



**HAL**  
open science

# Kinetic theory and large deviations for the dynamics of geophysical flows

Tomás Tangarife

► **To cite this version:**

Tomás Tangarife. Kinetic theory and large deviations for the dynamics of geophysical flows. Statistical Mechanics [cond-mat.stat-mech]. Ecole normale supérieure de lyon - ENS LYON, 2015. English. NNT : 2015ENSL1037 . tel-01241523

**HAL Id: tel-01241523**

**<https://theses.hal.science/tel-01241523>**

Submitted on 10 Dec 2015

**HAL** is a multi-disciplinary open access archive for the deposit and dissemination of scientific research documents, whether they are published or not. The documents may come from teaching and research institutions in France or abroad, or from public or private research centers.

L'archive ouverte pluridisciplinaire **HAL**, est destinée au dépôt et à la diffusion de documents scientifiques de niveau recherche, publiés ou non, émanant des établissements d'enseignement et de recherche français ou étrangers, des laboratoires publics ou privés.

# THÈSE

en vue de l'obtention du grade de

**Docteur de l'Université de Lyon, délivré par l'École  
Normale Supérieure de Lyon**

**Discipline : Physique**

**Laboratoire de Physique de  
l'École Normale Supérieure de Lyon**

**École doctorale de Physique et d'Astrophysique de Lyon**

présentée et soutenue publiquement le 16 Novembre 2015

par Monsieur Tomás TANGARIFE

---

## **Théorie cinétique et grandes déviations en dynamique des fluides géophysiques**

---

Directeur de thèse : M. Freddy BOUCHET

Devant la commission d'examen composée de :

M. Freddy BOUCHET,	CNRS et ENS Lyon, Directeur,
M. Krzysztof GAWĘDZKI,	CNRS et ENS Lyon, Examineur,
M. Petros J. IOANNOU,	National and Kapodistrian Univ. (Athènes), Rapporteur,
M. Jorge KURCHAN,	ENS (Paris), Examineur,
M. Grigorios A. PAVLIOTIS,	Imperial College (Londres), Examineur,
M. Tobias M. SCHNEIDER,	École Polytechnique Fédérale de Lausanne, Rapporteur,
M. Eric VANDEN-EIJNDEN,	Courant Institute (New York), Examineur,
M. William R. YOUNG,	Scripps Institution of Oceanography, Examineur.

# Contents

<b>Acknowledgements</b>	<b>5</b>
<b>Introduction</b>	<b>6</b>
<b>1 Zonal jets in mid–latitude atmospheres</b>	<b>11</b>
1.1 Observations . . . . .	11
1.2 Phenomenology of mid–latitude zonal jets . . . . .	13
1.2.1 Basic equations of large scale mid–latitude atmospheric dy- namics . . . . .	13
1.2.2 “Eddy–driven” jets . . . . .	15
1.2.3 On the role of rotation in jet dynamics . . . . .	15
1.2.4 Dimensional analysis in the beta–plane model . . . . .	16
1.2.5 Rare events in numerical simulations of zonal jets . . . . .	18
1.3 Current understanding of zonal jet dynamics . . . . .	19
1.3.1 Formation of jets through turbulent energy cascades . . . . .	20
1.3.2 Mixing of potential vorticity . . . . .	21
1.3.3 Quasi–linear and statistical approaches . . . . .	21
1.3.4 Equilibrium statistical mechanics theory . . . . .	24
1.4 Kinetic theory and Large Deviation theory . . . . .	24
<b>2 Statistics of slow–fast dynamical systems</b>	<b>26</b>
2.1 Heuristic derivation . . . . .	27
2.1.1 Law of Large Numbers and averaging . . . . .	27
2.1.2 Central Limit Theorem and typical fluctuations . . . . .	28
2.1.3 Large Deviation Principle and large fluctuations . . . . .	29
2.2 Stochastic averaging — Formal derivation . . . . .	29
2.2.1 Fokker–Planck formalism . . . . .	30
2.2.2 Stationary distribution of the fast variable . . . . .	31
2.2.3 Effective slow dynamics . . . . .	31
2.3 Large Deviation Principle — Formal derivation . . . . .	32
2.3.1 Gärtner–Ellis theorem . . . . .	32
2.3.2 Large deviation functions for the slow variable . . . . .	34
2.3.3 Link with stochastic averaging . . . . .	35
2.4 Validity of the results . . . . .	35
<b>3 Kinetic theory of zonal jets</b>	<b>37</b>
3.1 Time scale separation in the barotropic equation . . . . .	37
3.1.1 Non–dimensional equation . . . . .	37
3.1.2 Decomposition into zonal and non zonal flows . . . . .	38

3.1.3	Analogy with generic slow–fast systems . . . . .	39
3.2	Deterministic kinetic equation . . . . .	40
3.2.1	Link with the quasi–linear approximation and cumulant expansions . . . . .	41
3.2.2	Alternative derivation using the vorticity probability distribution functions . . . . .	43
3.3	Stochastic kinetic equation . . . . .	45
3.4	Perspectives . . . . .	46
<b>4</b>	<b>Implementation of the kinetic theory</b>	<b>48</b>
4.1	Some useful definitions for chapters 4 and 5 . . . . .	49
4.1.1	Expectations and limits . . . . .	49
4.1.2	Fourier decomposition . . . . .	50
4.2	Inviscid damping of the deterministic linearized equation . . . . .	50
4.2.1	A finite dimensional example . . . . .	51
4.2.2	Correlation functions from the solution of the deterministic linear equation . . . . .	52
4.2.3	Orr mechanism and depletion of the vorticity at the stationary streamlines . . . . .	53
4.3	Deterministic kinetic equation . . . . .	56
4.3.1	Pseudomomentum balance . . . . .	56
4.3.2	Numerical computation of the average Reynolds’ stress divergence . . . . .	58
4.4	Stochastic kinetic equation . . . . .	60
4.4.1	The integrated autocorrelation function in terms of two–points correlation functions . . . . .	61
4.4.2	Explicit computation in the case of a constant shear . . . . .	62
4.5	Perspectives . . . . .	64
<b>5</b>	<b>Theoretical justification of the kinetic theory</b>	<b>66</b>
5.1	Stationary distribution of the eddy vorticity in the inertial limit . . . . .	67
5.1.1	The stationary vorticity correlation function is a distribution . . . . .	68
5.1.2	Regularization of the eddy enstrophy due to a small linear friction . . . . .	70
5.2	Typical fluctuations of Reynolds’ stresses in the inertial limit . . . . .	71
5.2.1	The integrated autocorrelation function is a distribution . . . . .	72
5.2.2	The covariance is a distribution . . . . .	75
5.2.3	Influence of the forcing spectrum . . . . .	75
5.3	Consequences for the kinetic theory . . . . .	76
5.3.1	Summary of the technical results . . . . .	76
5.3.2	Consequences for the zonal energy balance . . . . .	77
5.3.3	Consequences for the ergodicity of the linearized dynamics . . . . .	78
5.3.4	Self–consistency of the time scale separation hypothesis . . . . .	79
5.4	Perspectives . . . . .	80
<b>6</b>	<b>Large deviations of zonal jets</b>	<b>82</b>
6.1	Estimation of the large deviation function from time series analysis . . . . .	83
6.1.1	Estimation of the decorrelation time . . . . .	84
6.1.2	Estimation of the scaled cumulant generating function . . . . .	85

6.2	Large deviations of quadratic forms of gaussian processes . . . . .	86
6.2.1	The Ricatti equation . . . . .	88
6.2.2	Link with the Lyapunov equation . . . . .	89
6.2.3	An explicit solution . . . . .	89
6.3	Barotropic dynamics on a rotating sphere . . . . .	90
6.3.1	Energy balance and non-dimensional equations . . . . .	91
6.3.2	Decomposition into zonal and non-zonal components . . . . .	92
6.3.3	Quasi-linear and linear dynamics . . . . .	92
6.3.4	Numerical implementation . . . . .	94
6.4	Zonal energy balance in the inertial limit . . . . .	95
6.4.1	Effective slow dynamics and effective zonal energy balance . . . . .	95
6.4.2	Average Reynolds' stresses in the inertial limit . . . . .	97
6.4.3	Fluctuations of Reynolds' stresses in the inertial limit . . . . .	101
6.4.4	Empirical validation of the time scale separation hypothesis . . . . .	102
6.5	Large deviations of Reynolds' stresses . . . . .	102
6.5.1	Large Deviation Principle for the time-averaged Reynolds' stresses . . . . .	103
6.5.2	Decomposition of the scaled cumulant generating function . . . . .	105
6.5.3	Numerical results . . . . .	106
6.6	Perspectives . . . . .	109
<b>7</b>	<b>Equilibrium dynamics of zonal jets</b>	<b>111</b>
7.1	The generalized Langevin equation . . . . .	111
7.1.1	Motivation . . . . .	111
7.1.2	Stationary distribution . . . . .	112
7.1.3	Stochastic averaging and fluctuation-dissipation relations . . . . .	114
7.1.4	Conserved quantities of the two-dimensional Euler equation . . . . .	116
7.2	Energy-entropy distribution . . . . .	117
7.2.1	Construction and properties of the energy-entropy distribution . . . . .	117
7.2.2	An explicit stationary solution of the Lyapunov equation . . . . .	119
7.3	Kinetic theory of Langevin models . . . . .	121
7.3.1	Construction of the equilibrium distribution . . . . .	121
7.3.2	Time scale separation in the Langevin equation . . . . .	123
7.3.3	Effective dynamics of the zonal jet . . . . .	126
7.3.4	Fluctuation-dissipation relations . . . . .	126
7.4	Perspectives . . . . .	128
	<b>Conclusion</b>	<b>130</b>
	<b>Appendices</b>	<b>131</b>
<b>A</b>	<b>Stochastic averaging — Formal derivation</b>	<b>132</b>
A.1	Perturbative expansion of the Fokker-Planck equation . . . . .	132
A.2	Explicit computation of the operators . . . . .	133
<b>B</b>	<b>Large Deviation Principle — Formal derivation</b>	<b>136</b>
B.1	The Gärtner-Ellis theorem applied to the slow process . . . . .	136
B.2	Expansion of the SCGF in powers of $\theta$ . . . . .	138

<b>C</b>	<b>Kinetic equation from the generalized LMN hierarchy</b>	<b>140</b>
C.1	The LMN hierarchy for the 2D stochastic Euler equation . . . . .	140
C.2	Young measure solution in the inertial limit . . . . .	141
C.3	Comparison with stochastic averaging . . . . .	142
C.3.1	Perturbative expansion in powers of $\alpha$ . . . . .	142
C.3.2	The case of a zonal jet . . . . .	144
C.3.3	Discussion . . . . .	145
<b>D</b>	<b>Convergence of the vorticity auto-correlation function to a distribution</b>	<b>147</b>
D.1	Sokhotskyi–Plemelj formula . . . . .	148
D.1.1	Regularization due to a small linear friction . . . . .	148
D.1.2	Expressions of the Cauchy Principal Value distribution . . . . .	148
D.2	Resolvent of the linearized Euler operator . . . . .	148
D.3	Proof of the convergence . . . . .	149
D.3.1	Points such that $U(y_1) = U(y_2)$ . . . . .	149
D.3.2	Points such that $U(y_1) \neq U(y_2)$ . . . . .	150
<b>E</b>	<b>Algorithms to compute the average Reynolds’ forcing</b>	<b>153</b>
E.1	Integral Lyapunov equation . . . . .	153
E.2	Integration of the resolvent over frequencies . . . . .	155
E.3	Using the pseudomomentum balance . . . . .	156
<b>F</b>	<b>Fluctuations of the Reynolds’ forcing for any background flow</b>	<b>158</b>
F.1	Two-points correlation functions . . . . .	158
F.2	Four-points correlation functions . . . . .	161
F.3	Temporal decay of some integrals . . . . .	162
<b>G</b>	<b>Large deviations of quadratic forms of gaussian processes</b>	<b>165</b>
G.1	Derivation of the Ricatti equation . . . . .	165
G.2	Explicit solution of the Ricatti equation . . . . .	166
<b>H</b>	<b>Most probable state of the equilibrium distribution</b>	<b>168</b>
<b>I</b>	<b>Decomposition of the Langevin equation</b>	<b>170</b>
I.1	Advection term . . . . .	170
I.2	Dissipation term . . . . .	170
I.3	Decomposed equations . . . . .	171
	<b>Bibliography</b>	<b>172</b>
	<b>Publications</b>	<b>181</b>
	<b>Main results</b>	<b>182</b>

# Acknowledgements

First I would like to thank Freddy for his constant support and involvement in the project of this thesis. His intuitive rigour and rigorous intuition have played a fundamental role in this work.

I also thank the people I had the chance to collaborate with. First of all Cesare Nardini, who has participated in many projects related to this thesis. Together with Freddy, Cesare has largely participated in teaching me what research is. Later during my PhD, I've had the chance to work with Brad Marston, I hope I'll have the opportunity to keep working with him in the future. I am also grateful to Cerasela Calugaru and all the staff of the PSMN for their support. I thank Tapio Schneider for inviting me to Zurich and for getting me involved in an interesting research project. Many people have also partly contributed to this thesis through very interesting and inspiring discussions: Petros Ioannou, Nikos Bakas, Navid Constantinou, Farid Ait-Chaalal, Eric Simonnet, Hugo Touchette, Eric Vanden-Eijnden and Tobias Grafke, among others. I had the chance to attend several conferences, thanks to a funding from the European Research Council under the European Unions seventh Framework Programme (FP7/2007-2013 Grant Agreement no. 616811).

I really enjoyed the friendly interaction with all the PhD students and young researchers in the lab, especially with Jason Laurie, Antoine Venaille, Rytis Paškauskas, Nathanaël Machicoane, Julien Reygner, Takahiro Nemoto, Leonardo Grigorio, Antoine Renaud, Eric Woillez, Thibaut Lestang; I also thank the constant participants to the PhD student's seminar, among them Clément Tauber, Irénée Frérot, ... I'd like to thank the people from the Physics departement for giving me the opportunity to do some teaching during my thesis, and the secretaries of the laboratory for their help, especially Fatiha Bouchneb for dealing with my repeated errors in administrative tasks.

---

Merci beaucoup à toutes les personnes qui m'ont accueilli à Lyon pendant la dernière année de ma thèse, en particulier Fanny, Clément, Anne, Antoine, Irénée, Fosca, Robert, Marie-Lou, Evelyne et Claude. Vous ne comprendrez peut-être pas tous les détails de cette thèse, mais sachez que vous y avez contribué directement avec votre hospitalité et votre dévouement. J'ai aussi une pensée pour le train Bellegarde-Lyon, dans lequel une partie significative de ce manuscrit a été rédigée.

Mes parents seraient très déçus de ne pas être mentionnés dans ces remerciements, et ils auraient raison. Merci à eux pour leur soutien constant durant toutes ces années. Enfin merci à Lauren, pour tout le reste.

# Introduction

Geophysical flows on large scales are turbulent, and have the striking property to self-organise into long-lived coherent structures. On Earth's atmosphere and on giant gaseous planets, strong east-west parallel currents —called zonal jets— are at the basis of mid-latitude atmosphere dynamics [110]. Quantifying their dynamics and statistics is fundamental in order to understand climate dynamics.

One of the motivations of this work is the description of fluctuations and rare events in zonal jet dynamics. For instance, the atmospheric polar jet stream fluctuates typically on time scales of a few weeks [111]. Larger fluctuations sometimes lead to a blocking of the Northern polar jet stream, which has major consequences on the weather in Western Europe and North America [54]. On Jupiter, observations suggest that one of the Southern jets has been lost in the late 30's through an extremely rare hydrodynamic instability [118]. None of the previous theoretical descriptions of zonal jets took into account typical and large fluctuations.

In mid-latitudes, zonal jets are on one hand slowly dissipated, mainly due to a large-scale friction mechanism, and on the other hand maintained by small-scale turbulent perturbations. This phenomenology has been identified for the polar jet streams on Earth in the 20's [51], and observed more recently on giant planets like Jupiter [100].

Because of turbulence, jet dynamics involve many spatial scales, from the scale of dissipation of turbulent perturbations to the scale of the jets themselves. Non-equilibrium statistical mechanics is a very natural framework to study the interactions and energy transfers between all these degrees of freedom. In many cases of interest, zonal jets evolve much slower than the surrounding turbulence [90]. This allows a quasistatic description of jet dynamics. In this thesis, we will show that in this regime of time scale separation, classical tools from statistical mechanics (stochastic averaging, large deviation theory) can be applied to give such effective description of jet dynamics and statistics. Such a task, an example of turbulent closure, is usually extremely hard to perform for turbulent flows.

Using stochastic averaging, we will obtain an effective equation for the slow dynamics of zonal jets, called the kinetic equation. This equation is a stochastic differential equation for the zonal velocity field, with multiplicative noise. The kinetic equation describes the attractors for the dynamics (alternating zonal jets), the relaxation towards those attractors, and the typical fluctuations around those attractors. The deterministic part of the kinetic equation was obtained previously using a quasilinear approximation of the dynamics [104] (S3T in [38] and CE2 in [106]). An example of numerical simulation of zonal jets, in the stochastic quasi-geostrophic barotropic model and in the related S3T approximation, is shown in

figure 1 [33]. In this case, the S3T approximation gives a qualitative description of the attractor of zonal jet dynamics. This description can be quantitatively accurate in some regimes, as discussed in chapter 3 of this thesis.

Our kinetic theory explains on a theoretical ground the past successes of quasi-linear approaches. It also allows to go further, as the stochastic part of the kinetic equation can explain departures from S3T-CE2 types of approximations, and describe fluctuations around the attractors of the slow dynamics.

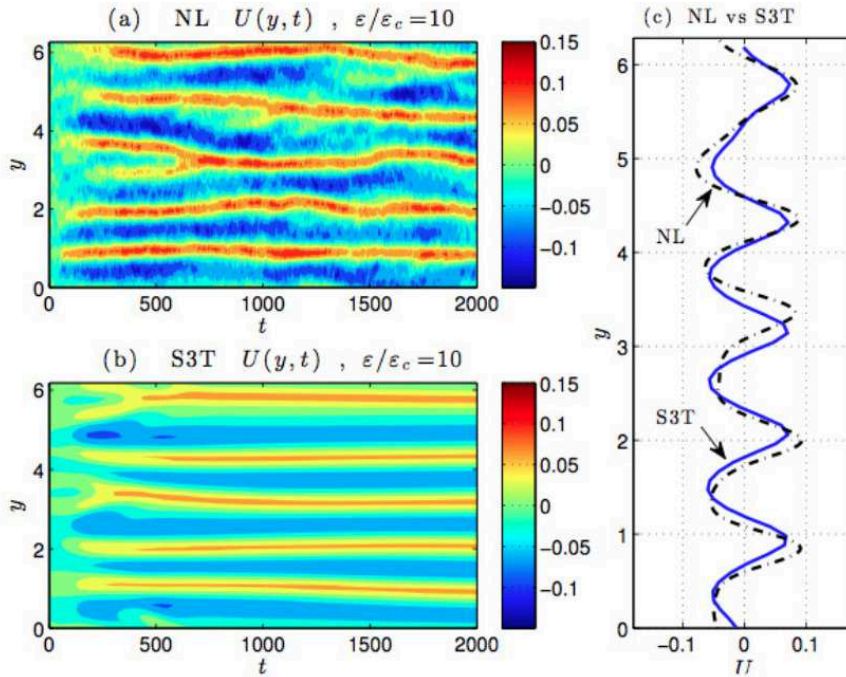


Figure 1: Formation of zonal jets in the stochastic quasi-geostrophic barotropic model and in the related S3T approximation, from [33]. The zonal velocity profile  $U(y,t)$  is represented as a function of latitude  $y$  and of time  $t$  (Hovmöller diagram), for the full model (upper panel) and for the S3T dynamics (bottom panel). The time-averaged velocity profile is also represented in the right panel, for both the full (NL) model, and for the S3T simulation, showing good qualitative agreement. However, the fluctuations of zonal jets visible in the NL simulation are not reproduced in the S3T simulation. The kinetic theory presented in this thesis is able to describe such fluctuations. Courtesy Navid Constantinou.

However, kinetic theory is not able to describe arbitrarily large fluctuations of zonal jets. Such rare fluctuations can have major consequences on weather and climate [28, 49, 107, 115], predicting their statistics is a major challenge in current climate studies.

Approaches through direct numerical simulations are prohibitive, because they imply that the total duration of the simulation increases as the probability of the event of interest decreases. As an example, in figure 2 is represented the evolution of zonal jets in the stochastic quasi-geostrophic barotropic model over very long time scales (when compared to the typical time scale of formation of jets), showing rare and abrupt transitions between two-jets and three-jets configurations. Such

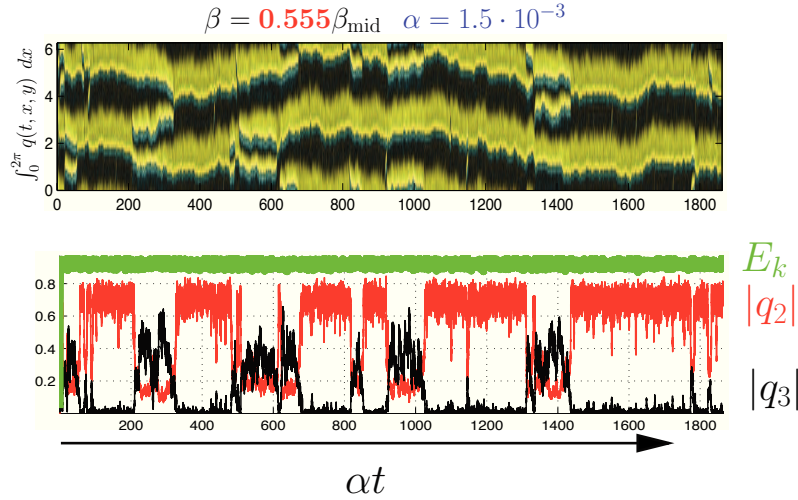


Figure 2: Zonal jets in a numerical simulation of the stochastic quasi-geostrophic barotropic equation. Top pannel: Hovmöller (spatio-temporal) diagram of the zonally averaged vorticity, showing rare and abrupt transitions between two-jets and three-jets configurations. Bottom pannel: time series of the vorticity Fourier components, showing both typical fluctuations and large fluctuations leading to transitions. Courtesy Eric Simonnet.

observation of a few transitions is not enough to get relevant statistics of those transitions (average residence time in each attractor, typical transition path from one attractor to another one). This observation calls for a theoretical approach instead.

Large deviation theory is a very interesting framework to study the statistical dynamics of both typical and rare events in complex systems. We will show that in the limit of time scale separation described above, large deviation theory gives the whole probability of paths of zonal jets, through the so-called large deviation principle. The large deviation principle gives access to both the effective dynamics (attractors, effective energy balance, typical transition path from one attractor to another one) and statistics (relative probability of two attractors, rate of transition between attractors).

To our knowledge, it is the first time this kind of approach (large deviation principle for slow-fast dynamical systems [39]) is applied in practice, using numerical simulations, to a complex system such as a turbulent flow. We will present original methods to implement the large deviation principle in practice, for the problem of interest (zonal jet dynamics), and that can be easily applied to a much larger class of non-equilibrium systems. In particular, those methods allow to study arbitrarily rare events extremely easily, in contrast with approaches through direct numerical simulations.

Stochastic averaging and the large deviation principle can be applied rigorously to a large class of systems with time scale separation [39, 84, 86]. However, we will

see that the stochastic quasi-geostrophic model does not fulfill the hypothesis for those theorems. Understanding under which conditions the results still apply is thus a crucial theoretical question, it can have very interesting physical consequences and could lead to new mathematical problems.

From a physical point of view, the regime of time scale separation between large scales and small scales turns out to be also the limit of small forces and dissipation. At leading order, the evolution of turbulent perturbations is described by the linearized dynamics close to the fixed zonal flow, in the regime of interest this linear dynamics is stochastically forced but not dissipated. The question of whether this linear dynamics actually reaches a stationary state or not is thus crucial for the self-consistency of our theory, answering this question is a central point of this thesis.

In the case of the stochastic two-dimensional Navier-Stokes equation (i.e. with no differential rotation), the linearized dynamics actually leads to an inviscid damping of turbulent perturbations, known as the Orr mechanism [11, 82], even in the absence of external dissipation. Using the Orr mechanism, we will study the mathematical properties of the linear stochastic dynamics. In particular, we will study the low-order statistics (average and covariance) of Reynolds' stresses, which are the terms appearing in the kinetic equation for zonal jets.

We will see that the inviscid damping ensures the self-consistency of the kinetic theory at leading order (deterministic part of the kinetic equation involving the average Reynolds' stress). At next order (stochastic part of the kinetic equation involving the typical fluctuations of Reynolds' stresses), the issue is more subtle and we will see that some quantities of interest converge to finite values in the limit of small dissipation, while some other quantities diverge. More precisely, we will obtain results of convergence in a weak sense, i.e. in the sense of distributions. An important physical consequence of those results is that the typical fluctuations of Reynolds' stresses cannot be neglected in the effective dynamics of zonal jets. All those theoretical results will also be confronted with numerical computations.

In the limit of no forcing and dissipation, approaches through equilibrium statistical mechanics explain both the self-organization of the flow and why zonal jets are natural attractors of the dynamics [14]. The formal generalization of these results to the case with forcing and dissipation can be done using a Langevin equation, a classical tool in statistical mechanics. Such Langevin model of zonal jet dynamics is presented in the end of this thesis. The interest of this approach is that we can construct the stationary distribution of the flow (generalized canonical equilibrium distribution), and obtain explicit results for the zonal jet evolution and statistics.

We will present a class of equilibrium distributions that leads to a time scale separation between the evolution of large scales and small scales, and apply the stochastic averaging procedure to obtain an equivalent of the kinetic equation. The relation with previous studies [10, 19, 61] will also be discussed.

The basic phenomenology of planetary zonal jets and a brief review of previous descriptions is first presented in chapter 1.

The effective description of zonal jets presented in this thesis is based on classical results of statistics: the Law of Large Numbers, the Central Limit Theorem and the Large Deviation Principle. These theoretical tools are presented in a general

framework in chapter 2.

In chapter 3, the Law of Large Numbers and the Central Limit Theorem are applied to the stochastic quasi-geostrophic barotropic model, leading to an effective equation describing the attractors and typical fluctuations of zonal jets (kinetic equation).

The practical implementation of the kinetic equation is discussed in chapter 4. This naturally leads to wonder about the self-consistency of the kinetic theory, in relation with the behaviour of linearized dynamics in the absence of dissipation. Those questions are addressed in chapters 4 and 5.

In chapter 6, tools from Large Deviation Theory are applied to the stochastic quasi-geostrophic barotropic model, which allows the description of rare events statistics in zonal jets dynamics.

Finally in chapter 7, an academic model describing the equilibrium dynamics of zonal jets is presented, and the effective dynamics of jets within this model is studied.

A general conclusion is given in page 130, and a list of the main results can be found in page 182.

# Chapter 1

## Zonal jets in mid–latitude atmospheres

### 1.1 Observations

Geophysical turbulent flows are characterized by their self-organisation into large-scale, long-lived structures: cyclones and anti-cyclones, parallel jets, ocean rings... In particular, atmospheric flows in mid-latitudes have a tendency to self-organise into robust horizontal currents parallel to the equator, called zonal jets.

This phenomenon is striking on giant planets like Jupiter. The velocity field in the outer layer can be analysed from observations [43], and the zonal (east-west) wind averaged over a line of constant latitude can be estimated as a function of latitude (zonal velocity profile). Measures of the zonal velocity profile separated by an interval of 20 years shows very few changes [90]. In contrast, the pictures of Jupiter’s external layer on smaller scales show that the turbulence evolves on time scales of order of the day [90]. These observations show that zonal jets are much more coherent than the surrounding turbulence.

On Earth, two intense eastward zonal jets are found in each hemisphere. The so-called sub-tropical jet streams are located at latitudes around  $\pm 30^\circ$ , and the so-called polar jet streams are located between  $\pm 40^\circ$  and  $\pm 70^\circ$ . Figures 1.1(a), 1.1(b) show the horizontal velocity field in the tropopause (around 10km height) for the southern hemisphere, at a given day and averaged over a southern hemisphere winter (june-july-august). These figures show that the instantaneous velocity field is far from the time-averaged one, meaning that these jets undergo strong fluctuations.

This variability is also observed in the northern hemisphere, where the polar jet stream visits two states: a nearly zonally invariant state, and a “blocked” state [54]. This phenomenon has very important consequences for weather, indeed the occurrences of blocked states are related with extreme heat waves in Western Europe and extreme cold waves in North America [49, 115]. This is illustrated in figures 1.2(a), 1.2(b). A simple analogy of this phenomenon has been obtained in a rotating tank experiment [116]. The time series of velocity shows bistability between these states, with sporadic and abrupt transitions. This phenomenon has also been reproduced in numerical simulations of simplified models [27, 57, 111].

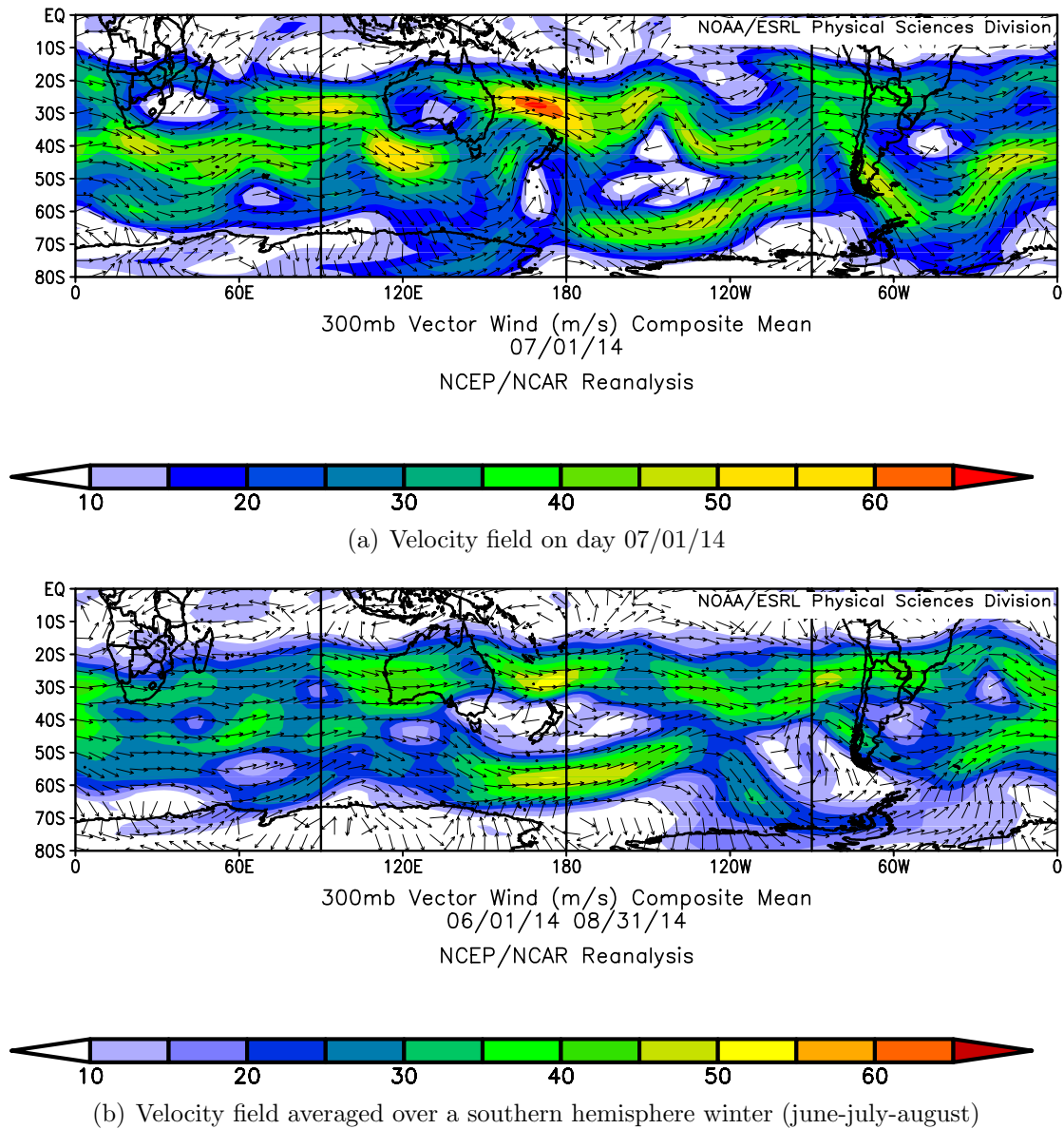


Figure 1.1: Map of the wind in the southern hemisphere, in the tropopause (pressure level 300 mb, i.e. around 10 km height), from data reanalysis [52] (image provided by the NOAA/ESRL Physical Sciences Division, Boulder Colorado from their Web site at <http://www.esrl.noaa.gov/psd/data/composites/day/>). The arrows indicate the direction of the wind and the colours show the intensity of the wind (in  $\text{m}\cdot\text{s}^{-1}$ ). The subtropical and polar jet streams appear on these maps, even though they are confounded in some locations. The comparison between both maps shows that these jets undergo strong fluctuations.

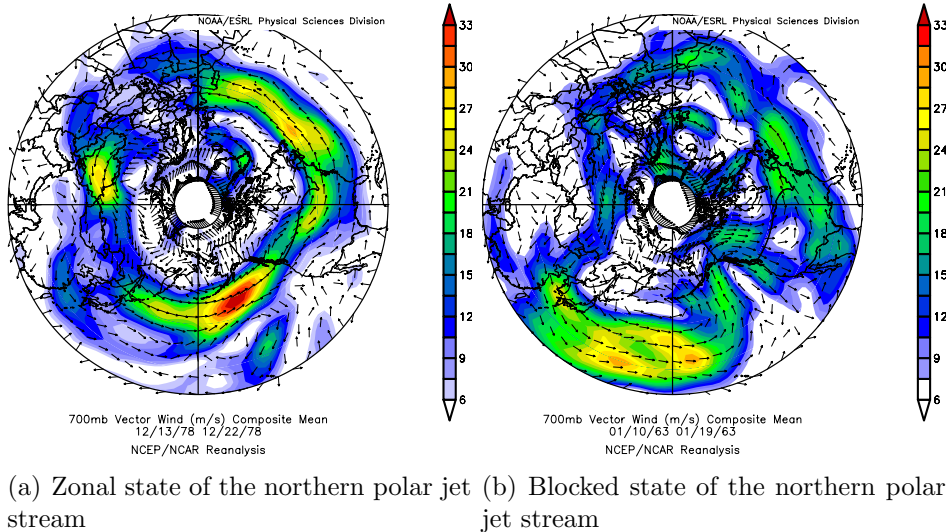


Figure 1.2: Map of the wind in the northern hemisphere, averaged over 10 days (at pressure level 700 mb, i.e. around 3 km height), from data reanalysis [52] (image provided by the NOAA/ESRL Physical Sciences Division, Boulder Colorado from their Web site at <http://www.esrl.noaa.gov/psd/data/composites/day/>). The averaging dates are the same as in [116]. The arrows indicate the direction of the wind and the colours show the intensity of the wind (in  $\text{m}\cdot\text{s}^{-1}$ ). The left panel (a) shows the nearly zonally invariant state, and the right panel (b) shows the blocked state, associated with strong meandering over North America and over Central Asia.

It has been suggested that planetary zonal jets may also have a large impact on abrupt climate changes [28, 107]. Such abrupt change has been observed on Jupiter in the end of the 40's [95, 118], and the relevance of such abrupt changes for past and future Earth climate changes is still an open question.

## 1.2 Phenomenology of mid-latitude zonal jets

### 1.2.1 Basic equations of large scale mid-latitude atmospheric dynamics

Climate dynamics involves many different phenomena, occurring over a wide range of temporal and spatial scales [88]. For this reason, the theoretical description of the climate system involves a large set of coupled equations. For practical reasons, and in order to extract the basic ingredients responsible for the phenomenon of interest, we have to use simplified equations.

In the study of atmospheric flows, the basic equations are the three-dimensional Navier-Stokes equations in the rotating frame of reference of the planet. Dimensional analysis of the different terms involved in these equations allow to perform major simplification [110]

- If the typical length scale of the horizontal motion  $L$  is much larger than the depth of the atmosphere, then the vertical motion resumes to the hydrostatic

balance  $\partial_z p = -\rho g$ , where  $\partial_z p$  is the vertical pressure gradient,  $\rho$  is the volumetric mass and  $g$  is the acceleration of gravity.

- If the horizontal velocity field evolves on time scales much larger than the period of rotation of the planet, then the horizontal motion resumes to a balance between the Coriolis acceleration and pressure gradients, as known as geostrophic balance:  $\rho \mathbf{f} \times \mathbf{v} = -\nabla p$ , where  $\mathbf{f} = 2\Omega \sin \theta \mathbf{e}_z$  is the Coriolis parameter ( $\Omega$  is the planet rotation rate,  $\theta$  is the latitude and  $\mathbf{e}_z$  is the vertical unit vector),  $\mathbf{v}$  is the horizontal velocity field and  $\nabla p$  is the horizontal pressure gradient. Geostrophic balance is expected to be accurate when the so-called Rossby number, defined as the ratio of the orders of magnitude of advective and Coriolis accelerations, is small:  $Ro = U/Lf \ll 1$ , where  $U$  is the typical order of magnitude of the horizontal velocity.

The hydrostatic and geostrophic balances describe accurately the winds and air mass fluxes in mid-latitudes, on time scales up to a week (typical time scale of evolution of the weather). On larger time scales (i.e. at next order in  $Ro$ ), advection and dissipation have to be taken into account. This leads to the class of quasi-geostrophic models.

Such models are known to produce realistic zonal jets [106], and even reproduce their variability and transitions [27, 57]. Among quasi-geostrophic models, the simplest model that produces multiple zonal jets is the stochastic barotropic beta-plane equation

$$\frac{\partial \omega}{\partial t} + \mathbf{v} \cdot \nabla \omega + \beta v = -\kappa \omega - \nu_n (-\Delta)^n \omega + \sqrt{\sigma} \eta, \quad (1.1)$$

where  $\omega = (\nabla \times \mathbf{v}) \cdot \mathbf{e}_z$  is the component of the vorticity that is perpendicular to the layer of fluid, and  $\mathbf{v} = (u, v)$  is the incompressible horizontal velocity field. The coordinates  $x$  and  $y$  are called respectively the zonal and meridional coordinates, and the velocity components  $u$  and  $v$  are called zonal and meridional velocities. Equation (1.1) essentially describes the two-dimensional motion of a fluid on the plane that is tangent to the surface of a rotating sphere, at a given latitude. Then,  $\beta$  is the gradient of the Coriolis parameter  $f$  at this latitude.

The first term on the right-hand side is a common way used to describe large-scale dissipation due to bottom drag [9, 110]. The coefficient  $\kappa$  is usually called Rayleigh friction or Ekman drag. The last two terms on the right-hand side are used to parametrize the effects of smaller-scale phenomena, which we do not want to describe in detail here. Such phenomena are essentially baroclinic and convective instabilities, which provide stirring of the quasi-2D flow and dissipate energy at the smallest resolved scales. The hyper-viscous term  $\nu_n (-\Delta)^n$  is essentially introduced for practical reasons in numerical simulations [3, 104]. The force term  $\sqrt{\sigma} \eta$  is the curl of a force (per unit of mass), it is usually taken to be a random noise. The simplest case—and this is the case we will consider in this thesis—is a gaussian white noise, with zero mean and correlations  $\mathbb{E}[\eta(\mathbf{r}_1, t_1)\eta(\mathbf{r}_2, t_2)] = C(\mathbf{r}_1, \mathbf{r}_2)\delta(t_1 - t_2)$ , where  $\mathbb{E}[\cdot]$  represents the average over realizations of the noise  $\eta$ . For an introduction to random processes and stochastic differential equations, see for example [44]. The parameter  $\sigma$  is a measure of the intensity of the random force in (1.1), it will be defined more precisely in section 1.2.4.

In this thesis (except in chapter 6), we will consider equation (1.1) in the bi-periodic domain  $(x, y) \in \mathcal{D} = [0, 2\pi L_x) \times [0, 2\pi L_y)$ , in order to avoid boundary effects.

In chapter 6, we will study the dynamics of zonal jets in a spherical geometry, the equation of motion will be introduced then.

### 1.2.2 “Eddy-driven” jets

When the flow is dominated by a coherent zonal jet, the velocity field reads  $\mathbf{v}(\mathbf{r}) = (U(y) + u'(\mathbf{r}), v'(\mathbf{r}))$ , where  $U(y)$  is the zonal velocity profile and  $\mathbf{v}' = (u', v')$  is the perturbation velocity. Typically,  $\mathbf{v}'$  is a turbulent velocity field, all along this thesis we will refer to this perturbation as “eddies” or “turbulence”, without distinction.

For the dynamics (1.1), zonal jets are mainly dissipated by the linear friction (term  $-\kappa\omega$ ). This dissipation is balanced by the transfer of energy by the turbulence  $\mathbf{v}'$ , from the forcing scale to the jet scale. Such zonal jets are said to be eddy-driven.

The previous statement can be made more precise, using the projected equation for the zonal jet velocity profile

$$\frac{\partial U}{\partial t} = -\frac{\partial}{\partial y} \langle u'v' \rangle - \kappa U, \quad (1.2)$$

where  $\langle \cdot \rangle$  denotes the average over the zonal direction, and where we have neglected viscosity and the stochastic force acting directly on  $U$ . This equation will be derived in more detail in chapter 3. On the right-hand side of (1.2), the term  $\langle u'v' \rangle$  is a zonally averaged horizontal flux of momentum, and is similar to a Reynolds’ stress used in the turbulence community [89]. Then,  $-\partial_y \langle u'v' \rangle$  is the convergence of momentum flux, or (minus) the divergence of the Reynolds’ stress. In this thesis,  $-\partial_y \langle u'v' \rangle$  will be called the Reynolds’ force<sup>1</sup>.

In a steady state,

$$U \simeq -\frac{1}{\kappa} \frac{\partial}{\partial y} \langle u'v' \rangle, \quad (1.3)$$

expressing the balance between large scale dissipation and forcing through the turbulent field  $(u', v')$ . In the case of eddy-driven jets, we should observe a clear correlation between the zonal jet velocity profile and the Reynolds’ force  $-\partial_y \langle u'v' \rangle$ .

This is the case in numerical simulations of mid-latitude jets on Jupiter [102]. On Earth, the polar jet streams are essentially eddy-driven, which was first argued in [51], and observed more recently [48, 88]. In contrast, the subtropical jet streams are not associated with convergence of horizontal momentum fluxes. Instead, their formation is understood in relation with large scale convections cells (Hadley cells), which are essentially three-dimensional [110].

### 1.2.3 On the role of rotation in jet dynamics

A purely zonal flow is characterized by  $v = 0$ . In the limit of a large value of  $\beta$ , we readily see from (1.1) that  $v$  should be correspondingly small in order to balance the advection term  $\mathbf{v} \cdot \nabla \omega$ . This basic argument (that is essentially equivalent to angular momentum and energy conservations [110]) explains why differential rotation (evolution of the Coriolis parameter with latitude) leads to predominantly zonal flows. More elaborated arguments that also involve differential rotation as a fundamental ingredient will be presented in section 1.3.

<sup>1</sup>Actually  $-\rho \partial_y \langle u'v' \rangle$  with  $\rho$  the mass per unit of area has the dimensions of a force. However, in this incompressible fluid dynamics context, we abusively call  $-\partial_y \langle u'v' \rangle$  a force.

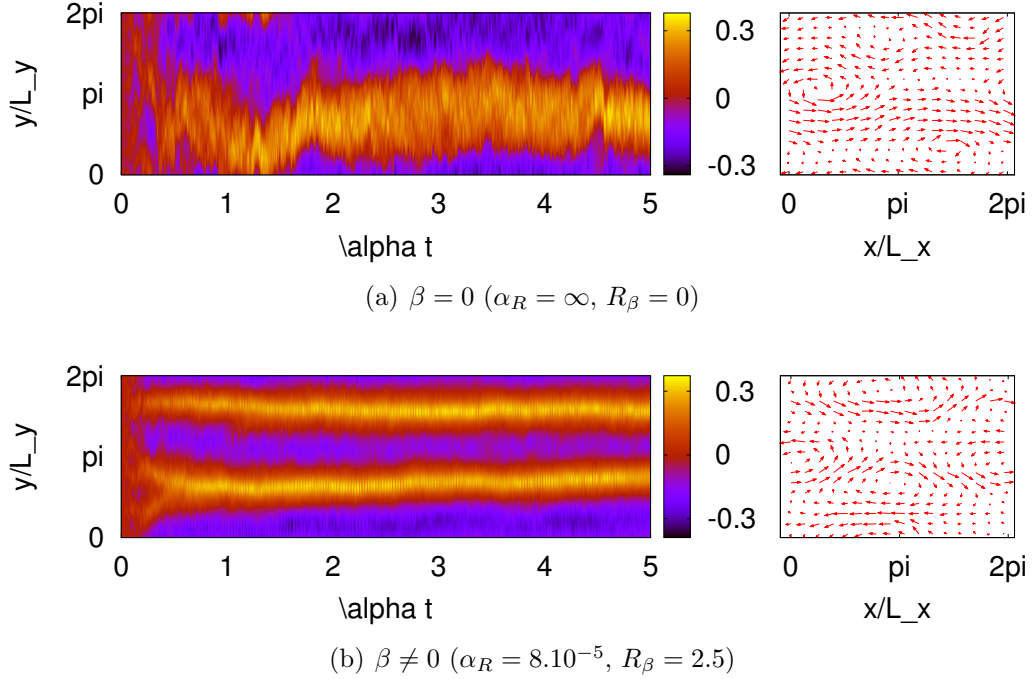


Figure 1.3: Zonal jets formation in simulations of the stochastic barotropic equation (1.1). Left panels: zonal velocity profile  $U(y)$  as a function of time (Hovmöller diagram), right panels: velocity field at  $t = 5/\alpha$ , with (a)  $\beta = 0$  and (b)  $\beta \neq 0$ . In both cases, robust zonal jets are formed. This shows that the beta effect is not necessary for jet formation in general, but that  $\beta$  changes the number and shape of the jets. The aspect ratio is  $L_x/L_y = 0.7$ , and  $\alpha = 10^{-3}$ . The parameters  $\alpha$ ,  $\alpha_R$  and  $R_\beta$  are defined in section 1.2.4. The numerical simulations were performed with a pseudo-spectral code, at resolution  $256 \times 256$ , with a homogeneous isotropic forcing peaked around wavenumber  $k_f = 8$ .

However, it should be noted that zonal flows can also form in the absence of rotation, i.e. in two-dimensional turbulence. In this case, turbulence leads to the concentration of the energy in the largest scale [9, 55], so the coherent structure depends crucially on the geometry [14]. Consider for instance the two-dimensional Navier-Stokes equation (equation (1.1) with  $\beta = 0$ ) in the bi-periodic domain  $(x, y) \in \mathcal{D} = [0, 2\pi L_x) \times [0, 2\pi L_y)$  with aspect ratio  $l_x = L_x/L_y$ . If  $l_x < 1$ , the largest scale corresponds to the  $k_y = 1$  mode, i.e. to a zonal flow. Conversely, if  $l_x > 1$  the coherent structure will be a meridional flow (in the  $y$  direction). In the square case  $l_x = 1$ , the large-scale flow will be made of a dipole of vortices. This effect is observed in numerical experiments, as illustrated in figure 1.3, and can even lead to bistability between the dipole and unidirectional flow attractors when  $l_x \simeq 1$  [13].

#### 1.2.4 Dimensional analysis in the beta-plane model

We have seen in section 1.1 that zonal jets in planetary atmospheres can have very different structures and dynamics. For instance, zonal jets on Jupiter evolve over time scales of decades [90], while the polar jet stream on Earth has strong fluctuations over time scales of a few weeks (see figure 1.1(a)). These different behaviours

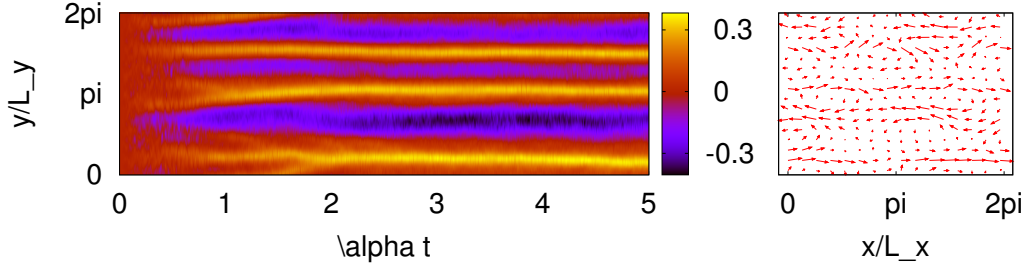


Figure 1.4: Hovmöller diagram of the zonal velocity profile (left) and velocity field at  $t = 5/\alpha$  (right), with  $\alpha = 2.10^{-3}$  and  $\beta$  such that  $\alpha R = 8.10^{-5}$  (and thus  $R_\beta = 2.5$ ), as in figure 1.3(b). Strong jets are formed also in this case.

can be understood from a dimensional analysis of the stochastic barotropic equation (1.1).

The inertial barotropic equation ((1.1) without dissipation and forcing) conserves the energy<sup>2</sup>

$$\mathcal{E}[\omega] = \frac{1}{2} \int_{\mathcal{D}} \mathbf{v}^2 = -\frac{1}{2} \int_{\mathcal{D}} \omega \psi, \quad (1.4)$$

where the last equality follows from an integration by parts and the use of the incompressibility condition<sup>3</sup>; and the relative enstrophy

$$\mathcal{Z}[\omega] = \frac{1}{2} \int_{\mathcal{D}} \omega^2. \quad (1.5)$$

By application of the Itô formula [44] to (1.1), we easily show that the total average energy injection rate by the stochastic force is  $\frac{\sigma}{2} \int_{\mathcal{D}} \mathbf{dr} (-\Delta^{-1} C)(\mathbf{r}, \mathbf{r})$ , where  $\Delta^{-1}$  represents the inverse Laplacian operator applied to either of the arguments of  $C$ , the correlation function of the force in (1.1). Multiplying  $C$  by an arbitrary positive constant amounts at renormalizing  $\sigma$ . Then, we can assume without loss of generality that  $\int \mathbf{dr} (-\Delta^{-1}) C(\mathbf{r}, \mathbf{r}) = 2$ , so  $\sigma$  is the total injection rate of energy per unit of mass. The energy balance for (1.1) thus reads

$$\frac{dE}{dt} = -2\kappa E - 2\nu_n H_n + \sigma \quad (1.6)$$

where  $E \equiv \mathbb{E}[\mathcal{E}[\omega]]$  and  $H_n = -\frac{1}{2} \mathbb{E} \left[ \int_{\mathcal{D}} \psi (-\Delta)^n \omega \right]$ .

For atmospheric flows, viscosity is negligible in the global energy balance:  $\nu_n H_n \ll \kappa E$ . This is the regime that we will study in the following. In a stationary state, we then have  $E_{stat} \simeq \sigma/2\kappa$ , expressing the balance between forces and dissipation. Assuming that most of the energy is contained in the zonal jet, we get an estimate of the order of magnitude of the jet velocity  $U \sim \sqrt{E_{stat}}/L \sim \sqrt{\epsilon/2\kappa}$ , where  $L$  is the typical length scale of the domain and  $\epsilon = \sigma/L^2$  is the average energy injection rate per unit of area. Then the typical time scale of advection and stirring of a turbulent eddy by the coherent structure is  $\tau_{eddy} = L/U$ .

<sup>2</sup>Actually, the total kinetic energy of the system is  $\rho \mathcal{E}[\omega]$ , with  $\rho$  the mass per unit of area. As usual in incompressible fluid dynamics, we call  $\mathcal{E}[\omega]$  the energy for simplicity.

<sup>3</sup>The incompressibility condition  $\partial_x u + \partial_y v = 0$  is usually written defining a stream function  $\psi(\mathbf{r})$ , such that  $u = -\partial_y \psi$ ,  $v = \partial_x \psi$ . Then  $\omega = \Delta \psi$  where  $\Delta = \partial_x^2 + \partial_y^2$  is the horizontal Laplacian operator.

The regime of formation of large-scale coherent structures is defined comparing  $\tau_{eddy}$  with the typical time scale of evolution of the coherent structure, given by the dissipative time scale  $\tau_{jet} = 1/\kappa$ . The regime of interest can thus be defined by<sup>4</sup>

$$\alpha \equiv \frac{\tau_{eddy}}{\tau_{jet}} = L\sqrt{\frac{2\kappa^3}{\epsilon}} \ll 1. \quad (1.7)$$

In this thesis, we will perform a perturbative expansion of (1.1) in powers of  $\alpha$ , i.e. in the regime where the turbulent eddies evolve much faster than the zonal jets. We will obtain effective descriptions of zonal jets dynamics in this regime, averaging out the fast turbulence.

Note however that  $\tau_{eddy}$  might not be the most relevant time scale for the evolution of turbulent perturbation. Indeed, when it comes to eddy-driven jet dynamics, the most relevant time scale of eddies dynamics is the decorrelation time of the Reynolds' stresses. This crucial point will be discussed all along the thesis.

When advective and Coriolis terms in (1.1) are of the same order, another length scale appears in the system. This length scale is known as the Rhines scale [110], and can be expressed as

$$L_R = \sqrt{\frac{U}{\beta}}.$$

It is often argued that  $L_R$  represents the typical meridional width of the jets [36, 106, 110]. The time scale of stirring of a turbulent eddy over the distance  $L_R$  is  $\tau_R = L_R/U$ , then the ratio of advective and dissipative time scales is

$$\alpha_R \equiv \kappa\tau_R = L_R\sqrt{\frac{2\kappa^3}{\epsilon}}.$$

$L/L_R$  is an estimation of the number of jets, so we can consider that the  $\beta$  effect is relevant when  $L_R \leq L$ . Then  $\alpha_R \leq \alpha$ , so the regime of interest  $\alpha \ll 1$  also implies  $\alpha_R \ll 1$ .

We notice that  $\alpha_R \propto (R_\beta)^{-5}$  where  $R_\beta = 2^{-1/2}\beta^{1/10}\epsilon^{1/20}\kappa^{-1/4}$  is the zonostrophy index introduced in [34, 42]. Direct numerical simulations [106] and data analysis [43] tend to show that  $R_\beta \gtrsim 2.5$  (which roughly implies  $\alpha_R \ll 1$ ) is a criterion for the robustness of zonal jets in beta-plane turbulence. As an example, estimates give  $R_\beta = 5.2$  for Jupiter [43] and  $R_\beta = 1.2$  for Earth's atmosphere [3], which explains the qualitative difference between zonal jets on Earth and on Jupiter.

This is also illustrated in figure 1.4, where we have used parameters such that  $\alpha_R$  is the same as in figure 1.3(b), but with a larger value of  $\alpha$ . We also observe strong jets in this case. Then, the comparison of figures 1.3 and 1.4 shows that a criterion for zonal jet formation would involve both  $\alpha$  and  $\alpha_R$  (or equivalently  $R_\beta$ ). This point will be further discussed in section 3.2.1.

### 1.2.5 Rare events in numerical simulations of zonal jets

As discussed in section 1.1, the Northern polar jet stream visits two states: a nearly zonally invariant state and a “blocked” state, see figures 1.2(a), 1.2(b). This phe-

<sup>4</sup>This condition can also be obtained comparing the typical length scale of dissipation by linear friction and the size of the domain, reasoning analogously to the Kolmogorov theory of 3D turbulence [14].

nomenon has also been reproduced in numerical simulations of simplified models [111], and has been related to a possible bistable property of the polar jet stream dynamics [27, 54, 57].

Similar bistability phenomena have been reported recently in numerical simulations by Eric Simonnet. As explained in the previous section, the value of  $\beta$  in the stochastic barotropic model (1.1) roughly determines the number of jets in the steady state. For example, in the simulation corresponding to the bottom panel of figure 1.3 the value of  $\beta$  leads to the formation of two jets, while in figure 1.4 the value of  $\beta$  is changed and we observe four jets.

When  $\beta$  takes a value that is intermediate between, say, a two-jets situation and a three-jets situation, rare transitions between those attractors occur on very long times scales (when compared to the dissipative time scale). This phenomenon is illustrated in figure 2 (page 8). The time series of  $q_2$  and  $q_3$ , respectively the second and third components in the Fourier decomposition of the zonally averaged vorticity  $q \equiv \langle \omega \rangle$ , shows the sporadic and abrupt transitions between the two-jets and three-jets configurations. The parameters here are  $\alpha = 1.5 \cdot 10^{-3}$  and  $\alpha_R = 1.1 \cdot 10^{-4}$  ( $R_\beta = 2.3$ ).

Those transitions occur on time scales of order  $100/\alpha$ . It is then extremely difficult to get relevant statistics of these rare events using direct numerical simulations. Using involved numerical methods such as the Adaptive Multilevel Splitting algorithm of [26, 97], one can get access to quantities like the probability of transitions between different configurations, or the typical path of the transition<sup>5</sup>. For instance in figure 1.5 is represented a Hovmöller diagram of the typical transition from a two-jets to a three-jets configuration, obtained using the Adaptive Multilevel Splitting algorithm.

An interesting observation to make is that this transition occurs on a time scale of order  $1/\alpha$  (dissipative time scale in (1.1)), of the order of the the typical time of evolution of zonal jets (see chapter 3 for more details). In the regime  $\alpha \ll 1$ , there is thus a clear time scale separation between

- the fast dynamics of turbulent eddies (time scale of order 1),
- the dynamics of zonal jets, including the transitions between attractors (time scale  $O(1/\alpha)$ ),
- the typical time of residence in each attractor (here  $O(100/\alpha)$ ).

## 1.3 Current understanding of zonal jet dynamics

We now review previous theories describing the formation and dynamics of zonal jets in the framework of barotropic models. Most of these theories are presented in geophysical fluid dynamics textbooks [87, 110], see also the introduction of [32].

---

<sup>5</sup>The Adaptive Multilevel Splitting method is given here as an example, it will not be further discussed in the thesis.

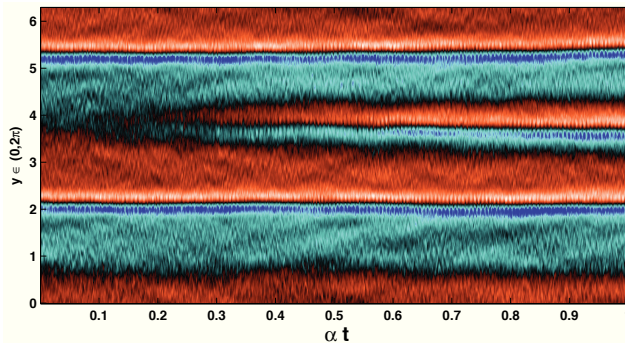


Figure 1.5: Hovmöller diagram of the zonally averaged vorticity, showing the typical transition from a configuration with two zonal jets to a configuration with three zonal jets, in a numerical simulation of the stochastic barotropic equation (1.1) (accessed using the Adaptive Multilevel Splitting algorithm of [26, 97]). Parameters are  $\alpha = 6 \cdot 10^{-4}$  and  $\alpha_R = 2.1 \cdot 10^{-5}$  ( $R_\beta = 3.3$ ). Courtesy Eric Simonnet.

### 1.3.1 Formation of jets through turbulent energy cascades

As explained in previous sections, the presence of zonal jets in mid-latitude can be seen in a first approximation as a phenomenon of self-organisation of a turbulent flow (eddy-driven jets). Then, describing jet dynamics is a genuine turbulence problem, and some previous approaches rely upon a phenomenological description of energy cascades in geostrophic turbulence.

Two-dimensional turbulence is characterized by a self-similar cascade of energy towards the large scales [9, 55], called “inverse cascade” in comparison with the cascade of energy towards small scales observed in three-dimensional turbulence [89]. Consider a two-dimensional fluid initially at rest, with stochastic forces localized on small scales. The non-linear advective interactions lead to the formation of the inverse energy cascade. If the typical length scale of dissipation by linear friction is larger than the size of the domain (which is equivalent to the condition  $\alpha \ll 1$  where  $\alpha$  is defined in (1.7) [14]), then energy piles up at the domain scale. In a domain stretched in the meridional direction, energy stored in the largest scale corresponds to a single zonal jet, as illustrated in figure 1.3.

An important characteristic of two-dimensional flows (as described by equation (1.1) with  $\beta = 0$ ) is that most zonal flows typically support no linear waves (the associated linear operator has no eigenmodes [11]). In contrast, barotropic dynamics (with  $\beta \neq 0$ ) is associated with the propagation of waves known as Rossby waves [98]. Since the beta effect introduces an anisotropy between meridional and zonal directions, Rossby waves are characterized by an anisotropic dispersion relation [110]. Vallis and Maltrud [112] suggested that the competition between Rossby waves and nearly isotropic turbulence leads to a concentration of energy in the modes associated with large scales and invariance in the zonal direction, i.e. into zonal jets. This phenomenology of jet formation has been observed in numerical simulations of the inertial barotropic model (equation (1.1) with no forces and dissipation) with an initial spectrum localized on small scales [112]. A similar phenomenology of jet formation has also been identified in a weak turbulence approach [76].

This simple picture is only valid at the early times of the system evolution, indeed non-inertial effects such as large-scale dissipation have to be taken into account to describe equilibration of jets [110]. Moreover, when strong zonal jets are formed the structures of both Rossby waves and smaller-scale turbulence are altered by the jets. Rossby waves are then observed to coexist with turbulence at all scales [105], leading to different self-similar energy cascades. This turbulent regime has been called zonostrophic turbulence, and has been observed in numerical simulations [34, 42] and observations of Jupiter’s jets [43].

### 1.3.2 Mixing of potential vorticity

The inertial barotropic equation ((1.1) without forces and dissipation) is equivalent to the conservation of potential vorticity  $q(\mathbf{r}) = \omega(\mathbf{r}) + \beta y$  [110]. Then, turbulence leads to the homogenization of  $q$ , i.e. to a linear profile of zonal vorticity. Such linear zonal vorticity corresponds to a parabolic velocity profile satisfying  $U''(y) = \beta$ . However, the presence of Rossby waves inhibiting turbulent mixing leads instead to a staircase profile of potential vorticity (piece-wise linear), or equivalently to an asymmetric zonal jet velocity profile (piece-wise parabolic) [36].

The prediction of such zonal velocity profile is qualitatively confirmed in observations of Jupiter’s jets [36], but is far from being quantitative and is probably not the most general case [7, 8].

The approaches presented in sections 1.3.1 and 1.3.2 are based on a phenomenological description of geostrophic turbulence (self-similar energy cascades and mixing). These works thus suggest that zonal jet formation is a highly non-linear phenomenon, where local energy transfers through scales are predominant. This picture is probably correct during jet formation for a fluid initially at rest and when the forcing or initial spectrum is localized on small scales, as shown by numerical simulations [34, 42, 112]. However, another picture can be drawn looking at the interactions of large scale zonal jets with turbulent vortices at smaller scales. Evidence of such non-local energy transfers has been observed in numerical experiments [48] and in a spectral analysis of atmosphere dynamics [103]. The closure theories presented in next paragraph, as well as the effective dynamics of jets presented in the rest of this thesis, give another picture of zonal jet dynamics where the main interactions into play are non-local in scales.

### 1.3.3 Quasi-linear and statistical approaches

A very natural and interesting way to study jet dynamics is to try access the statistics of the flow directly, instead of the extremely complex flow field itself. This is actually a very old idea in the study of complex systems, going back to the foundations of statistical mechanics by Ludwig Boltzmann in the late 19<sup>th</sup> century.

Reynolds (1894 [92]) was the first to try a direct statistical approach in order to describe turbulent flows. This led to what is often called Reynolds’ averaging [89], and to the closure problem, which we explain now. In equation (1.2), the evolution

of the zonal flow velocity profile  $U(y, t)$  depends on the turbulent velocity field  $\mathbf{v}'$ . More precisely, taking an ensemble average (for instance an average over realisations of the noise  $\eta$  in (1.1), here denoted with an overbar) of (1.2), one realizes that the mean flow  $\bar{U}$  is coupled to the velocity two-points correlation function  $\overline{u'v'}$ , the so-called Reynolds' stress [89]. This is directly due to the non-linear advection term in (1.1). For the same reason, the equation for  $\overline{u'v'}$  involves a three-points correlation function, and so on, leading to an infinite set of coupled equations for the statistics of the flow.

Faced with this difficulty one may consider either a phenomenological approach in order to model Reynolds' stresses from sensible dynamical considerations, or one may tackle the problem theoretically. The phenomenological approach was first attempted by Boussinesq (1877, see [89]), who modeled the Reynolds' stresses as proportional to the velocity gradients, advocating the analogy with viscosity in dilute gases theory. Nowadays, many modellings in turbulence or climate science are based on this phenomenological approximation [89, 100, 110].

A more refined approximation consists in computing the Reynolds' stresses according to the linearized dynamics of perturbations to the mean flow, the so-called quasi-linear approximation. In the hierarchy for cumulants of the velocity, this amounts at neglecting the three-points correlations in the equation for  $\overline{u'v'}$ , leading to a closed couple of equation for the statistics of the flow. This is a very natural approximation, and it is actually very similar to kinetic theories previously developed in different fields. Examples of such kinetic theories include wave turbulence in the context of weakly non-linear dispersive waves [75], and classical kinetic theories for plasmas and self-gravitating systems (Lenard-Balescu equation, Landau equation [4, 78]).

In the context of two-dimensional and geostrophic turbulence, the first closure approaches mainly focused on the regime of inverse cascade of energy, with relative success —for a review of closures in two-dimensional turbulence see [55], for an application in beta-plane turbulence see [25]. The first closure approach focused on zonal jet formation instead of the turbulent cascade was proposed in 2003 by Farrell and Ioannou [38], and named Stochastic Structural Stability Theory (S3T). This has then led to a wide litterature on extensions and tests of this theory [33, 85], also called CE2 (closure at second order) in [104, 106]. Related approximations have been studied before, known as wave-mean flow interaction theory [58] and modulational instability theory [7, 8, 31]. The S3T-CE2 approximation can be seen as a generalization of these approaches [2, 32].

A linear stability analysis of the S3T-CE2 system gives a qualitative description of the bifurcation leading to zonal flow formation [104], and allows to describe the merging of jets that is observed in many numerical simulations [85]. The analysis of most unstable wavenumbers also brings out cases of multistability in the barotropic equation [33]. An important result of S3T-CE2 is that the turbulent cascade of energy is not necessary to maintain robust zonal jets. Indeed, transfers of energy in the S3T-CE2 system are only non-local by construction, going directly from the scale of the eddies to the scale of the jets.

From a practical point of view, the S3T-CE2 closure is a very powerful tool for studying zonal jet formation and dynamics. However, the approximation leading

to the S3T-CE2 equations is presented with no theoretical justification. In all previous studies, the validity of S3T-CE2 has been assessed using a purely empirical method, comparing explicit results or numerical results of S3T-CE2 equations to direct numerical simulations of the equations of motion (1.1), for different values of the control parameters.

A more precise theoretical approach, similar to Boltzmann equation for the kinetic theory of dilute gases or Lenard-Balescu equation for plasmas [4], is much more demanding and has been actually attempted only rarely for turbulent flows. Obtaining such a kinetic theory for the dynamics of zonal jets is the main motivation of the work presented in this thesis.

A very strong analogy between two-dimensional flows and quasi-geostrophic dynamics on one hand and plasma physics on the other hand has been observed in the late 40's. In particular, the linear dynamics close to a mean state display similar spectral structure [5, 113], inviscid damping mechanism [11, 78, 82] and conserved quantities [110]. For this reason, it is natural to look for a kinetic description of two-dimensional and quasi-geostrophic flows that is similar to the one developed in plasma physics. Such quasi-linear approximation for the relaxation towards equilibria of either the 2D Euler equation [29] or the point vortex dynamics [30] have actually been proposed and studied in the past.

In a work preliminary to this thesis, the classical kinetic theory for long-range interacting systems (Lenard-Balescu equation) has been extended to the stochastically forced case [73, 74]. A similar kinetic theory for the stochastic quasi-geostrophic model (1.1) is the topic of chapters 3–5 of this thesis. One of the main results presented in these chapters is that a perturbative expansion of the barotropic equation (1.1) in the regime where the turbulence evolves much faster than the zonal jets gives the S3T-CE2 equations at leading order. This result gives both an indication of a relevant regime for zonal jet formation, and a strong theoretical support to the S3T-CE2 closure.

Finally, we note that some extensions of the S3T-CE2 closure have been proposed, either considering the formation of coherent non-zonal structures, like vortices embedded into the zonal jets [3], or taking into account higher cumulants in the hierarchy [68, 106]. We also note that approximations similar to the ones that lead to the S3T-CE2 system have been applied to different systems, such as more complete climate models [1, 80], or in the barotropic equation with deterministic forcing [67]. Similar ideas have been applied to the case of coherent vortices formation in two-dimensional turbulence, either with stochastic [60] or deterministic forcing [41], and to the study of unstable flows in a regime of moderate Reynolds number [65]. To finish, another way to study the statistics of turbulent flows, based on a hierarchy of equations for the  $n$ -points vorticity distribution functions, was also proposed in the 60's by Lundgren [63], Monin [70] and Novikov [79]. The applications of these ideas to the stochastic barotropic equation (1.1) is discussed in chapter 3, section 3.2.2.

### 1.3.4 Equilibrium statistical mechanics theory

To finish this short review of theories of zonal jet formation, we present briefly the equilibrium statistical mechanics theory of two-dimensional and geophysical flows, first proposed by Onsager in the 40's [81], and generalized in the 90's by Robert, Miller and Sommeria [69, 94] and called RMS theory, see [14] for a review.

Consider the stochastic two-dimensional Navier-Stokes equation ((1.1) with  $\beta = 0$ ). The inertial dynamics  $\partial_t \omega + \mathbf{v} \cdot \nabla \omega = 0$  has the particular property to conserve an infinite number of independent quantities: the energy functional (1.4) and the casimir functionals

$$\mathcal{C}_f[\omega] = \int_{\mathcal{D}} f(\omega), \quad (1.8)$$

for any sufficiently smooth function  $f$ . This gives a strong constraint on the flow field. The idea of RMS theory is to look for the most probable large-scale flow (macroscopic state), given these constraints. This is analogous to the microcanonical formulation of equilibrium statistical mechanics theory for systems of particles.

Basically, RMS theory predicts that inertial two-dimensional and geostrophic turbulence leads to a concentration of energy in the largest scale of the domain [14]. Real flows are forced and dissipated, so these results cannot be applied directly. However, in most physical applications forcing and dissipation are negligible compared to advection. The attractors of non-inertial dynamics are then very close to the attractors of the inertial dynamics [13]. This is observed for instance in figure 1.3(a), where forcing and dissipation are present and still the flow is very close to a single jet at the largest scale of the domain, which is the equilibrium state of the inertial 2D Euler equation in this case [14].

Like in statistical mechanics for systems of particles, the link between equilibrium theory for inertial (hamiltonian) dynamics and stochastic dynamics can be made using Langevin equations. Assuming Einstein's relation, dissipation and forcing in a Langevin equation balance each other (detailed balance), leading to a canonical stationary measure [46]. A generalization of these ideas has been considered recently [10, 61], and will be the topic of chapter 7.

## 1.4 Kinetic theory and Large Deviation theory

The works briefly presented in sections 1.3.1 and 1.3.2 give a satisfying understanding of jet formation, either through an inverse energy cascade when the forcing or initial spectrum is localized on small scales [112], or through the turbulent mixing of potential vorticity [36]. When a beta-effect is present, such non-linear turbulent phenomena interact with Rossby waves, which gives rise to multiple jet structures. However, these mechanisms cannot explain the long-time dynamics of jets, where energy transfers that are non-local in scales can play an important role [48, 103].

Approaches through statistical closures or cumulant expansions such as Stochastic Structural Stability Theory (S3T [38]) and Cumulant Expansion at Second Order (CE2 [104, 106]) are able to give a more quantitative description of the dynamics of zonal jets, in particular of their merging [85] and of the long-term attractors [33]. Understanding in which regime such approximations of the dynamics give quantita-

tive agreement with the original system is a very natural question to ask. However, previous works only used empirical tests of the theory (comparing results of S3T-CE2 to direct numerical simulations of the barotropic equation), and mainly did not agree on the relevant regime for such approximations to be valid, as can be seen comparing [33, 104, 106].

In contrast, the kinetic theory developed in [18] and presented in chapter 3 of this thesis is based on a perturbative expansion in powers of a small parameter (the parameter  $\alpha$  defined in section 1.2.4). The result at leading order is equivalent to S3T-CE2, as will be discussed in section 3.2.1 (page 41).

The interest of our approach is that it is precise and controlled, and it gives a general picture of zonal jet dynamics in the regime of interest. In contrast, S3T-CE2 phenomenological approaches are useful precisely because they allow to investigate different regimes where no time scale separation occurs, but do not allow to draw general conclusions beyond the particular cases studied in numerical simulations.

None of the works presented in section 1.3 tackle the problem of understanding rare events in jet dynamics. Such rare events are known to exist on Earth [54] and on Jupiter [95], as discussed in section 1.1. Being able to predict the statistics of such rare events (as for example the average transition rate between two jet configurations) is a very important issue in jet dynamics. Large Deviation Theory is a very natural tool to tackle this problem. We will show in chapters 2 and 6 that Large Deviation Theory can be applied to the stochastic barotropic model (1.1) in the limit of time scale separation described in section 1.2.4.

# Chapter 2

## Statistics of slow–fast dynamical systems

As explained in the previous chapter, zonal jets in planetary atmosphere typically evolve on a time scale that is much longer than the time scale of evolution of the surrounding turbulence [90]. It is then natural to look for an effective description of zonal jet dynamics using a quasi-static approximation. Such procedure is analogous to kinetic theories of dilute gases or plasmas (Bogolyubov hypothesis [4]). Before deriving the effective dynamics of zonal jets in chapters 3 and 6, it is useful to present the underlying mathematical results in a more general framework. It is the goal of this chapter.

In section 3.1 (page 37), we will show that in the time scale separation regime, the stochastic barotropic equation (1.1) can be put into the form

$$\begin{cases} \frac{\partial z}{\partial t} = \alpha f(z, w) \\ \frac{\partial w_i}{\partial t} = b_i(z, w) + \eta_i \end{cases} \quad (2.1)$$

where, as in (1.1),  $\eta$  is a white gaussian random vector of components  $\eta_i$ , with zero mean and correlations  $\mathbb{E}[\eta_i(t_1)\eta_j(t_2)] = C_{ij}\delta(t_1 - t_2)$ ; and where  $\alpha \ll 1$  is the parameter defined in section 1.2.4.

In (2.1),  $z$  typically evolves on a time scale of order  $1/\alpha$ , while  $w$  typically evolves on a time scale of order one. In the limit  $\alpha \ll 1$ , the evolution of  $w$  is thus much faster than the evolution of  $z$ . We call (2.1) a (stochastic) slow-fast system of equations.

In our geophysical fluid dynamics problem,  $z$  will be the zonal jet velocity profile and  $w$  will be the vorticity of the smaller-scale turbulence (eddy vorticity). For simplicity, we will consider in this chapter the case where  $z$  is scalar and  $w$  is an  $m$ -dimensional vector ( $i = 1, \dots, m$ ). The formal generalization to the infinite-dimensional (field) problem is straightforward, see chapters 3, 6 and 7.

We are interested in the effective dynamics and statistics of the slow process  $z$  in the time scale separation limit  $\alpha \ll 1$ . We will present the following results [39, 86]

- the Law of Large Numbers, that describes the *average* behaviour of  $z$ . This is explained in section 2.1.1.
- the Central Limit Theorem, that describes the *typical fluctuations* of  $z$ . This is explained in section 2.1.2.

- the Large Deviation Principle, that describes the *large fluctuations* of  $z$ . This is explained in section 2.1.3.

We first present these results from a qualitative point of view in section 2.1, and then give a more formal derivation in sections 2.2 and 2.3. The validity of these results, both from qualitative and rigorous points of view, will be discussed in section 2.4.

We note that in most of the mathematical literature on slow-fast systems [86, 114], the system (2.1) is written

$$\begin{cases} \dot{z} = f(z, w) \\ dw = \frac{1}{\alpha} b(z, w) dt + \frac{1}{\sqrt{\alpha}} \sigma dW_t \end{cases} \quad (2.2)$$

where  $W_t$  is a vector of  $m$  independent Wiener processes and  $C = \sigma\sigma^T$  is the covariance matrix with coefficients  $C_{ij}$ . As usually done in physics, we abusively denote  $\eta(t) = \frac{dW_t}{dt}$ , then we recover (2.1) from (2.2) by a rescaling of time.

In the units used in (2.2), the slow process  $z$  evolves on a time scale of order 1, which is more natural in order to study the effective dynamics of  $z$ . In our case, we chose the seemingly unnatural time unit corresponding to (2.1) because, as will be shown in chapter 3, it leads to an average total energy equal to 1 in the stationary state of the stochastic barotropic model (1.1).

We also note that the stochastic barotropic model is not exactly of the form (2.1). Indeed, as will be shown in chapter 3, non-linear terms and dissipative terms of order  $\sqrt{\alpha}$  and  $\alpha$  are also present in the equation for the fast process  $w$ . Such terms are usually not considered in mathematical studies, but they can be formally included, as done in section 2.2. Whether such terms influence or not the effective dynamics of  $z$  is actually a very important issue, that will be discussed in details in chapters 4 and 5.

## 2.1 Heuristic derivation

### 2.1.1 Law of Large Numbers and averaging

The Law of Large Numbers is the first result in the mathematical theory of probabilities, going back to the work of Jacques Bernoulli in the 18th century. For the canonical example of the fair coin tossing<sup>1</sup>, the Law of Large Numbers states that as the number of tosses increases, the number of heads and the number of tails get closer to each other. More precisely, if we denote by  $x_n$  the result of the  $n$ -th coin tossing ( $x_n = 1$  if we get heads and  $x_n = -1$  if we get tails), then

$$S_N = \frac{1}{N} \sum_{n=1}^N x_n \xrightarrow[N \rightarrow \infty]{} \mathbb{E}[x] = 0, \quad (2.3)$$

where  $\mathbb{E}[x]$  is the average of the random variable  $x$  (result of a single tossing). The Law of Large Numbers is empirically obvious in this simple example, due to the fact

---

<sup>1</sup>*Pile ou face en français.*

that successive tosses are independent.

In the slow-fast problem (2.1), the fast process  $w$  plays the role of the coin. Indeed, we can consider that  $w(s + \delta s)$  and  $w(s)$  are almost independent for delays  $\delta s$  larger than 1, while  $z$  has barely changed over the time interval  $[s, s + \delta s]$  if  $\delta s \ll 1/\alpha$ . It is thus natural to define the virtual fast process

$$\frac{\partial \tilde{w}_z}{\partial s} = b(z, \tilde{w}_z) + \eta, \quad (2.4)$$

where  $z$  is held fixed. The evolution of the slow process  $z$  is given by integration of the first equation in (2.1). In the time scale separation limit  $\alpha \rightarrow 0$ , the evolution of  $z$  between  $t$  and  $\Delta t$  is roughly given by

$$\frac{\partial z}{\partial t} \simeq \frac{z(t + \Delta t) - z(t)}{\Delta t} \simeq \frac{1}{\Delta t} \int_t^{t+\Delta t} \alpha f(z, \tilde{w}_z(s)) ds \quad (2.5)$$

for  $1 \ll \Delta t \ll 1/\alpha$ , with  $z = z(t)$  and where  $\tilde{w}_z(s)$  evolves according to (2.4), i.e. with  $z$  held fixed.

The expression (2.5) of  $\frac{\partial z}{\partial t}$  is very close to the expression of  $S_N$  for the coin tossing problem: it is a sum of almost independent random variables ( $\Delta t$  is the equivalent of  $N$  and  $w(s)$  is the equivalent of  $x_n$ , the integral over  $s$  is the analog of the sum over  $n$ ). Then, it is natural to guess that the effective evolution  $\bar{z}$  of  $z$  is given by the average of  $f(z, \tilde{w}_z(s))$  over the realizations of  $\tilde{w}_z(s)$ , computed in the stationary state of  $\tilde{w}_z(s)$  (with  $z$  held fixed),

$$\frac{\partial \bar{z}}{\partial t} \underset{\alpha \rightarrow 0}{=} \alpha F(\bar{z}) \equiv \alpha \mathbb{E}_{\bar{z}} [f(\bar{z}, w)]. \quad (2.6)$$

Equation (2.6) is the Law of Large Numbers for (2.1). The precise statement of the convergence of  $z$  towards  $\bar{z}$  with appropriate hypothesis will be given in section 2.4. In practice, we need the stationary probability distribution function  $Q_{\bar{z}}$  of the virtual fast process (2.4). In general,  $Q_{\bar{z}}$  depends parametrically on  $\bar{z}$ . Then, the average force  $F$  in (2.6) is given by  $F(\bar{z}) \equiv \int f(\bar{z}, w) Q_{\bar{z}}(w) dw$ .

### 2.1.2 Central Limit Theorem and typical fluctuations

The Central Limit Theorem is another early result of the theory of probabilities, first studied by de Moivre in the 18th century. It describes the moderately small fluctuations around the mean, described by the Law of Large Numbers. In the fair coin tossing problem, the Central Limit Theorem states that, for large  $N$ , the empirical average  $S_N$  is distributed according to a gaussian distribution with mean  $\mathbb{E}[S_N] \sim \mathbb{E}[x] = 0$  and variance  $\text{var}(S_N) \sim \text{var}(x)/\sqrt{N} = 1/\sqrt{N}$ .

Going back to the slow-fast system (2.1), we define the fluctuation of  $z$  around its mean  $\bar{z}$  as  $\Delta z = z - \bar{z}$ . Using again the fact that  $\frac{\partial z}{\partial t}$  in (2.5) is a sum of almost independent random variables, the Central Limit Theorem roughly states that  $\Delta z$  is of order  $\sqrt{\alpha}$  and is a gaussian stochastic process. This statement is equivalent to the following effective equation for  $z$

$$\frac{\partial z}{\partial t} \underset{\alpha \rightarrow 0}{\simeq} \alpha F(z) + \alpha^2 F_1(z) + \sqrt{\alpha^2} \xi(z), \quad (2.7)$$

where  $\xi(z)$  is a gaussian random noise with zero mean and correlation (with a fixed  $z$ )  $\mathbb{E}[\xi(z, t_1)\xi(z, t_2)] = \delta(t_1 - t_2)\Xi(z)$ , and  $F_1(z)$  is a correction to the drift  $F$ . The fact that  $\xi(z)$  is white in time is a consequence of the infinite time scale separation in the limit  $\alpha \rightarrow 0$ . The factor  $\Xi(z)$  represents the correlation of the typical fluctuations of  $f(z, w)$  in the stationary state of the virtual fast process (2.4).  $\Xi(z)$  and  $F_1(z)$  will be written explicitly in section 2.2 (see equation (2.20)). Again, a more precise statement of the convergence of  $z$  towards (2.7) with appropriate hypothesis will be given in section 2.4.

### 2.1.3 Large Deviation Principle and large fluctuations

The Large Deviation Principle is a more recent development in the theory of probabilities, first considered by Cramér in the early 20th century, and formalised by Varadhan in the 60's. The basic question is the following one: after a very large number  $N$  of tosses of our coin, what is the probability  $p_N(s)$  that  $S_N$  is equal to a given number  $s$ ? For  $s = 0$ , the Law of Large Numbers says that  $p_N(0)$  is equal to one as  $N \rightarrow \infty$ . The Central Limit Theorem gives an estimate of  $p_N(s)$ , that is valid for  $s \lesssim 1/\sqrt{N}$ . Another simple case is  $s = 1$  (or  $s = -1$ ), which means that we have obtained only heads (or only tails) in all of the  $N$  tosses. The probability to observe this phenomenon is  $p_N(\pm 1) = (1/2)^N$ . Cramér's theorem states that the probability to have  $S_N = s$  is always of the form  $\phi(s)^N$  for large  $N$  [108]. The function  $\phi(s)$  thus characterizes the whole distribution of  $S_N$  at leading order in  $N \gg 1$ . The function  $I(s) = -\ln \phi(s)$  is called the large deviation rate function, then the probability of  $S_N = s$  is logarithmically equivalent to  $\exp(-NI(s))$ , which is usually denoted  $p_N \asymp \exp(-NI(s))$ . We say that  $S_N$  satisfies a Large Deviation Principle.

Using again expression (2.5) of  $\frac{\partial z}{\partial t}$  as a sum of almost independent random variables, we understand that  $z(t)$  satisfies a Large Deviation Principle in the limit  $\alpha \rightarrow 0$ . In practice, the Large Deviation Principle gives a simple formulation for the probability of any path  $\{z(t)\}_{0 \leq t \leq T}$ , in the limit  $\alpha \rightarrow 0$ . In particular, this contains the Law of Large Numbers (2.6) and the Central Limit Theorem (2.7) as special cases (respectively most probable path and typical fluctuations around it), but it also gives access to arbitrarily rare fluctuations of  $z$ .

The formal derivation of the Large Deviation Principle for (2.1) is presented in section 2.3. More details about the rigorous theorems and associated hypothesis are given in section 2.4.

## 2.2 Stochastic averaging — Formal derivation

We now give a formal derivation of the Law of Large Numbers and Central Limit Theorem presented in sections 2.1.1, 2.1.2. In the cases studied in this thesis, the slow-fast system of interest is slightly different from (2.1), and can be written

$$\begin{cases} \frac{\partial z}{\partial t} = \alpha f(z, w) + \sqrt{\alpha}\eta_0 \\ \frac{\partial w}{\partial t} = -L_z \cdot w + \sqrt{\alpha}b_1(z, w) + \eta \end{cases} \quad (2.8)$$

In this equation, the evolution of the fast variable  $w$  is given at leading order by the linear operator  $L_z$ , and the term  $b_1(z, w)$  represents corrections to this behaviour. In the fluid mechanics problem considered in this thesis, the term  $b_1$  is related to the non-linear advection term. We also have added a forcing term  $\eta_0$  in the evolution of  $z$ , to remain as general as possible. We assume that  $\eta_0$  is a white in time gaussian noise with zero mean and variance  $C_0$ .

In general, the linear operator  $L_z$  depends parametrically on  $z$ , so the evolution of  $(z, w)$  through the coupled system (2.8) is non-linear. However, as can be guessed from the heuristic derivation of the Law of Large Numbers and Central Limit Theorem, the coefficients in the effective equation for the slow variable  $\bar{z}$  will be given by the *linear* virtual fast process

$$\frac{\partial \tilde{w}_{\bar{z}}}{\partial s} = -L_{\bar{z}} \cdot \tilde{w}_{\bar{z}} + \eta, \quad (2.9)$$

where  $\bar{z}$  is fixed. Then, the Law of Large Numbers and Central Limit Theorem will give a very simple description of the effective behaviour of  $z$ .

The formal derivation presented here follows the lines described in [44, 93], and is the one we used in our publication [18].

### 2.2.1 Fokker-Planck formalism

The stochastic differential equation (2.8) is equivalent to the Fokker-Planck equation for the probability density function  $P(z, w, t)$ ,

$$\frac{\partial P}{\partial t} = \mathcal{L}_0 P + \sqrt{\alpha} \mathcal{L}_1 P + \alpha \mathcal{L}_s P, \quad (2.10)$$

where

$$\begin{aligned} \mathcal{L}_0 P &\equiv \nabla_w \cdot (L_z \cdot w P) + \frac{1}{2} \nabla_w \nabla_w : (C P) \\ &= \sum_i \frac{\partial}{\partial w_i} \left[ (L_z \cdot w)_i P + \frac{1}{2} \sum_j \frac{\partial}{\partial w_j} C_{ij} P \right] \end{aligned} \quad (2.11)$$

is the Fokker-Planck operator that describes the leading order behaviour of  $w$ ,

$$\mathcal{L}_1 P \equiv -\nabla_w \cdot (b_1(z, w) P) \quad (2.12)$$

is the Fokker-Planck operator that describes the non-linear corrections to the evolution of  $w$ , and

$$\mathcal{L}_s P \equiv -\nabla_z \cdot (f(z, w) P) + \frac{1}{2} \nabla_z \nabla_z : (C_0 P) \quad (2.13)$$

describes the evolution of  $z$ . In these expressions,  $C : C' \equiv C_{ij} C'_{ij}$  represents the contraction of matrices  $C$  and  $C'$ .

The stochastic averaging procedure, which leads to the Law of Large Numbers and Central Limit Theorem equations, is a perturbative expansion of the Fokker-Planck equation (2.10) in powers of  $\alpha$ , in the time scale separation regime  $\alpha \ll 1$ . It is also called adiabatic reduction of the variables, indeed it describes only the evolution of the slow variable  $z$ , with the fast variable  $w$  adiabatically relaxed to its stationary state (with  $z$  held fixed). This is in agreement with the time scale separation, and with the definition of the virtual fast process (2.9).

## 2.2.2 Stationary distribution of the fast variable

At leading order, the Fokker-Planck equation (2.10) reads  $\partial_t P = \mathcal{L}_0 P$ . It describes only the linear evolution of  $w$ . For a fixed slow variable  $z$ , i.e. for  $P(z, w, t) = \delta(z - z_0) Q_{z_0}(w, t)$ , this is exactly the Fokker-Planck associated with the virtual fast process (2.9), where  $z_0$  is fixed.

In order to eliminate adiabatically the fast variable  $w$ , we need to consider the stationary distribution of  $\tilde{w}_{z_0}$ , i.e. the asymptotic expression of  $Q_{z_0}(w, t)$ . For the linear stochastic process (2.9) (Ornstein-Uhlenbeck process), the stationary distribution is a gaussian, independently of the initial condition [44]. (2.9) has no constant drift so  $\tilde{w}_{z_0}$  has a zero mean, and the correlation matrix  $(g_{z_0})_{ij}(t) = \mathbb{E}[\tilde{w}_{z_0,i}(t)\tilde{w}_{z_0,j}(t)]$  is the solution of

$$\frac{\partial g_{z_0}}{\partial t} + L_{z_0} g_{z_0} + g_{z_0} L_{z_0}^T = C. \quad (2.14)$$

Equation (2.14) is called the Lyapunov equation associated with the Ornstein-Uhlenbeck process (2.9), and can be obtained using the Itô formula [44].

Then, the stationary distribution of  $\tilde{w}_{z_0}$  is

$$G_{z_0}(w) = \frac{1}{Z_{z_0}} \exp\left(-\frac{1}{2} w^T (g_{z_0}^\infty)^{-1} w\right), \quad (2.15)$$

where  $g_{z_0}^\infty = \lim_{t \rightarrow \infty} g_{z_0}(t)$  is the stationary solution of the Lyapunov equation (2.14) and  $(g_{z_0}^\infty)^{-1}$  is its inverse, and where  $Z_{z_0}$  is a normalisation constant.

The average  $\mathbb{E}_{z_0}$  introduced in section 2.1.1 is the average over the gaussian distribution (2.15),

$$\bar{\phi}_{z_0} \equiv \mathbb{E}_{z_0}[\phi(\tilde{w}_{z_0})] = \int \phi(w) G_{z_0}(w) dw, \quad (2.16)$$

for any function  $\phi$ . The correlation between observables  $\phi(\tilde{w}_{z_0}(s))$  at time  $s$  and  $\psi(\tilde{w}_{z_0}(0))$  at time 0 in the stationary state of (2.9) reads

$$\mathbb{E}_{z_0}[\phi(\tilde{w}_{z_0}(s))\psi(\tilde{w}_{z_0}(0))] = \int \phi(w) e^{s\mathcal{L}_0} \psi(w) G_{z_0}(w) dw. \quad (2.17)$$

We also define the covariance of  $\phi(\tilde{w}_{z_0}(s))$  and  $\psi(\tilde{w}_{z_0}(0))$  as

$$\mathbb{E}_{z_0}[[\phi(\tilde{w}_{z_0}(s))\psi(\tilde{w}_{z_0}(0))] ] \equiv \mathbb{E}_{z_0}[(\phi(\tilde{w}_{z_0}(s)) - \bar{\phi}_{z_0})(\psi(\tilde{w}_{z_0}(0)) - \bar{\psi}_{z_0})]. \quad (2.18)$$

## 2.2.3 Effective slow dynamics

The statistics of  $z$  are described by the marginal distribution  $R(z, t) = \int P(z, w, t) dw$ . At leading order, the complete system  $(z, w)$  is described by the distribution  $G_z(w)R(z, t)$ , which means that at each instant  $t$ , the fast variable  $w$  is adiabatically relaxed to its stationary gaussian distribution  $G_z(w)$ .

More generally, for any distribution  $Q(z, w)$ , we define the projection  $(\mathcal{P}Q)(z, w) = G_z(w) \int Q(z, w) dw$ . Then  $P = G_z R + P_f$ , where  $P_f = (1 - \mathcal{P})P$  represents the corrections to the leading order behaviour of the system. In other words,  $P_f$  is the fastly evolving part of  $P$ . The stochastic averaging procedure is a perturbative expansion of  $P_f$  from the Fokker-Planck equation (2.10), leading to a closed Fokker-Planck equation for  $R(z, t)$ . This procedure is described in appendix A (page 132).

The resulting effective Fokker-Planck equation for  $R(z, t)$  is equivalent to the stochastic differential equation

$$\frac{\partial z}{\partial t} = \alpha F(z) + \sqrt{\alpha} \eta_0 + \alpha^{3/2} F_1(z) + \alpha \xi(z, t), \quad (2.19)$$

where  $F(z) = \mathbb{E}_z[f(z, w)]$ ,  $\xi(z, t)$  is a white in time gaussian noise with zero mean and correlations (for a fixed  $z$ )  $\mathbb{E}[\xi(z, t_1)\xi(z, t_2)] = \delta(t_1 - t_2)\Xi(z)$  with<sup>2</sup>

$$\Xi(z) = 2 \int_0^\infty \mathbb{E}_z [[f(z, \tilde{w}_z(s)) f(z, \tilde{w}_z(0))] ] ds, \quad (2.20)$$

and  $F_1(z)$  is given in appendix A<sup>3</sup>. The integrand in (2.20) is usually called in random processes theory the autocorrelation function of  $f(z, \tilde{w}_z(s))$  [44, 77]. Then,  $\Xi(z)$  will be called the integrated autocorrelation function.

$F$  represents the average effect of the fast variable  $w$  on  $z$ , as described at the level of the Law of Large Numbers.  $\xi(z, t)$  represents the effects of the fluctuations of  $w$  on  $z$ , this corresponds to the level of the Central Limit Theorem.  $F_1$  is a correction to the drift  $F$  that appears at next order in  $\alpha$ , due to the term  $b_1$  in (2.8) and to the fact that  $G_z$  and  $F$  depend on  $z$ .

Equation (2.19) describes the effective dynamics of the slow degrees of freedom  $z(t)$ . In chapters 3 and 7, we will apply this result to the barotropic equation, and discuss the physical consequences. Chapter 5 is devoted to the study of the terms  $F$  and  $\Xi(z)$  appearing in (2.19).

## 2.3 Large Deviation Principle — Formal derivation

In this section we present the Large Deviation Principle for slow-fast systems like (2.1) or (2.8), both from a theoretical and a practical point of view. We first present a very general and important result of the theory of large deviations in section 2.3.1: the Gärtner-Ellis theorem. Then in section 2.3.2 we see how this result applies to the case of slow-fast systems. Finally in section 2.3.3 we discuss the relations between the Large Deviation Principle and the results of stochastic averaging (Law of Large Numbers and Central Limit Theorem).

### 2.3.1 Gärtner–Ellis theorem

Consider again the fair coin tossing problem, like in section 2.1. We recall that by definition,  $p_N(s)$  is the probability that the mean result of  $N$  tosses  $S_N = \frac{1}{N} \sum_{n=1}^N x_n$

<sup>2</sup>If the slow process is a vector (or a field), the covariance matrix of the noise  $\xi(z)$  has elements

$$\Xi_{ij}(z) = \int_0^\infty \mathbb{E}_z [[f_i(z, \tilde{w}_z(s)) f_j(z, \tilde{w}_z(0)) + f_j(z, \tilde{w}_z(s)) f_i(z, \tilde{w}_z(0))] ] ds,$$

hence the factor 2 in the scalar case.

<sup>3</sup>Note that the correction term  $F_1$  arising from the perturbative expansion performed in this section and in appendix A is generically different from the drift given by the Central Limit Theorem [84]. However, as this term is an order  $\alpha$  smaller than  $F$ , such difference is not expected to have practical consequences on the effective dynamics of  $z$ .

is equal to  $s$ . For this type of problem, Cramér's theorem states that  $S_N$  satisfies a Large Deviation Principle, i.e. that

$$\ln p_N(s) \underset{N \rightarrow \infty}{\sim} -NI(s) \quad (2.21)$$

with  $I(s)$  the large deviation rate function. The Gärtner-Ellis theorem gives a more constructive way to state the Large Deviation Principle and to compute explicitly  $I(s)$ . Consider the function

$$\lambda(k) \equiv \lim_{N \rightarrow \infty} \frac{1}{N} \ln \mathbb{E} [e^{NkS_N}], \quad (2.22)$$

where the average is taken over the distribution of the  $N$  tossing events  $(x_1, \dots, x_n)$ . The structure in  $\ln \mathbb{E} [\exp]$  indicates that  $\lambda(k)$  is a cumulant generating function, a very classical tool in statistics and probabilities (see also section 2.3.3). With the large- $N$  limit,  $\lambda(k)$  is called the *scaled cumulant generating function* of  $S_N$ .

From (2.22),

$$\mathbb{E} [e^{NkS_N}] \underset{N \rightarrow \infty}{\sim} e^{N\lambda(k)}.$$

Assuming the Large Deviation Principle (2.21), we also have

$$\mathbb{E} [e^{NkS_N}] \underset{N \rightarrow \infty}{\sim} \int e^{Nks} e^{-NI(s)} ds \underset{N \rightarrow \infty}{\sim} \exp \left( N \sup_s \{ks - I(s)\} \right),$$

where we have used the fact that in the limit  $N \rightarrow \infty$ , the integral over  $s$  is almost equal to the largest term of the integrand (saddle-point or Laplace approximation). Identifying these two expressions of  $\mathbb{E} [e^{NkS_N}]$ , we get

$$\lambda(k) = \sup_s \{ks - I(s)\}. \quad (2.23)$$

The scaled cumulant generating function  $\lambda(k)$  is the Legendre-Fenchel transform of the large deviation rate function  $I(s)$ . Assuming that  $\lambda(k)$  is everywhere differentiable, this relation can be inverted to give

$$I(s) = \sup_k \{ks - \lambda(k)\}. \quad (2.24)$$

These simple formal computations show the importance of defining the scaled cumulant generating function. Now let's consider a sequence of random processes  $X_N$ . The Gärtner-Ellis theorem states that if its scaled cumulant generating function  $\lambda(k) = \lim_{N \rightarrow \infty} \frac{1}{N} \ln \mathbb{E} [e^{NkX_N}]$  exists and is differentiable for all  $k$ , then  $X_N$  satisfies a Large Deviation Principle with rate function  $I(x) = \sup_k \{kx - \lambda(k)\}$ .

When  $\lambda(k)$  has a singularity (a discontinuity in its first derivative), the Legendre-Fenchel transform  $x \rightarrow \sup_k \{kx - \lambda(k)\}$  only gives the convex envelope of the rate function  $I(x)$  [108]. This point is crucial for instance in cases of multistability (when  $I(x)$  has more than one minimum). In the context of equilibrium statistical mechanics, this phenomenon is related to phase transitions. In non-equilibrium cases, this is related to rare transitions between attractors of the dynamics.

### 2.3.2 Large deviation functions for the slow variable

We now show how the Gärtner-Ellis theorem can be applied to study the large deviations of the slow process  $z(t)$  in the slow-fast system (2.1).

In the heuristic derivation presented in section 2.1, we have seen that when  $\alpha \ll 1$  the instantaneous evolution of  $z$  (through  $\dot{z}$ ) is given by the long-term evolution of the virtual fast process  $\tilde{w}_z$ , with  $z$  held fixed —consistently with the time scale separation. It is thus natural to consider the random process  $\dot{z} \equiv \frac{\partial z}{\partial t}$  given by (2.5) and (2.4), where we recall that  $z$  is held fixed. We denote the random process  $\frac{z(t+\Delta t) - z(t)}{\Delta t}$  by  $\dot{z}_z(\Delta t)$ , by definition it reads<sup>4</sup>

$$\dot{z}_z(\Delta t) \equiv \frac{1}{\Delta t} \int_0^{\Delta t} f(z, \tilde{w}_z(s)) ds. \quad (2.25)$$

In order to describe the whole statistics of  $\dot{z}_z$  (typical behaviour and rare fluctuations), let's consider the scaled cumulant generating function for this stochastic process, denoted<sup>5</sup>

$$\begin{aligned} H(z, \theta) &\equiv \lim_{\Delta t \rightarrow \infty} \frac{1}{\Delta t} \ln \mathbb{E} [e^{\Delta t \theta \dot{z}_z}] \\ &= \lim_{\Delta t \rightarrow \infty} \frac{1}{\Delta t} \ln \mathbb{E}_z \exp \left( \theta \int_0^{\Delta t} f(z, \tilde{w}_z(s)) ds \right). \end{aligned} \quad (2.26)$$

The Gärtner-Ellis theorem states that if  $\theta \rightarrow H(z, \theta)$  exists and is differentiable, then the probability density function  $p_{\Delta t}$  of the random variable  $\dot{z}_z$  satisfies the Large Deviation Principle

$$p_{\Delta t}(\dot{z}_z) \underset{\Delta t \rightarrow \infty}{\asymp} e^{-\Delta t L(z, \dot{z})} \quad (2.27)$$

with rate function  $L(z, \dot{z}) = \sup_{\theta} \{\theta \dot{z} - H(z, \theta)\}$ . Because of the clear analogy with classical mechanics,  $H(z, \theta)$  is also called the Hamiltonian and  $L(z, \dot{z})$  the Lagrangian of  $z$ .

The Large Deviation Principle for the slow variable  $z$  in the limit  $\alpha \rightarrow 0$  gives the logarithmic equivalent of the probability density functional of paths  $\{z(t)\}$ , namely<sup>6</sup> [16, 39, 114]

$$P[z] \underset{\alpha \rightarrow 0}{\asymp} \exp \left( -\frac{1}{\alpha} S[z] \right), \quad (2.28)$$

with rate function

$$S[z] = \int L(z(t), \dot{z}(t)) dt, \quad (2.29)$$

also called the action of  $z$ . This can be proved applying the Gärtner-Ellis theorem directly to the process  $z(t)$ , as explained in appendix B.

<sup>4</sup>This expression is obtained from (2.5) with a change of time origin in the integral (the origin of time is not relevant for the fast process  $\tilde{w}_z(s)$ ) and with a rescaling with  $\alpha$  (which has no consequence in the final expression of the Large Deviation Principle).

<sup>5</sup>Here  $\Delta t$  is the equivalent of  $N$  and  $\theta$  is the equivalent of  $k$ . See also appendix B.1.

<sup>6</sup>The Large Deviation Principle is usually written for the process  $z$  in units (2.2), such that the natural time scale of evolution of  $z$  is of order one.

### 2.3.3 Link with stochastic averaging

As explained in the heuristic derivation 2.1.3, the Large Deviation Principle contains the Law of Large Numbers and Central Limit Theorem as approximations for small deviations from the mean. This can also be recovered directly from the expression of the scaled cumulant generating function (2.26). Indeed, a Taylor expansion in powers of  $\theta$  gives (see appendix B for details)

$$H(z, \theta) \simeq \theta F(z) + \frac{1}{2} \theta^2 \Xi(z) + O(\theta^3). \quad (2.30)$$

We recover the term appearing in the effective equation for  $z$ , (2.7): average drift  $F(z)$  at the level of the Law of Large Numbers (first order in  $\theta$ ) and integrated autocorrelation function  $\Xi(z)$  at the level of the Central Limit Theorem (second order in  $\theta$ )<sup>7</sup>. Higher orders in  $\theta$  give the deviations from Law of Large Numbers and Central Limit Theorem, i.e. deviations from the effective dynamics (2.7).

## 2.4 Validity of the results

The convergence of the slow process  $z$  in (2.1) to the effective dynamics (2.7) can be proved under the following hypothesis<sup>8</sup> [86]

- The effective slow dynamics (2.7) is well defined, i.e.  $F(z)$ ,  $F_1(z)$  and  $\Xi(z)$  are finite.
- The virtual fast process (2.4) is ergodic<sup>9</sup>: for any observable  $\phi(\tilde{w}_z)$ ,

$$\lim_{t \rightarrow \infty} \frac{1}{t} \int_0^t ds \phi(\tilde{w}_z(s)) = \mathbb{E}_z [\phi(\tilde{w}_z)], \quad (2.31)$$

where we recall that  $\mathbb{E}_z$  is the average in the statistically stationary state (over the invariant measure) of  $\tilde{w}_z$ .

The first hypothesis is very natural, it simply requires that the limiting process is well defined. The second hypothesis is also easy to understand qualitatively, we used it implicitly in the heuristic derivation (see equation (2.5)).

Consider the case where the virtual fast process is the linear process (2.9) with a diagonalizable linear operator  $L_z$  with strictly positive eigenvalues. Then the above hypothesis are satisfied and the convergence in (2.31) is exponential with rate given by the smallest eigenvalue of  $L_z$ . One way to characterize the convergence speed in practice is to compute the decorrelation time of the process  $f(z, \tilde{w}_z)$  in the stationary state of  $\tilde{w}_z$ , defined as [77, 84]

$$\tau_{corr}(z) \equiv \frac{\int_0^\infty \mathbb{E}_z [[f(z, \tilde{w}_z(s)) f(z, \tilde{w}_z(0))] ] ds}{\mathbb{E}_z [[f(z, \tilde{w}_z)^2]]}. \quad (2.32)$$

<sup>7</sup>At a more formal level, the effective slow dynamics (2.7) can be recovered using the quadratic approximation of  $H$  and using Freidlin-Wentzell theory [16, 39].

<sup>8</sup>Note that these rigorous results are generally proved in the finite dimensional case. It is easy to generalize them formally in infinite dimensional cases, like in fluid mechanics problems, and some rigorous results also exist [21, 37].

<sup>9</sup>The meaning of the limit in (2.31) will be defined in section 5.3.3, page 78.

$\tau_{corr}(z)$  gives the typical decorrelation time of the term that forces  $z$  in (2.8). It is thus the most relevant time scale related to the fast process when it comes to the dynamics of the slow process. In the case where the linear operator  $L_z$  is diagonalizable with strictly positive eigenvalues,  $\tau_{corr}$  will typically be related to the smallest eigenvalue of  $L_z$ .

In the fluid mechanics problem we are interested in, this issue is more subtle. Indeed, in our case the linear operator for the virtual fast process (linearized barotropic dynamics close to a zonal jet) is an infinite dimensional operator. It turns out that the linear operator typically has no eigenmodes [11], and that the asymptotic behaviour of the linear deterministic dynamics  $\partial_t + L_z$  is characterized by algebraic decays (see chapter 4 for details). This will lead to an algebraic convergence in expressions like (2.31). A qualitative way to characterize the convergence of the virtual fast process is then given by the condition that the time scale of evolution of  $\tilde{w}_z$  is much smaller than the time scale of evolution of  $z$ ,

$$\tau_{corr}(z) \ll \frac{1}{\alpha}. \quad (2.33)$$

The computation of  $\tau_{corr}$  and the validity of the above hypothesis (well-definiteness of the effective slow process and ergodicity) for the dynamics of zonal jets is the topic covered in chapter 5.

# Chapter 3

## Kinetic theory of zonal jets

We have seen in chapter 1 that some mid-latitude zonal jets have the property to evolve much slower than the surrounding turbulence [90]. In section 1.2.4, we have seen that this behaviour is characterized by a non-dimensional parameter  $\alpha$ , defined in (1.7) as the ratio of the typical time scale of turbulence evolution (advective time scale) and of the typical time scale of zonal jet evolution (dissipative time scale). Then,  $\alpha \ll 1$  is a criterion for the emergence of robust zonal jets in the stochastic barotropic equation (1.1).

In this chapter, we will prove that (1.1) can be written in the form of a slow-fast system like (2.8), where the zonal velocity profile  $U(y, t)$  is the slow variable, the eddy vorticity  $\omega'(x, y, t)$  is the fast variable and  $\alpha$  is the small parameter. Using the results presented in chapter 2, we will obtain equation (3.7) which describes the effective evolution of  $U$ , at the level of the Law of Large Numbers and the Central Limit Theorem. We call this equation the kinetic equation.

In sections 3.2 and 3.3, we describe the terms appearing in the kinetic equation, and discuss the physical consequences. In chapters 4 and 5, we will discuss in more details the applicability of the kinetic equation (3.7).

### 3.1 Time scale separation in the barotropic equation

The goal of this section is to write the stochastic barotropic equation (1.1) introduced in chapter 1 (page 11) in a form that is similar to the generic slow-fast system (2.8) presented in chapter 2 (page 26). Then, we will be able to apply the results presented in the previous chapter and to obtain an effective description of zonal jets dynamics.

#### 3.1.1 Non-dimensional equation

We perform a transformation to non-dimensional variables such that in the new units the domain is  $\mathcal{D} = [0, 2\pi l_x) \times [0, 2\pi)$  and the approximate average energy is 1. This is done introducing a non-dimensional time  $t' = t/\tau$  and a non-dimensional spatial variable  $\mathbf{r}' = \mathbf{r}/L$  where  $\tau = \tau_{eddy} = L\sqrt{2\kappa/\epsilon}$  is the typical time scale of stirring of the eddies by the zonal jet, defined in section 1.2.4, and where the aspect ratio is  $l_x = L_x/L_y$  and  $L = L_y$ .

The non-dimensional physical variables are  $\omega' = \tau\omega$ ,  $\mathbf{v}' = \tau\mathbf{v}/L$ , and the non-dimensional parameters are defined by  $\nu'_n = \nu_n\tau/L^{2n} = \nu_n\sqrt{2\lambda/\sigma}/L^{2n-2}$ ,

$$\kappa' = \kappa\tau = L\sqrt{\frac{2\kappa^3}{\epsilon}} = \alpha,$$

and

$$\beta' = L\tau\beta = \left(\frac{L}{L_R}\right)^2,$$

where we recognize the time scales ratio  $\alpha$  and the Rhines scale  $L_R$  defined in section 1.2.4. We consider a rescaled stochastic gaussian field  $\eta'$  with  $\mathbb{E}[\eta'(\mathbf{r}'_1, t'_1)\eta'(\mathbf{r}'_2, t'_2)] = C'(\mathbf{r}'_1 - \mathbf{r}'_2)\delta(t'_1 - t'_2)$  with  $C'(\mathbf{r}') = L^4C(\mathbf{r})$ . Performing this non-dimensionalization procedure, the barotropic equation reads

$$\frac{\partial\omega}{\partial t} + \mathbf{v} \cdot \nabla\omega + \beta v = -\alpha\omega - \nu_n(-\Delta)^n\omega + \sqrt{2\alpha}\eta, \quad (3.1)$$

where, for simplicity, we drop here and in the following the primes. We note that  $\alpha$  represents an inverse Reynolds number based on the large scale dissipation of energy and  $\nu_n$  is an inverse Reynolds number based on the viscosity or hyper-viscosity term that acts predominantly at small scales. Then, the regime of turbulence and of formation of zonal jets is defined by  $\nu_n \ll \alpha \ll 1$ , consistently with the scalings presented in section 1.2.4.

In this regime, we expect the influence of hyper-viscosity to be negligible, both in the global energy balance and in the dynamics of the large scales. Without loss of generality, we will consider the case of usual viscosity  $n = 1$ , the generalisation to  $n \neq 1$  being straightforward. For simplicity in the notation, we will use  $\nu \equiv \nu_1$ .

### 3.1.2 Decomposition into zonal and non zonal flows

For simplicity, we consider the case where the zonal symmetry (invariance by translation along  $x$ ) is not broken. Then the large scale structure will be a zonal jet characterized by either a zonal velocity field  $\mathbf{v}_z = U(y)\mathbf{e}_x$  or its corresponding zonal relative vorticity  $\omega_z(y) = -U'(y)$ .

Looking at (3.1), we see that the stochastic force produces turbulent eddies with amplitude  $\sqrt{\alpha}$ . Then, it is natural to assume that the perturbations to the zonal velocity field  $U(y)$  are of order  $\sqrt{\alpha}$ . Actually, this assumption is natural if the dynamics of those perturbations is damped on a time scale of order one. The goal of chapters 4 and 5 is to wonder about the self-consistency of this assumption.

Defining the zonal projection  $\langle \cdot \rangle$  as

$$\langle f \rangle(y) = \frac{1}{2\pi l_x} \int_0^{2\pi l_x} dx f(\mathbf{r}),$$

the zonal part of the vorticity will be denoted by  $\omega_z \equiv \langle \omega \rangle$ ; the rescaled non-zonal part of the flow  $\omega_m$  is then defined through the decomposition

$$\omega(\mathbf{r}) = \omega_z(y) + \sqrt{\alpha}\omega_m(\mathbf{r}).$$

The zonal and non-zonal velocities are then defined through  $U'(y) = -\omega_z(y)$ , the periodicity condition, and

$$\mathbf{v}(\mathbf{r}) = U(y)\mathbf{e}_x + \sqrt{\alpha}\mathbf{v}_m(\mathbf{r}).$$

We now project the barotropic equation (3.1) into zonal

$$\frac{\partial \omega_z}{\partial t} = -\alpha \frac{\partial}{\partial y} \langle v_m \omega_m \rangle - \alpha \omega_z + \nu \frac{\partial^2 \omega_z}{\partial y^2} + \sqrt{2\alpha} \eta_z \quad (3.2)$$

and non-zonal part

$$\frac{\partial \omega_m}{\partial t} + L_U [\omega_m] = \sqrt{2} \eta_m - \sqrt{\alpha} \mathbf{v}_m \cdot \nabla \omega_m + \sqrt{\alpha} \langle \mathbf{v}_m \cdot \nabla \omega_m \rangle, \quad (3.3)$$

where  $\eta_z = \langle \eta \rangle$  is a Gaussian field with correlation function  $\mathbb{E} [\eta_z(y_1, t_1) \eta_z(y_2, t_2)] = C_z(y_1 - y_2) \delta(t_1 - t_2)$  with  $C_z = \langle C \rangle$ ,  $\eta_m = \eta - \langle \eta \rangle$  is a Gaussian field with correlation function  $\mathbb{E} [\eta_m(\mathbf{r}_1, t_1) \eta_m(\mathbf{r}_2, t_2)] = C_m(\mathbf{r}_1 - \mathbf{r}_2) \delta(t_1 - t_2)$  with  $C_m = C - \langle C \rangle$ . Observe that the cross correlation between  $\eta_z$  and  $\eta_m$  is exactly zero, due to the translational invariance along the zonal direction of  $C$ .

The term in the left-hand side of (3.3) reads

$$L_U [\omega_m] = U(y) \frac{\partial \omega_m}{\partial x} + (\beta - U''(y)) \frac{\partial \psi_m}{\partial x} + \alpha \omega_m - \nu \Delta \omega_m \quad , \quad \omega_m = \Delta \psi_m. \quad (3.4)$$

It is the operator for the linearized evolution of eddies  $\omega_m$  close to the mean flow  $U$ .

The equation for the zonal potential vorticity evolution (3.2) can readily be integrated in order to get an equation for the zonal flow evolution

$$\frac{\partial U}{\partial t} = \alpha \langle v_m \omega_m \rangle - \alpha U + \nu \frac{\partial^2 U}{\partial y^2} + \sqrt{2\alpha} \zeta, \quad (3.5)$$

where  $\zeta$  is a gaussian noise such that  $\frac{\partial}{\partial y} \zeta = -\eta_z$ .

We see that the zonal potential vorticity is coupled to the non-zonal one through the zonal average of the advection term. We also clearly see that the natural time scale for the evolution of the zonal flow is  $1/\alpha$ . By contrast the natural time scale for the evolution of the non-zonal perturbation is one. These remarks show that in the limit  $\alpha \ll 1$ , we have a time scale separation between the slow zonal evolution and a rapid non-zonal evolution.

### 3.1.3 Analogy with generic slow–fast systems

The system (3.3),(3.5) is thus a particular case of the slow-fast system (2.8) presented in chapter 2 (page 26). Indeed, we have the analogy

$$\begin{aligned} z &\equiv U \quad , \quad w \equiv \omega_m \\ f(z, w) &\equiv \langle v_m \omega_m \rangle - U + \frac{\nu}{\alpha} \frac{\partial^2 U}{\partial y^2} \\ \eta_0 &\equiv \zeta \quad , \quad \eta \equiv \eta_m \\ L_z \cdot w &\equiv L_U [\omega_m] \\ b_1(z, w) &\equiv -\mathbf{v}_m \cdot \nabla \omega_m + \langle \mathbf{v}_m \cdot \nabla \omega_m \rangle. \end{aligned} \quad (3.6)$$

Using this analogy and equation (2.19), we get the effective evolution of the zonal jet velocity profile

$$\frac{\partial U}{\partial t} = \alpha F[U] + \sqrt{2\alpha} \zeta + \alpha^{3/2} F_1[U] + \alpha \xi[U]. \quad (3.7)$$

In the following, we will refer to equation (3.7) as the kinetic equation. In the next sections, we describe each term appearing in this equation, and discuss the physical consequences. To do this, we first need to define the analog of the virtual fast process (2.9) for the barotropic equations (3.3, 3.5). Using the analogy (3.6), we see that it reads

$$\frac{\partial \omega_m}{\partial t} = -L_U[\omega_m] + \sqrt{2}\eta_m, \quad (3.8)$$

where we have dropped the tilde for sake of simplicity in the notations. (3.8) describes the linear stochastic dynamics close to the jet velocity profile  $U(y)$ , which is held fixed.

We note that the dynamics (3.8) includes terms of order  $\alpha$  and  $\nu$  (see (3.4)). These dissipation terms could have equivalently been included in  $\mathcal{L}_s$  in the Fokker-Planck equation (2.10) associated with (3.3, 3.5), but we keep them in (3.8) for later convenience. However, an important part of our work was to prove that in the limit  $\nu_n \ll \alpha \ll 1$ , at leading order, the virtual fast process (3.8) with or without these dissipation terms has the same stationary distribution. This is a crucial point that will be made clear in chapters 4 and 5.

## 3.2 Deterministic kinetic equation

The term appearing at first order in (3.7) arises from the Law of Large Numbers (see section 2.1.1). It is the average of  $f$  defined in (3.6), in the stationary state of the virtual fast process (3.8),

$$F[U](y) = F_0[U](y) - U(y) + \frac{\nu}{\alpha} \frac{\partial^2 U}{\partial y^2}(y), \quad (3.9)$$

with

$$F_0[U](y) \equiv \mathbb{E}_U \langle v_m \omega_m \rangle (y). \quad (3.10)$$

$F_0$  is the average Reynolds' force in the stationary state of the linearized eddy evolution (3.8).  $F_0$  is a second-order moment of the gaussian stationary distribution of (3.8), it can thus be computed as a linear transform of the stationary two-points correlation function  $g_U^\infty[\omega_m](\mathbf{r}_1, \mathbf{r}_2) = \mathbb{E}_U[\omega_m(\mathbf{r}_1)\omega_m(\mathbf{r}_2)]$ . As explained in section 2.2,  $g_U^\infty$  is the stationary solution of the Lyapunov equation, which we report here for convenience

$$\frac{\partial g}{\partial t} + \left( L_U^{(1)} + L_U^{(2)} \right) g = 2C_m, \quad (3.11)$$

where  $L_U^{(i)}$  is the linear operator (3.4) applied to the  $i$ -th variable  $\mathbf{r}_i$ . Note that because  $L_U$  also contains dissipative terms of order  $\alpha$  and  $\nu$ , the definitions of  $F_0$  and  $g_U^\infty$  implicitly assume that the limit  $\nu \ll \alpha$ ,  $\alpha \rightarrow 0$  is taken. Whether  $F_0$  and the stationary solution of (3.11) are finite in this limit or not is the topic of chapters 4 and 5.

At this order of approximation, the dynamics reads

$$\frac{\partial U}{\partial t} = \alpha F_0[U] - \alpha U + \nu \frac{\partial^2 U}{\partial y^2} + \sqrt{2\alpha}\zeta, \quad (3.12)$$

where  $F_0$  can be easily computed from the stationary solution of (3.11), where  $U$  is held fixed. An efficient numerical algorithm to compute  $F_0$  will be presented in

section 4.3.2.

In the cases of interest for geophysical applications, the stochastic noise  $\eta$  does not act at the largest scales of the flow. In particular,  $\zeta = 0$ . This is why we refer to (3.12) as the deterministic kinetic equation. When  $\zeta = 0$ , (3.12) describes the relaxation of jets towards the attractors of the dynamics.

### 3.2.1 Link with the quasi-linear approximation and cumulant expansions

We note that in the leading order description (3.12), the non-linear eddy-eddy interaction term  $b_1$  does not appear. Neglecting the non-linear eddy-eddy term in the original equations (3.3,3.5) leads to the so-called quasi-linear barotropic equations:

$$\begin{cases} \frac{\partial U}{\partial t} = \alpha \langle v_m \omega_m \rangle - \alpha U + \nu \frac{\partial^2 U}{\partial y^2} + \sqrt{2\alpha} \zeta \\ \frac{\partial \omega_m}{\partial t} + L_U [\omega_m] = \sqrt{2} \eta_m. \end{cases} \quad (3.13)$$

The approximation leading to the quasi-linear dynamics (3.13) amounts at suppressing some of the triad interactions. As a consequence, the inertial quasi-linear dynamics has the same quadratic invariants as the initial barotropic equations: the energy and the relative enstrophy (see section 1.2.4). Quasi-linear dynamics has been studied as a simplified model of anisotropic turbulence, mainly on an empirical basis [104]. The result of stochastic averaging shows that at leading order, the quasi-linear barotropic equations (3.13) and the fully non-linear equations (3.3, 3.5) lead to the same zonal flow dynamics in the regime of time scale separation  $\alpha \ll 1$ , and are given by the system (3.11, 3.12).

An important physical consequence of this result deals with energy transfers among scales. Indeed, the fully non-linear barotropic dynamics (3.3, 3.5) is characterized by an inverse turbulent cascade of energy towards the largest scales, qualitatively similar to the inverse cascade in isotropic two-dimensional turbulence [9, 55], with quantitative differences due to anisotropy [42]. Then, it is commonly argued that the formation of large-scale coherent structures (vortices, jets) in two-dimensional and geophysical turbulent flows is the consequence of this inverse turbulent cascade of energy [14]. In contrast, in the quasi-linear barotropic dynamics (3.13) the transfers of energy from the eddies  $\omega_m$  to the mean flow  $U$  through the Reynolds' stresses  $\langle v_m \omega_m \rangle$  are non-local in scales. The result of stochastic averaging thus shows that in the large time scale separation limit  $\alpha \rightarrow 0$ , the dynamics of zonal jets on long time scales is actually accurately described by non-local energy transfers only.

A system very close to (3.11,3.12), known as Stochastic Structural Stability Theory (S3T, [3, 33]) or Cumulant Expansion at Second order (CE2, [106]) has been the subject of various studies over the past few years, from numerical and theoretical points of view [85, 104]. The S3T-CE2 equations are obtained assuming that the quasi-linear approximation is valid, and identifying zonal averages with ensemble averages. In this theory, the zonal flow equation (3.12) and the Lyapunov equation (3.11) evolve simultaneously, and  $F_0$  in (3.12) is computed accordingly. In the limit

of large time scale separation  $\alpha \ll 1$ , the Lyapunov equation evolves much faster than the mean flow equation. Then, the S3T-CE2 description is very close to the deterministic kinetic theory, in the regime  $\alpha \ll 1$ . Moreover, in a statistically stationary state, neither the jet profile  $U(y)$  nor the correlation functions  $g$  evolve. As a consequence, the deterministic kinetic equation (3.12) and the S3T-CE2 system have exactly the same attractors.

In previous studies, the validity of the S3T-CE2 theory has been assessed comparing numerical simulations of the barotropic equation to numerical resolutions of the S3T-CE2 system. For instance in the work of Tobias and Marston [106], it is argued that the strength of jet is related to the value of the zonostrophy index  $R_\beta$ , introduced in section 1.2.4. It is observed that a large value of  $R_\beta$  leads to a flow made of robust jets, while a small value leads to the formation of weak, meandering jets. Moreover, the comparison between CE2 calculations and direct non-linear simulations shows a very good agreement for large values of  $R_\beta$ , and a poor agreement for smaller values of  $R_\beta$ .

We now compare these results with the deterministic kinetic theory. First, using that  $\alpha_R \propto R_\beta^{-5}$ , the regime  $R_\beta \gg 1$ , in which robust jets and good accuracy of CE2 are found, coincides with the regime  $\alpha_R \ll 1$ . Let's now look more precisely at the different parameters considered in [106].

Three simulations are presented in this paper, corresponding to figures 2(a), 2(b) and 2(c), or 4(a), 4(b) and 4(c) for the comparison with the CE2 simulation. We find the following results:

- With the parameters of the case (a), we have  $\alpha = 0.068$  and  $\alpha_R = 0.0021$ , which are both very small. This is in accordance with the fact that robust jets are found, and that the quasi-linear approximation is accurate.
- With the parameters of the case (b), we find the values  $\alpha = 0.068$  and  $\alpha_R = 0.0029$ , which are still very small. Again, this is in accordance with the fact that strong jets are found, and that the quasi-linear approximation is accurate.
- With the parameters of the case (c), we have  $\alpha = 1.45 > 1$  and  $\alpha_R = 0.030$ , which is still quite small. The case (c) corresponds to weak and meandering jets, and to a very poor agreement between CE2 and non-linear simulation.

To conclude this discussion, we find that small values of  $\alpha_R$  and  $\alpha$  lead to the formation of strong jets, and to a very good accuracy of the S3T-CE2 equation. This observation can also be made from the numerical simulations presented in other papers [3, 33, 104]. However, the last case (c) suggests that  $\alpha$  might be more relevant than  $\alpha_R$  in order to characterise the robustness of jets and the validity of the quasi-linear approximation. This can also be seen in figure 6 of the work of Srinivasan and Young [104], where the ratio of energy contained in the jets is plotted as a function of an adimensionalized friction  $\mu_*$  and of an adimensionalized gradient of potential vorticity  $\beta_*$ . We find that strong jets, together with a good accuracy of the quasi-linear approximation, is obtained for small values of  $\mu_*$ , almost independently of the value of  $\beta_*$ . Then, it seems that the value of  $\beta$  does not control the robustness of jets and the validity of the quasi-linear approximation, suggesting again that  $\alpha$  —and not  $\alpha_R$  that depends on  $\beta$ — is the relevant small parameter for the kinetic theory of zonal jets.

Our approach thus justifies the S3T-CE2 theory in the time scale separation regime  $\alpha \ll 1$ , and indicates that this regime may be the regime where the quasi-linear approximation is accurate.

### 3.2.2 Alternative derivation using the vorticity probability distribution functions

Closed equations that describe the effective relaxation dynamics of zonal jets can be obtained using stochastic averaging (leading to the deterministic kinetic equation (3.12)), or using cumulant expansions (leading to the S3T-CE2 systems [3, 33, 106]).

In the stochastic averaging procedure, we consider the probability density functional of the whole vorticity field  $P[\omega]$ , and perform a perturbative expansion at the level of the Fokker-Planck equation (see chapter 2 and appendix A).

In the cumulant expansion approach, we consider the hierarchy of equations for the  $n$ -points vorticity correlation functions. This is a very classical approach in turbulence, and is usually referred to as Reynolds' equations [89].

An alternative approach is to consider the probability distribution of vorticity at given points in space. Like in the cumulant expansion approach, the non-linear terms in the barotropic equation lead to an infinite hierarchy of coupled equations known as the LMN hierarchy, from Lundgren [63], Monin [70] and Novikov [79]. This approach has been applied to different situations such as two-dimensional and three-dimensional, homogeneous and non-homogeneous, isotropic and anisotropic turbulence (see [71] and references therein), as a theoretical tool or combined with numerical simulations [40].

The LMN hierarchy is very similar to the BBGKY hierarchy in the kinetic theory of gases, plasmas and gravitational systems [4]. In a work anterior to this thesis [73, 74], the BBGKY hierarchy for systems of long-range interacting particles has been extended to the stochastically forced case. This can also be done in the fluid mechanics case, leading to a generalized LMN hierarchy. We sketch this procedure here, the detailed derivation is given in appendix C. We also assume for simplicity that  $\beta = 0$  and  $\nu = 0$ , the generalization to  $\beta \neq 0$ ,  $\nu \neq 0$  being straightforward.

We are interested in the evolution of the  $n$ -points equal-time vorticity distribution

$$p_n(\mathbf{r}_1, \sigma_1, \dots, \mathbf{r}_n, \sigma_n, t) = \mathbb{E}[\delta(\omega(\mathbf{r}_1, t) - \sigma_1) \dots \delta(\omega(\mathbf{r}_n, t) - \sigma_n)]. \quad (3.14)$$

By definition,  $p_n(\mathbf{r}_1, \sigma_1, \dots, \mathbf{r}_n, \sigma_n, t) d\sigma_1 \dots d\sigma_n$  represents the probability that at time  $t$ , the vorticity  $\omega(\mathbf{r}_k, t)$  has a value between  $\sigma_k$  and  $\sigma_k + d\sigma_k$ , for all  $k = 1 \dots n$ . Then, the knowledge of the function  $p_n$  for a given  $n$  gives all the moments of the vorticity, up to moments of order  $n$ . For instance, the average vorticity field is given by

$$\bar{\omega}(\mathbf{r}_1, t) \equiv \mathbb{E}[\omega(\mathbf{r}_1, t)] = \int_{\mathbb{R}} d\sigma_1 \sigma_1 p_1(\mathbf{r}_1, \sigma_1, t), \quad (3.15)$$

the two-points vorticity correlation function is given by

$$\tilde{g}(\mathbf{r}_1, \mathbf{r}_2, t) = \mathbb{E}[\omega(\mathbf{r}_1, t)\omega(\mathbf{r}_2, t)] = \int_{\mathbb{R}^2} d\sigma_1 d\sigma_2 \sigma_1 \sigma_2 p_2(\mathbf{r}_1, \sigma_1, \mathbf{r}_2, \sigma_2, t), \quad (3.16)$$

and so on.

The equation for the evolution of  $p_n$  is obtained from the barotropic equation (3.1) applying the Itô formula. Because of the non-linear terms, the evolution of

$p_n$  involves  $p_{n+1}$ . This kind of approach thus relies upon a closure in the hierarchy, and the results strongly depend on the closure (see the discussion in section 1.3.3, page 21). In our case, the closure appears naturally as a perturbative expansion in powers of  $\alpha \ll 1$ , like in the finite-dimensional analog [73, 74].

At order zero in  $\alpha$ , the barotropic equation is inertial so the equations for  $p_n$  form the usual LMN hierarchy. Then, a particular class of solutions is given by Young measures, defined by

$$\forall n, \quad p_n(\mathbf{r}_1, \sigma_1, \dots, \mathbf{r}_n, \sigma_n) = p(\mathbf{r}_1, \sigma_1) \dots p(\mathbf{r}_n, \sigma_n) \quad (3.17)$$

with  $p \equiv p_1$ . Distributed according to this measure, vorticity values at different points are statistically independent random variables. This means that Young measures represent the mean-field behaviour of the system, consistently with the RMS equilibrium statistical mechanics theory of two-dimensional flows [14, 15].

When  $\alpha \neq 0$ , we consider perturbations of the Young measure solution as

$$p_2(1, 2) = p(1)p(2) + \alpha q_2(1, 2), \quad (3.18)$$

$$p_3(1, 2, 3) = p(1)p(2)p(3) + \alpha \{q_2(1, 2)p(3)\} + \alpha^2 q_3(1, 2, 3), \quad (3.19)$$

and so on. In these expressions, we have used the usual short-hand notations of kinetic theory, see appendix C for details. These expressions define the functions  $q_n$ , our assumption is thus that  $q_n = O(1)$  as  $\alpha \rightarrow 0$ . This type of ansatz has been proposed since the beginning of the study of the LMN hierarchy, using an analogy with the BBGKY hierarchy of the classical kinetic theory of plasmas [63]. The functions  $q_n$  are called the connected parts of the probability distribution functions  $p_n$ . They describe the correction to the equilibrium statistical mechanics theory due to the small forcing and dissipation present in (3.1).

Injecting the expressions of  $p_n$  in the hierarchy and neglecting terms of order  $\alpha^2$ , we obtain a closed set of equations for  $p$  and  $q_2$ . Using (3.15) and (3.16), we obtain the corresponding equations for the average vorticity and for the vorticity two-points correlation function. Assuming that the mean flow is a parallel flow in the  $x$  direction and that the stochastic forces do not act directly on the zonal degrees of freedom, we obtain

$$\partial_t \bar{\omega}(y_1, t) = \alpha R[g_m](y_1, t) - \alpha \bar{\omega}(y_1, t), \quad (3.20)$$

and

$$\partial_t g_m + \left( L_{\bar{U}}^{0(1)} + L_{\bar{U}}^{0(2)} \right) g_m = 2C_m, \quad (3.21)$$

where  $g_m$  is the two-points correlation function of the non-zonal vorticity, and  $R[g_m]$  represents the forcing acting on  $\bar{\omega}$  due to Reynolds stresses. In these equations,  $\bar{\omega}$  and  $g_m$  evolve simultaneously. The system (3.20), (3.21) is thus exactly the S3T-CE2 system. As pointed out before, when  $\alpha \ll 1$  the dynamics of  $\bar{\omega}$  occurs on a time scale of order  $1/\alpha$ , while the time scale of evolution of  $g_m$  is of order 1, so we recover the deterministic kinetic equation (3.12).

To obtain this result, we have to make the assumption that the stochastic forcing does not act directly on the zonal jet. When this is not the case, we can prove that the assumption  $q_2 = O(1)$  breaks down (see appendix C). This illustrates the weaknesses of this approach: there is no control of the assumptions, and the way to truncate the hierarchy is not unique, probably leading to different effective equations [71]. As an example, another perturbative expansion in the limit of large time scale separation is proposed in [109], for the case of 3D isotropic turbulence.

### 3.3 Stochastic kinetic equation

The terms appearing at second order in (3.7) arise from the Central Limit Theorem (see section 2.1.2 and equation (2.19)). The expression of the drift term  $F_1[U]$  can be found in appendix A. The stochastic term  $\xi[U]$  is a gaussian random field that depends on the meridional coordinate  $y$ , white in time, with zero mean and correlations (for a fixed  $U$ )  $\mathbb{E}[\xi[U](y_1, t_1)\xi[U](y_2, t_2)] = \delta(t_1 - t_2)\Xi[U](y_1, y_2)$  where  $\Xi[U]$  is given by (2.20) in chapter 2 (page 32). Here,

$$\begin{aligned} \Xi[U](y_1, y_2) = \int_0^\infty \mathbb{E}_U [ [ \langle v_m \omega_m \rangle (y_1, s) \langle v_m \omega_m \rangle (y_2, 0) \\ + \langle v_m \omega_m \rangle (y_2, s) \langle v_m \omega_m \rangle (y_1, 0) ] ] ds, \end{aligned} \quad (3.22)$$

where we recall that  $\mathbb{E}_U[[\cdot]]$  denotes the covariance in the statistically stationary state of the virtual fast process (3.8). As discussed in section 2.1.2,  $\Xi[U]$  represents the typical fluctuations of the Reynolds' stress  $\langle v_m \omega_m \rangle$  around the mean  $F_0[U]$ <sup>1</sup>.  $\xi[U]$  is white in time, consistently with the time scale separation between the dynamics of the mean flow  $U$  and the dynamics of the eddies  $\omega_m$ .

An important remark to make is that the first order term in  $F_1[U]$  (in equation (3.7)) is exactly zero. Its general expression can be found in appendix A (equation (A.4)). In the case of the barotropic equation, it reads

$$F_1[U](y) = - \int_0^\infty ds \int \mathcal{D}[\omega_m] \langle v_m \omega_m \rangle (y) e^{s\mathcal{L}_0} \int d\mathbf{r} \frac{\delta}{\delta \omega_m(\mathbf{r})} [b_1[\omega_m]G_U[\omega_m]] + O(\sqrt{\alpha}), \quad (3.23)$$

where  $b_1[\omega_m]$  is the non-linear eddy-eddy interaction term (see (3.6)) and  $G_U[\omega_m]$  is the stationary gaussian distribution of the virtual fast process (3.8).  $b_1$  is quadratic so the functional derivative with respect to  $\omega_m$  will produce terms linear or quartic in  $\omega_m$ . When multiplied by  $\langle v_m \omega_m \rangle$  and averaged over the centered gaussian  $G_U$ , this gives zero.

The consequence is that corrections to the drift term  $F_0[U] = \mathbb{E}_U \langle v_m \omega_m \rangle$  only appear at order  $\alpha^2$ . These terms lead to corrections of the attractors of the effective dynamics that are of order  $\alpha$ . In the limit  $\alpha \ll 1$ , these terms are negligible in the effective dynamics of zonal jets.

The stochastic term  $\xi[U]$  also appears at next order in  $\alpha$ . However, its effect on the kinetic equation (3.7) is qualitatively very different from the drift term  $F_1[U]$ . Indeed, the deterministic kinetic equation (3.12) is unable to describe the statistics of the small fluctuations close to an attractor. A very interesting result that can be derived from (3.7) is the statistics for the Gaussian fluctuations of the jet close to its most probable value.

The initial purpose of the study of the stochastic kinetic equation (3.7) was to investigate the statistics of rare event in zonal jets dynamics. Assume for instance that the deterministic kinetic equation (3.12) has more than one attractor, as in figure 3.1. Then it is natural to guess that the small noise  $\xi[U]$  can describe the

<sup>1</sup>The dissipative terms contained in  $f$  (see equation (3.6)) do not appear in  $\Xi[U]$  because  $\mathbb{E}_U[[\cdot]]$  is the covariance of  $f$ , and not just the correlation.

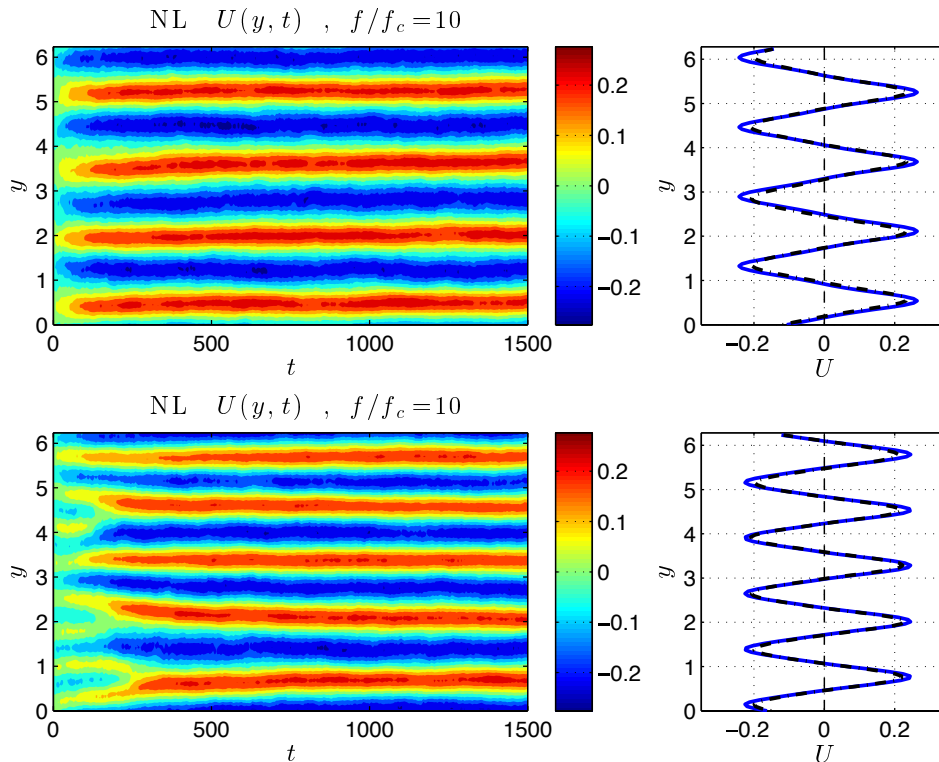


Figure 3.1: Evolution of the zonally averaged velocity profile  $U(y)$  as obtained from non-linear simulations (left) and comparison of the stationary velocity profile obtained from non-linear simulations and from the deterministic kinetic equation (3.12), or equivalently S3T [33]. The upper and lower pictures are obtained for the same values of the physical parameters but with different initial conditions. The figure shows that for a given set of parameters it can converge towards two attractors with a different number of jets. Courtesy Navid Constantinou.

relative probability of the two attractors and the probability of transitions between them. However, as discussed in section 2.1.3, the Central Limit Theorem can only describe small fluctuations around the attractors. To study large deviations such as transitions between attractors, we need to go to the level of the Large Deviation Principle. This is the subject of chapter 6.

### 3.4 Perspectives

The deterministic kinetic equation (3.12) describes a quasi-linear approximation of the barotropic equation, previously studied numerically [104]. One of the interests of the present approach is to give a precise regime of validity of this approximation, based on theoretical arguments (perturbative expansion). A very natural perspective of the present work is to apply the stochastic averaging procedure to different systems in which quasi-linear approximations are known to work in some cases. This is for instance the case in more complex models of geophysical fluid dynamics, such as an idealized Global Circulation Model (GCM), see figure 3.2. We see that the accuracy of the quasi-linear approximation depends on the rotation rate of the planet. A theoretical study could explain this behaviour, and help determine a ro-

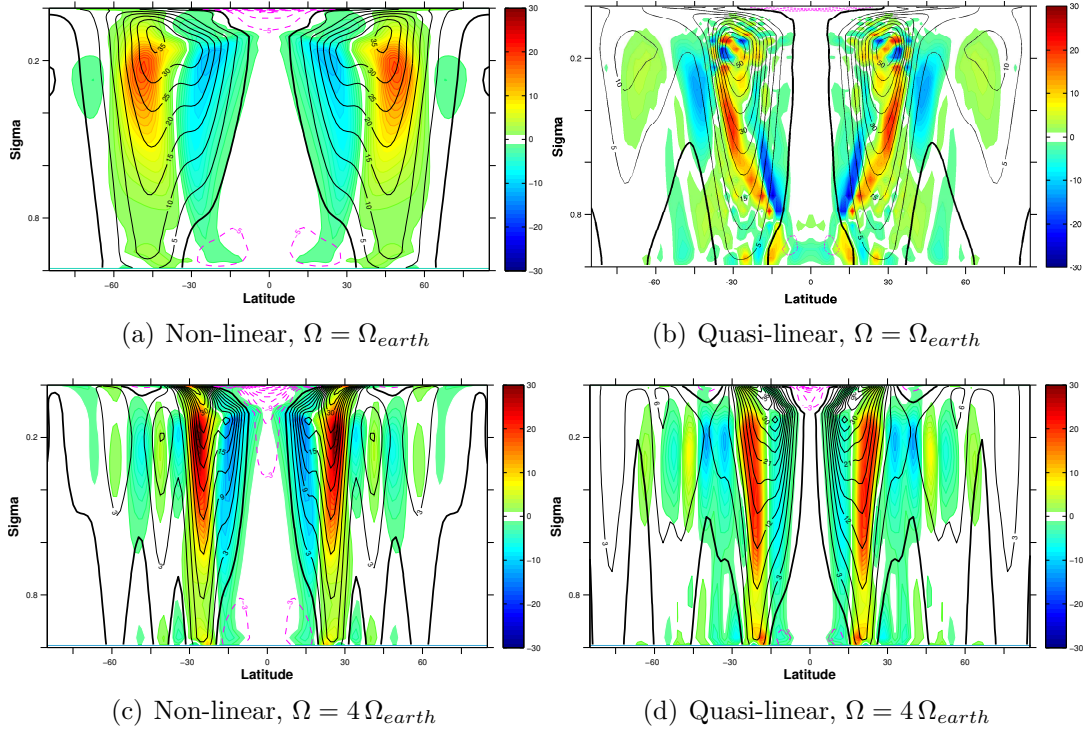


Figure 3.2: Zonally averaged zonal velocity (contours, in  $\text{m.s}^{-1}$ ) and zonally averaged momentum flux convergence (colors, in  $10^{-6} \text{ m.s}^{-2}$ ), as a function of latitude and sigma level (depth), from numerical simulations of an idealized GCM [1]. Black (resp. pink) contours represent eastward (resp. westward) winds. In all the simulations, strong eddy-driven eastward zonal jets are formed. The two left (resp. right) figures are simulations of the non-linear (resp. quasi-linear) equations.  $\Omega$  is the planet rotation rate in the simulation and  $\Omega_{earth}$  is the rotation rate of Earth. The quasi-linear approximation is not accurate for  $\Omega = \Omega_{earth}$ , but gives a very good agreement for  $\Omega = 4\Omega_{earth}$ . Courtesy Farid Ait-Chaalal.

but criterion for the accuracy of the quasi-linear approximation.

The deterministic kinetic equation (or equivalently S3T-CE2 systems) has been widely studied from a numerical point of view in the past [3, 33, 85, 104, 106]. An interesting perspective of this work is to simulate numerically the stochastic kinetic equation (3.7) in order to study the typical fluctuations of zonal jets. An algorithm to compute directly the integrated autocorrelation function  $\Xi[U]$  for a given base flow  $U$  will be presented in chapter 4 (section 4.4 page 60). Such simulation would provide a direct description of zonal jet statistics around the attractors of the deterministic kinetic equation (3.12).

# Chapter 4

## Implementation of the kinetic theory

In chapter 3, the stochastic averaging procedure was applied to the stochastic barotropic equation in the limit of small forces and dissipation (inertial limit), which was assumed to be the regime where zonal jets evolve much slower than turbulent eddies. This led to an effective description of jet dynamics, summarized by equations (3.7, 3.8), page 39.

The kinetic equation (3.7) arises from the Law of Large Numbers and the Central Limit Theorem, as explained in chapter 2. As a consequence, it involves quantities related to the low-order statistics of the Reynolds' stress divergence (Reynolds' force)  $\langle \omega_m v_m \rangle$ . Apart from dissipative terms, the most physically relevant terms in (3.7) are the average Reynolds' force  $F_0[U]$  given by (3.10) and the integrated autocorrelation function of the Reynolds' force  $\Xi[U]$  given by (3.22). We discuss in this chapter the basic properties of these quantities, and explain how to compute them explicitly.

The computation of  $F_0[U]$  and  $\Xi[U]$  involves averages in the stationary state of the linearized equation for eddies (3.8), denoted  $\mathbb{E}_U$  (see equations (3.10) and (3.22)). It is not obvious that the average  $\mathbb{E}_U$  of any observable of the eddy vorticity  $\omega_m$  gives a finite value. Indeed, the linear dynamics (3.8) is forced but not dissipated in the inertial limit  $\nu \ll \alpha \ll 1$ . Thus, in order to have finite large time limits, we have to rely on an inviscid damping mechanism. In the case of the linearized Euler equation such a mechanism is known as the Orr mechanism [82]. We will rely on this mechanism to express  $F_0[U]$  and  $\Xi[U]$ , and to prove that  $F_0[U]$  is finite. This implies in particular that the deterministic kinetic equation (3.12) is well defined. The extension of this result to the full stochastic kinetic equation (3.7) (which involves  $\Xi[U]$ ) is discussed in next chapter.

In the preliminary sections 4.1 and 4.2, we give some definitions and notations, and we recall classical results on the Orr mechanism for the two-dimensional Euler equation ( $\beta = 0$ ) [82], and present their generalisation to any jet profile [11], holding when the base flow has no modes neither unstable nor neutral.

Then in section 4.3, we give a simple expression of the average Reynolds' force  $F_0[U]$  in terms of a deterministic eddy enstrophy, and we propose a method to compute it numerically extremely fast in the limit of zero viscosity and small linear friction.

In section 4.4, we give an expression of the integrated autocorrelation function of the Reynolds' force  $\Xi[U]$ , and propose a method to compute it numerically in the limit of zero viscosity and small linear friction.

## 4.1 Some useful definitions for chapters 4 and 5

### 4.1.1 Expectations and limits

Because quantities of interest such as  $F_0$  and  $\Xi$  are defined with large-time and small-dissipation limits, it is useful to fix some notations, in order to clarify the following discussion. First of all, we recall the linear dynamics of the eddy vorticity  $\omega_m$  with linear friction and viscosity

$$\frac{\partial \omega_m}{\partial t} + L_U^0[\omega_m] = -\alpha \omega_m + \nu \Delta \omega_m + \sqrt{2} \eta_m, \quad (4.1)$$

where  $\eta_m$  is a gaussian white noise with zero mean and spatial correlations  $C_m$ , and with the inertial linear operator

$$L_U^0[\omega] = U(y) \frac{\partial \omega}{\partial x} + (\beta - U''(y)) \frac{\partial \psi}{\partial x}, \quad \omega = \Delta \psi. \quad (4.2)$$

The average of an observable  $\phi[\omega_m(\mathbf{r}, t)]$  with respect to realizations of the noise  $\eta_m$  in (4.1) will be denoted  $\mathbb{E}[\phi[\omega_m(\mathbf{r}, t)]]$ .

Formally, the terms appearing in the kinetic equation (3.7) for  $U(y)$  are expectations in the statistically stationary state of the inertial linearized barotropic dynamics

$$\frac{\partial \omega_m}{\partial t} + L_U^0[\omega_m] = \sqrt{2} \eta_m. \quad (4.3)$$

Such expectations have been denoted  $\mathbb{E}_U[\phi[\omega_m(\mathbf{r})]]$ , formally we can write

$$\mathbb{E}_U = \lim_{t \rightarrow \infty} \lim_{\alpha \rightarrow 0} \lim_{\nu \rightarrow 0} \mathbb{E}. \quad (4.4)$$

All the results presented in chapters 4 and 5 are derived with  $\nu = 0$ , and it turns out that most of these results can be alternatively obtained taking first the limit  $t \rightarrow \infty$ , and then  $\alpha \rightarrow 0$ . Moreover, in order to interpret those results it will be useful to consider the stationary state of the dynamics (4.1) with  $\nu = 0$ <sup>1</sup>, but with a small, non-zero damping rate  $\alpha$ . We thus define the expectation

$$\mathbb{E}_U^\alpha = \lim_{t \rightarrow \infty} \lim_{\nu \rightarrow 0} \mathbb{E}, \quad (4.5)$$

and abusively denote  $\mathbb{E}_U = \lim_{\alpha \rightarrow 0} \mathbb{E}_U^\alpha$ . The consequences of the ordering of limits  $t \rightarrow \infty$  and  $\alpha \rightarrow 0$  will be further discussed along chapters 4 and 5.

---

<sup>1</sup>We could also study the stationary statistics of (4.1) with  $\alpha = 0$  and  $\nu \ll 1$ , or with both  $\alpha$  and  $\nu$  non-zero. This would lead to different behaviour in the inertial limit, see the discussions in section 5.4 and in [18] for more details.

### 4.1.2 Fourier decomposition

The dynamics of  $\omega_m$  in (4.1) or (4.3) is linear, it is thus useful to study the dynamics of each Fourier mode independently, the global results will be obtained by simply adding the contribution from each mode. We treat here the simple case of a flow in a bi-periodic domain  $\mathcal{D} = [0, 2\pi l_x) \times [0, 2\pi)$ , the generalization to different geometries will be also discussed.

We expand the force correlation function  $C_m$  in Fourier series,

$$C_m(x, y) = \sum_{k>0, l} c_{kl} \cos(kx + ly), \quad (4.6)$$

with  $c_{kl} \geq 0$ . We note that because  $C_m$  is a correlation, it is a positive definite function. This explains why sin contribution are zero in this expansion. The expression  $c_{kl} \cos(kx + ly) + c_{k,-l} \cos(kx - ly)$  is the most general positive definite function involving the Fourier components  $e^{ikx}$  and  $e^{ily}$  or their complex conjugates, (4.6) is thus the most general homogeneous correlation function. The generalization to the case of an inhomogeneous force, for instance for the case of a channel would be straightforward.

The noise correlation function  $C_m$  corresponds to the noise

$$\eta_m(\mathbf{r}, t) = \sum_{k=-\infty}^{\infty} \sum_{l=-\infty}^{\infty} \sqrt{\frac{c_{kl}}{2}} e^{ikx+ily} \eta_{kl}(t) \quad (4.7)$$

where  $\eta_{kl}^* = \eta_{-k,-l}$  and  $\mathbb{E}[\eta_{k_1, l_1}(t_1) \eta_{k_2, l_2}(t_2)] = \delta_{k_1, -k_2} \delta_{l_1, -l_2} \delta(t_1 - t_2)$ , and  $c_{k,l}$  is defined for  $k < 0$  by  $c_{k,l} = c_{-k,-l}$  (we recall that  $c_{kl}$  are real and positive), and for  $k = 0$  by  $c_{0,l} = 0$ . By linearity of (4.1) and because the linear operator  $L_U = L_U^0 + \alpha - \nu \Delta$  is invariant under translations in the  $x$  direction, the non-zonal vorticity field can be written as

$$\omega_m(\mathbf{r}, t) = \sum_{k=-\infty}^{\infty} \sum_{l=-\infty}^{\infty} \sqrt{\frac{c_{kl}}{2}} e^{ikx} \omega_{kl}(y, t). \quad (4.8)$$

The eddy vorticity  $\omega_m$  evolves according to (4.1), so  $\omega_{kl}$  evolves according to

$$\frac{\partial \omega_{kl}}{\partial t} + L_{U,k}[\omega_{kl}] = \sqrt{2} e^{ily} \eta_{kl}, \quad (4.9)$$

where

$$L_{U,k}[\omega_{kl}] = ikU(y)\omega_{kl} + ik(\beta - U''(y))\psi_{kl} + \alpha\omega_{kl} - \nu\Delta_k\omega_{kl} \quad (4.10)$$

with  $\Delta_k = \partial_y^2 - k^2$  and  $\omega_{kl} = \Delta_k \psi_{kl}$ .

## 4.2 Inviscid damping of the deterministic linearized equation

In this introductory section we show how to compute quantities such as correlation functions for stochastic linear processes from associated deterministic problems. This will lead us to consider the asymptotic behaviour of the deterministic linear barotropic dynamics.

### 4.2.1 A finite dimensional example

To give a very simple example, we consider the one-dimensional linear stochastic equation (1D Ornstein-Uhlenbeck process)

$$\frac{dq}{dt} = -\lambda q + \sqrt{\sigma}\eta(t), \quad (4.11)$$

where  $\eta$  is a gaussian noise with zero mean and correlations  $\mathbb{E}[\eta(t)\eta(t')] = \delta(t-t')$ ,  $\lambda \geq 0$ ,  $\sigma > 0$ , and with initial condition  $q(0) = 0$ . We investigate the large-time limit of the variance of  $q$ . Integrating equation (4.11) as

$$q(t) = \sqrt{\sigma} \int_0^t e^{-\lambda(t-t_1)} \eta(t_1) dt_1, \quad (4.12)$$

we get

$$\mathbb{E} [q(t)^2] = \sigma \int_0^t e^{-2\lambda t_1} dt_1, \quad (4.13)$$

where  $\mathbb{E}$  denotes the average with respect to realisation of the noise  $\eta$ .

From this simple analysis, we can conclude that the convergence of the variance when  $t \rightarrow \infty$  depends on the value of the friction coefficient  $\lambda$ . Indeed, if  $\lambda > 0$ , the variance converges to the finite value  $\sigma/2\lambda$ , while for  $\lambda = 0$ , the variance diverges as  $\sigma t$ .

Observe that in equation (4.13), the variance is expressed from the solution  $\tilde{q}(t_1) = e^{-\lambda t_1}$  of the deterministic equation  $\partial_{t_1} \tilde{q} = -\lambda \tilde{q}$  with initial condition  $\tilde{q}(0) = 1$ . We thus conclude that the convergence of the variance depends on the large-time behaviour of the associated deterministic linear evolution, and particularly on the damping mechanisms that occur in this deterministic dynamics.

This discussion is very general, and an expression similar to (4.13) can be obtained for any Ornstein-Uhlenbeck process [44]. The computation of correlation functions can be discussed similarly to the computation of the variance (see section 4.2.2). We thus understand that in the problem we are interested in, whether the average Reynolds' force  $F_0[U] = \mathbb{E}_U \langle v_m \omega_m \rangle$  and the integrated autocorrelation function  $\Xi[U]$  are finite or not depend on the small-dissipation and large-time behaviour of the deterministic linear equation<sup>2</sup>

$$\frac{\partial \tilde{\omega}_m}{\partial t} + L_U^0[\tilde{\omega}_m] = -\alpha \tilde{\omega}_m + \nu \Delta \tilde{\omega}_m, \quad (4.14)$$

where  $L_U^0$  the linearized inertial evolution operator close to the zonal flow  $U$ , given in (4.2).

For finite values of  $\alpha$  and  $\nu$ , and for a stable linear operator  $L_U^0$ , the linear friction and viscosity are the main damping mechanisms. Then, the vorticity autocorrelation function, and all the quantities we are interested in will converge to finite values. However, we are interested in the particular limit where  $\nu \ll \alpha \ll 1$  and, for the self-consistency of the theory we need a uniform convergence independent of the values of  $\nu$  and  $\alpha$ . Then we need to rely on another damping mechanism, through

<sup>2</sup>Note that in this chapter the tilde represents the deterministic version of the fields. This should not be confused with the tilde used to represent the virtual fast process (4.1) in the previous chapter.

the linear operator  $L_U^0$ . For the linearized Euler equation ( $\beta = 0$ ), such inviscid damping mechanism is known as the Orr mechanism and the depletion of vorticity at the stationary streamlines. These mechanisms are summarised in section 4.2.3.

Moreover, we can see directly from (4.13) that if the linear operator is unstable ( $\lambda > 0$ ), the deterministic evolution diverges exponentially, so the auto-correlation function also diverges. The same way, if the linear operator has neutral eigenmodes ( $\lambda = 0$ ), then the auto-correlation function diverges linearly in time.

It is thus essential for the self-consistency of the theory to assume that the base flow  $U$  has no modes at all<sup>3</sup>. This is possible for a non-normal linear operator acting in an infinite-dimensional space, such as  $L_U^0$ , and this is actually the generic case. When  $\beta = 0$ , the only known stable base flows  $U$  with neutral modes are cases with localized vorticity profile [101] or the cosine flow in a square domain [11]. In some relevant jet situations (with  $\beta \neq 0$ ), the dynamics is also known to expel neutral modes from the spectrum [53].

However this is not the general case, and in particular in the barotropic equation ( $\beta \neq 0$ ), neutral modes such as Rossby waves are known to be of great importance in the dynamics of zonal jets [110]. Generalisation of the present theory to those cases is discussed in section 4.5.

In the following paragraph we detail the relation between correlation functions of the Ornstein-Uhlenbeck process  $\omega_m$  and the deterministic dynamics (4.14). Then in next paragraph, we present the Orr mechanism and the depletion of the vorticity at the stationary streamlines for the linearized 2D Euler equation.

## 4.2.2 Correlation functions from the solution of the deterministic linear equation

In this section, we show how to compute formally the vorticity two-points correlation function  $g_U(\mathbf{r}_1, \mathbf{r}_2, t) = \mathbb{E}[\omega_m(\mathbf{r}_1, t)\omega_m(\mathbf{r}_2, t)]$  where the vorticity  $\omega_m$  is given by (4.1), using the solution of the deterministic dynamics (4.14) with appropriate initial conditions. Those computations are very general, so we consider here that  $\alpha, \nu$  and  $t$  are finite, for simplicity. The expectation  $\mathbb{E}$  in the above definition of  $g_U$  is the average over realisations of the noise  $\eta_m$  in (4.1), it is different from the expectation  $\mathbb{E}_U$  which implicitly contains the limits  $\nu \ll \alpha$ ,  $\alpha \rightarrow 0$ ,  $t \rightarrow \infty$  (see section 4.1.1).

We will denote  $g \equiv g_U$  in this chapter and in the following one, to simplify the notation.

Observe that because of (4.7),  $\omega_{k_1, l_1}$  and  $\omega_{k_2, l_2}^*$  are statistically independent for  $(k_1, l_1) \neq (k_2, l_2)$ . Then, using (4.8), the vorticity two-points correlation function

---

<sup>3</sup>Remark first that because  $L_U^0$  is invariant under time reversal  $t \rightarrow -t$ ,  $U \rightarrow -U$  (recall that here  $\beta = 0$ ), the existence of a stable mode necessarily implies the existence of an unstable mode. Remark also that the action of  $L_U^0$  on zonally invariant functions  $f(y)$  is trivial: any such function is a neutral mode of  $L_U^0$ . We will thus consider the operator  $L_U^0$  acting on non-zonally invariant functions only, and assume that  $L_U^0$  restricted to such functions has no mode at all.

reads

$$\begin{aligned} g(\mathbf{r}_1, \mathbf{r}_2, t) &= \sum_{k=-\infty}^{\infty} \sum_{l=-\infty}^{\infty} \frac{c_{kl}}{2} e^{ik(x_1-x_2)} \mathbb{E} [\omega_{kl}(y_1, t) \omega_{kl}^*(y_2, t)] \\ &= \sum_{k>0, l} c_{kl} g_{kl}(\mathbf{r}_1, \mathbf{r}_2, t) \end{aligned} \quad (4.15)$$

with  $g_{kl}(\mathbf{r}_1, \mathbf{r}_2, t) = \frac{1}{2} e^{ik(x_1-x_2)} \mathbb{E} [\omega_{kl}(y_1, t) \omega_{kl}^*(y_2, t)] + \text{c.c.}$ , where c.c. stands for the complex conjugate. The linear stochastic differential equation (4.9) can be formally solved using the Itô stochastic integral representation

$$\omega_{kl}(y, t) = \sqrt{2} \int_0^t e^{-t_1 L_{U,k}} [e_l](y) dW_{kl}(t_1)$$

with  $e_l(y) = e^{ily}$ . Like in the one-dimensional case studied before, let's denote  $\tilde{\omega}_{kl}(y, t_1) = e^{-t_1 L_{U,k}} [e_l](y)$  the solution at time  $t_1$  of the deterministic linear dynamics  $\partial_t + L_{U,k}$  with initial condition  $e_l$ . Then,<sup>4</sup>

$$g_{kl}(\mathbf{r}_1, \mathbf{r}_2, t) = e^{ik(x_1-x_2)} \int_0^t \tilde{\omega}_{kl}(y_1, t_1) \tilde{\omega}_{kl}^*(y_2, t_1) dt_1 + \text{c.c.} \quad (4.16)$$

The vorticity-vorticity correlation function  $g_{kl}$  is expressed as a time-integral of a product of the deterministic vorticity  $\tilde{\omega}_{kl}$ , with appropriate initial condition. Such expression can be easily generalized to any kind of correlation functions, this will be extensively used in chapters 4 and 5.

### 4.2.3 Orr mechanism and depletion of the vorticity at the stationary streamlines

We have seen in the previous paragraph that stationary correlation functions of the Ornstein-Uhlenbeck process  $\omega_m$  can be computed from time-integrals like (4.16), involving solutions of the associated deterministic problem. We consider here the linear deterministic equation (4.14) with  $\beta = 0$ , and with no viscosity or linear friction,  $\alpha = \nu = 0$ .

The phenomenology is the following: while the vorticity shows filaments at finer and finer scales when time increases, non-local averages of the vorticity (such as the one leading to the computation of the streamfunction or the velocity) converge to zero in the long time limit.

As an example, consider the case of the linear Euler equation in a channel  $(x, y) \in \mathcal{D} = [0, 2\pi L_x] \times [0, L_y]$ , or in an infinite domain  $(x, y) \in \mathcal{D} = [0, 2\pi L_x] \times \mathbb{R}$ , where the background flow is  $U(y) = sy$  with a constant shear  $s$ . Then  $U''(y) = 0$  and  $L_{U,k} = ik sy$ . This is actually the case first studied by Orr [82]. According to the discussion of the previous paragraph, we consider the deterministic linear dynamics

$$\frac{\partial \tilde{\omega}_{k,l}}{\partial t} + ik sy \tilde{\omega}_{k,l}(y, t) = 0 \quad , \quad \tilde{\omega}_{k,l}(y, 0) = e^{ily}, \quad (4.17)$$

<sup>4</sup>A similar formula can easily be deduced for any stochastic force of the form  $C(\mathbf{r}_1, \mathbf{r}_2) = \sum_k e^{ik(x_1-x_2)} \sum_l c_{kl}(y_1) c_{kl}^*(y_2)$  from the explicit solution of the Ornstein-Uhlenbeck process as the stochastic integral  $\int_0^t e^{-t_1 L_{U,k}} [c_{kl}] dW_{kl}(t_1)$ . Here the key point is that the Fourier basis diagonalizes any translationally invariant correlation function.

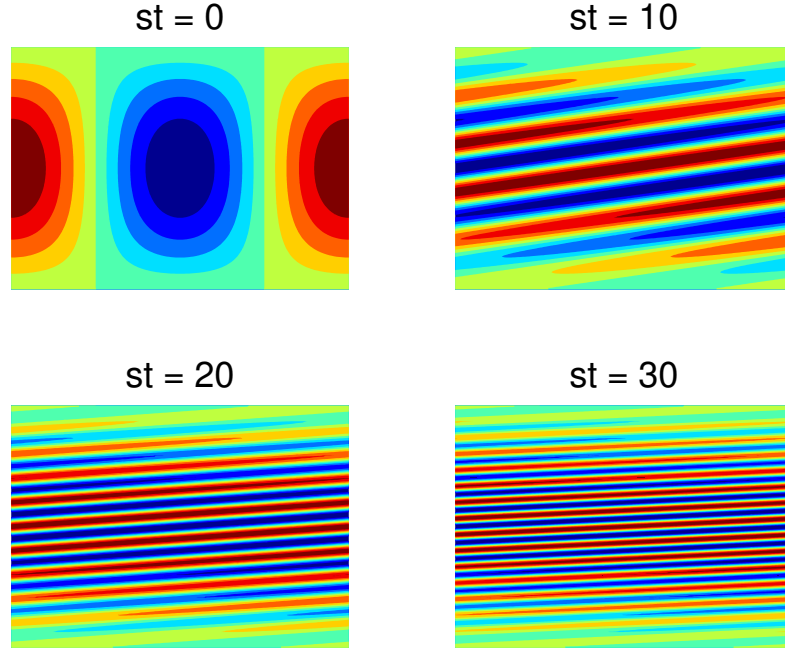


Figure 4.1: Evolution of the perturbation vorticity, advected by the constant shear base flow  $U(y) = sy$ .

which can be solved as  $\tilde{\omega}_{k,l}(y, t) = e^{-iksyt+ily}$ . This increasing filamentation of the vorticity field as time goes on can be seen in figure 4.1. The streamfunction is then computed as

$$\tilde{\psi}_{kl}(y, t) = \int dy' H_k(y, y') \tilde{\omega}_{k,l}(y', t), \quad (4.18)$$

where  $H_k$  is the Green function of the Laplacian  $\Delta_k = \partial_y^2 - k^2$ , i.e. such that  $\Delta_k H_k(y, y') = \delta(y - y')$ . Such integral is an oscillating integral. In the limit  $t \rightarrow \infty$ , it decays algebraically to zero with a power that depends on the order of differentiability of  $H_k$ . In this case, we can prove that

$$\tilde{\psi}_{kl}(y, t) \underset{t \rightarrow \infty}{\sim} \frac{\tilde{\omega}_{kl}^\infty(y) e^{-iksyt}}{(iks)^2 t^2}. \quad (4.19)$$

The velocity components can be computed from the stream function, using (4.19) we can thus show that the perturbation velocity also decays to zero algebraically. This is the so-called Orr mechanism [82]. The filamentation and the related relaxation mechanism with no dissipation for the velocity and streamfunction is very general for advection equations and it has an analog in plasma physics in the context of the Vlasov equation, where it is called Landau damping [78].

We note that in (4.19), the shear  $s$  plays the role of an effective damping rate. The generalization of the Orr mechanism to the case of any strictly monotonic profile  $U(y)$  —i.e. when the shear is always non-zero— has been first considered [22]. However, zonal jets necessarily have velocity extrema. The generalization of the

Orr mechanism to non-monotonic background flows  $U(y)$  has only been considered recently, in a work preliminary to this thesis [11]. As explained in paragraph 4.2.1, it is natural to assume that the linear operator  $L_{U,k}^0$  has no modes. With this hypothesis, it has been shown that [11]

$$\tilde{\omega}_{kl}(y, t) \underset{t \rightarrow \infty}{\sim} \tilde{\omega}_{kl}^\infty(y) e^{-ikU(y)t}, \quad (4.20)$$

where the function  $\tilde{\omega}_{kl}^\infty(y)$  depends on the whole velocity profile  $U(y)$ . The Orr mechanism for  $U(y) = sy$  is a particular case of (4.20), where  $\tilde{\omega}_{kl}^\infty(y) = e^{ily}$ . Using again results on oscillating integrals and the properties of the Laplacian Green function  $H$ , we have the asymptotic decay of the velocity components and of the streamfunction [11]

$$\tilde{u}_{kl}(y, t) \underset{t \rightarrow \infty}{\sim} \frac{\tilde{\omega}_{kl}^\infty(y)}{ikU'(y)} \frac{e^{-ikU(y)t}}{t}, \quad (4.21)$$

$$\tilde{v}_{kl}(y, t) \underset{t \rightarrow \infty}{\sim} \frac{\tilde{\omega}_{kl}^\infty(y)}{ik(U'(y))^2} \frac{e^{-ikU(y)t}}{t^2}, \quad (4.22)$$

and

$$\tilde{\psi}_{kl}(y, t) \underset{t \rightarrow \infty}{\sim} \frac{\tilde{\omega}_{kl}^\infty(y)}{(ikU'(y))^2} \frac{e^{-ikU(y)t}}{t^2}. \quad (4.23)$$

In all the above formulas, higher order corrections are present and decay with higher powers in  $1/t$ . From these expressions, it is clear that the local shear  $U'(y)$  acts as an effective damping mechanism.

Mathematical proofs of the asymptotic behaviour (4.20–4.23) have been given recently, either for the case of a strictly monotonic profile  $U(y)$  [119, 120] or for the relaxation of the non-linear 2D Euler equation after a small perturbation of the constant shear profile  $U(y) = sy$  [6], following the analogous theorem for non-linear Landau damping [72].

At this stage, a natural question is: what happens when the local shear vanishes? Indeed, a jet profile necessarily presents extrema of the velocity, at points  $y_0$  such that  $U'(y_0) = 0$ . Such points are called stationary points of the zonal jet profile. It can be shown that at the stationary points, the perturbation vorticity also decays for large times:  $\tilde{\omega}_{kl}^\infty(y_0) = 0$  [11]. This phenomenon has been called vorticity depletion at the stationary streamlines. It has been observed numerically that the extend of the area for which  $\tilde{\omega}_{kl}^\infty(y_0) \simeq 0$  can be very large, up to half of the total domain, meaning that in a large part of the domain, the shear is not the explanation for the asymptotic decay. The formula for the vorticity (4.20) is valid for any  $y$ . The formulas for the velocity and stream functions are valid for any  $y \neq y_0$ . Exactly at the specific point  $y = y_0$ , the damping is still algebraic with preliminary explanation given in [11], but a complete theoretical prediction is not yet available.

Equations (4.20),(4.21),(4.22),(4.23) give the asymptotic behaviour of vorticity, velocity and stream function in the deterministic linear 2D Euler equation, with no external damping mechanism. In the following, we will also be interested in the behaviour of these fields when a small friction or viscosity are present. For simplicity, we will only treat the case of a small friction (which acts uniformly at all scales):

$\nu = 0$ . Then, the linear friction leads to an exponential damping of all fields, with rate  $\alpha$ . It will be useful to generalize (4.20) as

$$\tilde{\omega}_{kl}^\alpha(y, t) = \tilde{\omega}_{kl}^\infty(y) e^{-(ikU(y)+\alpha)t} + \tilde{\omega}_{kl}^{r,\alpha}(y, t). \quad (4.24)$$

The above formula defines  $\tilde{\omega}_{kl}^{r,\alpha}$ . The classical Orr mechanism (4.20) is equivalent to the statement that for all values of  $\alpha$  (even for  $\alpha = 0$ ),  $\tilde{\omega}_{kl}^{r,\alpha}(y, t)$  is a bounded function both in  $y$  and  $t$ , and decays to 0 as  $t \rightarrow \infty$ . Actually, a refined formulation of the Orr mechanism is that  $\tilde{\omega}_{kl}^{r,\alpha}(y, t) \underset{t \rightarrow \infty}{\sim} O(e^{-\alpha t}/t^\gamma)$ , with  $\gamma > 0$  [11].

We have thus seen that, under the hypothesis that  $\beta = 0$  and that the linear operator  $L_U^0$  has no modes, the deterministic linear dynamics of the eddies leads to an inviscid damping of the velocity and of the streamfunction. As explained in the finite dimensional example, this is the key ingredient that can ensure the convergence of quantities like  $F_0[U]$ . We investigate this points in the following section.

### 4.3 Deterministic kinetic equation

The deterministic kinetic equation (3.12) describes the effective dynamics of zonal jets at the level of the Law of Large Numbers. It thus involves the average Reynolds' stress divergence  $F_0[U] = \mathbb{E}_U \langle \omega_m v_m \rangle$ , averaged over the stationary distribution of the inertial linear process (4.3). Using a pseudomomentum balance, we now show how to compute  $F_0[U]$  in practice, for a given zonal base flow  $U(y)$ .

#### 4.3.1 Pseudomomentum balance

In this paragraph we present the pseudomomentum balance for the linear dynamics of non-zonal degrees of freedom close to the zonal jet  $U$  (4.1) with  $\nu = 0$ . This yields the expression (4.30) of the average Reynolds' stress divergence  $F_0[U]$  as a function of a deterministic enstrophy density.

Let us first observe that using (4.8), the average Reynolds' force in the stationary state and in the inertial limit<sup>5</sup> can be decomposed into its contributions coming from each independent  $(k, l)$  forced mode

$$F_0[U](y) = \lim_{\alpha \rightarrow 0} \sum_{k>0, l} c_{kl} f_{kl}^\alpha(y), \quad (4.25)$$

with  $f_{kl}^\alpha(y) = \lim_{t \rightarrow \infty} f_{kl}(y, t)$  where

$$f_{kl}(y, t) = \pi l_x \mathbb{E} [v_{kl}(y, t) \omega_{kl}^*(y, t)] + \text{c.c.} = ik\pi l_x \mathbb{E} [\psi_{kl}(y, t) \omega_{kl}^*(y, t) - \text{c.c.}], \quad (4.26)$$

with  $\mathbb{E}$  the average over realisations of the noise  $\eta_m$  in the dynamics of  $\omega_m$  (or equivalently (4.9)) with a finite  $\alpha$  (here we already take the limit  $\nu = 0$ ).

<sup>5</sup>Here we consider first the limit  $t \rightarrow \infty$  and then  $\alpha \rightarrow 0$ , for simplicity. The opposite could be done easily and would give the same result (4.30). See also section 5.1 for details on the ordering of limits.

We introduce the pseudomomentum density  $P(y, t) = \frac{1}{2(U''(y) - \beta)} \mathbb{E} \langle \omega_m^2 \rangle$ . It is the ratio of the zonally averaged eddy enstrophy density and of (minus) the gradient of the jet vorticity.  $-P$  is also called the wave activity density. In linearized quasi-geostrophic dynamics like the linearized inertial barotropic equation, the total pseudomomentum  $\int dy P(y, t)$  is conserved (Eliassen-Palm relation [110]). This is in contrast with the eddy kinetic energy or the eddy enstrophy, which are exchanged with the zonal jet through Reynolds' stresses. Then, this is a very powerful tool to diagnose the sources and sinks of waves (like Rossby waves for instance) in data of geophysical flows or numerical simulations [47, 111].

Like for  $F_0$ , we can write  $P = \lim_{\alpha \rightarrow 0, t \rightarrow \infty} \sum_{k>0, l} c_{kl} p_{kl}$  with  $p_{kl}(y, t) = \frac{\pi l_x}{U''(y) - \beta} \mathbb{E} |\omega_{kl}(y, t)|^2$ . The evolution of  $p_{kl}$  is obtained applying the Itô formula to (4.9), which gives

$$f_{kl}(y, t) = \frac{\partial p_{kl}}{\partial t} + 2\alpha p_{kl} - \frac{2\pi l_x}{U''(y) - \beta}. \quad (4.27)$$

Note that (4.27) is a particular case of the pseudomomentum conservation law, indeed the integral over  $y$  of the l.h.s vanishes<sup>6</sup>, and the last two terms in the r.h.s come from the dissipation and forcing in (4.9).

The l.h.s of (4.27) gives the average Reynolds' force through (4.25), this is why pseudomomentum conservation is particularly relevant in our problem. If  $\alpha$  is non zero, then  $p_{kl}(y, t)$  has a finite limit  $p_{kl}^\alpha(y)$  as  $t \rightarrow \infty$ , and  $\partial p_{kl}/\partial t \rightarrow 0$  in the large time limit. (4.27) then becomes

$$f_{kl}^\alpha(y) = 2\alpha p_{kl}^\alpha(y) - \frac{2\pi l_x}{U''(y) - \beta}. \quad (4.28)$$

Using (4.16), the first term in the r.h.s of (4.28) can be written

$$2\alpha p_{kl}^\alpha(y) = \frac{4\alpha\pi l_x}{U''(y) - \beta} \int_0^\infty |\tilde{\omega}_{kl}(y, t_1)|^2 dt_1. \quad (4.29)$$

Assuming that the Orr mechanism (4.24) applies, we easily get  $2\alpha p_{kl}^\alpha(y) \rightarrow \frac{2\pi l_x}{U''(y) - \beta} |\tilde{\omega}_{kl}^\infty(y)|^2$  in the limit  $\alpha \rightarrow 0$ . Using this relation and (4.25), we get

$$F_0[U](y) \equiv \lim_{\alpha \rightarrow 0} \sum_{k>0, l} c_{kl} f_{kl}^\alpha(y) = 2\pi l_x \sum_{k>0, l} c_{kl} \frac{|\tilde{\omega}_{kl}^\infty(y)|^2 - 1}{U''(y) - \beta}. \quad (4.30)$$

In section 4.3.2, we will explain how to compute numerically  $F_0[U]$  using (4.30). In practice, such numerical computation can only be done with a non-zero  $\alpha$ . The convergence in the limit  $\alpha \rightarrow 0$  can be checked implementing (4.30) for various small values of  $\alpha$ , as illustrated in figure 4.2.

<sup>6</sup>By definition of  $f_{kl}$ ,

$$\int dy f_{kl}(y, t) = -k\pi l_x \text{Im} \mathbb{E} \int dy \psi_{kl}(y, t) \omega_{kl}^*(y, t) = 0$$

using  $\omega_{kl} = \Delta_k \psi_{kl}$  and two successive integrations by parts for the last equality.

### Behaviour at the extrema of the zonal vorticity profile

We remark that the expression (4.30) for  $F_0[U]$  could diverge at points  $y_0$  such that  $U''(y_0) - \beta = 0$  (extrema of the zonal vorticity profile). Actually, looking at the expression of the inertial linear operator  $L_{U,k}^0$  (equation (4.10) with  $\alpha = \nu = 0$ ), we see that at such points, the non-local term  $ik(U''(y_0) - \beta)\tilde{\psi}_{kl}$  vanishes. Then, the deterministic dynamics can be solved explicitly and gives the asymptotic vorticity profile  $\tilde{\omega}_{kl}^\infty(y_0) = \tilde{\omega}_{kl}(y_0, 0) = e^{iy_0}$ . This explains why  $F_0[U]$  does not diverge as  $y \rightarrow y_0$  (see also appendix E.3).

### Behaviour at the stationary points of the zonal velocity profile

At the stationary points  $y_s$  such that  $U'(y_s) = 0$ , the so-called depletion of vorticity [11] leads to  $\tilde{\omega}_{kl}^\infty(y_s) = 0$ , and to algebraic decays of the velocity components that are different from (4.21), (4.22). We can prove that the average Reynolds' force at such points  $F_0[U](y_s)$  also converges to a finite value in the inertial limit. This is presented in details in our publication [18]. Here, we only remark that the average Reynolds' force given by (4.30) can be computed also for  $y = y_s$  and is finite if  $U''(y_s) \neq 0$ . This is also observed in numerical computations, see figure 4.2.

### Expression with a more general type of forcing

As noted in section 4.2.2, the computations in this section can be easily generalized to the case of a forcing with spatial correlations of the form  $C(\mathbf{r}_1, \mathbf{r}_2) = \sum_k e^{ik(x_1 - x_2)} \sum_l c_{kl}(y_1)c_{kl}^*(y_2)$ . In particular, such forcing can describe cases with no invariance under translations in the  $y$  direction. The resulting average Reynolds' stress divergence then reads

$$F_0[U](y) = 2\pi l_x \sum_{k>0,l} \frac{|\tilde{\omega}_{kl}^\infty(y)|^2 - |c_{kl}(y)|^2}{U''(y) - \beta}, \quad (4.31)$$

where  $\tilde{\omega}_{kl}^\infty$  is the asymptotic vorticity profile defined in the Orr mechanism (4.20), for the deterministic dynamics  $\partial_t + L_{U,k}^0$  with initial condition  $c_{kl}(y)$ .

### 4.3.2 Numerical computation of the average Reynolds' stress divergence

In practice, the study of the effective dynamics of zonal jets reduces to the computation of the average Reynolds' force  $F_0$ . This cannot be done explicitly in general, except in some very particular cases [18, 23, 24, 104]. The investigation of zonal jets effective dynamics thus requires an efficient numerical computation of  $F_0$ .

$F_0$  can be computed as a linear transform of the solution of the Lyapunov equation (3.11). A natural way to solve the Lyapunov equation is to discretize the linear operator  $L_U^{(1)} + L_U^{(2)}$  and to directly solve the approximate dynamics. This is the traditional way and such a technique has for instance been used in most of previous works using S3T-CE2 [3, 33, 85, 104, 106].

However, we are here specifically interested in the inertial limit. One could solve the Lyapunov equation for finite values of  $\alpha$  and  $\nu$  and then study the asymptotic

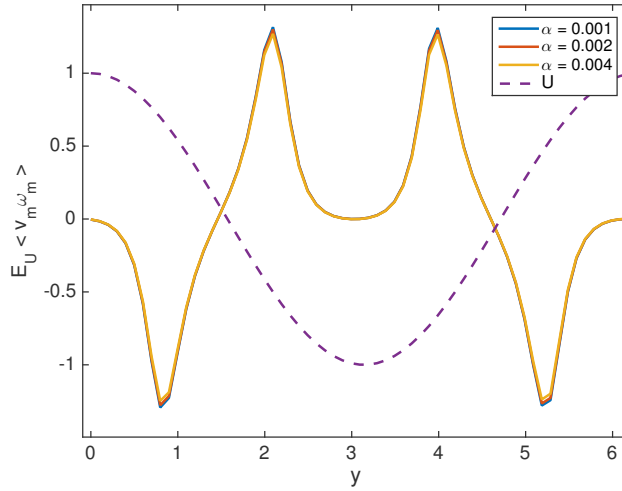


Figure 4.2: The Reynolds' stress divergence  $F_0[U](y) = \mathbb{E}_U \langle v_m \omega_m \rangle$  in the case of a cosine base profile  $U(y) = \cos y$ , with forcing at wavenumber  $k = 1.5$ ,  $l = 2$ .  $F_0[U]$  was computed using (4.30) and with the algorithm detailed in section 4.3.2 and appendix E, with different values of the friction coefficient  $\alpha$ . We observe the convergence of this calculation when  $\alpha \rightarrow 0$ , even at the stationary points  $y = 0$  and  $y = \pi$ .  $F_0[U]$  gives the instantaneous evolution of the zonal jet velocity:  $U$  will not change at the jet extrema  $y = 0$  and  $y = \pi$ , and  $U$  will weaken around the zeros at  $y = \pi/2$  and  $y = 3\pi/3$ . The Reynolds' stresses thus tend to narrow the jet.

behavior of the results when these parameters go to zero. While feasible, this route seems extremely difficult, as the numerical discretization would have to be increased as  $\nu$  goes to zero. One of the goals of this thesis was to find alternative ways to compute the average Reynolds' force. We now briefly present those methods, the details are summarized in appendix E.

### Integral form of the Lyapunov equation

The first idea has been to turn the stationary Lyapunov equation into an integral equation for  $f_{kl}^\alpha$ , which is known to be well-behaved in the inertial limit. The integral equation was then solved iteratively. This is presented in detail in [18] and in appendix E.1. The main limitation of this method is that the convergence of the iterative scheme for a given  $U$  cannot be predicted.

### Integration over frequencies of the resolvent

Another way to proceed is to compute  $f_{kl}^\alpha$  from the resolvent of the linear operator  $L_{U,k}^0$ , defined as the solution of the ordinary differential equation

$$\left( \frac{d^2}{dy^2} - k^2 \right) \phi - \frac{U''(y)}{U(y) - c - i\epsilon} \phi = \frac{e^{ily}}{ik(U(y) - c - i\epsilon)}, \quad (4.32)$$

see appendix D.2 for details. (4.32) can be solved numerically very easily [11]. The computation of  $f_{kl}^\alpha$  then reduces to an integration over frequencies  $c$  of a function

of the resolvent. This method is presented in another publication [12], and in appendix E.2.

### Computation using the pseudomomentum balance

The last method relies on the expression of  $f_{kl}^\alpha$  deduced from the pseudomomentum balance, (4.30). The computation of  $f_{kl}^\alpha$  reduces to the computation of  $\tilde{\omega}_{kl}^\infty$ , the asymptotic vorticity profile defined in the Orr mechanism (4.20). This is simple as  $\tilde{\omega}_{kl}^\infty$  is related to the asymptotic solution of a deterministic linear equation. Actually, a very simple way to compute  $\tilde{\omega}_{kl}^\infty$  as a function of the resolvent given by (4.32) is proposed in [11], see also appendix E.3 of this thesis. In contrast with the second method, it does not involve an integration over frequencies, but only the computation of the resolvent at a given frequency for each  $y$ . The computation is then much faster. The result for  $F_0$  is shown in figure 4.2.

Note that in all of the three proposed ways to compute  $F_0$ , the viscosity is exactly zero, and the limit  $\alpha \rightarrow 0$  can be achieved very easily, as illustrated in figure 4.2. Being able to compute the average Reynolds' force in the stationary state of the eddy dynamics, in the limit of no dissipation is an important result in itself. In particular, an interesting perspective is to use these methods to study the effective evolution of jets through the deterministic kinetic equation (3.12). Another way to proceed would be to compute directly the attractors of zonal jet dynamics (in the case where  $\zeta = 0$  in (3.12)) as the solutions of

$$F_0[U] = U - \frac{\nu}{\alpha} \frac{\partial^2 U}{\partial y^2}, \quad (4.33)$$

for instance using an iterative scheme.

## 4.4 Stochastic kinetic equation

We now consider the effective dynamics of zonal jets at second order in  $\alpha$ , equation (3.7) in page 39. In particular, this equation involves a noise term  $\xi[U]$  that represents the typical fluctuations of the time averaged Reynolds' force  $\frac{1}{\Delta t} \int_0^{\Delta t} \langle v_m \omega_m \rangle(s) ds$ . More precisely,  $\xi[U]$  is a gaussian noise with zero mean and correlations (for a fixed  $U$ )

$$\mathbb{E} [\xi[U](y_1, t_1) \xi[U](y_2, t_2)] = \delta(t_1 - t_2) \Xi[U](y_1, y_2) \quad (4.34)$$

with  $\Xi[U]$  given in (3.22), page 45. The integrand in (3.22) is usually called the autocorrelation function of  $f(z, \tilde{w}_z(s))$  [44, 77]. Then,  $\Xi[U]$  is called the integrated autocorrelation function.

Like  $F_0$  in (4.25),  $\Xi[U]$  is defined<sup>7</sup> as the limit when  $\alpha \rightarrow 0$  of an expectation in the steady state of  $\omega_m$ . For future convenience, we define  $\Xi^\alpha$  as the integrated autocorrelation function of the Reynolds' force with a small but non-zero  $\alpha$ , such that

$$\Xi[U] = \lim_{\alpha \rightarrow 0} \Xi^\alpha[U], \quad (4.35)$$

<sup>7</sup>Formally, we should first take the limit  $\alpha \rightarrow 0$  and then  $t \rightarrow \infty$  to compute  $\Xi$ . Inverting the ordering of limits does not have any consequences here, as will be argued in chapter 5.

where  $\Xi^\alpha$  is defined as

$$\begin{aligned} \Xi^\alpha[U](y_1, y_2) = & \int_0^\infty \left\{ \mathbb{E}_U^\alpha [\langle v_m \omega_m \rangle (y_1, s) \langle v_m \omega_m \rangle (y_2, 0)] \right. \\ & \left. - \mathbb{E}_U^\alpha [\langle v_m \omega_m \rangle (y_1, s)] \mathbb{E}_U^\alpha [\langle v_m \omega_m \rangle (y_2, 0)] + (y_1 \leftrightarrow y_2) \right\} ds, \end{aligned} \quad (4.36)$$

where  $\mathbb{E}_U^\alpha[\cdot]$  is the average in the stationary state of (4.1) (with  $\nu = 0$ ), and  $(y_1 \leftrightarrow y_2)$  is the symmetric expression with  $y_1$  and  $y_2$  interchanged.

In this section we give an expression of  $\Xi^\alpha[U]$  that enables its numerical computation, and that will be useful in chapter 5 in order to address the convergence of  $\Xi^\alpha$  in the limit  $\alpha \rightarrow 0$ . We also present a simple case where  $\Xi^\alpha[U]$  can be computed explicitly.

#### 4.4.1 The integrated autocorrelation function in terms of two-points correlation functions

To state these results more precisely, we need to decompose  $\Xi^\alpha[U]$  into its contributions coming from each forcing mode. Using (4.8) and (4.36), we get

$$\begin{aligned} \Xi^\alpha[U](y_1, y_2) = & \sum_{(k, k', l, l') \in \mathbb{Z}^4} \frac{c_{kl}}{2} \frac{c_{k'l'}}{2} \int_0^\infty \mathbb{E}_U^\alpha [ [ (v_{kl} \omega_{-k, -l}) (y_1, s) (v_{k'l'} \omega_{-k', -l'}) (y_2, 0) \\ & + (y_1 \leftrightarrow y_2) ] ] ds, \end{aligned}$$

where  $\mathbb{E}_U^\alpha[[\cdot]]$  denotes the covariance. The vorticity  $\omega_{kl}$  (defined in (4.9) page 50) and the associated meridional velocity  $v_{kl}$  are Ornstein-Uhlenbeck processes with zero initial condition, so they are gaussian random variables at all times [44]. Then Isserli-Wick theorem can be applied, and the four-points correlation functions can be written as products of two-points correlation functions. Using the fact that  $\omega_{k_1, l_1}$  and  $\omega_{k_2, l_2}^*$  are statistically independent for  $(k_1, l_1) \neq (k_2, l_2)$ , we get

$$\Xi^\alpha[U](y_1, y_2) = \sum_{(k, l) \in \mathbb{Z}^2} c_{kl}^2 \left\{ \Xi_{kl}^\alpha(y_1, y_2) + \Xi_{kl}^\alpha(y_2, y_1) \right\} \quad (4.37)$$

with  $\Xi_{kl}^\alpha(y_1, y_2) = C_{kl}^\alpha(y_1, y_2) + D_{kl}^\alpha(y_1, y_2)$  where

$$C_{kl}^\alpha(y_1, y_2) = \frac{1}{4} \int_0^\infty \mathbb{E}_U^\alpha [v_{kl}(y_1, s) v_{-k, -l}(y_2, 0)] \mathbb{E}_U^\alpha [\omega_{-k, -l}(y_1, s) \omega_{kl}(y_2, 0)] ds \quad (4.38)$$

and

$$D_{kl}^\alpha(y_1, y_2) = \frac{1}{4} \int_0^\infty \mathbb{E}_U^\alpha [v_{kl}(y_1, s) \omega_{-k, -l}(y_2, 0)] \mathbb{E}_U^\alpha [\omega_{-k, -l}(y_1, s) v_{kl}(y_2, 0)] ds. \quad (4.39)$$

Note that, by definition of the covariance  $\mathbb{E}_U^\alpha[[\cdot]]$ , the correlations  $\mathbb{E}_U^\alpha [v_{kl}(y_1, s) \omega_{-k, -l}(y_1, s)]$  and  $\mathbb{E}_U^\alpha [v_{k'l'}(y_2, 0) \omega_{-k', -l'}(y_2, 0)]$  have been cancelled in the computation of  $\Xi_{kl}^\alpha[U]$ .

Following the procedure described in section 4.2.2, the two-points correlation functions appearing in (4.38) and (4.39) can be expressed as

$$T_{\omega\omega}^\alpha(k, l, y_1, y_2, s) \equiv \frac{1}{2} \mathbb{E}_U^\alpha [\omega_{-k, -l}(y_1, s) \omega_{k, l}(y_2, 0)] = \int_0^\infty dt_1 \tilde{\omega}_{-k, -l}(y_1, s+t_1) \tilde{\omega}_{k, l}(y_2, t_1), \quad (4.40)$$

$$T_{vv}^\alpha(k, l, y_1, y_2, s) \equiv \frac{1}{2} \mathbb{E}_U^\alpha [v_{k,l}(y_1, s) v_{-k,-l}(y_2, 0)] = \int_0^\infty dt_1 \tilde{v}_{k,l}(y_1, s+t_1) \tilde{v}_{-k,-l}(y_2, t_1), \quad (4.41)$$

$$T_{v\omega}^\alpha(k, l, y_1, y_2, s) \equiv \frac{1}{2} \mathbb{E}_U^\alpha [v_{k,l}(y_1, s) \omega_{-k,-l}(y_2, 0)] = \int_0^\infty dt_1 \tilde{v}_{k,l}(y_1, s+t_1) \tilde{\omega}_{-k,-l}(y_2, t_1), \quad (4.42)$$

$$T_{\omega v}^\alpha(k, l, y_1, y_2, s) \equiv \frac{1}{2} \mathbb{E}_U^\alpha [\omega_{-k,-l}(y_1, s) v_{k,l}(y_2, 0)] = \int_0^\infty dt_1 \tilde{\omega}_{-k,-l}(y_1, s+t_1) \tilde{v}_{k,l}(y_2, t_1), \quad (4.43)$$

where  $\tilde{\omega}_{kl}$  is the solution of the deterministic linear dynamics  $\partial_t + L_{U,k}$  with initial condition  $e_l$ , and  $\tilde{v}_{kl}$  is the associated meridional velocity.

The second numerical method explained in section 4.3.2 can be easily generalized to compute  $\Xi^\alpha[U]$ . Indeed, the two-points correlation functions defined in equations (4.40–4.43) can be expressed as integrals over frequency of products of the resolvent (see appendices D.2 and E.2). Then, the integrals over  $s$  in (4.38, 4.39) can also be expressed as integrals over frequencies, which can be computed numerically. These computations are very similar to those presented in appendix E.2, so we do not report them here. Instead, we present a case where  $\Xi_{kl}^\alpha$  can be computed explicitly, which is easier to interpret qualitatively.

#### 4.4.2 Explicit computation in the case of a constant shear

Consider the case of the linear Euler equation in a channel  $(x, y) \in \mathcal{D} = [0, 2\pi L_x) \times [0, L_y]$ , or in an infinite domain  $(x, y) \in \mathcal{D} = [0, 2\pi L_x) \times \mathbb{R}$ , where the background flow is  $U(y) = sy$  with a constant shear  $s$ . Then the linearized deterministic dynamics of  $\tilde{\omega}_{k,l}$  reads

$$\partial_{t_1} \tilde{\omega}_{k,l}(y, t_1) + (iksy + \alpha) \tilde{\omega}_{k,l}(y, t_1) = 0 \quad , \quad \tilde{\omega}_{k,l}(y, 0) = e^{ily}, \quad (4.44)$$

which can be solved as  $\tilde{\omega}_{k,l}(y, t_1) = e^{-(iksy+\alpha)t_1+ily}$ . The associated velocity field is then obtained as

$$\tilde{v}_{k,l}(y, t_1) = ik \int dy' H_k(y, y') e^{-(iksy'+\alpha)t_1+ily'}, \quad (4.45)$$

where  $H_k(y, y')$  is the Green function of the Laplacian  $\Delta_k = \partial_y^2 - k^2$ , i.e. such that  $\Delta_k H_k(y, y') = \delta(y - y')$ .

The correlation functions defined in equations (4.40–4.43) can be easily computed using these explicit expressions of  $\tilde{\omega}_{kl}$  and  $\tilde{v}_{kl}$ . Then,  $\Xi^\alpha[U]$  is computed using (4.37, 4.38, 4.39). The results are reported in details in section 5.2.1 (page 72).

In figure 4.3 is represented the real part of  $\Xi_{kl}^\alpha$  for  $k = l = 1$ ,  $s = 1$  and  $\alpha = 0.01$ . We observe that  $\Xi_{kl}^\alpha(y, y')$  is dominated by its value on the diagonal  $y = y'$ . In chapter 5, we will actually prove that the value of  $\Xi_{kl}^\alpha(y, y')$  at points such that  $U(y) = U(y')$  (i.e. on the diagonal  $y = y'$  for the constant shear flow  $U(y) = sy$ ) is expected to diverges as  $1/\alpha$  in the inviscid limit  $\alpha \rightarrow 0$ , while it is expected to converge to a finite value elsewhere. This is consistent with the qualitative behaviour observed in figure 4.3. This behaviour is related to the well-definiteness of the kinetic equation (3.7), as discussed in more details in next chapter.

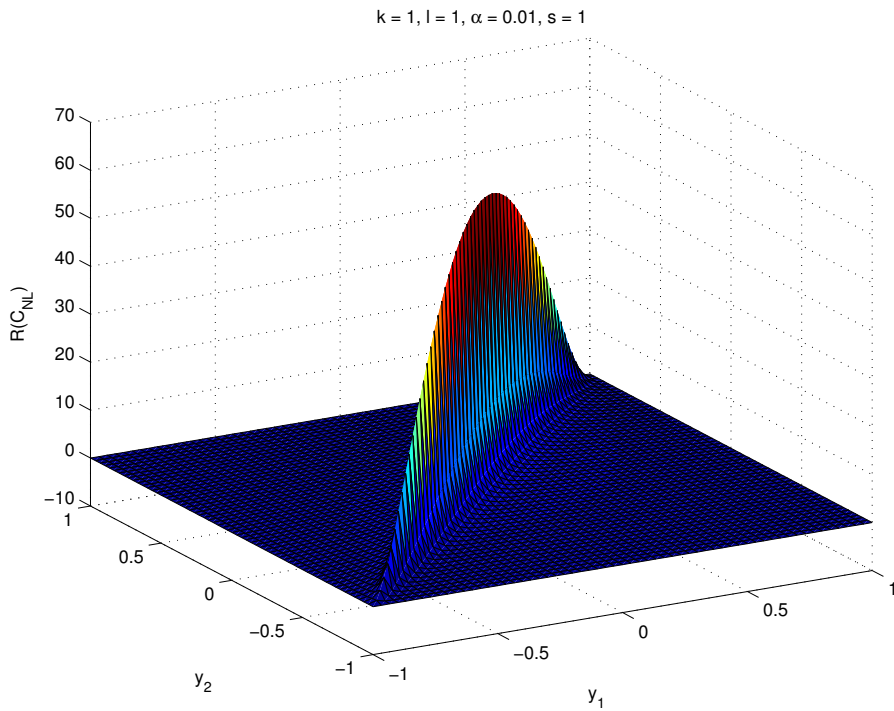


Figure 4.3: Real part of the integrated autocorrelation function  $\Xi_{kl}^\alpha(y_1, y_2)$  (defined in (4.37)) as a function of  $(y_1, y_2)$  in the case of a constant shear base flow  $U(y) = sy$ , computed with equations (5.16, 5.18) for given values of the parameters:  $k = l = 1$ ,  $s = 1$  and  $\alpha = 0.01$ . This quantity is clearly dominated by the values on the diagonal  $y_1 = y_2$ , where it is expected to diverge as  $1/\alpha$  when  $\alpha \rightarrow 0$ .

## 4.5 Perspectives

In section 4.3, we have given an explicit expression of the average Reynolds' force  $F_0$  in terms of the asymptotic profile of deterministic vorticity. This led both to a simple proof of the fact that  $F_0$  is finite, and to a very efficient way to compute it numerically. Those results apply to the linearized Euler equation, i.e. to the case  $\beta = 0$ . For geophysical applications, it would be very interesting to understand if these results also apply to the linearized beta-plane equation.

So far, the asymptotic behavior of the linearized barotropic equation has been mostly studied in the particular case of a parabolic jet profile, such that the gradient of potential vorticity  $U''(y) - \beta$  either exactly vanishes [24], or is small [23]. In the first case, the deterministic linear dynamics can be solved explicitly, and it can be shown that an inviscid damping mechanism (very similar to the Orr mechanism in the constant shear case) leads to an algebraic decay of the stream function as  $\tilde{\psi}_k \sim t^{-1/2}$ . This decay is not fast enough to insure the convergence of the average Reynolds' force. In this very particular case, the deterministic kinetic theory is not self-consistent. However, this case might be a very singular one, indeed the case of a small but strictly negative potential vorticity gradient [23] leads to a decay of the stream function as  $\tilde{\psi}_k \sim t^{-3/2}$ . Then the average Reynolds' force converges, and the theory is self-consistent at first order.

The other hypothesis made to obtain the previous results is that the linear operator  $L_U^0$  has no modes, neither unstable nor neutral. While the assumption that there is no unstable mode is very natural, it can seem at first restrictive to assume that no neutral mode exist. However, this is the generic case for the 2D Euler equation. The only examples of stable flows for the 2D Euler dynamics with neutral modes we are aware of are cases with localized vorticity profile [101] or the cosine flow in a square domain [11].

When it comes to the linear barotropic equation, this assumption might be more restrictive. Indeed, the Rossby waves are very common neutral modes of the linearized barotropic dynamics, and are expected to exist in geophysical situations [87]. However, we note that a mechanism of expulsion of modes in the presence of a background zonal jet has been observed in specific cases, and seems to hold in the atmosphere [53]. In the case where the linear dynamics would still have neutral modes, the typical time scale of propagation of the wave would be an intermediate time scale between the evolution of the jet and the evolution of the eddies. This contribution should thus be extracted from the dynamics of eddies, and the effective equation of jets dynamics would be modified. Investigating this point would be very interesting for the kinetic theory.

Another natural perspective of the results of this chapter is the numerical integration of the kinetic equation (3.7). As discussed in sections 3.2.1 and 4.3.2, the deterministic part of the kinetic equation is very close to the S3T-CE2 system, which has been simulated and compared with direct numerical simulations of the stochastic barotropic model in many cases [3, 33, 85, 104, 106]. In all those studies, the average Reynolds' force  $F_0$  is computed solving the Lyapunov equation in a standard way (discretizing the linear operator), with finite viscosity and linear friction. The use of the expression (4.30) of  $F_0$  through the algorithm described in section

4.3.2 provides a way to investigate stationary zonal jets in the limit of no viscosity and small dissipation  $\alpha \rightarrow 0$ . Moreover, an efficient implementation of such algorithm could possibly provide an extremely fast simulation of large scale dynamics in barotropic models, which is part of a very challenging issue in geophysical fluid dynamics modelling [66].

Besides, the stochastic part of the kinetic equation has never been simulated. Such simulation could be done using the numerical method proposed in section 4.4. It would provide a direct description of zonal jet statistics around the attractors of the deterministic kinetic equation (3.12), which is not possible through simulations of the deterministic kinetic equation (or equivalently S3T-CE2).

# Chapter 5

## Theoretical justification of the kinetic theory

Using a stochastic averaging approach (equivalent to the Law of Large Numbers and the Central Limit Theorem), we derived in chapter 3 the following effective dynamics of zonal jets in the limit of small forces and dissipation<sup>1</sup>:

$$\frac{\partial U}{\partial t} = \alpha F_0[U] - \alpha U + \alpha \xi[U], \quad (5.1)$$

where  $F_0[U](y) = \mathbb{E}_U \langle \omega_m v_m \rangle$  and  $\xi[U]$  is a gaussian white noise with spatial correlations  $\Xi[U]$ , given in (3.22) page 45.  $F_0$  and  $\Xi$  are averages in the statistically stationary state of the linear inertial dynamics

$$\frac{\partial \omega_m}{\partial t} + L_U^0[\omega_m] = \sqrt{2} \eta_m, \quad (5.2)$$

where  $L_U^0$  is the operator for the linearized barotropic dynamics close to the fixed base flow  $U(y)$  with no dissipation (see (4.2) page 49). The effective dynamics (5.1) is called the kinetic equation and the linearized dynamics (5.2) is called the virtual fast process.

We discuss in this chapter the hypothesis for the validity of this effective equation, as already discussed in a more general setting in section 2.4 (page 35). We first enumerate those hypothesis, and then present the main results of this chapter.

1. We first need to make sure that (5.2) has a stationary distribution (invariant measure), so that the expectations  $\mathbb{E}_U$  actually have a meaning.

As already pointed out in the previous chapter, this is not obvious as (5.2) is forced but not dissipated. The existence of such stationary distribution is the consequence of an inviscid damping mechanism, known in the case of the 2D Euler equation as the Orr mechanism (presented in section 4.2 page 50). However, such damping is not uniform on all observables, and we will see that the expectation  $\mathbb{E}_U$  of some observables is actually infinite.

---

<sup>1</sup>We focus here on the physically most relevant terms, i.e. we assume  $\zeta = 0$  and we neglect both viscosity and the correction drift of order  $\alpha^2$  (recall that the term of order  $\alpha^{3/2}$  in (3.7) is exactly zero, see section 3.3).

2. For this reason, we have to make sure that the kinetic equation (5.1) is well-defined, in the sense that  $F_0$  is finite and  $\Xi$  is a distribution (generalized function).

From the qualitative point of view of the averaging procedure (see section 2.4), we have to make sure that:

3. The fast process (5.2) is ergodic (in a sense that will be precised later on).
4. The time scale separation between slow and fast components is satisfied in the effective description (5.1, 5.2) (self-consistency).

In the previous chapter, we have already seen that the average Reynolds stress divergence  $F_0$  is finite (see section 4.3.1), using the Orr mechanism (4.20). In this chapter, we will use the Orr mechanism to prove that

- the stochastic inertial linear dynamics (5.2) has a stationary distribution. This is done in section 5.1; it proves point 1.
- the integrated autocorrelation function of the Reynolds' stress divergence  $\Xi[U]$  is a distribution (generalized function). This is presented in section 5.2. This result, together with the result of the previous chapter about  $F_0[U]$ , proves point 2.

The properties of  $\Xi[U]$  have important consequences for the zonal jet energy balance, as explained in section 5.3.2. It will also be further discussed in chapter 6.

Then in section 5.3 we discuss points 3. and 4., using the theoretical computations of section 5.2. We will prove ergodicity of the fast process in a weak sense that will be precised, and we will prove that a time scale separation exists between the effective dynamics of  $U$  in the kinetic equation (5.1) and the dynamics of  $\omega_m$  in (5.2), in the sense of (2.33) (page 36).

Some of the technical points studied in this chapter will be illustrated with numerical simulations of the linearized barotropic equation in chapter 6.

## 5.1 Stationary distribution of the eddy vorticity in the inertial limit

As discussed in chapter 3, it is essential to make sure that the linear stochastic process corresponding to the inertial linearized evolution of non-zonal degrees of freedom (eddies) close a base flow  $U$  has a stationary distribution. We discuss this issue in this section.

We consider the linear dynamics with no dissipation (5.2), this equation describes a linear stochastic Gaussian process, or Ornstein-Uhlenbeck process. Whatever the initial condition, its stationary distribution is the gaussian functional [44]

$$G_U[\omega_m] = \frac{1}{Z_U} \exp \left( -\frac{1}{2} \int d\mathbf{r}_1 d\mathbf{r}_2 \omega_m(\mathbf{r}_1) (g^\infty)^{-1}(\mathbf{r}_1, \mathbf{r}_2) \omega_m(\mathbf{r}_2) \right), \quad (5.3)$$

where  $(g^\infty)^{-1}$  is the inverse of the stationary vorticity auto-correlation function  $g^\infty$  (here understood as a linear operator). We recall that  $g^\infty$  depends parametrically on  $U$ .

We thus have to make sure that  $g^\infty$  actually exists. By definition,  $g^\infty$  is the large-time limit of the vorticity two-points correlation function  $g(\mathbf{r}_1, \mathbf{r}_2, t) = \mathbb{E}[\omega_m(\mathbf{r}_1, t)\omega_m(\mathbf{r}_2, t)]$ . The evolution of  $g$  is given by the Lyapunov equation

$$\frac{\partial g}{\partial t} + \left(L_U^{0(1)} + L_U^{0(2)}\right)g = 2C_m, \quad (5.4)$$

where  $L_U^{0(i)}$  is the operator  $L_U^0$  acting on the variable  $\mathbf{r}_i$ . We will prove that equation (5.4) has as asymptotic solution  $g^\infty$  for large time. This may seem paradoxical as we deal with a linearized dynamics with a stochastic force and no dissipation mechanism. We explain in this section that the Orr mechanism presented in section 4.2.3 (page 53) acts as an effective dissipation. However this effect is not uniform on all observables. We will prove that  $g$  has a limit  $g^\infty$  in the sense of distributions, from which we will be able to prove that velocity-like observables (like the kinetic energy contained in the non-zonal degrees of freedom) are finite in the large-time limit. By contrast, observables involving only vorticity (like the non-zonal enstrophy) will diverge in the large-time limit.

The statement that “the Gaussian process corresponding to the inertial linearized evolution close to a base flow  $U$  has a stationary distribution” must thus be understood with care: not all observable converge.

### 5.1.1 The stationary vorticity correlation function is a distribution

We study here the behaviour for large times of  $g_{kl}(\mathbf{r}_1, \mathbf{r}_2, t) \equiv \frac{1}{2}e^{ik(x_1-x_2)}\mathbb{E}[\omega_{kl}(y_1, t)\omega_{kl}^*(y_2, t)] + \text{c.c.}$  where  $\mathbb{E}$  is the average over realizations of the gaussian white noise  $\eta_{kl}$  in the linear dynamics

$$\frac{\partial \omega_{kl}}{\partial t} + L_{U,k}^0[\omega_{kl}] = \sqrt{2}e^{ily} \eta_{kl} \quad (5.5)$$

with  $L_{U,k}^0 = ikU + ik(\beta - U'')\Delta_k^{-1}$  (see section 4.1.2 in page 50 for details of the Fourier decomposition).

From (4.16) and the Orr mechanism (4.20), we get

$$\begin{aligned} g_{kl}(\mathbf{r}_1, \mathbf{r}_2, t) &= e^{ik(x_1-x_2)} \int_0^t \tilde{\omega}_{kl}(y_1, t_1)\tilde{\omega}_{kl}^*(y_2, t_1) dt_1 + \text{c.c.} \\ &= e^{ik(x_1-x_2)} \tilde{\omega}_{kl}^\infty(y_1)\tilde{\omega}_{kl}^{\infty*}(y_2) \int_0^t e^{-ik[U(y_1)-U(y_2)]t_1} dt_1 + g_{kl}^r(\mathbf{r}_1, \mathbf{r}_2, t) + \text{c.c.}, \end{aligned} \quad (5.6)$$

where  $g_{kl}^r$  contains the corrections due to the decaying part of  $\tilde{\omega}_{kl}$ . We readily see that if  $U(y_1) \neq U(y_2)$ , then  $g_{kl}(y_1, y_2, t)$  has a finite limit when  $t \rightarrow \infty$ . By contrast, if  $U(y_1) = U(y_2)$  then the first term in (5.6) diverges linearly with  $t$ . In section 5.1.2, we will argue that  $g_{kl}^r(\mathbf{r}_1, \mathbf{r}_2, t)$  is subdominant with respect to this divergence, so the leading order divergence of  $g_{kl}$  at points such that  $U(y_1) = U(y_2)$  is given by the first term in (5.6).

Using Plemelj formula (D.2) in appendix D.1, we get  $g_{kl} \rightarrow g_{kl}^\infty$  in the limit  $t \rightarrow \infty$ , with

$$g_{kl}^\infty(\mathbf{r}_1, \mathbf{r}_2) = e^{ik(x_1-x_2)} \left\{ \frac{\pi |\tilde{\omega}_{kl}^\infty(y_1)|^2}{|kU'(y_1)|} \delta(y_1 - y_2) - iPV \left( \frac{\tilde{\omega}_{kl}^\infty(y_1) \tilde{\omega}_{kl}^{\infty*}(y_2)}{k(U(y_1) - U(y_2))} \right) \right\} + g_{kl}^r(\mathbf{r}_1, \mathbf{r}_2, \infty) + \text{c.c.}, \quad (5.7)$$

where  $PV$  denotes the Cauchy Principal Value distribution.

To write this formula, we have assumed that  $U$  is a monotonic profile. Then each frequency  $kU(y)$  in the asymptotic oscillations of the deterministic vorticity (4.20) corresponds to a single streamline  $y = \text{cte}$ . If  $U$  is non-monotonic, two streamlines may have the same frequency, and resonances between streamlines should be considered. The formula would then be more intricate, but the result can be easily obtained from (4.20) and the conclusion that  $g_{kl}$  converges to a distribution is still true. We note that the difficult theoretical result related to those resonances is to establish (4.20) [11].

We recall that  $g$  is the weighted sum of  $g_{kl}$  over  $(k, l)$ , see equation (4.15). We conclude that the Lyapunov equation (5.4) has a stationary solution understood as a distribution.

Equation (5.7) also implies that at all points such that  $y_1 = y_2$ ,  $g$  diverges in the stationary state. This means that the enstrophy contained in the non-zonal degrees of freedom  $\frac{1}{2}g^\infty(\mathbf{r}, \mathbf{r}) = \frac{1}{2}\mathbb{E}_U[\omega_m(\mathbf{r})^2]$  is infinite. In paragraph 5.1.2, we will see how this divergence is regularized by a small linear friction. By contrast, any observable that can be computed as an integral of  $g^\infty$  multiplied by a continuous function is finite.

As an example, consider the velocity auto-correlation function and the kinetic energy density. The velocity two-points correlation function is a quadratic quantity, that can be obtained directly as a linear transform from the vorticity auto-correlation function  $g$ , or from the deterministic solution to the linearized operator. From (4.15), we see that the contributions from each forcing mode add up:

$$\mathbb{E}_U[\mathbf{v}_m(\mathbf{r}_1, t) \cdot \mathbf{v}_m(\mathbf{r}_2, t)] = \sum_{k>0, l} c_{kl} E_{kl}(\mathbf{r}_1, \mathbf{r}_2),$$

with

$$E_{kl}(\mathbf{r}_1, \mathbf{r}_2) = e^{ik(x_1-x_2)} \int_0^\infty \tilde{\mathbf{v}}_{kl}(y_1, t_1) \cdot \tilde{\mathbf{v}}_{kl}^*(y_2, t_1) dt_1 + \text{c.c.}, \quad (5.8)$$

where  $\tilde{\mathbf{v}}_{kl}$  is the velocity of the deterministic solution to the linearized equation  $\partial_t \tilde{\omega}_{kl} + L_{U,k}^0[\tilde{\omega}_{kl}] = 0$ , with initial condition  $\mathbf{e}_l$ . Alternatively,  $E_{kl} = \mathbf{V}^{(1)} \mathbf{V}^{(2)*} g_{kl}^\infty$ , where  $\mathbf{V} = -\nabla[\Delta^{-1}(\cdot)] \times \mathbf{e}_z$  is the linear operator giving the velocity from the vorticity and  $\mathbf{V}^{(1)}$ , resp.  $\mathbf{V}^{(2)}$  are the operator  $\mathbf{V}$  acting on the first, or second variable respectively. From (4.21, 4.22), it is clear that  $E_{kl}$  and thus the velocity two-points correlation functions are finite, even if no dissipation is present in the dynamics of  $\mathbf{v}_m$ .

We note that  $\alpha \mathbb{E}_U[\mathbf{v}_m^2(\mathbf{r}_1, t)]$  is the eddy kinetic energy density (the kinetic energy contained in the non-zonal degrees of freedom). We thus conclude that in the limit of very small  $\alpha$ , the non-zonal kinetic energy is proportional to  $\alpha$ , and that its value can be estimated from the Lyapunov equation with  $\alpha = 0$ . Those results are

extremely important, as they prove that the assumption that velocity perturbations close to the zonal flow are of order  $\sqrt{\alpha}$  is self-consistent.

### 5.1.2 Regularization of the eddy enstrophy due to a small linear friction

We have proved in the previous paragraph that the average eddy kinetic energy density and the velocity two-points correlation functions have limit values independent on  $\alpha$  or the viscosity in the inertial limit. This behaviour is similar to the behaviour of the average Reynolds' force  $F_0$ , as explained in chapter 4. By contrast, the vorticity two-points correlation function  $g^\infty(\mathbf{r}_1, \mathbf{r}_2)$  diverges point-wise for any two points such that  $U(y_1) = U(y_2)$ , and is well defined as a distribution, as shown in equation (5.7). This also implies that the enstrophy contained in non-zonal degrees of freedom for  $\alpha = 0$ ,  $\frac{1}{2}g^\infty(\mathbf{r}, \mathbf{r}) = \frac{1}{2}\mathbb{E}_U[\omega_m(\mathbf{r})^2]$ , is infinite. We now address how this is regularized for small values of  $\alpha$ .

We will prove that in the vicinity of  $y_1 = y_2$ , the singular behavior of  $g_{kl}^\infty$  is regularized in a universal way (with shape functions independent on  $U$ ) over a scale  $\alpha/|kU'(y_1)|$ . Moreover we can prove that  $\mathbb{E}_U^\alpha[\omega_m^2(\mathbf{r})]$  diverges proportionally to  $1/\alpha$ , such that the actual non-zonal enstrophy density  $\frac{1}{2}\alpha\mathbb{E}_U^\alpha[\omega_m^2(\mathbf{r})]$  has a finite limit when  $\alpha \rightarrow 0$  (see section 4.1.1 page 49 for the definition of the expectations). This behaviour could have been expected in order to balance the finite enstrophy input rate provided by the stochastic force.

We now consider the dynamics of the eddy vorticity  $\omega_m$  with a small but non-zero friction  $\alpha$ . We then denote  $g_{kl}^\alpha \equiv \frac{1}{2}e^{ik(x_1-x_2)}\mathbb{E}_U^\alpha[\omega_{kl}(y_1, t)\omega_{kl}^*(y_2, t)] + \text{c.c.}$  where  $\mathbb{E}_U^\alpha$  is the average in the stationary state of the linear dynamics

$$\frac{\partial\omega_{kl}}{\partial t} + L_{U,k}^\alpha[\omega_{kl}] = \sqrt{2}e^{ily} \eta_{kl} \quad (5.9)$$

with  $L_{U,k}^\alpha = ikU + ik(\beta - U'')\Delta_k^{-1} + \alpha$  (see section 4.1.2 in page 50 for details of the Fourier decomposition).

Using (4.16) and the Orr mechanism (4.24), we get

$$g_{kl}^\alpha(\mathbf{r}_1, \mathbf{r}_2) = e^{ik(x_1-x_2)} \frac{\tilde{\omega}_{kl}^\infty(y_1)\tilde{\omega}_{kl}^{\infty*}(y_2)}{ik(U(y_1) - U(y_2)) + 2\alpha} + g_{kl}^{r,\alpha}(\mathbf{r}_1, \mathbf{r}_2) + \text{c.c.}, \quad (5.10)$$

where,  $g_{kl}^{r,\alpha}$  contains the corrections due to the correction term  $\tilde{\omega}_{kl}^{r,\alpha}$  in (4.24). We readily see in (5.10) that if  $U(y_1) \neq U(y_2)$  then  $g_{kl}^\alpha(\mathbf{r}_1, \mathbf{r}_2)$  is finite when  $\alpha \rightarrow 0$ . By contrast, if  $U(y_1) = U(y_2)$  then the first term in (5.10) diverges as  $1/\alpha$  when  $\alpha \rightarrow 0$ . In appendix D, we prove that  $g_{kl}^{r,\alpha}(\mathbf{r}_1, \mathbf{r}_2) = o(1/\alpha)$  when  $\alpha \rightarrow 0$ , so the leading order divergence of  $g_{kl}^\alpha$  at points such that  $U(y_1) = U(y_2)$  is given by the first term in (5.10).

When  $y_1 \sim y_2$ , the first term in (5.10) can be written

$$\frac{\tilde{\omega}_{kl}^\infty(y_1)\tilde{\omega}_{kl}^{\infty*}(y_2)}{ik(U(y_1) - U(y_2)) + 2\alpha} \underset{y_1 \sim y_2}{\sim} \frac{\tilde{\omega}_{kl}^\infty(y_1)\tilde{\omega}_{kl}^{\infty*}(y_2)}{ikU'(y_1)} \frac{-i}{(y_1 - y_2) - \frac{2i\alpha}{kU'(y_1)}}.$$

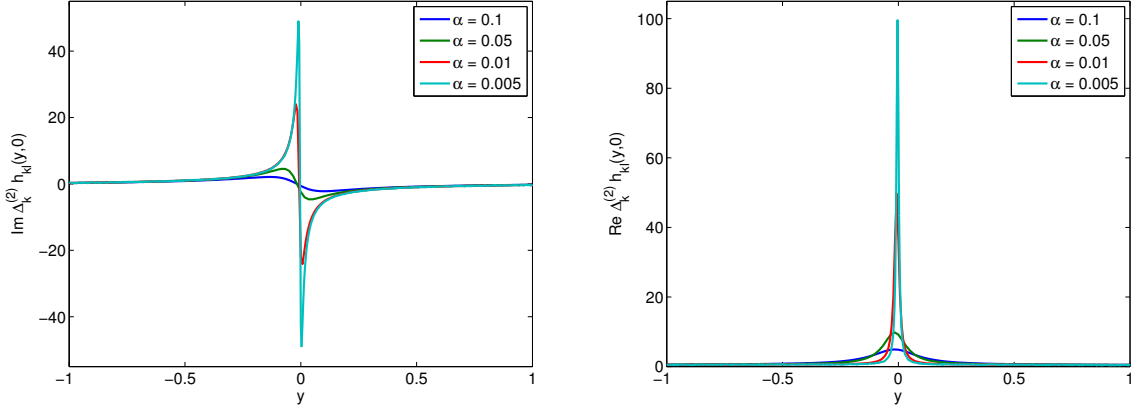


Figure 5.1: Real and imaginary parts of the  $k$ -th Fourier component of the stationary vorticity two-points correlation function  $g_{kl}^\alpha(x, y, x, 0)$  in the case of a parabolic base profile in a channel geometry (with no stationary points), with  $k = l = 1$  and different values of the friction coefficient  $\alpha$ . The plots clearly show the expected divergence at  $y = 0$ . A closer look at the divergence is shown in figure 5.2. These numerical results were obtained using an integral representation of the Lyapunov equation, see section 4.3.2 and [18] for details.

Using the results of appendix D.1, we get in the small  $\alpha$  limit

$$g_{kl}^\alpha(\mathbf{r}_1, \mathbf{r}_2) \underset{\lambda_\alpha \ll 1, y_1 \sim y_2}{\sim} 2 \left\{ \cos k(x_1 - x_2) \frac{|\tilde{\omega}_k^\infty(y_1)|^2}{|kU'(y_1)|} \operatorname{Re} [F_{\lambda_\alpha}(y_1 - y_2)] + \frac{\operatorname{Im} [\tilde{\omega}_k^\infty(y_1) \tilde{\omega}_k^{\infty*}(y_2) e^{ik(x_1 - x_2)}]}{kU'(y_1)} \operatorname{Im} [F_{\lambda_\alpha}(y_1 - y_2)] \right\} + 2 \operatorname{Re} g_{kl}^{r, \alpha}(\mathbf{r}_1, \mathbf{r}_2), \quad (5.11)$$

with  $\lambda_\alpha = 2\alpha/|kU'(y_1)|$  and  $F_\lambda(y) = \frac{-i}{y - i\lambda}$ . Comparing (5.7) with (5.11), we conclude that the vorticity two-points correlation function is regularized in a universal way close to  $y_1 = y_2$  when  $\alpha$  is small but non-zero, through the function  $F_\lambda(y)$ .

In figure 5.1 are represented the real and imaginary parts of  $g_{kl}^\alpha$  for different values of  $\alpha$ , for a parabolic base velocity in a channel (with no extrema). The expected divergence at  $y_1 = y_2$  clearly appears in this figure. In figure 5.2, the comparison of this divergence and of the theoretical prediction (5.11) shows a very good agreement.

In particular, (5.10) implies

$$\mathbb{E}_U^\alpha |\omega_{kl}(y, t)|^2 = g_{kl}^\alpha(\mathbf{r}, \mathbf{r}) \underset{\alpha \rightarrow 0}{\sim} \frac{|\tilde{\omega}_{kl}^\infty(y)|^2}{\alpha}, \quad (5.12)$$

so the eddy enstrophy density  $\frac{1}{2}\alpha \mathbb{E}_U^\alpha [\omega_m^2]$  remains finite as  $\alpha \rightarrow 0$ . This is also the relation we have used in order to prove that the average Reynolds' force  $F_0$  is finite in section 4.3 (page 56).

## 5.2 Typical fluctuations of Reynolds' stresses in the inertial limit

In section 4.3, we have proved that the average Reynolds' force  $F_0$ , computed in the stationary state of  $\omega_m$  without dissipation, is finite. In this section we address the

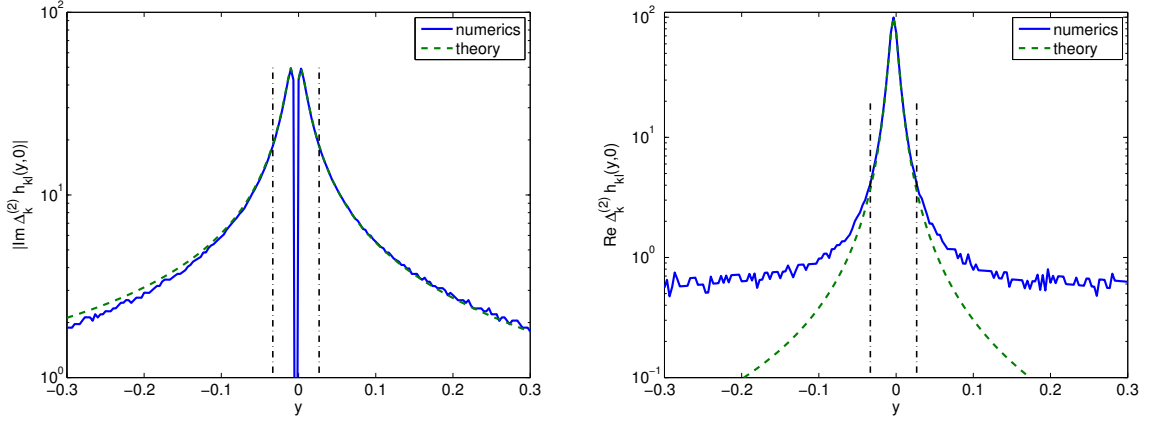


Figure 5.2: Divergence of the stationary vorticity two-points correlation function  $g_{kl}^\alpha(x, y, x, 0)$  near  $y = 0$  in semi-log scale, in the case of a parabolic base profile in a channel geometry (with no stationary points), with  $k = l = 1$  and  $\alpha = 0.005$ . As expected, the comparison between the numerical result and the universal shape (5.11) is very good in the range  $1 \gg y \gg \frac{2\alpha}{ks_0} \simeq 0.006$  (the area between the vertical lines). These numerical results were obtained using an integral representation of the Lyapunov equation, see section 4.3.2 and [18] for details.

similar question for the integrated autocorrelation function of the Reynolds' force  $\Xi[U]$ , defined in (3.22) (page 45).

More precisely, we study the behaviour for small  $\alpha$  of  $\Xi^\alpha[U]$ , defined in (4.36) (page 61), and that satisfies  $\Xi[U] = \lim_{\alpha \rightarrow 0} \Xi^\alpha[U]$ . Formally, we should first take the limit  $\alpha \rightarrow 0$ , and then  $t \rightarrow \infty$ , like we did in section 5.1.1. Like it is the case for the average Reynolds' force  $F_0$  (see section 4.3.1) and for the vorticity auto-correlation function  $g^\infty$  (see section 5.1), the result for  $\Xi$  is independent of the ordering of limits. For simplicity, we will only present the derivation corresponding to taking first  $t \rightarrow \infty$  and then  $\alpha \rightarrow 0$ . Moreover, the behaviour of  $\Xi^\alpha$  for small  $\alpha$  will be very important in the following discussion, in section 5.3.

### 5.2.1 The integrated autocorrelation function is a distribution

The formal computations of section 4.4 led to the following expression of  $\Xi^\alpha[U]$ :

$$\Xi^\alpha[U](y_1, y_2) = \sum_{(k,l) \in \mathbb{Z}^2} c_{kl}^2 \{ \Xi_{kl}^\alpha(y_1, y_2) + \Xi_{kl}^\alpha(y_2, y_1) \} \quad (5.13)$$

where

$$\Xi_{kl}^\alpha(y_1, y_2) = \frac{1}{4} \int_0^\infty [T_{\omega\omega}^\alpha \cdot T_{vv}^\alpha + T_{v\omega}^\alpha \cdot T_{\omega v}^\alpha](k, l, y_1, y_2, s) ds, \quad (5.14)$$

where  $T_{\omega\omega}^\alpha$ ,  $T_{vv}^\alpha$ ,  $T_{v\omega}^\alpha$  and  $T_{\omega v}^\alpha$  are two-points time-correlation functions, defined in (4.40–4.43).

Using the Orr mechanism (4.20–4.24) to estimate the large- $s$  behaviour of  $T_{\omega\omega}^\alpha$ ,

$T_{vv}^\alpha$ ,  $T_{vw}^\alpha$  and  $T_{ww}^\alpha$ , we will prove that

$$\Xi_{kl}^\alpha(y_1, y_2) \underset{\alpha \rightarrow 0}{\sim} \frac{A_{kl}(y_1, y_2)}{ik(U(y_1) - U(y_2)) + 2\alpha}, \quad (5.15)$$

where  $A_{kl}$  is a regular function. At points such that  $y_1 = y_2$ , we readily see that  $\Xi_{kl}^\alpha(y_1, y_2)$  behaves like  $1/\alpha$ , as explained before. Using Plemelj formula (D.2), we also see that  $\Xi_{kl}^\alpha(y_1, y_2)$  converges in the sense of distributions as  $\alpha \rightarrow 0$ .

In the following, we first prove (5.15) in a simple, explicitly solvable case. Then we consider the generalisation of this result to any background flow  $U(y)$ .

### Explicit computation in the case of a constant shear

Like in section 4.4.2, consider the case of the linear Euler equation in a channel  $(x, y) \in \mathcal{D} = [0, 2\pi L_x] \times [0, L_y]$ , or in an infinite domain  $(x, y) \in \mathcal{D} = [0, 2\pi L_x] \times \mathbb{R}$ , where the background flow is  $U(y) = sy$  with a constant shear  $s$ .

In this case, the deterministic linear equation can be solved explicitly, and all the quantities of interest can be expressed in terms of spatial integrals involving  $H_k$ , the Green function of the Laplacian  $\Delta_k = \partial_y^2 - k^2$ . In the following, we will not need the explicit expression of  $H_k$ , but only the fact that  $H_k$  is a continuous function of its two variables, and that the first derivative  $\partial_y H_k(y, y')$  is discontinuous at  $y = y'$  [11].

The correlation functions  $T_{vv}^\alpha$  and  $T_{ww}^\alpha$  can be easily computed injecting the expressions of  $\tilde{\omega}_{kl}$  and  $\tilde{v}_{kl}$  into (4.40) and (4.41), leading to

$$\begin{aligned} C_{kl}^\alpha(y_1, y_2) &\equiv \frac{1}{4} \int_0^\infty [T_{ww}^\alpha \cdot T_{vv}^\alpha](k, l, y_1, y_2, s) ds \\ &= -\frac{i}{ks^3} \frac{e^{-il(y_1 - y_2)}}{y_1 - y_2 + \frac{2\alpha}{ks}i} \int dy'_1 \int dy'_2 \frac{H_k(y_1, y'_1) H_{-k}(y_2, y'_2) e^{il(y'_1 - y'_2)}}{(y'_2 - y'_1 + \frac{2\alpha}{ks}i)(y_1 - y'_1 + \frac{2\alpha}{ks}i)}. \end{aligned} \quad (5.16)$$

$H_k$  is a continuous function, so the spatial integrals appearing in the above expression converge to a finite quantity in the limit  $\alpha \rightarrow 0$ :

$$\int dy'_1 \int dy'_2 \frac{H_k(y_1, y'_1) H_{-k}(y_2, y'_2) e^{il(y'_1 - y'_2)}}{(y'_2 - y'_1 + \frac{2\alpha}{ks}i)(y_1 - y'_1 + \frac{2\alpha}{ks}i)} \xrightarrow{\alpha \rightarrow 0} A(k, l, y_1, y_2) \quad (5.17)$$

where  $A$  is a regular function independent of  $\alpha$ , that can be written explicitly using Plemelj formula (D.2). Then, we clearly see that, due to the pre-factor in (5.16),  $C_{kl}^\alpha(y_1, y_2)$  is finite for  $y_1 \neq y_2$  and diverges as  $1/\alpha$  for  $y_1 = y_2$ .

Similarly, we can compute

$$\begin{aligned} D_{kl}^\alpha(y_1, y_2) &\equiv \frac{1}{4} \int_0^\infty [T_{vw}^\alpha \cdot T_{vw}^\alpha](k, l, y_1, y_2, s) ds \\ &= -\frac{i}{ks^3} \left( \int dy'_1 \frac{H_k(y_1, y'_1) e^{-il(y'_1 - y_2)}}{(y_2 - y'_1 + \frac{2\alpha}{ks}i)(y_1 - y'_1 + \frac{2\alpha}{ks}i)} \right) \times \\ &\quad \left( \int dy'_2 \frac{H_k(y_2, y'_2) e^{-il(y'_2 - y_1)}}{y_1 - y'_2 + \frac{2\alpha}{ks}i} \right). \end{aligned} \quad (5.18)$$

We observe that this expression is the product of two integrals. The second one converges to a finite quantity when  $\alpha \rightarrow 0$ , for any  $y_1$  and  $y_2$ . Moreover, if  $y_1 \neq y_2$  the first integral also has a finite limit, using again that the Green function  $H_k$  is continuous. However, when  $y_1 = y_2$ , the integral over  $y'_1$  becomes

$$\int dy'_1 \frac{H_k(y_1, y'_1) e^{-il(y'_1 - y_1)}}{(y_1 - y'_1 + \frac{2\alpha}{ks}i)^2} = \int dy'_1 \frac{\frac{\partial}{\partial y'_1} (H_k(y_1, y'_1) e^{-il(y'_1 - y_1)})}{y_1 - y'_1 + \frac{2\alpha}{ks}i}, \quad (5.19)$$

where we used an integration by parts. We now see that this integral diverges when  $\alpha \rightarrow 0$  because the quantity at the numerator is not continuous exactly at  $y_1 = y'_1$ . This implies that  $D_{kl}^\alpha(y, y)$  diverges as  $\ln \alpha$  when  $\alpha \rightarrow 0^2$ .

Using (5.16) and the fact that  $D_{kl}^\alpha(y, y) \sim \ln \alpha$ , we deduce<sup>3</sup> the asymptotic behaviour of the integrated autocorrelation function  $\Xi_{kl}^\alpha(y_1, y_2)$  (defined in (4.37))

$$\Xi_{kl}^\alpha(y_1, y_2) \underset{\alpha \rightarrow 0}{\sim} \frac{A_{kl}(y_1, y_2)}{iks(y_1 - y_2) + 2\alpha} \quad (5.20)$$

where  $A_{kl}(y_1, y_2)$  is a finite function independent of  $\alpha$ . We have thus proved the result (5.15) in this simple case.

### Generalization to any background flow

We now generalize the result of the previous paragraph to the case of a generic base flow  $U(y)$ . We will prove that the main contribution to  $\Xi_{kl}^\alpha$  in the limit  $\alpha \rightarrow 0$  comes from  $C_{kl}^\alpha$ , and that it is of the form (5.15).

To do this, it is enough to observe that the most divergent part of  $\Xi_{kl}^\alpha$  comes from the vorticity-vorticity correlations  $T_{\omega\omega}^\alpha$ . Indeed, it is the integral of a function that oscillates without decaying in the limit  $\alpha \rightarrow 0$ , see (4.40) and (4.20). In comparison, all the other correlation functions involve integrals of the velocity field, that decays algebraically for large time, see (4.22). The computation of  $T_{\omega\omega}^\alpha$  is very similar to the computation of the equal-time two-points vorticity correlation function  $g_{kl}^{\alpha, \infty}$  in section 5.1.2. For that reason, the limits  $t \rightarrow \infty$  and  $\alpha \rightarrow 0$  could be taken in either order, leading to the same result for  $\Xi$ .

Using (4.40) and (4.24), we get

$$T_{\omega\omega}^\alpha(k, l, y_1, y_2, s) = \frac{\tilde{\omega}_{-k, -l}^\infty(y_1) \tilde{\omega}_{kl}^\infty(y_2)}{ik(U(y_1) - U(y_2)) + 2\alpha} e^{ikU(y_1)s - \alpha s} + T_{\omega\omega}^{r, \alpha}(k, l, y_2, y_2, s), \quad (5.21)$$

where  $T_{\omega\omega}^{r, \alpha}$  is subdominant with respect to the first term in the limit  $\alpha \rightarrow 0$  when  $U(y_1) = U(y_2)$  (see appendix F). We recover the divergent part of (5.15) for  $U(y_1) = U(y_2)$ .

To finish the proof, we need to find bounds on  $T_{vv}^\alpha$ ,  $T_{v\omega}^\alpha$  and  $T_{\omega v}^\alpha$ . This is done in appendix F. In particular, it is shown that in the limit  $\alpha \rightarrow 0$  and at points such that  $U(y_1) = U(y_2)$ ,  $|D_{kl}^\alpha(y_1, y_2)| \lesssim C |\ln \alpha|$  with some positive constant  $C$ , like in the constant shear case studied in the previous paragraph. Then, the same conclusion holds, and (5.15) is proved in the general case.

<sup>2</sup>To understand the rate of this divergence with  $\alpha$ , it is enough to observe that the divergence arises from the neighbourhood  $y'_1 \in [y_1 - \epsilon, y_1 + \epsilon]$ . Then, as  $y'_1 \rightarrow \frac{\partial}{\partial y'_1} H_k(y_1, y'_1)$  is analytic in both the neighbourhoods  $y'_1 \in [y_1 - \epsilon, y_1]$  and  $y'_1 \in [y_1, y_1 + \epsilon]$ , we can expand it in Taylor series. By direct computation, one finally obtains that the integral in (5.19) diverges as  $\ln \alpha$ .

<sup>3</sup>See section F.2 in appendix F for details.

### 5.2.2 The covariance is a distribution

The typical fluctuations of Reynolds' stresses are also characterized by the covariance of the Reynolds' stress divergence at points  $y_1$  and  $y_2$ , defined as

$$C[U](y_1, y_2) \equiv \mathbb{E}_U [\langle v_m \omega_m \rangle (y_1) \langle v_m \omega_m \rangle (y_2)]. \quad (5.22)$$

This quantity enters for instance into the expression of the correlation time  $\tau_{corr}$  (denominator of (2.32), page 35, see also section 5.3.4).

The computation of  $C[U](y_1, y_2)$  can be done the same way as the computation of  $\Xi[U]$  in section 4.4: decomposition into contributions from each forcing mode, use of Isserli-Wick theorem and expression using the two-points correlation functions  $T_{\omega\omega}^\alpha$ ,  $T_{vv}^\alpha$ ,  $T_{v\omega}^\alpha$  and  $T_{\omega v}^\alpha$  (defined in equations (4.40–4.43) in page 61). This procedure leads to  $C = \lim_{\alpha \rightarrow 0} C^\alpha$  where

$$C^\alpha[U](y_1, y_2) \equiv \sum_{(k,l) \in \mathbb{Z}^2} c_{kl}^2 [T_{vv}^\alpha(k, l, y_1, y_2, 0) T_{\omega\omega}^\alpha(k, l, y_1, y_2, 0) + T_{v\omega}^\alpha(k, l, y_1, y_2, 0) T_{\omega v}^\alpha(k, l, y_1, y_2, 0)]. \quad (5.23)$$

Using the computations of previous section and of appendix F, we understand from (5.23) that the covariance  $C^\alpha$  and is of the form

$$C^\alpha[U](y_1, y_2) \underset{\alpha \rightarrow 0}{\sim} \sum_{(k,l) \in \mathbb{Z}^2} \frac{c_{kl}^2 A'_{kl}(y_1, y_2)}{ik(U(y_1) - U(y_2)) + 2\alpha}, \quad (5.24)$$

where  $A'_{kl}$  is a regular function, independent of  $\alpha$ . The consequences of this result are discussed in section 5.3.

### 5.2.3 Influence of the forcing spectrum

The results of previous sections (5.15, 5.24) essentially show that the typical fluctuations of the Reynolds' force  $\langle \omega_m v_m \rangle (y)$  diverge point-wise in the large time and inertial limit  $t \rightarrow \infty$ ,  $\alpha \rightarrow 0$ . The consequences of this result for the ergodicity of the stochastic linear barotropic equation (5.2) will be discussed in section 5.3.

So far, we have essentially considered the case where one or a few modes  $(k, l)$  are stochastically forced. When a large number, say  $K \gg 1$ , of modes is forced, another type of averaging occurs, and the divergences (5.15, 5.24) can be regularized. Here we only give qualitative arguments, a more rigorous study would be necessary to make those arguments more precise.

Using the Fourier decomposition defined in section 4.2.2 (page 52), we can write the average and integrated autocorrelation function of the Reynolds' force, computed in the stationary state of  $\omega_m$  with a small non-zero  $\alpha$ , as

$$F^\alpha = \sum_{(k,l) \in \mathbb{Z}^2} c_{kl} f_{kl}^\alpha, \quad \Xi^\alpha = \sum_{(k,l) \in \mathbb{Z}^2} c_{kl}^2 \Xi_{kl}^\alpha, \quad (5.25)$$

where  $f_{kl}^\alpha$  is defined in section 4.3.1 (page 56), and  $\Xi_{kl}^\alpha$  is defined in section 4.4 (page 60). The results of sections 4.3 and 5.2 imply that  $\Xi^\alpha(y, y)/F^\alpha(y) \sim 1/\alpha$  as  $\alpha \rightarrow 0$ , when one or a few Fourier modes are forced.

The Fourier coefficients of the noise correlation function  $c_{kl}$  are constrained by the total energy balance. Namely, we have assumed that the average energy injection rate by the noise  $\eta$  in the original stochastic barotropic equation (1.1) (page 14) is equal to  $\sigma$ , i.e.  $\sum_{k,l} e_{kl} = 1$  where  $e_{kl} \equiv \frac{c_{kl}}{2(k^2+l^2)}$  is the average energy injection rate in mode  $(k, l)$ . A natural choice of forcing spectrum is  $e_{kl} = e = \text{cte}$  on a set of  $K$  modes. Then, the energy constraint imposes  $e = 1/K$ .

Using (5.25), this roughly implies that  $\Xi^\alpha(y, y)/F^\alpha(y) \sim 1/\alpha K$ . The strong fluctuations of  $\langle \omega_m v_m \rangle(y)$  could then be weakened in an asymptotic regime where  $\alpha \rightarrow 0$ ,  $K \rightarrow \infty$  in a specific manner. This is another form of the Law of Large Numbers, where now averaging arises from the addition of  $K \gg 1$  independent Fourier modes.

This simple argument is far from being accurate at this point. Indeed, we have neglected the  $(k, l)$  dependency of  $f_{kl}^\alpha$  and  $\Xi_{kl}^\alpha$ , which are most likely to be relevant in this computation.

Understanding such averaging when the number of forced modes  $K$  is large thus requires describing how  $f_{kl}^\alpha$  and  $\Xi_{kl}^\alpha$  depend on  $(k, l)$ , and considering different forcing spectra  $c_{kl}$ . This is a very promising perspective of this work.

## 5.3 Consequences for the kinetic theory

### 5.3.1 Summary of the technical results

In this paragraph we shortly summarize the technical results derived in chapter 4 and section 5.2. We will then discuss the practical consequences for the validity of the effective zonal jet dynamics (5.1).

In section 5.2, we have seen that the typical fluctuations of Reynolds' stresses, as quantified by the variance and integrated autocorrelation function of the Reynolds' force  $\langle \omega_m v_m \rangle(y)$ , diverge point-wise in the absence of external damping mechanism. It is thus useful to study the stationary statistics of Reynolds' stresses when a small but non-zero friction  $\alpha$  is present, and to consider the limit  $\alpha \rightarrow 0$  then.

We have defined the expectation  $\mathbb{E}_U^\alpha$  as the average in the statistically stationary state of the linear dynamics (4.1) with a non-zero damping rate  $\alpha$ , and the associated average Reynolds' force  $F^\alpha[U] \equiv \mathbb{E}_U^\alpha \langle \omega_m v_m \rangle$ , Reynolds' force covariance

$$C^\alpha[U](y_1, y_2) \equiv \mathbb{E}_U^\alpha [\langle \omega_m v_m \rangle(y_1) \langle \omega_m v_m \rangle(y_2)], \quad (5.26)$$

and integrated autocorrelation function

$$\Xi^\alpha[U](y_1, y_2) \equiv \int_0^\infty \mathbb{E}_U^\alpha [[\langle v_m \omega_m \rangle(y_1, s) \langle v_m \omega_m \rangle(y_2, 0) + (y_1 \leftrightarrow y_2)]] ds. \quad (5.27)$$

We have proved the following:

- In section 4.3, we have seen that  $F^\alpha$  converges to a finite function as  $\alpha \rightarrow 0$ .
- In section 5.2, we have seen that  $\Xi^\alpha[U](y_1, y_2)$  converges to a distribution. In particular,  $\Xi^\alpha[U](y_1, y_2)$  converges to a finite quantity if  $U(y_1) \neq U(y_2)$  while it diverges as  $1/\alpha$  if  $U(y_1) = U(y_2)$ .

- In section 5.2.2, we have seen that  $C^\alpha$  has the same behaviour as  $\Xi^\alpha$ , with the same point-wise divergence.

We recall that those results were derived assuming the Orr mechanism (4.20) and (4.24). In the case of the two-dimensional Euler equation (i.e. with  $\beta = 0$ ), the Orr mechanism is known to occur under the assumption that the linearized operator close to the base flow  $U$  has no modes (which is the generic case for the linearized Euler dynamics [11]). However, the results obtained in chapters 4 and 5 remain correct as long as a similar inviscid damping occurs in the deterministic linear dynamics, which is sometimes the case even if the above hypothesis are not fulfilled, in particular for  $\beta \neq 0$  (see section 4.5 for details).

### 5.3.2 Consequences for the zonal energy balance

The kinetic energy associated with the zonal jet is  $\mathcal{E}_z \equiv \pi l_x \int U^2(y) dy$ . Applying the Itô formula to the kinetic equation (5.1), we get the average zonal energy balance

$$\frac{dE_z}{dt} = 2\alpha\pi l_x \int \mathbb{E}[F_0[U](y)U(y)] dy - 2\alpha E_z + \alpha^2\pi l_x \int \mathbb{E}[\Xi[U](y, y)] dy, \quad (5.28)$$

with  $E_z = \mathbb{E}[\mathcal{E}_z]$  where  $\mathbb{E}$  is the average with respect to realizations of the noise  $\xi$  in (5.1).

In (5.28), the last term on the right-hand side represents the energy injection rate in the zonal mean flow by the fluctuations of Reynolds' stresses. Using the results of section 5.2, we see that this term is actually infinite, so the energy balance (5.28) and the kinetic equation (5.1) are formally ill-defined.

This problem is very similar to the infinite value of the eddy enstrophy density  $\frac{1}{2}\mathbb{E}_U[\omega_m^2]$  obtained in section 5.1. In fact, we have seen that considering the effect of a small friction  $\alpha$  in the dynamics of  $\omega_m$ , this divergence is regularized so that the actual eddy enstrophy density  $\frac{1}{2}\alpha\mathbb{E}_U^\alpha[\omega_m^2]$  remains finite in the limit  $\alpha \rightarrow 0$ .

The same argument can be applied here. Indeed, it is natural from a physical point of view to consider the dynamics of  $U$  through the kinetic equation (5.1) and of  $\omega_m$  through the linear equation (4.1) with the same friction coefficient  $\alpha \ll 1$ . Then, the results of section 5.2 imply that the last term in the r.h.s of (5.28) is actually of order  $\alpha$ .

From a formal point of view, this indicates that the perturbative expansion (stochastic averaging) is not well-posed when it comes to observables such as the energy in zonal degrees of freedom.

From a physical point of view, this result indicates that we should expect the fluctuations of Reynolds' stresses to be relevant in the zonal jet energy balance, even in the limit of very small  $\alpha$ . This effect was not considered in previous quasi-linear approaches like S3T-CE2 [3, 33, 85, 104, 106], where only the average Reynolds' stress divergence was taken into account. Our theoretical results suggest that a careful analysis of the zonal energy budget in the inertial limit  $\nu \ll \alpha \ll 1$  in S3T-CE2 approaches should give a quantitative disagreement with the original stochastic barotropic equations. Such analysis will be done in chapter 6, using numerical simulations of both the linearized barotropic equation and of a modified Lyapunov equation, that takes into account those fluctuations of Reynolds' stresses.

Finally, note that the inconsistency of the perturbative expansion can be compensated by the averaging effect due to a very large number  $K$  of forcing modes (see section 5.2.3). If such averaging occurs, the last term in the r.h.s of the energy balance (5.28) will be of order  $1/K \ll 1$  with respect to the first term. This means that in a regime  $\alpha \rightarrow 0$ ,  $K \rightarrow \infty$ , the fluctuations of Reynolds' stresses are negligible with respect to the mean, even at the level of the zonal energy balance.

### 5.3.3 Consequences for the ergodicity of the linearized dynamics

The fast process  $\omega_m(s)$  is said to be ergodic if for any observable  $\phi[\omega_m]$ , the time average and the average over the stationary distribution (5.3) are identical [86]

$$\lim_{t \rightarrow \infty} \frac{1}{t} \int_0^t \phi[\omega_m(s)] ds = \mathbb{E}_U[\phi[\omega_m]] . \quad (5.29)$$

This equality must be understood in a probabilistic sense, indeed the left-hand side is a random variable while the right-hand side is an averaged quantity. In the sense of a mean-square limit [44] (or limit in  $L^2$  norm [86]), the condition (5.29) is equivalent to  $\lim_{t \rightarrow \infty} \|\phi\|^2(t) = 0$  with

$$\|\phi\|^2(t) \equiv \mathbb{E}_U \left[ \left( \frac{1}{t} \int_0^t \phi[\omega_m(s)] ds - \mathbb{E}_U[\phi[\omega_m]] \right)^2 \right] . \quad (5.30)$$

Such definition of ergodicity is a classical one [83], but it is not the only possible one (mean-square convergence implies convergence in probability and in law, but we could consider almost-sure convergence).

In order to anticipate the divergences due to the singular fluctuations of Reynolds' stresses studied in section 5.2, we define the related quantity

$$\|\phi\|_\alpha^2(t) \equiv \mathbb{E}_U^\alpha \left[ \left( \frac{1}{t} \int_0^t \phi[\omega_m(s)] ds - \mathbb{E}_U^\alpha[\phi[\omega_m]] \right)^2 \right] , \quad (5.31)$$

where now the dynamics of  $\omega_m$  is dissipated by a non-zero friction  $\alpha$ , and  $\mathbb{E}_U$  is the expectation in the stationary state of  $\omega_m$ . Obviously  $\lim_{t \rightarrow \infty} \|\phi\|_\alpha^2(t) = 0$  whenever  $\alpha > 0$ , we will thus consider either the regime  $\alpha \ll 1$ ,  $t \gg 1$  or the limit  $\alpha = 0$ ,  $t \rightarrow \infty$ .

Using computations very similar to those reported in appendix B.2 (page 138), we get

$$\|\phi\|_\alpha^2(t) \underset{t \rightarrow \infty}{\sim} \frac{2}{t} \int_0^\infty \mathbb{E}_U^\alpha \left[ \phi[\omega_m(\tau)] \phi[\omega_m(0)] \right] d\tau . \quad (5.32)$$

A particularly interesting case is when  $\phi[\omega_m]$  is the Reynolds' stress divergence  $\langle \omega_m v_m \rangle$ . Indeed, in this case the ergodicity condition (5.29) is directly the Law of Large Numbers for  $\langle \omega_m v_m \rangle$ , as stated in section 2.1.1, and which led to the deterministic part of the kinetic equation (5.1). In this case, we recognize in the left-hand side of (5.32) the definition of the integrated autocorrelation function  $\Xi^\alpha[U]$ , defined in (5.27).

If we simply consider the ergodicity of  $\langle \omega_m v_m \rangle$  point-wise, using the results of section 5.2 (in particular (5.15)), we get

$$\| \langle \omega_m v_m \rangle(y) \|_\alpha^2(t) \underset{t \rightarrow \infty}{\sim} \frac{\Xi^\alpha[U](y, y)}{t} \underset{\alpha \rightarrow 0}{\sim} \frac{A}{\alpha t}, \quad (5.33)$$

with  $A$  a constant independent of  $\alpha$  and  $t$ . Taking first the limit  $\alpha \rightarrow 0$ , the above quantity diverges and ergodicity is clearly broken. From a qualitative point of view, the relevant range of values of  $t$  (time variable for the fast process) is  $t \ll 1/\alpha$ , and we still deduce from (5.33) that the ergodicity condition (5.29) for the Reynolds' force  $\langle \omega_m v_m \rangle(y)$  is not satisfied.

However, ergodicity can be understood in a weaker sense. Indeed, we have seen in section 5.2 that  $\Xi^\alpha[U]$  converges to a distribution in the inertial limit. We thus expect to observe convergence of quantities integrated over  $y$  when multiplied by a smooth test function. Let  $f(y)$  be such test function, consider the observable  $\phi_f[\omega_m] \equiv \int dy f(y) \langle \omega_m v_m \rangle(y)$ . In this case, (5.32) becomes

$$\| \phi_f \|_\alpha^2(t) \underset{t \rightarrow \infty}{\sim} \frac{2}{t} \int dy_1 dy_2 f(y_1) f(y_2) \Xi^\alpha[U](y_1, y_2) \underset{\alpha \rightarrow 0}{\sim} \frac{A_f}{t}, \quad (5.34)$$

with  $A_f$  a constant independent of  $\alpha$  and  $t$ . Then, ergodicity for  $\phi_f$  is satisfied. As an example,  $f(y) = e^{ily}$  is of particular interest as it leads to consider ergodicity for the  $l$ -th Fourier coefficient of the Reynolds' stress divergence. We conclude that ergodicity of the stochastic linearized equation (4.1) for the Fourier coefficients of the Reynolds' stress divergence is satisfied.

Again, the breaking of point-wise ergodicity can be regularized by the averaging effect due to a large number  $K$  of forced modes (see section 5.2.3). If such averaging occurs, then (5.33) becomes

$$\| \langle \omega_m v_m \rangle(y) \|_\alpha^2(t) \sim \frac{A}{\alpha K t} \quad (5.35)$$

in the regime  $t \gg 1$ ,  $K \gg 1$ ,  $\alpha \ll 1$ . In a regime where  $\alpha \rightarrow 0$  with the constraint  $\alpha K = \text{cte}$ , ergodicity is thus satisfied in a strong sense (point-wise).

We also stress that proving ergodicity in a general sense (i.e. the condition (5.32) for any observable  $\phi[\omega_m]$ ) is far from reach at this point. It would involve studying any moment of the time-averaged vorticity  $\omega_m$ , and like for the Reynolds' stress divergence considered here, ergodicity will be satisfied in a weak sense that would have to be determined precisely.

### 5.3.4 Self-consistency of the time scale separation hypothesis

To perform the stochastic averaging procedure, we have assumed that the zonal jet velocity profile  $U(y)$  evolves much slower than the turbulent eddy vorticity  $\omega_m$ . This led to the effective description, summarized by equations (5.1, 4.1).

A very interesting and natural question to ask is whether time scale separation indeed exists in the effective description. In other words: is the time scale separation hypothesis self-consistent?

Formally, we need to check the condition  $|\tau_{corr}^\alpha| \ll 1/\alpha$ , where the decorrelation time of the Reynolds' force at points  $y_1$  and  $y_2$  is defined as [77, 84]

$$\tau_{corr}^\alpha(y_1, y_2) = \frac{1}{2} \frac{\Xi^\alpha[U](y_1, y_2)}{C^\alpha[U](y_1, y_2)}. \quad (5.36)$$

In section 5.2, we have seen that both  $\Xi^\alpha[U](y_1, y_2)$  and  $C^\alpha[U](y_1, y_2)$  diverge point-wise if  $U(y_1) = U(y_2)$ , as  $\alpha \rightarrow 0$ . More precisely, we have seen that at those points, both quantities diverge exactly as  $1/\alpha$ . As a consequence, those divergences cancel out in the computation of (5.36), and  $\tau_{corr}^\alpha(y_1, y_2)$  has a finite value in the limit  $\alpha \rightarrow 0$ , at any points  $(y_1, y_2)$ .

We have thus proved that the time scale separation hypothesis is self-consistent, under the assumptions of the Orr mechanism:  $\beta = 0$  and the base flow has no modes. In chapter 6, we will study the validity of this result when  $\beta \neq 0$  using numerical simulations of the linearized barotropic equation.

## 5.4 Perspectives

The main conclusion of this chapter is that the kinetic approach (stochastic averaging) in the limit  $\alpha \rightarrow 0$  leads to divergences, related to strong fluctuations of Reynolds' stresses. The consequences of those divergences are inconsistent energy injections in the mean flow and breaking of ergodicity of the virtual fast process.

However, we have also seen that in the case where a very large number  $K$  of Fourier modes are forced, another Law of Large Numbers can possibly apply and those divergences can be regularized. In other words, in the regime  $\alpha \ll 1$ ,  $K \gg 1$  with  $\alpha K = \text{cte}$ , the small value of  $\alpha$  implies a time scale separation between mean flow and perturbations while the large value of  $K$  ensures the validity of the Law of Large Numbers, leading to a kinetic theory without divergences.

Similar behaviour can be expected in the cases with  $\beta \neq 0$  or  $\nu \neq 0$ . Indeed, numerical simulations of zonal jets typically show more fluctuations in the Navier-Stokes case ( $\beta = 0$ ) than in the beta-plane case, see for instance figure 1.3 in page 16. It indicates that the stochastic part of the kinetic equation (related to the fluctuations of Reynolds' stresses) could be negligible in a regime of large  $\beta$ .

All the theoretical results of chapters 4 and 5 were obtained with zero viscosity. This is in contrast with every previous empirical approaches, where viscosity (or hyper-viscosity) is necessary for numerical stability and is kept constant [3, 33, 85, 104, 106]. Proving that the kinetic description is valid even in the limit of zero viscosity is a great achievement of our theoretical approach. However, we also note that a different inertial regime  $\nu \ll \alpha \ll 1$ , where  $\nu$  and  $\alpha$  would be related to each other, could lead to a different asymptotic behaviour for  $F_0$  and  $\Xi$ . Preliminary results in the case of the constant shear base flow are reported in our publication [18], but a general picture is still missing.

All those possible regimes have to be stated more precisely. They could lead to different conclusions when it comes to the zonal energy balance (see section 5.3.2) or to the ergodicity of the linearized equation (see section 5.3.3). A more precise study of the effective dynamics of zonal jets in those regimes is a very interesting perspective of this work.

From a physical point of view, the main consequence of the asymptotic form of the integrated autocorrelation function  $\Xi^\alpha[U]$  in the inertial limit (see equation (5.15)) is that the average energy injection rate by the stochastic forcing  $\alpha\xi[U]$  in the effective equation of zonal jets at second order (stochastic kinetic equation (5.1)) is of order  $\alpha$ , like the energy injection by the drift  $\alpha F_0$  (see section 5.3.2). This means that in the limit  $\alpha \rightarrow 0$ , we do not expect the relative fluctuations of the mean flow to become negligible (in the energy norm). More precisely, consider the energy of the mean zonal flow  $E_{\overline{U}} = \int dy \overline{U}(y)^2$  and the mean energy of the zonal flow  $\overline{E} = \int dy \overline{U^2}(y)$ , where the overbar denotes for instance a time average, in a direct numerical simulation of the stochastic 2D Navier-Stokes equation. The theoretical results of section 5.2 suggest that  $\Delta E = \overline{E} - E_{\overline{U}}$  should converge to a constant as  $\alpha \rightarrow 0$ , which is counter-intuitive. A very interesting ongoing project is to study empirically the validity of this result in direct numerical simulations. Related results are presented in next chapter.

# Chapter 6

## Large deviations of zonal jets

In chapters 3–5, we have studied an effective equation for the dynamics of zonal jets in the regime where they evolve much slower than the surrounding turbulence. This effective equation (kinetic equation) can only describe the typical dynamics of zonal jets: attractors, relaxation towards the attractors and typical fluctuations around the attractors. In particular, the kinetic equation is not able to describe accurately rare events in zonal jet dynamics, such as extreme fluctuations that can lead to the transition from an attractor to another one.

Such rare transitions were for instance observed in numerical simulations of the stochastic barotropic model, see figure 2 (page 8) and section 1.2.5 (page 18). Describing the statistics of such rare events is a major challenge in the understanding of zonal jet dynamics, and yet this problem was never studied previously from a theoretical point of view.

In this chapter, we use tools from Large Deviation Theory to compute the probability of rare events in zonal jet dynamics, in the regime of time scale separation between the evolution of the jet and of the turbulent perturbations. We will present original methods to compute numerically or explicitly such probabilities, and apply these methods to the stochastic barotropic model.

Large Deviation Theory allows to study extremely rare events as well as typical events, as explained for instance in chapter 2. In our case, this means that the terms involved in the kinetic equation can be computed from the large deviations functions. As a consequence, the numerical methods presented in this chapter will also be used to quantify the relative influence of the terms in the kinetic equation for zonal jets, and to illustrate some of the theoretical results of chapters 4 and 5.

In the first two sections, we will present original methods to implement the Large Deviation Principle described in chapter 2. Those methods can be applied to any kind of slow-fast dynamical systems, or under some hypothesis that will be precised. In section 6.1 we explain how to compute the relevant large deviation functions from time series analysis, for instance coming from numerical simulations. In section 6.2 we show how to compute these large deviation functions from a simplified closed equation, for a specific class of systems. Those two first sections are rather technical, and can be skipped by the reader interested in geophysical applications.

All the numerical simulations presented in this chapter correspond to the stochastic quasi-geostrophic barotropic model on a rotating sphere. This model is presented

in section 6.3.

In section 6.4, we use the methods presented in sections 6.1 and 6.2 to study numerically the effective slow dynamics of zonal jets (kinetic equation).

Finally in section 6.5, we implement the Large Deviations Principle for zonal jets, and compute numerically the probabilities of rare events using the methods of sections 6.1 and 6.2.

The work presented in this chapters will be the subject of two publications [17, 16].

## 6.1 Estimation of the large deviation function from time series analysis

In this section we consider the stochastic process  $(z, w)$  given by the slow-fast system (2.1) (page 26), that we report here for convenience

$$\begin{cases} \frac{\partial z}{\partial t} = \alpha f(z, w) \\ \frac{\partial w}{\partial t} = b(z, w) + \eta, \end{cases} \quad (6.1)$$

where  $\eta$  is a vector of independent gaussian white noises with covariance matrix  $C$ . As described in section 2.3 (page 32), the slow process  $z$  satisfies a large deviation principle in the limit  $\alpha \rightarrow 0$ , that provides a simple way to compute rare events in the dynamics of  $z$  when  $\alpha \ll 1$ .

In practice, the most interesting quantity to compute is the scaled cumulant generating function (2.26)

$$H(z, \theta) = \lim_{\Delta t \rightarrow \infty} \frac{1}{\Delta t} \ln \mathbb{E}_z \exp \left( \theta \int_0^{\Delta t} f(z, \tilde{w}_z(s)) ds \right), \quad (6.2)$$

where  $\mathbb{E}_z$  is the average in the stationary state of the virtual fast process

$$\frac{\partial \tilde{w}_z}{\partial s} = b(z, \tilde{w}_z) + \eta, \quad (6.3)$$

where  $z$  is a fixed parameter. As explained in section 2.3, the infinite-time limit in (6.2) is consistent with the time scale separation between  $z$  and  $w$ , and  $\theta \rightarrow H(z, \theta)$  can be seen as the scaled cumulant generating function for the random process  $\dot{z}$  at a given  $z$ .

In this section we present a way to compute the scaled cumulant generating function (6.2) from a time series of the virtual fast process (6.3), for instance obtained from a direct numerical simulation.

Consider a time series  $\{\tilde{w}_z(s)\}_{0 \leq s \leq T}$  of the virtual fast process (6.3), with a given total time window  $s \in [0, T]$ . We use this continuous time series notation for simplicity, the generalization of the following formulas to the case of discrete time series is straightforward. We also denote for simplicity  $R(s) \equiv f(z, \tilde{w}_z(s))$ .

The basic idea to estimate the scaled cumulant generating function (6.2) is to divide the full data set  $\{\tilde{w}_z(s)\}_{0 \leq s \leq T}$  into blocks of length  $\Delta t$ , to compute the integrals  $\int_{t_0}^{t_0 + \Delta t} R(s) ds$  over those blocks, and then to average the quantity

$\exp\left(\theta \cdot \int_{t_0}^{t_0+\Delta t} R(s) ds\right)$ . For a small block length  $\Delta t$ , the large-time regime defined by the limit  $\Delta t \rightarrow \infty$  in the theoretical expression of  $H$  (6.2) is not attained. On the other hand, too large values of  $\Delta t$  —typically of the order of the total time  $T$ — lead to a low number of blocks, and thus to a very poor estimation of the empirical mean. Estimating  $H$  thus requires finding an intermediate regime for  $\Delta t$ . More precisely, we expect this regime to be attained for  $\Delta t$  equal to a few times the decorrelation time of the process  $R(s)$ , defined by [77, 84]

$$\tau \equiv \lim_{\Delta t \rightarrow \infty} \frac{\int_0^{\Delta t} \int_0^{\Delta t} \mathbb{E}_z [[R(s_1)R(s_2)]] ds_1 ds_2}{2\Delta t \mathbb{E}_z [[R^2]]} = \frac{\int_0^\infty \mathbb{E}_z [[R(s)R(0)]] ds}{\mathbb{E}_z [[R^2]]}, \quad (6.4)$$

where  $\mathbb{E}_z [[R(s_1)R(s_2)]]$  is the covariance of  $R$  at time  $s_1$  and at time  $s_2$ . The second equality is easily obtained using computations very similar to those reported in appendix B.2. Because of the infinite-time limit in (6.4), the estimation of  $\tau$  suffers from the same finite sampling problem as the estimation of  $H$ .

The interesting values of the block length  $\Delta t$  are given by the value of  $\tau$ , which itself depends on  $\Delta t$ . Finding a block length  $\Delta t$  such that the estimation of  $H$  and  $\tau$  is accurate is thus a tricky problem. In the following, we propose a method to find the optimal  $\Delta t$  and estimate the quantities we are interested in. The proposed method is close to the “data bunching” method used to estimate errors in Monte Carlo simulations [56].

### 6.1.1 Estimation of the decorrelation time

We will first consider the problem of the estimation of  $\tau$  in a simple solvable case, so the numerical results can be compared directly to explicit formulas. Consider the stochastic process  $R(s) = w(s)^2$  where  $w$  is the one-dimensional Ornstein-Uhlenbeck process

$$\frac{dw}{ds} = -w(s) + \eta(s), \quad (6.5)$$

where  $\eta$  is a gaussian white noise with correlation  $\mathbb{E}(\eta(s)\eta(s')) = \delta(s-s')$ . A direct calculation gives the decorrelation time of  $R$ ,  $\tau = 1/2$ . The scaled cumulant generating function can also be computed explicitly, as will be explained in section 6.2.

For a time series  $\{R(s)\}_{0 \leq s \leq T}$ , we denote  $\bar{R}_T = \frac{1}{T} \int_0^T R(s) ds$  and  $\text{var}_T(R) = \frac{1}{T} \int_0^T (R(s) - \bar{R}_T)^2 ds$  respectively the empirical mean and variance of  $R$  over the full time series. We then estimate the decorrelation time  $\tau$  defined in (6.4) using an average over blocks of length  $\Delta t$ ,

$$\tau_{\Delta t} = \frac{1}{2\Delta t \text{var}_T(R)} \mathbb{E}_{\frac{T}{\Delta t}} \left[ \left( \int_{t_0}^{t_0+\Delta t} (R(s) - \bar{R}_T) ds \right)^2 \right], \quad (6.6)$$

where  $\mathbb{E}_{\frac{T}{\Delta t}} [h_{t_0}]$  is the empirical average over realisations of the quantity  $h_{t_0}$  inside the brackets<sup>1</sup>.

<sup>1</sup>Explicitely,

$$\mathbb{E}_{\frac{T}{\Delta t}} \left[ \left( \int_{t_0}^{t_0+\Delta t} (R(s) - \bar{R}_T) ds \right)^2 \right] = \frac{\Delta t}{2T} \sum_{k=0}^{\frac{2T}{\Delta t}-2} \left( \int_{k\Delta t/2}^{k\Delta t/2+\Delta t} (R(s) - \bar{R}_T) ds \right)^2, \quad (6.7)$$

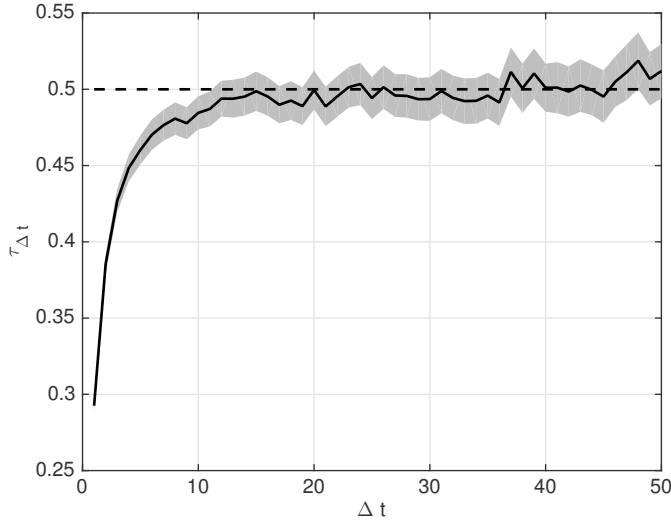


Figure 6.1: Plot of the estimated decorrelation time  $\tau_{\Delta t}$  (black line) and error bars (grey shading) as functions of  $\Delta t$ . For small values of  $\Delta t$ , the large-time limit in (6.4) is not achieved, which explains the low values of  $\tau_{\Delta t}$ . For too large values of  $\Delta t$ , the empirical average  $\mathbb{E}_{\frac{T}{\Delta t}}$  in (6.6) is not accurate due to the small value of  $\frac{T}{\Delta t}$ , which explains the increasing fluctuations in  $\tau_{\Delta t}$  as  $\Delta t$  increases. The optimal value  $\Delta t^*$  is the one in between these artificial behaviour. Here, one can read  $\Delta t^* \simeq 20$  and  $\tau_{\Delta t^*} \simeq 0.5$ , in agreement with the exact value  $\tau = 1/2$  (dashed line). The Ornstein-Uhlenbeck process (6.5) has been integrated over  $T = 5.10^4$  using the method proposed in [45], with time step  $10^{-3}$ .

To find the optimal value of  $\Delta t$ , we plot  $\tau_{\Delta t}$  as a function of  $\Delta t$ , see figure 6.1. For small values of  $\Delta t$ , the large-time limit in (6.4) is not achieved, which explains the low values of  $\tau_{\Delta t}$ . For too large values of  $\Delta t$ , the empirical average  $\mathbb{E}_{\frac{T}{\Delta t}}$  in (6.6) is not accurate due to the small value of  $\frac{T}{\Delta t}$  (small number of blocks), which explains the increasing fluctuations in  $\tau_{\Delta t}$  as  $\Delta t$  increases. The optimal value of  $\Delta t$ —denoted  $\Delta t^*$  in the following—is the one in between these artificial behaviours. It should satisfy  $T \gg \Delta t^* \gg \tau_{\Delta t^*}$ . Here, one can read  $\Delta t^* \simeq 10$  and  $\tau_{\Delta t^*} \simeq 0.5$ , so this optimal  $\Delta t^*$  satisfies the aforementioned condition. The estimated value  $\tau_{\Delta t^*}$  is in agreement with the theoretical value  $\tau = 1/2$ .

The error bars for  $\tau_{\Delta t}$  are given by  $\Delta\tau_{\Delta t} = \sqrt{\text{var}(\tau_{\Delta t})/N_{\text{terms}}}$ , where  $\text{var}(\tau_{\Delta t})$  is the empirical variance associated with the average  $\mathbb{E}_{\frac{T}{\Delta t}}$  defined in (6.7), and  $N_{\text{terms}}$  is the number of terms in this sum (roughly  $N_{\text{terms}} \simeq 2T/\Delta t$ ).

### 6.1.2 Estimation of the scaled cumulant generating function

The self-consistent estimation of the decorrelation time  $\tau$  presented in the previous section gives the optimal value  $\Delta t^*$  of the block length. Then, the scaled cumulant generating function is computed for a given value of  $\theta$  as

---

assuming for simplicity that  $T/\Delta t$  is an integer. Generalisations to any  $T, \Delta t$  is straightforward, replacing  $2T/\Delta t$  by its floor value. The 50% overlap is suggested by Welch's estimator of the power spectrum of a random process [117].

$$H_T(\theta) \equiv \frac{1}{\Delta t^*} \ln \mathbb{E}_{\frac{T}{\Delta t^*}} \left[ \exp \left( \theta \int_{t_0}^{t_0 + \Delta t^*} R(s) ds \right) \right], \quad (6.8)$$

where  $\mathbb{E}_{\frac{T}{\Delta t^*}}$  is the empirical average over the blocks, as defined in (6.7). However, as explained in chapter 2, the knowledge of  $H(z, \theta)$  for an arbitrarily large value of  $|\theta|$  leads to the probability of an arbitrarily rare event for  $\dot{z}$ . This is in contradiction with the fact that the available time series  $\{R(s)\}_{0 \leq s \leq T}$  is finite. In other words, the range of values of  $\theta$  for which the scaled cumulant generating function  $H_T(\theta)$  can be computed with accuracy depends on  $T$ .

Indeed, for large positive values of  $\theta$ , the sum  $\mathbb{E}_{\frac{T}{\Delta t^*}}$  in (6.8) is dominated by the largest term  $\exp(\theta I_{max})$  where  $I_{max} = \max_{t_0} \left\{ \int_{t_0}^{t_0 + \Delta t} R(s) ds \right\}$  is the largest value of  $\int_{t_0}^{t_0 + \Delta t} R(s) ds$  over the finite sample  $\{R(s)\}_{0 \leq s \leq T}$ . Then  $H_T(\theta) \sim \frac{1}{\Delta t^*} I_{max} \theta$  for  $\theta \gg 1$ . This phenomenon is known as linearization [96], and is clearly an artifact of the finite sample size. We denote  $\theta_{max}$  the value of  $\theta$  such that linearization occurs for  $\theta > \theta_{max}$ . Typically, we expect  $\theta_{max}$  to be a positive increasing function of  $T$ . The same way,  $H_T(\theta) \sim -\frac{1}{\Delta t^*} I_{min} \theta$  for  $\theta < 0$  and  $|\theta| \gg 1$ , with  $I_{min} = \min_{t_0} \left\{ \int_{t_0}^{t_0 + \Delta t} R(s) ds \right\}$ . We thus define similarly  $\theta_{min}$  such that linearization occurs for  $\theta < \theta_{min}$ . Typically, we expect  $\theta_{min}$  to be a negative decreasing function of  $T$ .

The convergence of estimators like (6.8) is studied in [96], in particular it is shown that error bars can be computed in the range  $[\theta_{min}/2, \theta_{max}/2]$  for a given time series  $\{R(s)\}_{0 \leq s \leq T}$ . An example of computation of  $H_T(\theta)$  is shown in figure 6.2 for the one-dimensional Ornstein-Uhlenbeck process, and compared to the explicit solution. The full error bars in figure 6.2 are given by the error from the estimation of  $\tau$  and the statistical error described in [96]. The method shows excellent agreement with theory, and allows to observe non-gaussian behaviours.

In sections 6.4 and 6.5, we will apply those tools (estimation of the decorrelation time and of the scaled cumulant generating function) to the study of Reynolds' stresses statistics in zonal jet dynamics.

In next section, we present a class of systems for which the computation of the large deviation functions can be done much easier. These theoretical tools will then be applied to the quasi-linear approximation of the barotropic model.

## 6.2 Large deviations of quadratic forms of gaussian processes

In the previous section we have explained how to compute naively the scaled cumulant generating function  $H(z, \theta)$  from a time series of the virtual fast process  $\tilde{w}_z$ . This allows to estimate precisely (with statistical error bars) the probability of typical and moderately rare events in the statistics of the time averaged process  $R(s) \equiv f(z, \tilde{w}_z(s))$ , for any kind of slow-fast system (6.1). However, studying the statistics of arbitrarily rare events with this method is still extremely difficult, as it implies that the length of the time series increases as the probability of the event of interest decreases.

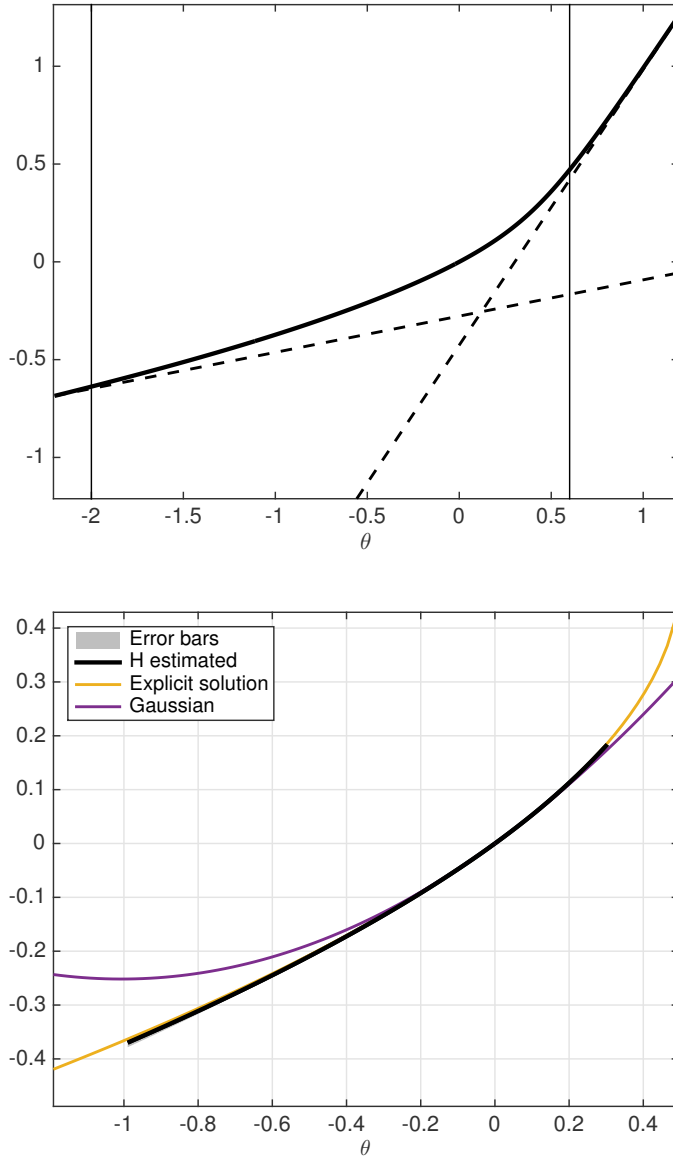


Figure 6.2: Computation of the scaled cumulant generating function from (6.8) for the one-dimensional Ornstein-Uhlenbeck process (6.5). Upper panel: illustration of the linearization effect for large values of  $|\theta|$ . The solid curve is the estimated scaled cumulant generating function  $H_T$ , and the dashed lines are the expected linear tails, which are artifacts of the finite sample size [96]. The thin vertical lines show the range  $\theta \in [\theta_{min}, \theta_{max}]$  for which we consider that linearization does not take place. Bottom panel: the converged scaled cumulant generating function estimator  $H_T$  on  $\theta \in [\theta_{min}/2, \theta_{max}/2]$  (thick black curve, with error bars in grey shading). The yellow curve is the exact scaled cumulant generating function (see section 6.2), it fits the estimated one within statistical errors. The purple curve is the quadratic fit, that corresponds to a gaussian process  $R(s)$  (see section 2.3.3 page 35). This quadratic fit is computed using the exact mean, variance and decorrelation time of  $R$ . The Ornstein-Uhlenbeck process (6.5) has been integrated over  $T = 5 \cdot 10^4$  using the method proposed in [45], with time step  $10^{-3}$ .

In this section we consider a specific class of system, for which the scaled cumulant generating function can be computed through a closed equation. This equation depends parametrically on  $\theta$ , and we will see that in cases of interest the duration of the numerical resolution of this equation does not depend on  $\theta$ . This means that solving this equation allows to study arbitrarily rare events extremely easily, and to compute very low probabilities in a given time.

We consider the class of stochastic processes of the form<sup>2</sup>

$$\begin{cases} \frac{\partial z}{\partial t} = \alpha (r_z + w^T \cdot M_z \cdot w) \\ \frac{\partial w}{\partial t} = -L_z \cdot w + \eta. \end{cases} \quad (6.9)$$

For simplicity in the notations, we will assume that  $z$  is a scalar variable and that  $w$  is  $m$ -dimensional (the generalization to different settings is straightforward, see section 6.5). Then,  $r_z$  is a scalar,  $M_z$  is a  $m \times m$  quadratic form and  $L_z$  is a  $m \times m$  linear operator, that can depend parametrically on the slow variable  $z$ , and  $\eta$  is a gaussian random vector with zero mean and covariance matrix  $C$ .

The virtual fast process (6.3) here reads

$$\frac{\partial \tilde{w}_z}{\partial s} = -L_z \cdot \tilde{w}_z + \eta. \quad (6.10)$$

This is a linear gaussian process (Ornstein-Uhlenbeck process). In this simple case, the scaled cumulant generating function (6.2) can be computed extremely easily, as we now explain.

### 6.2.1 The Ricatti equation

In appendix G.1, we show that the scaled cumulant generating function for the system (6.9) reads [16]

$$H(z, \theta) = \theta r_z + \text{tr} (CN_\infty(z, \theta)). \quad (6.11)$$

where  $N_\infty(z, \theta)$  is the stationary solution of the matrix Ricatti equation

$$\frac{\partial N}{\partial t} + L_z^T N(t, z, \theta) + N(t, z, \theta) L_z = 2N(t, z, \theta) C N(t, z, \theta) + \theta M_z. \quad (6.12)$$

Note that equation (6.12) may have more than one solution: we should take the one such that  $N_\infty(z, 0) = 0$ , so that  $H(z, 0) = 0$ .

In section 6.5, we will present a numerical resolution of (6.12) for the case of the quasi-linear barotropic equation on the sphere, and then compute directly the scaled cumulant generating function using (6.11). We will see that (6.12) can be very easily solved for a given value of  $\theta$ . This means that the result (6.11) allows to study arbitrarily rare events in zonal jet dynamics extremely easily, through the Large

<sup>2</sup>In the equation for  $\dot{z}$ , a linear term in  $w$  could be added. This is the case considered in our publication [16], and in appendix G. This slight generalization is not necessary for the application to the barotropic model, considered in section 6.5.

Deviation Principle. Such result is in clear contrast with approaches through direct numerical simulations, which require that the total time of integration increases as the probability of the event of interest decreases.

We now describe some basic properties of the Ricatti equation (6.12).

### 6.2.2 Link with the Lyapunov equation

As explained in section 2.3.3, the scaled cumulant generating function  $H(z, \theta)$  for small  $\theta$  contains the information about the Law of Large Numbers and the Central Limit Theorem. More precisely, from (2.30) (page 35) we expect to have

$$H(z, \theta) = \theta F(z) + O(\theta^2), \quad (6.13)$$

where we recall that in the Law of Large Numbers, the average drift is  $F(z) \equiv \mathbb{E}_z[f(z, \tilde{w}_z)]$ . At first order in  $\theta$ , equations (6.11) and (6.12) then give  $F(z) = r_z + \text{tr} \left( CN_\infty^{(1)}(z) \right)$  where  $N_\infty^{(1)}(z)$  is the stationary solution of the Ricatti equation at lowest non trivial order

$$\frac{\partial N^{(1)}}{\partial t} + L_z^T N^{(1)}(t, z) + N^{(1)}(t, z) L_z = M_z. \quad (6.14)$$

This equation can be solved as

$$N^{(1)}(t, z) = \int_0^t e^{-t_1 L_z^T} M_z e^{-t_1 L_z} dt_1, \quad (6.15)$$

so

$$F(z) = r_z + \int_0^\infty \text{tr} \left( C e^{-t_1 L_z^T} M_z e^{-t_1 L_z} \right) dt_1. \quad (6.16)$$

Using the properties of the trace, we can write  $F(z) = r_z + \text{tr} (M_z g_z)$  with  $g_z = \int_0^\infty e^{-t_1 L_z} C e^{-t_1 L_z^T} dt_1$ . We recognize in  $g_z$  the stationary solution of the Lyapunov equation associated with the virtual fast process  $\tilde{w}_z$ , which means that  $g_z$  is the stationary two-points correlation function of  $\tilde{w}_z$ <sup>3</sup>. We have thus recovered the definition  $F(z) = \mathbb{E}_z[f(z, \tilde{w}_z)]$  from the Ricatti equation.

The same procedure could be applied to recover the definition of the forcing covariance  $\Xi(z)$  from (2.30) and from the system (6.11), (6.12). The computations are straightforward, so we don't report them here.

### 6.2.3 An explicit solution

As we have seen in the previous paragraph, a natural way to tackle the Ricatti equation (6.12) is to solve it perturbatively in  $\theta$ . This is done in appendix G.2, and the result is the following:

If  $M_z L_z = L_z^T M_z$  and  $L_z$  commutes with  $CM_z$ , then

$$H(\theta) = \theta r_z + \frac{1}{2} \text{tr} \left[ L_z - \sqrt{L_z^2 - 2\theta CM_z} \right], \quad (6.17)$$

<sup>3</sup>Actually this last expression of  $g_z$  is exactly the equivalent of the formula (4.16) (in page 53) used in chapters 4 and 5.

whenever the square root  $\sqrt{L_z^2 - 2\theta CM_z}$  exists [16]. Note that in this expression, the square root should be chosen such that  $H(0) = 0$ .

Under those hypothesis, we are able to compute explicitly the probability of any deviation from the mean for the process  $\dot{z}$ . This is for instance the case when the fast process  $\tilde{w}_z$  is one-dimensional. Indeed, in this case the commutation conditions are automatically satisfied, and the explicit solution (6.17) takes a very simple form. This is the case considered in figure 6.2.

In the case of the barotropic model, it can be checked directly that the condition  $ML_U = L_U^T M$ , where  $L_U$  is the linearized equation close to the base flow  $U$  and  $M$  is the quadratic form that defines the Reynolds' stress divergence, is not fulfilled. As a consequence, the explicit solution (6.17) cannot be used in this context.

### 6.3 Barotropic dynamics on a rotating sphere

In sections 6.4 and 6.5, we will apply the tools of chapter 2 and previous sections (estimation of the scaled cumulant generating function and computation from the Ricatti equation) to the study of zonal jet statistics.

For practical reasons, we consider here the case of a barotropic flow on the surface of a rotating sphere. This system is first presented in this section. As we will see, this model is similar to the biperiodic barotropic model studied in chapters 1, 3–5. In particular, we will find a similar regime of time scale separation between the evolution of zonal jets and of turbulent eddies, and we will focus on a quasi-linear approximation of the dynamics, like the one defined in section 3.2.1 (page 41) for the biperiodic case.

We study the dynamics of zonal jets in the quasi-geostrophic one-layer barotropic model on a sphere of radius  $a$ , rotating at rate  $\Omega$ ,

$$\begin{cases} \frac{\partial \omega}{\partial t} + J(\psi, \omega) + \frac{2\Omega}{a^2} \frac{\partial \psi}{\partial \lambda} = -\kappa \omega - \nu_n (-\Delta)^n \omega + \sqrt{\sigma} \eta, \\ u = -\frac{1}{a} \frac{\partial \psi}{\partial \phi}, \quad v = \frac{1}{a \cos \phi} \frac{\partial \psi}{\partial \lambda}, \quad \omega = \Delta \psi \end{cases} \quad (6.18)$$

where  $\omega$  is the relative vorticity,  $\mathbf{v} = (u, v)$  is the horizontal velocity field,  $\psi$  is the stream function and  $J(\psi, \omega) = \frac{1}{a^2 \cos \phi} (\partial_\lambda \psi \cdot \partial_\phi \omega - \partial_\lambda \omega \cdot \partial_\phi \psi)$  is the jacobian operator. The coordinates are denoted  $(\lambda, \phi) \in [0, 2\pi] \times [-\pi/2, \pi/2]$ ,  $\lambda$  is the longitude and  $\phi$  is the latitude. All fields  $\omega, u, v$  and  $\psi$  can be decomposed onto the basis of spherical harmonics, for example

$$\psi(\lambda, \phi) = \sum_{\ell=0}^{\infty} \sum_{m=-\ell}^{\ell} \psi_{m,\ell} Y_\ell^m(\phi) e^{im\lambda}. \quad (6.19)$$

All fields  $\omega, u, v$  and  $\psi$  are  $2\pi$ -periodic in the zonal ( $\lambda$ ) direction, so we can also define the Fourier coefficients in the zonal direction,

$$\psi_m(\phi) \equiv \frac{1}{2\pi} \int_0^{2\pi} \psi(\lambda, \phi) e^{-im\lambda} d\lambda = \sum_{\ell=0}^{\infty} \psi_{m,\ell} Y_\ell^m(\phi). \quad (6.20)$$

In (6.18),  $\kappa$  is a linear friction coefficient, also known as Ekman drag or Rayleigh friction, that models the dissipation of energy at the large scales of the flow [110]. Hyper-viscosity  $\nu_n (-\Delta)^n$  accounts for the dissipation of enstrophy at small scales and is used mainly for numerical reasons. As we will discuss along the chapter most of the dynamical quantities are independent of the value of  $\nu_n$ , for small enough  $\nu_n$ .  $\eta$  is a gaussian noise with zero mean and correlations  $\mathbb{E}[\eta(\lambda_1, \phi_1, t_1) \eta(\lambda_2, \phi_2, t_2)] = C(\lambda_1 - \lambda_2, \phi_1, \phi_2) \delta(t_1 - t_2)$ , where  $C$  is a positive-definite function.  $C$  is assumed to be normalized such that  $\sigma$  is the average injection of energy per unit of time and per unit of mass by the stochastic force  $\sqrt{\sigma}\eta$ .

### 6.3.1 Energy balance and non-dimensional equations

The inertial barotropic model (eq. (6.18) with  $\kappa = \nu_n = \sigma = 0$ ) conserves the energy  $\mathcal{E}[\omega] = -\frac{1}{2} \int \omega \psi \, \mathbf{dr}$  (we denote  $\mathbf{dr} = a^2 \cos \phi \, d\phi d\lambda$ ), the moments of potential vorticity  $\mathcal{C}_m[\omega] = \int (\omega + f)^m \, \mathbf{dr}$  with the Coriolis parameter  $f(\phi) = 2\Omega \sin \phi$ , and the linear momentum  $L[\omega] = \int \omega \cos \phi \, \mathbf{dr}$ .

The average energy balance for the dissipated and stochastically forced barotropic equation is obtained applying the Ito formula to (6.18) [44], it reads

$$\frac{dE}{dt} = -2\kappa E - 2\nu_n Z_n + \sigma, \quad (6.21)$$

where  $E = \mathbb{E}[\mathcal{E}[\omega]]$  is the total average energy and  $Z_n = \mathbb{E}[-\frac{1}{2} \int \psi (-\Delta)^n \omega \, \mathbf{dr}]$ . The term  $-2\nu_n Z_n$  in (6.21) represents the dissipation of energy at the small scales of the flow. In the regime we are interested in, most of the energy is concentrated in the large-scale zonal jet, so the main mechanism of energy dissipation is the linear friction (first term in the right-hand side of (6.21)). In this turbulent regime, the energy dissipation by hyper-viscosity can be neglected. Then, in a statistically stationary state,  $E_{stat} \simeq \frac{\sigma}{2\kappa}$ , expressing the balance between stochastic forces and linear friction in (6.18).

This average total energy estimate yields the typical jet velocity  $U \sim \sqrt{\frac{\sigma}{2\kappa}}$ . The order of magnitude of the time scale of advection and stirring of turbulent eddies by this jet is  $\tau_{eddy} \sim \frac{a}{U}$ . We perform a non-dimensionalization of the stochastic barotropic equation (6.18) using  $\tau_{eddy}$  as unit time and  $a$  as unit length. This amounts at setting  $a = 1$  and at using the adimensionalized variables  $t' = t/\tau_{eddy}$ ,  $\omega' = \omega\tau_{eddy}$ ,  $\psi' = \psi\tau_{eddy}$ ,  $\Omega' = \Omega\tau_{eddy}$ ,

$$\alpha = \kappa\tau_{eddy} = \sqrt{\frac{2\kappa^3}{\sigma}}, \quad (6.22)$$

$\nu'_n = \nu_n\tau_{eddy}$ ,  $\sigma' = \sigma\tau_{eddy}^3 = 2\alpha$ , and a rescaled force  $\eta' = \eta\sqrt{\tau_{eddy}}$  such that  $\mathbb{E}[\eta'(\lambda_1, \phi_1, t'_1) \eta'(\lambda_2, \phi_2, t'_2)] = C(\lambda_1 - \lambda_2, \phi_1, \phi_2) \delta(t'_1 - t'_2)$ . In these new units, and dropping the primes for easiness in the notation, the stochastic barotropic equation (6.18) reads

$$\frac{\partial \omega}{\partial t} + J(\psi, \omega) + 2\Omega \frac{\partial \psi}{\partial \lambda} = -\alpha \omega - \nu_n (-\Delta)^n \omega + \sqrt{2\alpha} \eta. \quad (6.23)$$

In (6.23),  $\alpha$  is an inverse Reynolds' number based on the linear friction and  $\nu_n$  is an inverse Reynolds' number based on hyper-viscosity. The turbulent regime

mentioned before corresponds to  $\nu_n \ll \alpha \ll 1$ . In such regime and in the units of (6.23), the total average energy in a statistically stationary state is  $E_{stat} = 1$ .

We are interested in the dynamics of zonal jets in the regime of small forces and dissipation, defined as  $\alpha \ll 1$ . As we will see now, it corresponds to a regime where the zonal jet evolves much slower than the surrounding turbulent eddies.

### 6.3.2 Decomposition into zonal and non-zonal components

In order to decompose (6.23) into a zonally averaged flow and perturbations around it, we define the zonal projection of a field

$$\langle \psi \rangle (\phi) \equiv \psi_0(\phi) = \frac{1}{2\pi} \int_0^{2\pi} \psi(\lambda, \phi) d\lambda.$$

The zonal jet velocity profile is then defined by  $U(\phi) \equiv \langle u \rangle (\phi)$ . In most situations of interest, the stochastic force in (6.23) does not act directly on the zonal flow:  $\langle \eta \rangle = 0$ . Then the perturbations to the zonal jet will be proportional to the amplitude of the stochastic force in (6.23). We thus decompose the velocity field as  $\mathbf{v} = U\mathbf{e}_x + \sqrt{\alpha}\delta\mathbf{v}$  and the relative vorticity field as  $\omega = U + \sqrt{\alpha}\delta\omega$  with  $\omega_z \equiv \langle \omega \rangle$ , and where  $\alpha$  is the non-dimensional parameter defined in (6.22). The perturbation velocity  $\delta\mathbf{v}$  and vorticity  $\delta\omega$  will be called eddy velocity and eddy vorticity, respectively.

This ansatz is very similar to the one done in chapter 3 in the bi-periodic case. The self-consistency of this assumption has then been discussed in details in chapters 4 and 5, from a theoretical point of view. In this chapter, we will address this issue using direct numerical simulations, and we will recover some theoretical results of chapters 4 and 5.

With this decomposition of the vorticity field, the barotropic equation (6.23) reads

$$\begin{cases} \frac{\partial \omega_z}{\partial t} = \alpha R - \alpha \omega_z - \nu_n (-\Delta)^n \omega_z \\ \frac{\partial \delta\omega}{\partial t} = -L_U [\delta\omega] - \sqrt{\alpha} NL [\delta\omega] + \sqrt{2}\eta, \end{cases} \quad (6.24)$$

with  $R(\phi) \equiv -\langle J(\delta\psi, \delta\omega) \rangle$  the zonally averaged advection term, where the linear operator  $L_U$  reads

$$L_U [\delta\omega] = \frac{1}{\cos \phi} (U(\phi)\partial_\lambda \delta\omega + \gamma(\phi)\partial_\lambda \delta\psi) + \alpha \delta\omega + \nu_n (-\Delta)^n \delta\omega, \quad (6.25)$$

with  $\gamma(\phi) = \partial_\phi \omega_z(\phi) + 2\Omega \cos \phi$ , and where

$$NL [\delta\omega] = J(\delta\psi, \delta\omega) - \langle J(\delta\psi, \delta\omega) \rangle$$

is the non-linear eddy-eddy interaction term.

### 6.3.3 Quasi-linear and linear dynamics

In the limit of small forces and dissipation  $\alpha \ll 1$ , the perturbation flow is expected to be of small amplitude. Then the non-linear term  $NL[\delta\omega]$  in (6.24) is negligible

compared to the linear term  $L_U[\delta\omega]$ . Neglecting these non-linear eddy-eddy interaction terms, we then obtain the so-called quasi-linear approximation of the barotropic equation [104],

$$\begin{cases} \frac{\partial\omega_z}{\partial t} = \alpha R - \alpha\omega_z - \nu_n(-\Delta)^n\omega_z \\ \frac{\partial\delta\omega}{\partial t} = -L_U[\delta\omega] + \sqrt{2}\eta. \end{cases} \quad (6.26)$$

The approximation leading to the quasi-linear dynamics (6.26) amounts at suppressing some of the triad interactions. As a consequence, the inertial quasi-linear dynamics has the same quadratic invariants as the initial barotropic equations. The average energy balance for the quasi-linear barotropic dynamics (6.26) is thus the same as the one for the full barotropic dynamics (6.24).

Using  $\omega_z(\phi) = -\frac{1}{\cos\phi}\partial_\phi(U(\phi)\cos\phi)$  and the first equation of (6.26), we get the evolution equation for the zonal flow velocity  $U(\phi)$

$$\frac{\partial U}{\partial t} = \alpha f - \alpha U - \nu_n(-\Delta)^n U, \quad (6.27)$$

where  $f(\phi)$  is such that  $R(\phi) = -\frac{1}{\cos\phi}\partial_\phi(f(\phi)\cos\phi)$ .  $f$  is minus the divergence of the Reynolds' stress, also called Reynolds' force.

In many situations of interest, as for example in the case of Jovian jets, the turbulent eddies  $\delta\omega$  evolve much faster than the zonal jet velocity profile  $U$  (see chapter 1 and [90]). In (6.24) and (6.26), the natural time scale of evolution of the zonal jet is of order  $1/\alpha$ , while the typical time scale of evolution of the perturbation vorticity  $\delta\omega$  is of order 1. In the regime  $\alpha \ll 1$ , we thus expect to observe a separation of time scales between the evolution of  $\omega_z$  and  $\delta\omega$ . This is consistent with the definition of  $\alpha$  as the ratio of the inertial time scale  $\tau_{eddy}$  and of the dissipative time scale  $1/\kappa$ , see (6.22).

The quasi-linear barotropic equation can be put under the form of the slow-fast dynamical system (6.9), with the analogy

$$\begin{aligned} z &\equiv \omega_z, \quad w \equiv \delta\omega \\ r_z &\equiv -\omega_z - \frac{\nu_n}{\alpha}(-\Delta)^n\omega_z \\ w^T \cdot M_z \cdot w &\equiv -\langle J(\delta\psi, \delta\omega) \rangle \\ \eta &\equiv \sqrt{2}\eta \\ L_z \cdot w &\equiv L_U[\delta\omega]. \end{aligned} \quad (6.28)$$

The associated virtual fast process in the limit  $\alpha \rightarrow 0$  reads

$$\frac{\partial\delta\omega}{\partial t} = -L_U[\delta\omega] + \sqrt{2}\eta, \quad (6.29)$$

where  $U$  is held fixed. This equation describes the barotropic dynamics linearized close to the fixed base flow  $U(\phi)$ , through the linear operator (6.25). Like in the biperiodic case of chapters 3–5, equation (6.29) still contains terms of order  $\alpha$  and  $\nu_n$  in  $L_U$ . Using numerical simulations of (6.29), we will study the dependency in  $\alpha$  and  $\nu_n$  of (6.29) in the regime  $\nu_n \ll \alpha \ll 1$ , and discuss the physical consequences for the slow dynamics of zonal jets.

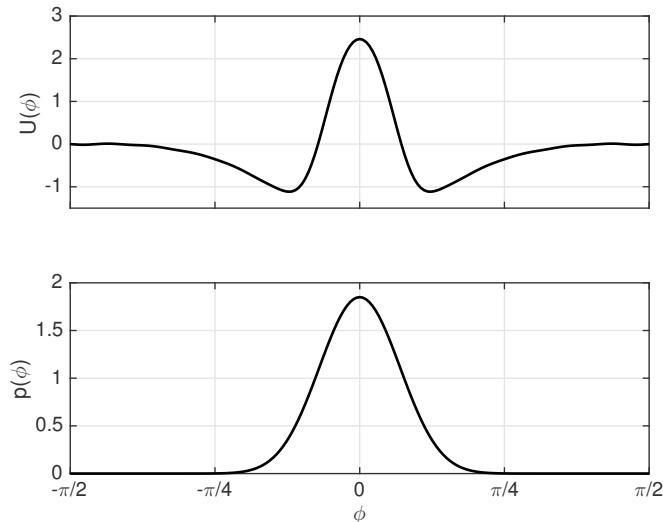


Figure 6.3: Top pannel: the zonal flow velocity profile  $U(\phi)$  used in numerical simulations of the linearized barotropic equation (6.29). Bottom pannel: zonally averaged energy injection rate by the stochastic force  $\eta$  in (6.23), (6.26) and (6.29).

### 6.3.4 Numerical implementation

Direct numerical simulations (DNS) of the barotropic equation (6.24), the quasi-linear barotropic equation (6.26) and the linear equation (6.29) are performed using a purely spectral code with a fourth-order-accurate Runge-Kutta algorithm with an adaptive time step<sup>4</sup>. The spectral cutoffs defined by  $\ell \leq L$ ,  $|m| \leq \min\{\ell, M\}$  in the spherical harmonics decomposition of the fields are taken to be  $L = 80$  and  $M = 20$ . In all the simulations, the rotation rate of the sphere is  $\Omega = 3.7$  in the units defined previously.

The stochastic noise is implemented using the method proposed in [62], with a non-zero renewal time scale  $\tau_r$  larger than the time step of integration. For  $\tau_r$  much smaller than the typical eddy turnover time scale, the noise can be considered as white in time.

The force only acts on the mode  $|m| = 10$ ,  $\ell = 10$ , which is concentrated around the equator (see figure 6.3). With such forcing spectrum and with  $\alpha = 0.073$ , the integration of the quasi-linear barotropic equation (6.26) leads to a stationary state characterized by a strong zonal jet with velocity  $U(\phi)$ , represented in figure 6.3. We use a truncation of this jet (first 25 spherical harmonics) as the mean flow in the simulation of the linear barotropic equation (6.29).

We use hyper-viscosity of order 4 with coefficient  $\nu_4$  such that the damping rate of the smallest mode is 4. To assess that hyper-viscosity is negligible in the large scale statistics, simulations of the linear equation with  $\nu_4 = 4$  and  $\nu_4 = 2$  are compared in sections 6.4 and 6.5.

<sup>4</sup>A program that implements spectral DNS, real-space DNS for the non-linear and quasi-linear equations, and includes all the graphical tools needed to visualize statistics, is freely available. The Objective-C++ and Swift programming languages are employed. C blocks and Grand Central Dispatch enable the efficient use of multiple CPU cores. The application “GCM” is available for OS X 10.9 and higher on the Apple Mac App Store at URL <http://appstore.com/mac/gcm>

## 6.4 Zonal energy balance in the inertial limit

In previous section was presented the stochastic quasi-geostrophic barotropic model on the surface of a rotating sphere, in particular we have seen that this model is very similar to the stochastic barotropic model in a bi-periodic domain: in the limit of weak forces and dissipation, there is a time scale separation between the evolution of the zonal velocity profile  $U(\phi)$  and of the turbulent perturbations (eddy) vorticity  $\delta\omega(\lambda, \phi)$ .

In this regime, an effective dynamics for the zonal velocity profile  $U(\phi)$ , where the turbulent eddies are averaged out, can be derived. This was explained in chapter 2 in a general framework, here we apply those results to zonal jet dynamics in the spherical barotropic model. In particular, we will study the average energy balance for the zonal flow, in the regime  $\nu_n \ll \alpha \ll 1$ .

The effective equation and effective energy balance for  $U(\phi)$  are very similar to those studied theoretically in chapters 3–5. In particular, the effective equation for  $U(\phi)$  is close to a second order closure of the dynamics [66, 68], the main difference being that our effective equation takes into account both the average and typical fluctuations of Reynolds' stresses in the evolution of zonal jets, while second order closures only keep the average Reynolds' stresses.

Here we will adopt an empirical point of view, and study those equations using numerical simulations. One of the goals of such approach is to quantify the influence of the fluctuations of Reynolds' stresses in zonal jet dynamics. We will also comment the numerical results in relation with the theoretical predictions of chapters 4 and 5.

### 6.4.1 Effective slow dynamics and effective zonal energy balance

The effective slow evolution of  $\omega_z$  (or equivalently of  $U$ ) is obtained using the analogy (6.28) and the results of stochastic averaging presented in chapter 2 (see equation (2.19) in page 32). Here we consider the quasi-linear dynamics, but we would obtain the same effective equation starting from the full non-linear dynamics (6.24). In both cases, the effective evolution of  $U(\phi)$  is given by

$$\frac{\partial U}{\partial t} = \alpha F^\alpha[U] - \alpha U + \alpha \xi^\alpha[U] \quad (6.30)$$

with  $F^\alpha[U](\phi) = \mathbb{E}_U^\alpha[f(\phi)]$ , where  $\xi^\alpha[U]$  is a gaussian noise with zero mean and correlations (for a fixed  $U$ )

$$\mathbb{E}[\xi^\alpha[U](\phi_1, t_1)\xi^\alpha[U](\phi_2, t_2)] = \delta(t_1 - t_2)\Xi^\alpha[U](\phi_1, \phi_2), \quad (6.31)$$

with  $\Xi^\alpha[U]$  given by (2.20) (we will not need the expression of  $\Xi^\alpha[U]$  here), and where we have neglected viscosity and drift terms of higher order in  $\alpha$ . In these expressions,  $\mathbb{E}_U^\alpha$  is the average in the statistically stationary state of (6.29) with  $U$  held fixed.

The hyperviscous terms in (6.27) essentially dissipate energy at the smallest scales of the flow. In the turbulent regime we are interested in, such small-scale dissipation is negligible in the global energy balance. For this reason, we have neglected those viscous terms in (6.30). Note however that some hyper-viscosity is still present in the numerical simulations of (6.29), in order to ensure numerical stability. For

consistency, we will make sure that those hyper-viscous terms have no influence on the numerical results (see figures 6.4, 6.8).

Note that in contrast with chapters 3–5, we consider here the effective dynamics (6.30) where the terms  $F^\alpha[U]$  and  $\Xi^\alpha[U]$  are computed from (6.29) with  $\alpha \neq 0$ . We will then study the regime  $\alpha \ll 1$  using numerical simulations of (6.29) with different values of  $\alpha$ . This corresponds to take first the limit  $t \rightarrow \infty$  and then  $\alpha \rightarrow 0$  in (6.29).

As explained in chapter 2, (6.30) can be seen as the Law of Large Numbers and the Central Limit Theorem for (6.26). Equation (6.30) describes the effective slow dynamics of zonal jets in the regime  $\nu_n \ll \alpha \ll 1$ , it is the analogous of the kinetic equation studied in chapter 3. In particular, the attractors of (6.30) are the same as the attractors of a second order closure of the barotropic dynamics (CE2 in [66, 68]). The noise term in (6.30) allows to describe the influence of fluctuations of Reynolds' stresses on zonal jet dynamics, while classical closures only take into account the average Reynolds' stresses. Quantifying the influence of these fluctuations is one of the goals of this study. This will be done at the level of the effective zonal energy balance, that we now derive.

The kinetic energy contained in zonal degrees of freedom reads  $E_z = \int d\phi E(\phi)$  with  $E(\phi) = \pi \cos \phi U^2(\phi)$ . Applying the Itô formula<sup>5</sup> to (6.30), we get the equation for the effective evolution of  $E(\phi)$ ,

$$\frac{1}{\alpha} \frac{dE}{dt} = p_{mean}(\phi) - 2E + \alpha p_{fluct}(\phi), \quad (6.32)$$

with the instantaneous energy injection rates into the zonal mean flow, respectively by the average Reynolds' stresses  $p_{mean}(\phi) \equiv 2\pi \cos \phi F^\alpha[U](\phi) U(\phi)$  and by the fluctuations of Reynolds' stresses  $\alpha p_{fluct}(\phi) \equiv \alpha \pi \cos \phi \Xi^\alpha[U](\phi, \phi)$ . Integrating (6.32) over latitudes, we obtain the total zonal energy balance

$$\frac{1}{\alpha} \frac{dE_z}{dt} = P_{mean} - 2E_z + \alpha P_{fluct}, \quad (6.33)$$

with  $P_{mean} \equiv \int d\phi p_{mean}(\phi)$  and  $\alpha P_{fluct} \equiv \int d\phi \alpha p_{fluct}(\phi)$ .

All the terms appearing in (6.32) and (6.33) can be easily estimated using data from a direct numerical simulation of the linearized barotropic equation (6.29). Indeed,  $F^\alpha[U](\phi)$  can be computed as the empirical average of  $f(\phi)$  in the stationary state of (6.29), and  $\Xi^\alpha[U]$  can be computed using the method described in section 6.1.1 to estimate correlation times<sup>6</sup>.

Besides,  $F^\alpha[U]$  and  $\Xi^\alpha[U]$  can be computed directly from the scaled cumulant generating function  $H$ , using (2.30) (page 35). Computing  $H$  using the Ricatti equation (6.11, 6.12) and then using (2.30), we have a very easy way to compute

<sup>5</sup>Formally, the Itô formula leads to an energy balance involving the expectations of  $p_{mean}$  and  $p_{fluct}$  over realizations of the noise  $\xi^\alpha$ , i.e. over realizations of  $U$  itself. Such average energy balance is not relevant physically, indeed we are interested here in the instantaneous energy balance, for a given base flow  $U$ . Relations like (6.32) can be derived formally, see for instance [17].

<sup>6</sup>The statistical error bars for  $p_{fluct}$  are computed from the error in the estimation of  $\Xi^\alpha[U]$ , which is similar to the estimation of the correlation time  $\tau$  described in section 6.1.1. The statistical error bars for  $p_{mean}$  are computed from the error in the estimation of the average  $F^\alpha$ , given by  $(\delta F^\alpha)^2 = \frac{1+2\tau/\Delta t}{N} \text{var}(F^\alpha)$  where  $\tau$  is the autocorrelation time of  $F^\alpha$ ,  $\Delta t$  the time step between measurements of the Reynolds' stress and  $N$  the total number of data points [77].

the terms appearing in the effective slow dynamics (6.30) or in the zonal energy balance equations (6.32) and (6.33), without having to simulate directly the fast process (6.29).

The energy injection rates  $P_{mean}$  and  $\alpha P_{fluct}$ , computed using both of the methods explained above, with different values of the non-dimensional damping rate  $\alpha$  are represented in figure 6.4. The first term  $P_{mean}$  (solid curve) is roughly of the order of magnitude of the dissipation term in (6.33) (recall we use units such that  $E_z \simeq 1$ ). The second term  $\alpha P_{fluct}$  is about an order of magnitude smaller than  $P_{mean}$ . In this case, the energy balance (6.33) implies that the zonal velocity is actually slowly decelerating.

In this case, neglecting  $\alpha P_{fluct}$  in (6.33) leads to an error in the zonal energy budget of about 5–10%. This confirms the fact that fluctuations of Reynolds' stresses are only negligible in a first approximation, but that they should be taken into account in order to have a quantitative description of zonal jet evolution. We further discuss this result in section 6.4.3.

We also observe that  $P_{mean}$  increases up to a finite value as  $\alpha \ll 1$ , while  $\alpha P_{fluct}$  is nearly constant over the range of values of  $\alpha$  considered. We will further comment on those behaviours below.

The spatial distribution of the energy injection rates  $p_{mean}(\phi)$  and  $p_{fluct}(\phi)$  are represented in figures 6.5 and 6.6(a), 6.6(b). Both  $p_{mean}(\phi)$  and  $p_{fluct}(\phi)$  are concentrated in the jet region  $\phi \in [-\pi/4, \pi/4]$ , which is also the region where the stochastic forces act (see figure 6.3). We also observe in figure 6.6(a) that  $p_{mean}$  is always positive, meaning that the turbulent perturbations  $\delta\omega$  are everywhere injecting energy into the zonal degrees of freedom, i.e. the average Reynolds' stresses are intensifying the zonal flow  $U(\phi)$  at each latitude. This effect is predominant at the jet maximum and around the jet minima (around  $\phi = \pm\pi/8$ ).

By definition,  $p_{fluct}(\phi)$  is always positive. However, we clearly see that this quantity is relatively small in the region of jet maximum  $\phi \simeq 0$ . This means that the fluctuations of Reynolds' stresses tend to force the mean zonal flow  $U(\phi)$  predominantly away from the jet extrema, near  $\phi = \pm\pi/16$ .

We now comment in details these numerical results, in relation with the theoretical results obtained in chapters 4 and 5. We first recall that those theoretical results were derived in the case of the bi-periodic barotropic model, with the hypothesis that the deterministic linear dynamics  $\partial_t + L_U$  leads to an inviscid damping of the eddy velocity (see section 4.2 page 50). In the case of the linearized Euler equation in a periodic domain, such inviscid damping is known as the Orr mechanism [82], and applies whenever the operator  $L_U$  has no modes [11]. In the present case of the barotropic dynamics on a sphere, no theoretical results are known, and yet we will see that the behaviour of  $p_{mean}$  and  $p_{fluct}$  obtained from numerical simulations of (6.29) is similar to the behaviour predicted for the bi-periodic case by the theory developed in chapters 4 and 5.

## 6.4.2 Average Reynolds' stresses in the inertial limit

In chapter 4, and under the hypothesis detailed previously, we have shown that  $F^\alpha[U](\phi)$  converges to a finite function of  $\phi$  as  $\alpha \rightarrow 0$  with  $\nu_n \ll \alpha$ . As a conse-

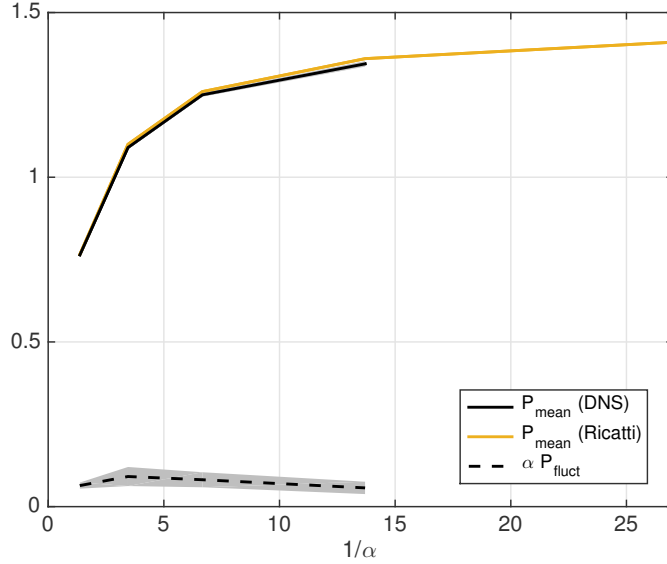


Figure 6.4: Total energy injection rate into the zonal flow by the mean Reynolds' stresses  $P_{mean}$  (first term in the r.h.s of (6.33), in solid line) and by the fluctuations of Reynolds' stresses  $\alpha P_{fluct}$  (last term in the r.h.s of (6.33), in dashed line with statistical error bars in grey shading) as a function of  $1/\alpha$ . Those quantities are estimated from direct numerical simulations (DNS) of the linearized barotropic equation (6.39) with parameters given in section 6.3.4, and  $P_{mean}$  is also computed directly using the Ricatti equation (6.12) (yellow curve). This allows to use finer resolution and smaller viscosity very easily, here the spectral cutoff in the Ricatti calculation is  $L = 120$  (compared to  $L = 80$  for the DNS), and the hyper-viscosity coefficient is such that the smallest scale has a damping rate of 4 (i.e. it is half of the hyperviscosity coefficient in the case  $L = 80$ ). The comparison of the solid black and yellow curves indicates that numerical resolution and hyper-viscosity are negligible in the computation of  $P_{mean}$ . We observe that  $P_{mean}$  is of the same order as the zonal energy dissipation rate due to linear friction (second term in the r.h.s of (6.33)), and that  $\alpha P_{fluct}$  is about an order of magnitude smaller. Neglecting  $\alpha P_{fluct}$  in (6.33) leads to an error in the zonal energy budget of about 5–10%. Besides,  $P_{mean}$  increases up to a finite value as  $\alpha \rightarrow 0$ , in agreement with theoretical predictions.

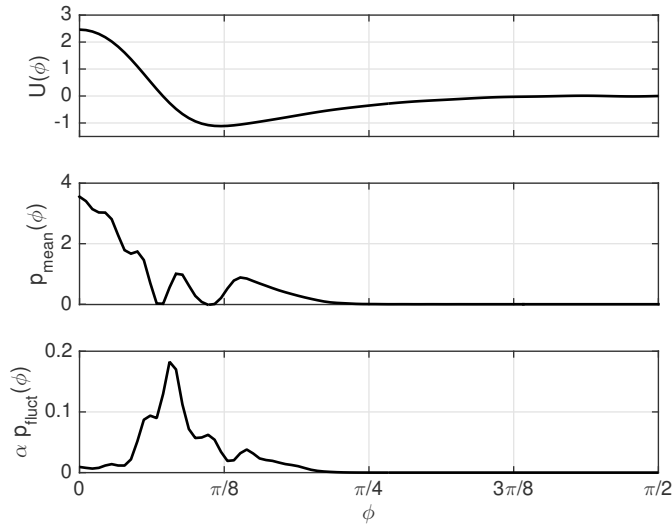
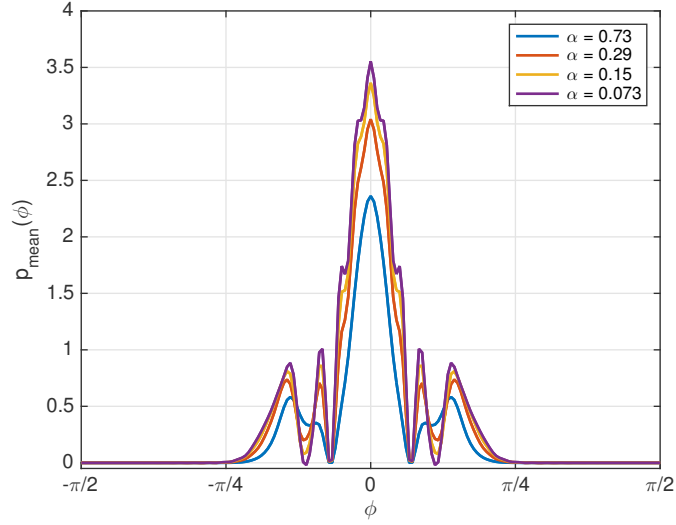
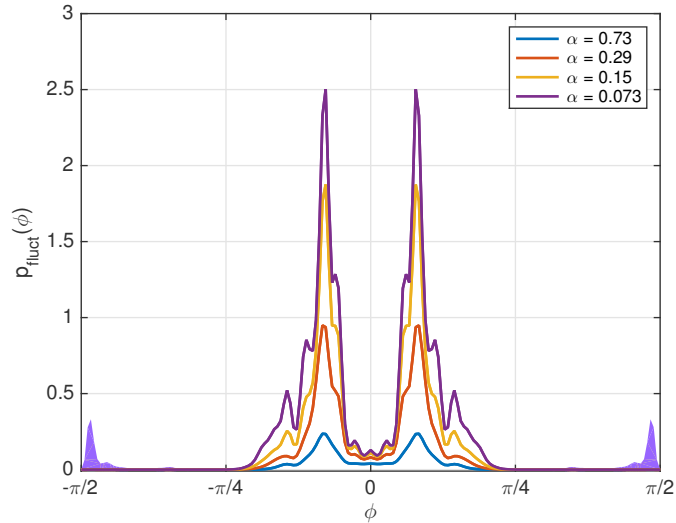


Figure 6.5: From top to bottom: zonal velocity profile  $U(\phi)$ , energy injection rate by the average Reynolds' stresses  $p_{mean}(\phi)$  and energy injection rate by the fluctuations of Reynolds' stresses  $\alpha p_{fluct}(\phi)$ , as functions of latitude  $\phi$  restricted to the Northern hemisphere. The values in the Southern hemisphere are symmetric with respect to those represented here, see figures 6.3, 6.6(a) and 6.6(b).  $p_{mean}$  and  $p_{fluct}$  are estimated from numerical simulations of (6.39) with parameters given in section 6.3.4, and  $\alpha = 0.073$ .  $p_{mean}$  is always positive, meaning that the average Reynolds' stresses are intensifying the zonal flow  $U(\phi)$  at each latitude. We see that fluctuations of Reynolds' stresses are lower at the jet extrema ( $p_{fluct}$  is relatively small), in particular close to the equator  $\phi = 0$ . This can be understood as a consequence of the depletion of vorticity at the stationary streamline [11]. Error bars are not shown here, see figures 6.6(a) and 6.6(b).



(a)



(b)

Figure 6.6: Energy injection rate into the zonal flow (a) by the mean Reynolds' stresses  $p_{mean}$  (first term in the r.h.s of (6.32)) and (b) by the fluctuations of Reynolds' stresses  $p_{fluct}$  (last term in the r.h.s of (6.32)), as functions of latitude  $\phi$ , estimated from direct numerical simulations of the linearized barotropic equation (6.39) with parameters given in section 6.3.4, and with different values of the damping rate  $\alpha$ . Shaded areas represent the statistical error bars. In figure (a), we observe the convergence of  $p_{mean}$  to a finite function of  $\phi$  as  $\alpha \rightarrow 0$ , in agreement with the theoretical predictions. In figure (b), we observe that the values of  $p_{fluct}$  are relatively weak close the jet maximum  $\phi = 0$ , while they keep increasing as  $\alpha \rightarrow 0$  in other locations, as expected from theory.

quence, we expect that  $p_{mean} = 2\pi \cos \phi F^\alpha[U](\phi)U(\phi)$  and  $P_{mean} = \int d\phi p_{mean}(\phi)$  also converge to finite values as  $\alpha \rightarrow 0$ . This is what is observed in figures 6.4 and 6.6(a).

This observation implies that the effective dynamics of  $U$  given by (6.30) is well defined at leading order in  $\alpha$ . This behaviour is very similar to the behaviour of the kinetic equation in the bi-periodic case discussed in chapter 4.

### 6.4.3 Fluctuations of Reynolds' stresses in the inertial limit

In chapter 5, and under the hypothesis detailed previously, we have shown that  $\Xi^\alpha[U](\phi, \phi)$  behaves as  $1/\alpha$  in the regime  $\nu_n \ll \alpha \ll 1$ . It implies that  $\alpha P_{fluct}$  should converge to a finite value as  $\alpha$  decreases. In figure 6.4, we see that  $\alpha P_{fluct}$  first increases slightly between  $\alpha = 0.73$  and  $\alpha = 0.29$ , and then decreases between  $\alpha = 0.29$  and  $\alpha = 0.073$ . Moreover, this evolution is of very weak amplitude compared to the statistical error bars. This indicates that we should have better statistics and go to smaller values of  $\alpha$  in order to state precisely whether the theoretical prediction for  $\alpha P_{fluct}$  is satisfied or not.

In figure 6.6(b), we see that  $p_{fluct}(\phi)$  keeps increasing as  $\alpha$  decreases in the region away from the jet maximum (roughly for  $|\phi| \in [\pi/16, \pi/4]$ ), while its value remains relatively small close to the equator  $\phi = 0$ . This can actually be understood qualitatively using the results of chapters 4 and 5. Indeed, we have seen in section 5.2 that  $\Xi^\alpha[U](\phi, \phi)$  diverges as  $1/\alpha$ , mainly because of the vorticity-vorticity correlations, and of the asymptotic behaviour of the deterministic vorticity given by the Orr mechanism (see (5.21) page 74). More precisely, we have proved such behaviour at every point where the local shear by the zonal jet  $U(\phi)$  is non-zero, i.e. at every point where the Orr mechanism applies. This explains why  $p_{fluct}(\phi)$  increases as  $\alpha$  decreases away from the jet maximum. At the shear-less points (for instance  $\phi = 0$ ), no precise theoretical prediction is available for  $\Xi^\alpha[U](\phi, \phi)$ . At such points, the deterministic vorticity actually decays for large times (depletion of vorticity at the stationary streamline, see section 4.2 page 50 and [11]). In this stochastic context, we can expect the fluctuations of  $\delta\omega$  to be weaker in this region  $\phi \simeq 0$ , and this is indeed what is observed in figure 6.6(b). We stress that no precise theoretical result applies here, but the phenomenology of the deterministic linear dynamics associated with (6.29) is in agreement with the numerical observations.

An important remark to make is that we have considered here the case where only one mode is stochastically forced (see section 6.3.4 for details). In chapter 5, we have discussed the influence of the forcing spectrum on the behaviour of  $\Xi^\alpha[U]$ , in particular we have seen that  $\Xi^\alpha[U](\phi, \phi)$  should behave as  $1/\alpha K$  in the regime  $\alpha \ll 1$ ,  $K \gg 1$ , where  $K$  is the number of forced modes. This implies that  $p_{fluct}(\phi) \sim 1/\alpha K$  and  $\alpha P_{fluct} \sim 1/K$ . Here  $K = 1$ , so we are basically considering the case where fluctuations of Reynolds' stresses are the most important in the zonal energy balance. In other words, this is the worst case test for CE2 types of closures. In most previous studies of second order closures like CE2, a large number of modes is forced [66, 68], so in these cases  $p_{fluct}(\phi)$  and  $\alpha P_{fluct}$  are most likely to be negligible in the zonal energy balance.

### 6.4.4 Empirical validation of the time scale separation hypothesis

Considering the linearized dynamics of the eddy vorticity  $\delta\omega$  close to a fixed zonal flow  $U(\phi)$  only makes sense if  $\delta\omega$  effectively evolves much faster than  $U(\phi)$ . An indication of whether this hypothesis is self-consistent or not is given by the maximal decorrelation time of the Reynolds' force  $f(\phi)$  for the linear barotropic equation (6.39), defined as<sup>7</sup>

$$\tau_{max}^\alpha \equiv \max_\phi \lim_{t \rightarrow \infty} \frac{1}{t} \int_0^t \int_0^t \frac{\mathbb{E}_U^\alpha [[f(\phi, s_1) f(\phi, s_2)]]}{2\mathbb{E}_U^\alpha [[f^2(\phi)]]} ds_1 ds_2, \quad (6.34)$$

In chapter 5 and under the hypothesis that the Orr mechanism applies (see previous section), we have proved that  $\tau_{max}^\alpha$  has a finite value independent of  $\alpha$  when  $\alpha \ll 1$ . Using the method described in section 6.1.1, the maximal decorrelation time (6.34) can be estimated from simulations of the linearized barotropic equation (6.39), with different values of  $\alpha$ .

The results are summarized in figure 6.7. We observe the convergence of  $\tau_{max}^\alpha$  to a finite value as  $\alpha$  decreases, and this value is smaller than the inertial time scale estimate (equal to one by definition of the time units). This means that the typical time scale of evolution of the Reynolds' stress divergence is much smaller than the dissipative time scale  $1/\alpha$ . As the jet typically evolves over this dissipative time scale, this result constitutes an empirically indication that the hypothesis of a time scale separation between the evolution of the zonal jet and of the eddies as  $\alpha \rightarrow 0$  is satisfied.

## 6.5 Large deviations of Reynolds' stresses

In section 6.4, we have studied the effective energy balance for the zonal flow  $U(\phi)$  using numerical simulations of the linearized barotropic dynamics (6.29). This effective description of zonal jet dynamics corresponds to the Law of Large Numbers and the Central Limit Theorem applied to the quasi-linear barotropic equations (6.26) in the regime  $\alpha \ll 1$ . In other words, this effective description takes into account the low-order statistics of Reynolds' stresses: average and covariance.

In order to study arbitrarily rare events in zonal jet dynamics, we have to go to the level of the Large Deviation Principle. We first formulate the Large Deviation Principle for the quasi-linear barotropic equations (6.26) and discuss qualitatively its implications for zonal jet statistics, and then give the numerical results.

The Large Deviation Principle presented in section 6.5.1 is exactly equivalent to the one presented in a more general setting in chapter 2, we just recall it here for convenience.

<sup>7</sup>In this spherical geometry the maximum is taken over the inner jet region  $\phi \in [-\pi/7, \pi/7]$ .

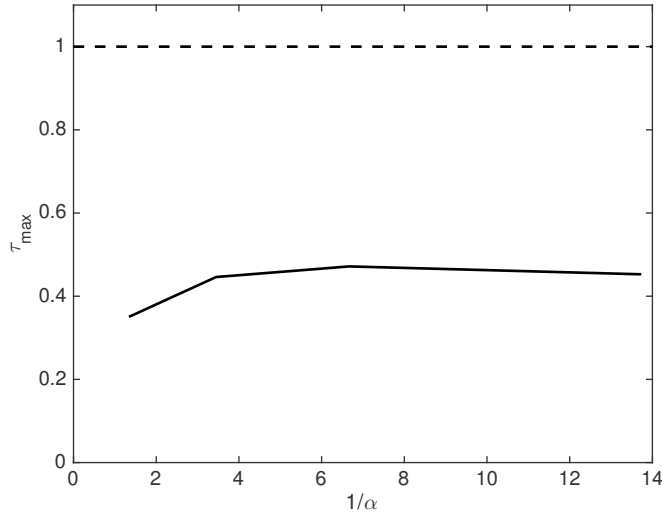


Figure 6.7: Solid line: decorrelation time of the Reynolds' stress divergence (6.34) as a function of the damping rate  $\alpha$ . We clearly see the convergence of  $\tau_{\max}^\alpha$  to a finite value as  $\alpha \rightarrow 0$ . The decorrelation time is of the order of the inertial time scale (equal to one by definition of the units, here represented by the dashed line), and much smaller than the dissipative time  $1/\alpha$  (not represented here), showing the time scale separation between dissipative and inertial processes in the quasi-linear barotropic dynamics. The parameters are the ones given in section 6.3.4.

### 6.5.1 Large Deviation Principle for the time-averaged Reynolds' stresses

Consider the evolution of  $\omega_z$  from the first equation of (6.26). Over a time scale  $\Delta t$  much smaller than  $1/\alpha$  but much larger than the decorrelation time  $\tau$  we can write

$$\frac{\Delta\omega_z}{\Delta t} \equiv \frac{1}{\alpha} \frac{\omega_z(t + \Delta t) - \omega_z(t)}{\Delta t} \simeq \frac{1}{\Delta t} \int_t^{t+\Delta t} R(s) ds - \omega_z(t), \quad (6.35)$$

where we have considered that  $\omega_z$  has almost not evolved between  $t$  and  $t + \Delta t$  (because  $\Delta t \ll 1/\alpha$ ), while  $R(s)$  has evolved according to (6.29) with a fixed  $\omega_z$  (or equivalently a fixed  $U$ ). We have also neglected hyper-viscosity in the evolution of  $\omega_z$ , which is natural in the turbulent regime we are interested in. Note however that some hyper-viscosity is still present in the numerical simulations of (6.29), in order to ensure numerical stability. For consistency, we will make sure that those hyper-viscous terms have no influence on the numerical results (see figure 6.8).

The approximation (6.35) is exactly the one we have done in chapter 2 in order to obtain heuristically the Large Deviation Principle (see section 2.1).

We denote by  $P_{\Delta t} \left[ \frac{\Delta\omega_z}{\Delta t} \right]$  the probability distribution function of  $\frac{\Delta\omega_z}{\Delta t}$ , with a fixed  $t$  (and thus a fixed  $\omega_z(t)$ ), but with an increasing  $\Delta t$ . Considering this regime is consistent with the limit of time scale separation  $\alpha \rightarrow 0$ , where  $\omega_z$  is nearly frozen while  $\delta\omega$  keeps evolving. From (6.35),  $P_{\Delta t} \left[ \frac{\Delta\omega_z}{\Delta t} \right]$  is also the probability density function of the time-averaged advection term  $\frac{1}{\Delta t} \int_t^{t+\Delta t} R(s) ds$ .

In the limit  $\Delta t \rightarrow \infty$ , the time-integral in (6.35) converges to a given value<sup>8</sup>, i.e.  $P_{\Delta t} \left[ \frac{\Delta \omega_z}{\Delta t} \right]$  approaches a  $\delta$  distribution centered on this value (Law of Large Numbers). The Large Deviation Principle gives the speed of convergence of  $P_{\Delta t} \left[ \frac{\Delta \omega_z}{\Delta t} \right]$  towards this  $\delta$  distribution, and provides the probability of fluctuations around the most probable value in the regime  $\Delta t \gg 1$ . Namely,

$$P_{\Delta t} \left[ \frac{\Delta \omega_z}{\Delta t} \right] \underset{\Delta t \rightarrow \infty}{\asymp} \exp \left( -\Delta t \mathcal{L} \left[ \frac{\Delta \omega_z}{\Delta t} \right] \right), \quad (6.36)$$

where  $\asymp$  stands for the equivalence in logarithmic scale. The function  $\mathcal{L}$  is called the large deviation rate function. It characterizes the whole distribution of  $\frac{\Delta \omega_z}{\Delta t}$  in the regime  $\Delta t \gg 1$ , including the most probable value and the typical fluctuations.

Our goal in the following is to compute numerically  $\mathcal{L} \left[ \frac{\Delta \omega_z}{\Delta t} \right]$ . To do this, we will use the Gärtner-Ellis theorem presented in chapter 2, and that we briefly recall here.

Using (6.35), the definition of the scaled cumulant generating function (6.2) can be reformulated as

$$H[\theta] = \lim_{\Delta t \rightarrow \infty} \frac{1}{\Delta t} \ln \int d\dot{\omega}_z P_{\Delta t} [\dot{\omega}_z] \exp (\theta \cdot \Delta t \dot{\omega}_z) \quad (6.37)$$

Because  $\omega_z$  is a field, here  $\theta$  is also a field depending on the latitude  $\phi$ , and  $H$  is a functional. For simplicity, we stop denoting the dependency in  $\omega_z$  in  $H$ . In (6.37), we also have used the notation  $\theta_1 \cdot \theta_2 \equiv \int d\phi \cos \phi \theta_1(\phi) \theta_2(\phi)$  for the canonical scalar product on the basis of spherical harmonics.

Using (6.36) in (6.37) and using a saddle-point approximation to evaluate the integral in the limit  $\Delta t \rightarrow \infty$ , we get  $H[\theta] = \sup_{\dot{\omega}_z} \{ \theta \cdot \dot{\omega}_z - \mathcal{L} [\dot{\omega}_z] \}$ , i.e.  $H$  is the Legendre-Fenchel transform of  $\mathcal{L}$ . Assuming that  $H$  is everywhere differentiable, we can invert this relation as

$$\mathcal{L} \left[ \frac{\Delta \omega_z}{\Delta t} \right] = \sup_{\theta} \left\{ \theta \cdot \frac{\Delta \omega_z}{\Delta t} - H[\theta] \right\}. \quad (6.38)$$

The scaled cumulant generating function  $H[\theta]$  can be computed either from a time series of  $\delta \omega$  (see section 6.1) or solving the Ricatti equation (see section 6.2). Then the large deviation rate function  $\mathcal{L}$  can be computed using (6.38), and this gives the whole probability distribution of  $\frac{\Delta \omega_z}{\Delta t}$  (or equivalently of the time-averaged Reynolds' stresses) through the Large Deviation Principle (6.36).

In the following, we implement this program and discuss the physical consequences for zonal jet statistics. We first give a simpler expression of  $H[\theta]$ , that makes its numerical computation easier.

<sup>8</sup>As discussed in chapter 5, ergodicity for the Reynolds' stress divergence is not satisfied pointwise, here it means that the large- $\Delta t$  limit of  $\frac{1}{\Delta t} \int_t^{t+\Delta t} R(s) ds$  might not be the average over the invariant measure of (6.29). This observation has no consequence here, we only have to make sure that  $\frac{1}{\Delta t} \int_t^{t+\Delta t} R(s) ds$  has a finite limit for  $\Delta t \rightarrow \infty$ , and this is what we observe for instance in figure 6.6(a).

## 6.5.2 Decomposition of the scaled cumulant generating function

Using the Fourier decomposition (6.20), we can decompose the perturbation vorticity as  $\delta\omega(\lambda, \phi) = \sum_m \omega_m(\phi)e^{im\lambda}$ , where  $\omega_m$  satisfies

$$\frac{\partial\omega_m}{\partial u} = -L_{U,m}[\omega_m] + \sqrt{2}\eta_m, \quad (6.39)$$

where the Fourier transform of the linear operator (6.25) reads

$$L_{U,m}[\omega_m](\phi) = -\frac{im}{\cos\phi} (U(\phi)\omega_m(\phi) + \gamma(\phi)\psi_m(\phi)) - \alpha\omega_m(\phi) - \nu_n(-\Delta_m)^n \omega_m(\phi). \quad (6.40)$$

In (6.39),  $\eta_m(\phi, t)$  is a gaussian white noise such that  $\eta_{-m} = \eta_m^*$ , with zero mean and with correlations

$$\mathbb{E}[\eta_m(\phi_1, t_1)\eta_m^*(\phi_2, t_2)] = c_m(\phi_1, \phi_2)\delta(t_1 - t_2),$$

$$\mathbb{E}[\eta_m(\phi_1, t_1)\eta_m(\phi_2, t_2)] = 0,$$

where  $c_m$  is the  $m$ -th coefficient in the Fourier decomposition of  $C$  in the zonal direction.

Using the Fourier decomposition, the zonally averaged advection term can be written  $R(\phi) = \sum_m R_m(\phi)$  with  $R_m(\phi) = -\frac{im}{\cos\phi}\partial_\phi(\psi_m \cdot \omega_{-m})$ . Using this expression and the fact that  $\omega_{m_1}$  and  $\omega_{m_2}^*$  are statistically independent for  $m_1 \neq m_2$ , the scaled cumulant generating function (6.37) can be decomposed as<sup>9</sup>

$$\begin{aligned} H[\theta] &\equiv \lim_{\Delta t \rightarrow \infty} \frac{1}{\Delta t} \ln \mathbb{E}_U^\alpha \left[ \exp \left( \theta \cdot \int_0^{\Delta t} (R(s) - \omega_z(0)) ds \right) \right] \\ &= -\theta \cdot \omega_z + \sum_m H_m[\theta], \end{aligned} \quad (6.41)$$

with

$$H_m[\theta] = \lim_{\Delta t \rightarrow \infty} \frac{1}{\Delta t} \log \mathbb{E}_U^\alpha \exp \left[ \int d\phi \cos\phi \theta(\phi) \int_0^{\Delta t} R_m(\phi, s) ds \right]. \quad (6.42)$$

We recall that  $\mathbb{E}_U^\alpha$  is the average in the statistically stationary state of (6.39).

In the following, we will consider the case where only one Fourier mode  $m$  is forced, for simplicity. If several modes are forced, their contributions to the scaled cumulant generating function add up, according to (6.41).

Finally, consider the decomposition of the zonally averaged advection term into spherical harmonics (6.19),  $R_m(\phi) = \sum_\ell R_{m,\ell} Y_\ell^0(\phi)$ . Using  $\theta(\phi) = \theta_\ell Y_\ell^0(\phi)$  in (6.42), we investigate the statistics of the  $\ell$ -th coefficient  $R_{m,\ell}$ . The associated scaled cumulant generating function (6.42) is denoted  $H_{m,\ell}(\theta) \equiv H_m[\theta Y_\ell^0(\phi)]$ , and the large deviation rate function is denoted

$$\mathcal{L}_{m,\ell}(\dot{\omega}_\ell) = \sup_{\theta_\ell} \{ \theta_\ell \dot{\omega}_\ell - H_{m,\ell}(\theta_\ell) \}. \quad (6.43)$$

<sup>9</sup>The time  $t$  in the upper and lower bounds of the integral in (6.41) are not relevant here, as we are considering the statistically stationary state of (6.39).

### 6.5.3 Numerical results

The function  $H_{m,\ell}$  can be computed either from a time series of  $\omega_m(\phi, s)$  using the method described in section 6.1, or solving the Ricatti equation as described in section 6.2. Then, the large deviation rate function is computed using (6.43). We now show the results of these computations.

#### Scaled cumulant generating function

An example of computation of  $H_{m,\ell}(\theta)$  is shown in figure 6.8, with  $m = 10$ ,  $\ell = 3$  and  $\alpha = 0.073$ . The linearized barotropic equation (6.39) is integrated over a time  $T_{max} = 54,500$ , with fixed mean flow given in figure 6.3, and the value of  $R_{m,\ell}$  is recorded every 0.03 time units (the units are defined in section 6.3.1).

The scaled cumulant generating function (6.42) is then estimated following the procedure described in section 6.1.2 (thick black curve in figure 6.8). Because the time series of  $R_{m,\ell}$  is finite,  $H_{m,\ell}(\theta)$  can only be computed with accuracy on a restricted range of values of  $\theta$  (see section 6.1.2 for details), here  $\theta \in [\theta_{min}/2, \theta_{max}/2] = [-0.6, 1.1]$ .

The scaled cumulant generating function (6.42) is also computed solving numerically the Ricatti equation (6.12) and using (6.11) (yellow curve in figure 6.8). The numerical integration of the Ricatti equation is very fast, this allows to use finer resolution and lower hyper-viscosity very easily.

We observe a perfect agreement between the direct estimation of  $H_{m,\ell}$  (black curve in figure 6.8) and the computation of  $H_{m,\ell}$  using the Ricatti equation (yellow curve). The integration of the Ricatti equation was done with a finer resolution and a lower hyper-viscosity than in the simulation of the linearized barotropic equation (6.39), the agreement between both results in figure 6.8 thus shows that the resolution used in the simulation of (6.39) is high enough, and that the effect of hyper-viscosity is negligible.

We stress that the computation of  $H_{m,\ell}(\theta)$  using the Ricatti equation (6.12) does not require the numerical integration of the linear dynamics (6.39). Typically, the integration of (6.39) over a time  $T_{max} = 54,500$  takes about one week, while the resolution of the Ricatti equation (6.12) for a given value of  $\theta$  is a matter of a few seconds. This allows to investigate the statistics of rare events (large values of  $|\theta|$  in figure 6.8) extremely easily, as we now explain in more details.

#### Rate function and departure from the Central Limit Theorem

The main goal of this study is to investigate the statistics of rare events in zonal jet dynamics, that cannot be described by the kinetic equation studied for instance in section 6.4. Using the previous numerical results, we will now show how to quantify the departure from the kinetic description.

We stress that the typical behaviour of zonal jets in the regime  $\alpha \ll 1$  is fully described by the kinetic equation (6.30). As a consequence, the numerical results shown in section 6.4 summarize how the low-order statistics of the time-averaged advection term depend on the physical parameters  $\alpha$  and  $\nu_n$  (see for instance figure 6.4). For this reason, we will focus here on the probabilities of very rare events, as

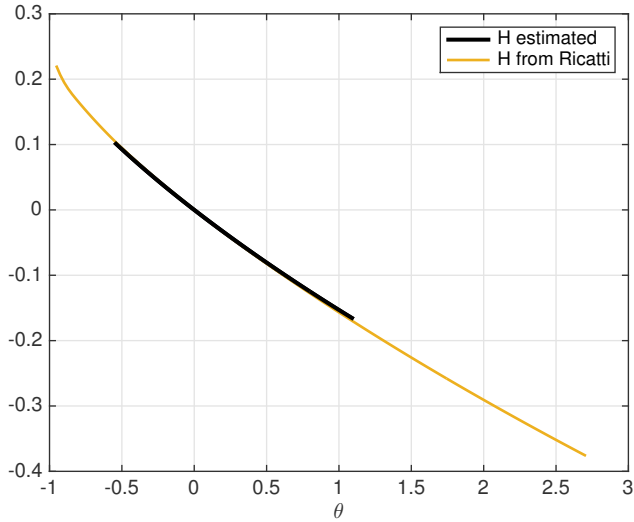


Figure 6.8: Thick black line: scaled cumulant generating function  $H_{10,3}(\theta)$  estimated from the numerical simulation of the linearized barotropic dynamics (6.39), with parameters defined in section 6.3.4 and  $\alpha = 0.073$ . Statistical error bars are smaller than the width of this curve. Yellow curve: scaled cumulant generating function  $H_{10,3}(\theta)$  computed from numerical integration of the Riccati equation (6.12), using (6.11). The spectral cutoff in the Riccati calculation is  $L = 120$  (compared to  $L = 80$  for the simulation of (6.39)), and the hyper-viscosity coefficient is such that the smallest scale has a damping rate of 4 (i.e. it is half of the hyperviscosity coefficient in the case  $L = 80$ ). The estimated scaled cumulant generating function is in agreement with the one computed from the Riccati equation, showing that the finite spectral cutoff and hyperviscosity are negligible in the calculation of  $H_{10,3}(\theta)$ . The numerical integration of the Riccati equation allows to investigate larger values of  $|\theta|$  (rarer events) extremely easily, see also figure 6.9.

described by the Large Deviation Principle (6.36).

The large deviation rate function  $\mathcal{L}_{m,\ell}$  entering in the Large Deviation Principle (6.36) can be computed from  $H_{m,\ell}$  using (6.43). The result of this calculation is shown in figure 6.9 (yellow curve<sup>10</sup>).

Because of the relation (6.35),  $\mathcal{L}_{m,\ell}$  can also be interpreted as the large deviation rate function for the time-averaged advection term, denoted  $\bar{R}_{m,\ell,\Delta t} \equiv \frac{1}{\Delta t} \int_0^{\Delta t} R_{m,\ell}(s) ds$ . In other words, the probability distribution function of  $\bar{R}_{m,\ell,\Delta t}$  in the regime  $\Delta t \gg 1$  is roughly

$$P_{m,\ell,\Delta t}(\bar{R}) \underset{\Delta t \gg 1}{\asymp} \exp(-\Delta t \mathcal{L}_{m,\ell}(\bar{R})). \quad (6.44)$$

The Central Limit Theorem states that for large but finite  $\Delta t$ , the statistics of  $\bar{R}_{m,\ell,\Delta t}$  around its mean  $F_{m,\ell} \equiv \mathbb{E}_U^\alpha[\bar{R}_{m,\ell,\Delta t}] = \mathbb{E}_U^\alpha[R_{m,\ell}]$  are nearly gaussian. A classical result in Large Deviation Theory is that the Central Limit Theorem can be recovered from the Large Deviation Principle. Indeed, using an expansion of  $H_{m,\ell}$  in powers of  $\theta$  (like the one done in section 2.3.3 page 35) and computing the Legendre-Fenchel transform (6.38), we get

$$\mathcal{L}_{m,\ell}(\bar{R}) = \frac{1}{2\Xi_{m,\ell}} (\bar{R} - F_{m,\ell})^2 + O\left((\bar{R} - F_{m,\ell})^3\right) \quad (6.45)$$

with  $\Xi_{m,\ell} \equiv 2 \int_0^\infty \mathbb{E}_U^\alpha[[R_{m,\ell}(s)R_{m,\ell}(0)]] ds$ . Using the Large Deviation Principle (6.44), this means that the statistics of  $\bar{R}_{m,\ell,\Delta t}$  for small fluctuations around  $F_{m,\ell}$  are gaussian with variance  $\Xi_{m,\ell}/\Delta t$ , which is exactly the result of the Central Limit Theorem. Then, the difference between the actual rate function  $\mathcal{L}_{m,\ell}(\bar{R})$  and its quadratic approximation (right-hand side of (6.45)) gives the departure from the gaussian behaviour of  $\bar{R}_{m,\ell,\Delta t}$ .

From (6.45), the gaussian behaviour is expected to apply roughly for  $|\bar{R} - F_{m,\ell}| \leq \sigma_{m,\ell,\Delta t}$  with  $\sigma_{m,\ell,\Delta t} \equiv \sqrt{\Xi_{m,\ell}/\Delta t}$ . The values of  $F_{m,\ell} \pm \sigma_{m,\ell,\Delta t}$  are represented by the black vertical lines in figure 6.9<sup>11</sup>. The quadratic approximation of the rate function is also shown in figure 6.9 (purple curve). As expected, both curves are indistinguishable between the vertical lines (typical fluctuations), and departures from the gaussian behaviour are observed away from the vertical lines (rare fluctuations). Namely, the probability of a large negative fluctuation is much larger than the probability of the same fluctuation for a gaussian process with same mean and variance as  $\bar{R}_{m,\ell,\Delta t}$ . On the contrary, the probability of a large positive fluctuation is much smaller than the the probability of the same fluctuation for a gaussian process with same mean and variance as  $\bar{R}_{m,\ell,\Delta t}$ .

The kinetic description basically amounts at replacing  $\bar{R}_{m,\ell,\Delta t}$  by a gaussian process with same mean and variance. From the results summarized in figure 6.9, we see that such approximation leads to a very inaccurate description of rare events statistics. Understanding the influence of those non-gaussian behaviour of  $\bar{R}_{m,\ell,\Delta t}$  on zonal jet dynamics is naturally a very interesting perspective of this work.

<sup>10</sup>Here the Legendre-Fenchel transform (6.38) is estimated as  $\mathcal{L}_{m,\ell}(\dot{\omega}_z) = \theta^* \cdot \dot{\omega}_z - H_{m,\ell}(\theta^*)$  where  $\theta^*$  is the solution of  $\dot{\omega}_z = H'_{m,\ell}(\theta^*)$ . Other estimators could be considered [96].

<sup>11</sup>The value of  $\Delta t$  used in this estimation is the optimal one  $\Delta t^*$ , defined in section 6.1.

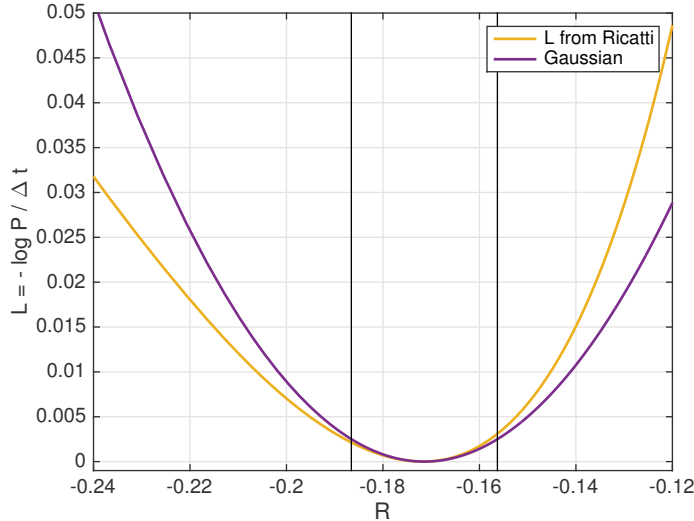


Figure 6.9: Yellow curve: large deviation rate function  $\mathcal{L}_{10,3}(\bar{R})$  computed from numerical integration of the Ricatti equation (6.12), using (6.11) and (6.38), with parameters defined in section 6.3.4 and  $\alpha = 0.073$ . Purple curve: quadratic fit (6.45) that corresponds to a gaussian process with same mean and variance as  $\bar{R}_{10,3,\Delta t}$ , the time-averaged advection term. Black vertical lines: standard deviation of  $\bar{R}_{10,3,\Delta t}$  around its mean. Outside those vertical lines, we observe non-gaussian behaviour of  $\bar{R}_{10,3,\Delta t}$ , in particular negative fluctuations are much more probable than positive ones.

## 6.6 Perspectives

We have seen in this chapter how to compute the large deviation function associated with the Reynolds' stress divergence  $H(z, \theta)$  as a function of  $\theta$ , either from a set of data or using the Ricatti equation (6.12). However, the problem of the well-definiteness of  $H$  in the inertial limit  $\alpha \rightarrow 0$  has not been discussed. This problem is similar to the subject of chapter 5, where we have studied the convergence of the terms appearing in the Law of Large Numbers and Central Limit Theorem in the inertial limit, using the asymptotic behaviour of the linearized 2D Euler equation. Such approach could be generalized to study the self-consistency of the Large Deviation Principle. Another interesting way to proceed would be to study the properties of the Ricatti equation in the limit  $\alpha \rightarrow 0$ . Moreover, as the Large Deviation Principle contains the Law of Large Numbers and Central Limit Theorem (see section 2.3.3 in page 35), we would recover the results of chapter 5.

The most interesting application of the Large Deviation Principle is the study of rare events, such as transitions between attractors of the barotropic model in cases of bistability, as illustrated for example in figures 2 and 3.1. We have shown how to compute the probability of very rare events, but we have not applied those tools to cases of bistability.

In the framework presented in this chapter, bistability would be related to singularities of the scaled cumulant generating function  $H_{m,\ell}(\theta)$  (discontinuity of the derivative with respect to  $\theta$ ). Then, interesting quantities such as transition proba-

bility and most probable transition path (instanton) could be investigated, possibly directly from the Riccati equation.

# Chapter 7

## Equilibrium dynamics of zonal jets

In this chapter we present the kinetic theory for a model related to the stochastic barotropic equation. The difference here is that we impose a constraint on the spectrum of the forcing, which leads to detailed balance between forcing and dissipation, in analogy with the Langevin equation in statistical mechanics for systems of particles. In general, those specific dissipation and forcing terms do not correspond to a realistic modelling of a geophysical flow, the Langevin model studied in this chapter should be considered as an academic theoretical tool.

In particular, one of the motivations of this study is to find cases where quantities of interest for the kinetic theory (average Reynolds' stress divergence  $F_0[U]$ , integrated autocorrelation function of the Reynolds' stress divergence  $\Xi[U]$ , see chapter 3) can be computed explicitly. The average Reynolds' stress divergence  $F_0[U]$  is basically given by the stationary solution of a Lyapunov equation (eq. (3.11) page 40). Here we will construct a model where the stationary Lyapunov equation can be solved explicitly, and compute  $F_0[U]$ . Then we will derive a relation between  $F_0[U]$  and  $\Xi[U]$ , which reflects the detailed balance property at the level of the kinetic equation.

The approach is actually very general, and some of the main results will be proved in an abstract framework before being applied to the turbulence problem.

### 7.1 The generalized Langevin equation

#### 7.1.1 Motivation

The original Langevin equation [59] describes the motion of a particle subjected to random forces and friction from the surrounding particles (brownian motion). If a particular relation holds between friction and random forces (Einstein's relation), then the stationary probability distribution function of the particle's velocity is exactly the canonical Gibbs distribution. This is in agreement with the fact that the particle is at statistical equilibrium with the surrounding environment (thermal bath). This procedure thus enables the description of statistical equilibrium by stochastic equations of motion. It is described in any textbook of statistical mechanics, see for example [46] or [93], and it is generalizable to any Hamiltonian system in contact with a thermal bath.

In contrast with the previous simple system, turbulence is a non-equilibrium phenomenon. Indeed, it is generally characterized by fluxes of energy among scales, either through self-similar cascades [9, 89], or through non-local transfers of energy as described in the kinetic theory presented in chapter 3. However, equilibrium statistical mechanics (RMS theory) provides a very precise description of the large scales of two-dimensional and geophysical turbulent flows in the inertial limit, as briefly described in section 1.3.4 (page 24, see [14] for a review). The goal of this chapter is to propose a description of the statistical equilibrium dynamics of zonal jets, through a generalization of the Langevin equation to the stochastic two-dimensional Navier-Stokes equation. We will thus recover at leading order the results from RMS theory, and describe the corrections due to forcing and dissipation.

The basic ingredient of RMS theory is the conservation of an infinite number of independent quantities by the inertial dynamics (see section 1.3.4). The equilibrium states are then given by the maximization of an entropy functional, constrained to the values of those conserved quantities [14] (microcanonical ensemble). In the Langevin approach presented here (canonical ensemble), the stationary distribution will be parametrized by those conserved quantities. In practice, this means that we can construct the model such that it admits one stationary distribution among the many possible equilibrium ones. This procedure is explained in details now.

### 7.1.2 Stationary distribution

We focus in this chapter on the Langevin dynamics associated with the 2D Euler equation, but all these results can be easily generalized to different dynamics: barotropic dynamics over a doubly-periodic topography, or in a channel.

Consider the stochastic equation

$$\frac{\partial \omega}{\partial t} + \mathbf{v} \cdot \nabla \omega = -\kappa \int d\mathbf{r}' C(\mathbf{r} - \mathbf{r}') \frac{\delta \mathcal{G}}{\delta \omega(\mathbf{r}')} + \sqrt{2\kappa\gamma} \eta(\mathbf{r}, t) \quad (7.1)$$

with  $\kappa, \gamma > 0$ , with  $\eta(\mathbf{r}, t)$  a gaussian white noise with zero mean and correlations

$$\mathbb{E} [\eta(\mathbf{r}, t) \eta(\mathbf{r}', t')] = \delta(t - t') C(\mathbf{r} - \mathbf{r}'), \quad (7.2)$$

and where  $\mathcal{G}[\omega]$  is a conserved quantity of the inertial dynamics (Euler dynamics). The dissipation term (first term in the r.h.s of (7.1)) involves the correlation function of the stochastic forcing  $C$ , this naturally comes from the fact that dissipation and forcing should balance each other at each scale in order to achieve statistical equilibrium. This property will be stated more precisely in the next paragraphs.

### Fokker-Planck equation

The evolution of the probability density functional for a finite dimensional stochastic process is given by a Fokker-Planck equation [44, 93]. In this infinite-dimensional (field) problem, the formal generalization of the Fokker-Planck equation reads

$$\frac{\partial P}{\partial t} = \mathcal{L}_{\text{in}} P + \mathcal{L}_{\kappa} P \quad (7.3)$$

for the probability density functional  $P[\omega]$ , where

$$\mathcal{L}_{\text{in}}P = \int d\mathbf{r} \frac{\delta}{\delta\omega(\mathbf{r})} [\mathbf{v} \cdot \nabla\omega(\mathbf{r}) P[\omega]] \quad (7.4)$$

is the inertial part of the Fokker-Planck operator, and

$$\mathcal{L}_{\kappa}P = \kappa \int d\mathbf{r} \frac{\delta}{\delta\omega(\mathbf{r})} \left[ \int d\mathbf{r}' C(\mathbf{r} - \mathbf{r}') \left( \frac{\delta\mathcal{G}}{\delta\omega(\mathbf{r}')} P[\omega] + \gamma \frac{\delta P}{\delta\omega(\mathbf{r}')} \right) \right] \quad (7.5)$$

is the operator associated with forcing and dissipation in (7.1).

Like in the construction of the original Langevin equation, the stationary probability distribution function (PDF)  $P[\omega]$  of equation (7.1) is known explicitly, it is the equilibrium distribution associated with the conserved quantity  $\mathcal{G}[\omega]$  (also called the potential),

$$P_{\text{eq}}[\omega] = \frac{1}{Z} \exp\left(-\frac{1}{\gamma} \mathcal{G}[\omega]\right), \quad (7.6)$$

where  $Z$  is a normalisation constant.

More precisely, the inertial and forced-dissipated parts of the Fokker-Planck equation (7.3) applied at  $P_{\text{eq}}$  vanish independently:  $\mathcal{L}_{\text{in}}P_{\text{eq}} = 0$  and  $\mathcal{L}_{\kappa}P_{\text{eq}} = 0$ . The latter is obvious from (7.5) and (7.6). The former can be proved using the following properties:

- the Liouville theorem

$$\int d\mathbf{r} \frac{\delta}{\delta\omega(\mathbf{r})} [\mathbf{v} \cdot \nabla\omega(\mathbf{r})] = \int d\mathbf{r} \nabla \cdot \frac{\delta}{\delta\omega(\mathbf{r})} [\mathbf{v}\omega] = 0. \quad (7.7)$$

- the conservation of  $\mathcal{G}[\omega]$  by the inertial dynamics

$$\int d\mathbf{r} (\mathbf{v} \cdot \nabla\omega)(\mathbf{r}) \frac{\delta\mathcal{G}}{\delta\omega(\mathbf{r})} = 0. \quad (7.8)$$

The fact that the inertial and forced-dissipated parts of the stationary Fokker-Planck equation vanish independently is the precise statement of detailed balance at the level of the stochastic dynamics (7.1).

The interest of the Langevin model (7.1) is that the potential in the stationary distribution (7.6) can be chosen among the conserved quantities  $\mathcal{G}$  of the inertial dynamics. This is particularly useful in the case of the 2D Euler dynamics, which conserves an infinite number of conserved quantities, as explained in section 7.1.4.

In particular, we will build in section 7.3 a potential  $\mathcal{G}_{\gamma}$  which depends parametrically on  $\gamma$ , such that the associated Langevin dynamics (7.1) leads to a time scale separation between the evolution of a zonal jet and the evolution of perturbations close to this jet in the regime  $\gamma \ll 1$ . We will then apply the Law of Large Numbers and the Central Limit Theorem (stochastic averaging) presented in chapter 2 in order to obtain an effective equation for jet dynamics (kinetic equation).

Since we know that the stationary distribution of the full Langevin equation is the equilibrium distribution (7.6), it is natural to wonder if the stationary distribution of the kinetic equation can be computed directly from (7.6). It is indeed the case, and

this leads to particular constraints on the slow Fokker-Planck equation associated to the kinetic equation. Those constraints are called fluctuation-dissipation relations for a reason that will be made clear in the following. We now derive those relations in an abstract framework, they will be applied to the turbulence Langevin model (7.1) in section 7.3.

### 7.1.3 Stochastic averaging and fluctuation–dissipation relations

The general stochastic averaging procedure is described in details in chapter 2 and appendix A. To understand the derivation of the fluctuation-dissipation relations, it is useful to recall the main steps of this procedure.

Consider the slow-fast stochastic dynamical system (2.1), that we recall here for convenience,

$$\begin{cases} \frac{\partial z}{\partial t} = \alpha f(z, w) \\ \frac{\partial w}{\partial t} = b(z, w) + \eta \end{cases} \quad (7.9)$$

where  $\eta$  is a (vector) white gaussian noise. The joint probability distribution function  $P(z, w, t)$  is the solution of the Fokker-Planck equation

$$\frac{\partial P}{\partial t} = \mathcal{L}_0 P + \alpha \mathcal{L}_s P, \quad (7.10)$$

where the Fokker-Planck operators  $\mathcal{L}_i$  describe the evolution of  $P$  at each order in  $\alpha$  (see section 2.2 for the expression of  $\mathcal{L}_i$ ). We treat here the simple case (7.9), the generalization to the more complex system of equations considered in section 7.3 is straightforward.

Consider the virtual fast process  $\tilde{w}_z$ , defined as the second equation of (7.9) with a fixed  $z$ . Assume  $\tilde{w}_z$  has a stationary distribution  $G_z$ , solution of  $\mathcal{L}_0 G_z = 0$ . We denote by  $\mathcal{P}$  the projection onto the subspace of PDFs with the fast variable  $w$  relaxed to its stationary distribution  $G_z$ ,

$$\mathcal{P}P(z, w, t) \equiv G_z(w) \int dw P(z, w, t). \quad (7.11)$$

We then denote by  $P_s \equiv \mathcal{P}P$  the slowly evolving part of the PDF and by  $P_f \equiv (1 - \mathcal{P})P$  the fastly evolving part of the PDF. Defining the marginal distribution of the slow process  $z$  as

$$R(z, t) \equiv \int dw P(z, w, t), \quad (7.12)$$

we have  $P_s = G_z \cdot R$ .

To obtain the equation for the evolution of  $P_s$ , we apply the projector  $\mathcal{P}$  on the full Fokker-Planck equation (7.10). Using that  $\mathcal{L}_0$  is a derivative with respect to the fast variable  $w$  (for details see section 2.2 page 29), we have  $\mathcal{P}\mathcal{L}_0 = 0$ , so

$$\partial_t P_s = \alpha \mathcal{P}\mathcal{L}_s (P_s + P_f). \quad (7.13)$$

Again, we see in this equation that the typical time scale of evolution  $P_s$  is of order  $1/\alpha \gg 1$ .

The stochastic averaging technique is a perturbative expansion in powers of  $\alpha$  of the correction PDF  $P_f$ , leading to a closed equation for  $P_s$ . Namely, we can write  $P_f = \mathcal{L}_n P_s + O(\alpha^n)$ , where  $\mathcal{L}_n P_s$  is the perturbative expansion of  $P_f$  up to terms of order  $\alpha^{n-1}$ . Then, the effective equation for  $P_s$  reads

$$\partial_t P_s = \alpha \mathcal{P} \mathcal{L}_s (1 + \mathcal{L}_n) P_s + O(\alpha^n). \quad (7.14)$$

This closed equation describes the effective statistics of  $z$  in the small- $\alpha$  limit, i.e. in the limit of a large time scale separation between slow and fast variables. We stress that the operator  $\mathcal{L}_n$  depends on  $\alpha$ , with terms up to order  $\alpha^{n-1}$ . The main technical difficulty of the stochastic averaging procedure is actually to compute explicitly the operator  $\mathcal{L}_n$ , this is done for instance in appendix A.

Now assume that the system (7.9) has a Langevin structure, like (7.1). This means that the drift terms  $f$  and  $b$  in (7.9) can be decomposed into inertial and dissipation parts, and that this decomposition satisfies a Liouville theorem and a conservation law, as explained above for (7.1).

We do not need to write these conditions explicitly here, all we need is to observe that there exists an equilibrium distribution  $P_{\text{eq}}$  which is a stationary solution of the Fokker-Planck equation (7.10), more precisely that the inertial and the forced-dissipated parts of the Fokker-Planck operator  $\mathcal{L}_0 + \alpha \mathcal{L}_s$  applied at  $P_{\text{eq}}$  vanish independently:

$$(\mathcal{L}_0^{\text{in}} + \alpha \mathcal{L}_s^{\text{in}}) P_{\text{eq}} = 0, \quad (7.15)$$

$$(\mathcal{L}_0^\kappa + \alpha \mathcal{L}_s^\kappa) P_{\text{eq}} = 0, \quad (7.16)$$

where the exponent ‘in’ (resp.  $\kappa$ ) refers to the inertial (resp. forced and dissipated) part of the dynamics.

Applying the projector  $\mathcal{P}$  on (7.15) and (7.16) and using again the fact that  $\mathcal{L}_0$  is a derivative with respect to  $w$ , we get

$$\mathcal{P} \mathcal{L}_s^{\text{in}} (P_{s,\text{eq}} + P_{f,\text{eq}}) = 0 \quad (7.17)$$

and

$$\mathcal{P} \mathcal{L}_s^\kappa (P_{s,\text{eq}} + P_{f,\text{eq}}) = 0, \quad (7.18)$$

where  $P_{s,\text{eq}} = \mathcal{P} P_{\text{eq}}$  and  $P_{f,\text{eq}} = (1 - \mathcal{P}) P_{\text{eq}}$ . Now using the result of the perturbative expansion  $P_f = \mathcal{L}_n P_s + O(\alpha^n)$ , (7.17) and (7.18) become

$$\mathcal{P} \mathcal{L}_s^{\text{in}} (1 + \mathcal{L}_n) P_{s,\text{eq}} = O(\alpha^n) \quad (7.19)$$

and

$$\mathcal{P} \mathcal{L}_s^\kappa (1 + \mathcal{L}_n) P_{s,\text{eq}} = O(\alpha^n). \quad (7.20)$$

We stress that (7.19), (7.20) are obtained from a perturbative expansion in powers  $\alpha$ , so they hold up to terms of order  $\alpha^{n-1}$ . Indeed, in the general case  $P_{s,\text{eq}}$  depends on  $\alpha$ . Then, equations (7.19) and (7.20) insure that the stationary solution of the effective Fokker-Planck equation (7.14) is given by the marginal equilibrium distribution  $P_{s,\text{eq}}$ , expanded at order  $\alpha^{n-1}$ .

More precisely, equations (7.19) and (7.20) relate the different terms appearing in the effective Fokker-Planck equation (7.14). On one hand, (7.19) is a relation between the terms coming from the inertial part of the dynamics, and on the other hand, (7.20) is a relation between the terms coming from forcing and dissipation.

At the level of approximation corresponding to  $n = 3$ , the effective Fokker-Planck equation (7.14) contains terms corresponding to a deterministic drift (in particular dissipation) of the slow process  $z$ , and other terms corresponding to a stochastic forcing of  $z$  (fluctuations). For this reason, the relations (7.19), (7.20) relating those terms are called fluctuation-dissipation relations.

In section 7.3 will be given an explicit example of such fluctuation-dissipation relations, for a class of Langevin models of the form (7.1) with a specific potential  $\mathcal{G}$ .

### 7.1.4 Conserved quantities of the two-dimensional Euler equation

In (7.1), the functional  $\mathcal{G}[\omega]$  is a conserved quantity of the inertial 2D Euler equation  $\partial_t \omega + \mathbf{v} \cdot \nabla \omega = 0$ . In a doubly-periodic domain, the inertial 2D Euler equation conserves an infinite number of independent quantities: the energy

$$\mathcal{E}[\omega] = -\frac{1}{2} \int \mathrm{d}\mathbf{r} \omega \psi, \quad (7.21)$$

and the so-called Casimir functionals

$$\mathcal{C}_f[\omega] = \int \mathrm{d}\mathbf{r} f(\omega(\mathbf{r})), \quad (7.22)$$

for any sufficiently smooth function  $f$ . The conservation of the Casimir functionals is related, through Noether's theorem, to the particle relabelling symmetry of fluid mechanics [99]. It can also be understood by the fact that the inertial 2D Euler equation is an advection equation for the vorticity field  $\omega$ , so the vorticity is conserved at a point moving with the fluid (Lagrangian point of view) [55].

This particular property is fundamental in the construction of RMS theory [14], and it will also be crucial in this chapter. Indeed, the choice of the potential  $\mathcal{G}[\omega] = \mathcal{E}[\omega] + \mathcal{C}_f[\omega]$  among the infinite number of conserved quantities (energy-Casimir functionals) leads to specific statistics of the flow in the statistically stationary state. This means that we can construct by hand the stationary state of (7.1): most probable flow, typical fluctuations, energy contained at each scale... In all the cases treated in this chapter, the most probable flow is a coherent zonal jet on the largest scale, and small-scale fluctuations are of smaller amplitude. This is consistent with the phenomenology of 2D and quasi-geostrophic turbulence in the regime we are interested in.

The simplest examples of energy-Casimir functionals we will consider are the quadratic ones, i.e. linear combinations of energy, enstrophy, and linear momentum or total circulation depending on the boundary conditions. In section 7.2, we will see that this case is singular for various reasons: the average total kinetic energy is infinite, while the average Reynolds' force acting on the zonal flow vanishes. Moreover, we will see that in the cases where the most probable flow is a zonal jet, the

most probable amplitude of this jet is not determined by the distribution  $P_{\text{eq}}[\omega]$ .

In order to be closer to a realistic situation, we will have to go to next order in the choice of the potential  $\mathcal{G}[\omega]$ , including non-quadratic terms in  $\omega$  in (7.22). This is done in section 7.3. We will first construct the energy-Casimir functional in order to have a time scale separation between the large-scale zonal flow and the small-scale eddies. Using stochastic averaging, we will then obtain the effective equations for the slow evolution of the large-scale jet (eqs. (7.59),(7.60)). The terms appearing in these effective equations are related to each other through fluctuation-dissipation relations, as described in an abstract framework in section 7.1.3. These fluctuation-dissipation relations will be written explicitly.

## 7.2 Energy–enstrophy distribution

The simplest case of energy-Casimir functional are the quadratic ones, that lead to gaussian statistics of the flow through (7.6).

As will be shown in section 7.2.2, such distributions are the stationary distribution of the original stochastic barotropic model (1.1) with specific values of the friction and viscosity coefficients. For this reason, these distributions have been studied before, either in the context of the truncated two-dimensional Euler equation [55], or in relation with the equilibrium statistical mechanics theory of geophysical fluid dynamics models [64].

### 7.2.1 Construction and properties of the energy–enstrophy distribution

Let's consider the case of the biperiodic barotropic equation on the domain  $\mathcal{D} = [0, 2\pi l_x) \times [0, 2\pi)$  with aspect ratio  $l_x < 1$ . Periodicity of the stream function and vorticity fields leads to a zero value of total circulation and linear momentum, so we will consider potentials only made of linear combinations of energy and enstrophy,  $\mathcal{G}_2 = \beta\mathcal{E} + \mathcal{Z}$  where the enstrophy  $\mathcal{Z}$  is the Casimir functional (7.22) defined by  $f(\omega) = \frac{1}{2}\omega^2$ , and  $\beta$  is the generalized inverse temperature (in this chapter we will not consider the beta-effect like in previous chapters, so we hope no confusion will be made).

In the doubly periodic domain  $\mathcal{D}$ , we can decompose the fields in Fourier modes,  $\omega(\mathbf{r}) = \sum_{\mathbf{k}} \omega_{\mathbf{k}} e^{i\mathbf{k}\cdot\mathbf{r}}$ . Periodicity of the velocity field implies that  $\omega_{\mathbf{0}} = \frac{1}{(2\pi)^2 l_x} \int \omega = 0$ , so the equilibrium distribution (7.6) reads

$$P_{\text{eq}}[\omega] \propto \exp \left( -\frac{1}{2\gamma} \sum_{\mathbf{k} \neq \mathbf{0}} \left( 1 + \frac{\beta}{\mathbf{k}^2} \right) |\omega_{\mathbf{k}}|^2 \right). \quad (7.23)$$

Then, a necessary and sufficient condition for the normalizability of  $P_{\text{eq}}$  is

$$\forall \mathbf{k} \neq \mathbf{0}, \frac{1}{\gamma} \left( 1 + \frac{\beta}{\mathbf{k}^2} \right) \geq 0 \quad (7.24)$$

For large  $\mathbf{k}^2$ , this implies that  $\gamma > 0$ . Then,  $\beta \geq -\mathbf{k}^2$  for all  $\mathbf{k} \neq \mathbf{0}$ , or equivalently,  $\beta \geq -\mathbf{k}_0^2$ , where  $\mathbf{k}_0 = (0, 1)$  is the first non-zero Fourier mode.

### Concentration of energy in the largest scale

Can this distribution lead to a concentration of the energy in the largest scale (mode  $\mathbf{k}_0$ )? The mean energy in the mode  $\mathbf{k}$  is easily computed as a moment of the multivariate gaussian distribution  $P_{\text{eq}}$  (7.23),

$$E_{\mathbf{k}} \equiv \frac{1}{2\mathbf{k}^2} \mathbb{E}|\omega_{\mathbf{k}}|^2 = \frac{1}{2} \frac{\gamma}{\mathbf{k}^2 + \beta}, \quad (7.25)$$

where  $\mathbb{E}$  is the average over the stationary distribution  $P_{\text{eq}}$ . Then, the ratio of the energy contained in a mode  $\mathbf{k}$  and of the energy in the smallest mode is

$$\frac{E_{\mathbf{k}}}{E_{\mathbf{k}_0}} = \frac{\mathbf{k}_0^2 + \beta}{\mathbf{k}^2 + \beta}. \quad (7.26)$$

We have a concentration of the energy in the largest scale if this quantity is of the form  $\epsilon g(\mathbf{k})$  with  $0 < \epsilon \ll 1$  for all  $\mathbf{k} \neq \mathbf{k}_0$ .  $g$  is defined up to a multiplicative constant, for instance given by  $g(\mathbf{k}_1) = 1$ . Then,

$$\mathbf{k}_0^2 + \beta = \epsilon (\mathbf{k}_1^2 + \beta) \quad \Rightarrow \quad \beta = -\mathbf{k}_0^2 + \epsilon (\mathbf{k}_1^2 - \mathbf{k}_0^2) + O(\epsilon^2). \quad (7.27)$$

We will then have a concentration of the energy in the smallest mode  $\mathbf{k}_0$  in the limit  $\beta \rightarrow -\mathbf{k}_0^2 = -1$ . Such negative temperatures are not surprising, they arise often in the equilibrium statistical mechanics theory of such models [14, 55].

### Most probable flow

The equilibrium distribution (7.23) is a centered gaussian, so the most probable flow is the zero mean flow. Now consider the case  $\beta = -\mathbf{k}_0^2 + O(\epsilon)$  with  $\mathbf{k}_0^2 = 1$  and  $0 < \epsilon \ll 1$ . From (7.25), the average energy in the mode  $\mathbf{k}_0$  diverges as  $1/\epsilon$ , while for  $\epsilon = 0$  the distribution does not depend any more on  $\omega_{\mathbf{k}_0}$  (see (7.23)). To conclude, the typical flow according to the energy-entropy distribution (7.23) with  $\epsilon \ll 1$  is a zonal jet on the largest scale  $\mathbf{k}_0 = (0, 1)$  that contains most of the energy of the flow, with a smaller amplitude flow on the smaller scales. This is in agreement with the general phenomenology of planetary zonal jets.

### The average total energy is infinite

The total average energy is given by (7.25),

$$E = \sum_{\mathbf{k}} E_{\mathbf{k}} = \sum_{\mathbf{k}} \frac{1}{2} \frac{\gamma}{\mathbf{k}^2 + \beta}, \quad (7.28)$$

This sum can be approximated by the following integral

$$E \simeq E_{k \leq K_0} + \frac{\gamma}{2} \int_{K_0}^{\infty} \frac{2\pi k \, dk}{k^2 + \beta} \quad (7.29)$$

with  $K_0 \gg 1$  and where  $E_{k \leq K_0}$  is the energy of the first modes, such that  $k \leq K_0$ . This integral is obviously divergent, so  $E$  is infinite. This singular property of energy-entropy ensembles was already discussed by Kraichnan and Montgomery in the context of truncated approximations of the Euler equation [55].

In section 7.3, we will present another equilibrium ensemble (with a non-quadratic potential  $\mathcal{G}[q]$ ), associated with a finite total average energy.

### Average Reynolds' force

In analogy with the kinetic theory of chapter 3, let's consider the average Reynolds' force acting on a fixed zonal flow  $U(y)$  due to the perturbations  $\delta\omega$  to this zonal flow. By definition,

$$F_0(y) \equiv \mathbb{E}_U \langle \delta\omega \delta v \rangle = \sum_{k \neq 0, l_1, l_2} \frac{ik}{k^2 + l_1^2} g_{k, l_1, l_2} e^{i(l_1 + l_2)y}, \quad (7.30)$$

with  $g_{k, l_1, l_2} = \mathbb{E}_U[\omega_{k, l_1} \omega_{-k, l_2}]$ , where  $\mathbb{E}_U$  is the average over the equilibrium distribution (7.23) conditioned on the fact that the zonal flow is  $U(y)$ . Because all Fourier modes are independent of each other according to the distribution (7.23), the two-points correlation function  $g_{k, l_1, l_2}$  can be computed explicitly:

$$g_{k, l_1, l_2} = \frac{\gamma}{1 + \beta/(k^2 + l_1^2)} \delta_{l_1, -l_2}. \quad (7.31)$$

Then,

$$F_0(y) = \sum_{k, l} \frac{ik\gamma}{k^2 + l^2 + \beta} = 0, \quad (7.32)$$

which is zero because it changes sign under the transformation  $k \rightarrow -k$ .

This result is not surprising in this simple case, indeed the equilibrium distribution (7.23) is invariant under translations in the  $y$  direction, and because all Fourier modes are independent of each other, this property remains true for the distribution conditioned on a fixed zonal flow. Then  $F_0(y)$  is a constant, and this constant is zero by conservation of total momentum.

However, the fact that  $F_0 = 0$  remains true even if the invariance under translations in the  $y$  direction is explicitly broken, for instance in the beta-plane equation or the barotropic equation over a doubly-periodic topography, or taking into account linear momentum in a channel geometry. To our knowledge, it is the first time this property is observed.

### Summary

The typical flow distributed according to the energy-ensrophy measure (7.23), in the regime  $\beta = -\mathbf{k}_0^2 + O(\epsilon)$  with  $\mathbf{k}_0 = (0, 1)$  and  $0 < \epsilon \ll 1$ , is a strong zonal jet on the largest scale, with smaller-scale and smaller-amplitude fluctuations. However, the total average energy contained in these fluctuations is infinite. Moreover, when  $\epsilon = 0$  ( $\beta = -1$ ), the probability of the jet amplitude is no more defined. These singularities can be avoided including higher-order Casimir functionals in the potential  $\mathcal{G}[\omega]$  that defines the equilibrium distribution (7.6). It will also allow to obtain a finite average total energy. This is the case we study in section 7.3.

### 7.2.2 An explicit stationary solution of the Lyapunov equation

In analogy with the kinetic theory of chapter 3 or with closure theories (S3T-CE2 for instance [2, 104, 106]), consider the linearized dynamics of perturbations close to a fixed zonal flow  $U(y)$ . According to the results of previous section, we consider the

case where this zonal flow is on the largest scale of the domain,  $U(y) = U_0 \cos(y + \phi)$  with  $U_0$  and  $\phi$  some constants. Then, the linearized 2D Navier-Stokes equation reads

$$\frac{\partial \delta \omega}{\partial t} + U(y) \frac{\partial}{\partial x} (\delta \omega + \delta \psi) = -\kappa \delta \omega + \nu \Delta \delta \omega + \sqrt{2} \eta, \quad (7.33)$$

with the perturbation vorticity  $\delta \omega$  and the perturbation streamfunction  $\delta \psi$ . Because this equation is linear and invariant under translations in the  $x$  direction, we can consider without loss of generality the case where a single zonal mode  $k$  is forced,

$$\frac{\partial \omega_k}{\partial t} + ikU(y) (\omega_k + \psi_k) = -\kappa \omega_k + \nu \Delta_k \omega_k + \sqrt{2} \eta_k, \quad (7.34)$$

where  $\omega_k(y, t)$  is the coefficient in the Fourier decomposition in the  $x$  direction of  $\delta \omega$ ,  $\psi_k = \Delta_k^{-1} \omega_k$  is the associated stream function with  $\Delta_k = \partial_y^2 - k^2$  the  $k$ -th coefficient of the Laplacian, and  $\eta_k(y, t)$  is a gaussian noise with zero mean and correlations

$$\mathbb{E} [\eta_k(y_1, t_1) \eta_k(y_2, t_2)] = 0, \quad (7.35)$$

$$\mathbb{E} [\eta_k(y_1, t_1) \eta_k^*(y_2, t_2)] = \delta(t_1 - t_2) c_k(y_1 - y_2). \quad (7.36)$$

Equation (7.34) is a linear stochastic process, called Ornstein-Uhlenbeck process. It is fully characterized by its two-points correlation function  $g_k(y_1, y_2, t) = \mathbb{E} [\omega_k(y_1, t) \omega_k^*(y_2, t)]$ , given by the Lyapunov equation

$$\frac{\partial g_k}{\partial t} + \left( L_{\text{in}}^{(1)} + L_{\text{in}}^{(2)*} \right) g_k + \left( L_{\kappa}^{(1)} + L_{\kappa}^{(2)*} \right) g_k = 2c_k, \quad (7.37)$$

where  $L_{\text{in}} = ikU(1 + \Delta_k^{-1})$ ,  $L_{\kappa} = \kappa - \nu \Delta_k$ , and the exponent ( $i$ ) indicates that the operator acts on the variable  $y_i$ . From (7.31), we look for a stationary solution  $g_k^\infty$  of (7.37) that satisfies<sup>1</sup>

$$(1 + \Delta_k^{-1}) g_k^\infty(y_1, y_2) = g_0 \delta(y_1 - y_2), \quad (7.38)$$

with  $g_0$  a constant to be determined. A direct calculation shows that  $\left( L_{\text{in}}^{(1)} + L_{\text{in}}^{(2)*} \right) g_k^\infty = 0$ . Then, the Lyapunov equation (7.37) is solved in the stationary state for the particular forcing

$$c_k = \frac{1}{2} \left( L_{\kappa}^{(1)} + L_{\kappa}^{(2)*} \right) g_k^\infty. \quad (7.39)$$

The fact that the inertial and forced-dissipated parts of the Lyapunov equation vanish independently is a direct consequence of the Langevin structure of this system. From (7.39), the constant  $g_0$  can be given by the normalization of the energy injection<sup>2</sup>.

<sup>1</sup>Note that this condition can be solved explicitly as  $g_k^\infty(y_1, y_2) = g_0 \left( \delta(y_1 - y_2) - H_{\sqrt{k^2 - 1}}(y_1 - y_2) \right)$  where  $H_K$  is the Green function of the Laplacian  $\Delta_K$ .

<sup>2</sup>The condition (7.39) leads to  $g_k = O(1/\kappa, 1/\nu)$ , which seems to be in contradiction with the results of section 5.1 (in page 67), in particular with the statement that  $g_k$  should converge point-wise in the limit  $\nu \ll \kappa \ll 1$  at any point such that  $U(y_1) \neq U(y_2)$ . This is because the condition (7.39) also means that  $c_k$  is a distribution, and not a smooth function. The fact that the results of section 5.1 do not apply when the forcing is a distribution can be understood easily in the case of the constant shear base flow  $U(y) = sy$ , in which case  $g_k(y_1, y_2) = \frac{2c_k(y_1 - y_2)}{iks(y_1 - y_2) + 2\kappa}$ . If  $c_k(y_1 - y_2) \propto \delta(y_1 - y_2)$  then  $g_k = O(1/\kappa)$ , in contradiction with the results of section 5.1.

The solution given by (7.38),(7.39) could be used to study the linear stability of the cosine mean flow in the framework of the kinetic theory (or equivalently S3T, CE2 systems), in the spirit of [2, 104]. Note that this solution can be easily generalized to the beta-plane equation or to the barotropic equation over a periodic topography.

## 7.3 Kinetic theory of Langevin models

As we have seen in the previous section, the energy-entropy distribution for the bi-periodic 2D Euler equation suffers from two singularities: the total average energy is infinite, and in the limit of a concentration of energy in the large-scale zonal jet, the probability distribution function does not depend on the zonal jet amplitude. In this section, we will include higher-order (non-quadratic) Casimir functionals in the definition of the stationary distribution (7.6) in order to avoid these singularities.

In paragraph 7.3.1, we will see how the higher-order Casimir functionals select the amplitude of the large-scale zonal jet and the typical perturbations of this jet.

In paragraph 7.3.2, we will investigate the Langevin dynamics associated with this energy-Casimir functional. In particular, we will see that a regime of time scale separation between the evolution of zonal jets and the evolution of the surrounding turbulence exists.

Using stochastic averaging (Law of Large Numbers and Central Limit Theorem), we can derive a closed effective dynamics for the zonal jet, where the perturbations are averaged out. This effective dynamics (kinetic equation) is presented in paragraph 7.3.3.

As explained in a general setting in section 7.1.3, the terms appearing in the kinetic equation are related to each other through so-called fluctuation-dissipation relations. Those relations are written explicitly in section 7.3.4, for the Langevin model considered in this section.

### 7.3.1 Construction of the equilibrium distribution

As in the previous section 7.2, we consider the 2D Euler Langevin dynamics in the domain  $\mathcal{D} = [0, 2\pi l_x) \times [0, 2\pi)$  with aspect ratio  $l_x < 1$ . We have seen that the energy-entropy distribution  $P_{\text{eq}} \propto \exp(-\mathcal{G}/\gamma)$  with potential  $\mathcal{G}[\omega] = \mathcal{G}_2[\omega] = (-1+\epsilon)\mathcal{E} + \mathcal{Z}$  where  $0 < \epsilon \ll 1$  and with  $\gamma > 0$  describes a concentration of the energy in a large-scale zonal jet. We now consider the more general class of potentials

$$\mathcal{G}[\omega] = (-1 + \epsilon)\mathcal{E}[\omega] + \mathcal{Z}[\omega] + \epsilon\mathcal{C}_f[\omega] = \int \text{d}\mathbf{r} \left( \frac{1 - \epsilon}{2}\omega\psi + \frac{1}{2}\omega^2 + \epsilon f(\omega) \right), \quad (7.40)$$

where  $f$  is a smooth function of the form  $f(\omega) = \sum_{n>2} a_n \omega^n$ , where the coefficients  $a_n$  are such that the distribution  $P_{\text{eq}} \propto \exp(-\mathcal{G}/\gamma)$  is normalizable.

#### Average total energy

An easy way to insure a finite average total energy is to impose that  $f(\omega)$  is defined on a bounded set of values of  $\omega$ , for instance  $f(\omega) = f_0 \left[ \left(1 - (\omega/\omega_{\text{max}})^4\right)^{-1/2} - 1 \right]$ .

It means that, distributed according to the equilibrium PDF with potential given by (7.40), the absolute value of the vorticity at any point cannot exceed  $\omega_{max}$  (more precisely, the event  $\omega(\mathbf{r}) > \omega_{max}$  at a given  $\mathbf{r}$  has probability zero, in particular this has to be fulfilled by the initial condition). Then, the average total energy is bounded by  $(2\pi)^4 \omega_{max}^2 \|H\|_\infty$ , where  $\|H\|_\infty$  is the maximum of the Green function of the Laplacian  $H$  over the domain  $\mathcal{D}$ .

### Most probable flow

At leading order in  $\epsilon$ , the potential reads

$$\mathcal{G}_0[\omega] = \frac{1}{2} \int d\mathbf{r} (\omega \Delta^{-1} \omega + \omega^2). \quad (7.41)$$

By construction, any large-scale jet with vorticity<sup>3</sup>  $\omega_0(\mathbf{r}) = -A \cos y - B \sin y$  is a minimizer of  $\mathcal{G}_0$ . For  $\epsilon \neq 0$ , the minimizer of the full potential  $\mathcal{G}$  reads  $\omega^*(\mathbf{r}) = -A^* \cos y - B^* \sin y + O(\epsilon)$ , where the values of  $A^*$  and  $B^*$  are selected by the higher-order Casimir functional  $\mathcal{C}_f$  in (7.40). This is shown in appendix H.

### Typical fluctuations

Let's now look at the gaussian fluctuations around the most probable state: for  $\omega = \omega^* + \delta\omega$ , we have

$$\mathcal{G}[\omega] \simeq \mathcal{G}[\omega^*] + \frac{1}{2} \int d\mathbf{r} d\mathbf{r}' \delta\omega(\mathbf{r}) \frac{\delta^2 \mathcal{G}}{\delta\omega(\mathbf{r}) \delta\omega(\mathbf{r}')} [\omega^*] \delta\omega(\mathbf{r}'). \quad (7.42)$$

Using (7.6), this means that the distribution of the fluctuations  $\delta\omega$  is approximately gaussian,

$$P[\delta\omega] = \exp\left(-\frac{1}{2\gamma} \int d\mathbf{r} d\mathbf{r}' \delta\omega(\mathbf{r}) M(\mathbf{r}, \mathbf{r}') \delta\omega(\mathbf{r}')\right) (1 + O(\delta\omega^3)) \quad (7.43)$$

where, using (7.40),

$$M(\mathbf{r}, \mathbf{r}') \equiv \frac{\delta^2 \mathcal{G}}{\delta\omega(\mathbf{r}) \delta\omega(\mathbf{r}')} [\omega^*] = H(\mathbf{r} - \mathbf{r}') + \delta(\mathbf{r} - \mathbf{r}') + O(\epsilon), \quad (7.44)$$

where  $H$  is the Green function of the Laplacian.

Consider first perturbations on the largest scale, with vorticity  $\delta\omega = \delta\omega_0 = -\delta A \cos y - \delta B \sin y$ . The terms of order  $\epsilon^0$  in the exponential in (7.43) vanish, so the argument of the exponential in (7.43) is of order  $\epsilon/\gamma$ . This means that the typical amplitude of those large-scale fluctuations  $\delta\omega_0$  is of order  $|\gamma/\epsilon|^{1/2}$ .

Consider now perturbations  $\delta\omega$  on the smaller scales, the terms of order  $\epsilon^0$  in the exponential in (7.43) do not vanish, so  $|\delta\omega| \sim |\gamma|^{1/2}$ .

<sup>3</sup>We use this notation in agreement with the reference papers [10, 19, 61].

## Summary

To summarize, for the equilibrium PDF (7.6) with potential (7.40), the typical vorticity field is of the form

$$\omega(\mathbf{r}) = -(A^* + \delta A) \cos y - (B^* + \delta B) \sin y + \sqrt{\gamma} \omega_p(\mathbf{r}) + O(\epsilon), \quad (7.45)$$

with  $\omega_p$  a perturbation field on the small scales, and where  $\delta A, \delta B \sim |\gamma/\epsilon|^{1/2}$ .

In the case  $\gamma \ll |\epsilon|$ , the flow is strongly concentrated around the most probable flow  $\omega^*$ , as expected from the general form of the equilibrium distribution  $P_{\text{eq}}$  (7.6). On the other hand, for  $\gamma \sim |\epsilon| \ll 1$  the large-scale jet undergoes strong fluctuations while the smaller-scale flow is still of smaller amplitude, and undergoes fluctuations of amplitude  $\sqrt{\gamma}$ . In this regime, the distribution  $P_{\text{eq}}$  has a variance of order 1 in the subspace spanned by  $(\cos y, \sin y)$ , and has a variance of order  $\gamma \ll 1$  in the orthogonal subspace.

Assuming  $\gamma \sim |\epsilon| \ll 1$ , we can write the potential vorticity field as

$$\omega(\mathbf{r}) = -A \cos y - B \sin y + \sqrt{\gamma} \omega_p(\mathbf{r}) \quad (7.46)$$

where  $A$  and  $B$  are fluctuating variables, and  $\omega_p$  represent the small-scale turbulent surrounding flow. This is in good agreement with the general phenomenology of planetary zonal jets, and with the ansatz used in the non-equilibrium kinetic theory in chapter 3 [18]. The main difference in this case is that we have built this typical flow by hand, by tuning the different parameters in the potential  $\mathcal{G}$ . The typical flow has been obtained from the *a priori* built in stationary distribution, and not from the one reached by the natural equations of motion. We thus now have to study the dynamics of  $A, B$ , and  $\omega_p$ . This is done in the next sections.

We will see that the time scale of evolution of  $(A, B)$  is of order  $1/\gamma$ , while the time scale of evolution of the perturbation  $\omega_p$  is of order 1. We will thus similarly perform a perturbative expansion in powers of  $\gamma$  following the stochastic averaging procedure (Law of Large Numbers and Central Limit Theorem, see chapter 2), and obtain an effective equation for the evolution of  $(A, B)$  in the limit  $\gamma \rightarrow 0$ .

### 7.3.2 Time scale separation in the Langevin equation

Consider the projections on the large-scale modes defined by

$$\langle \omega, \cos \rangle \equiv \int \frac{d\mathbf{r}}{2\pi^2 l_x} \omega(\mathbf{r}) \cos y \quad , \quad \langle \omega, \sin \rangle \equiv \int \frac{d\mathbf{r}}{2\pi^2 l_x} \omega(\mathbf{r}) \sin y. \quad (7.47)$$

Then, the decomposition of the vorticity field (7.46) is defined by  $A = -\langle \omega, \cos \rangle$ ,  $B = -\langle \omega, \sin \rangle$  and  $\sqrt{\gamma} \omega_p(\mathbf{r}) = \omega(\mathbf{r}) + (A \cos y + B \sin y)$ .

We project the Langevin equation (7.1) with potential  $\mathcal{G}$  given by (7.40) using these definitions. This is done in appendix I. The resulting equations read

$$\partial_t A = \gamma \langle \mathbf{v}_p \cdot \nabla \omega_p, \cos \rangle + \kappa \gamma C_0 \frac{\partial \tilde{\mathcal{G}}}{\partial A} + \sqrt{2\kappa\gamma} \eta_c, \quad (7.48)$$

$$\partial_t B = \gamma \langle \mathbf{v}_p \cdot \nabla \omega_p, \sin \rangle + \kappa \gamma C_0 \frac{\partial \tilde{\mathcal{G}}}{\partial B} + \sqrt{2\kappa\gamma} \eta_s, \quad (7.49)$$

$$\partial_t \omega_p + L_U[\omega_p] + \sqrt{\gamma} N L_U[\omega_p] + \gamma \kappa D_U[\omega_p] = \sqrt{2\kappa} \eta_p, \quad (7.50)$$

with  $\frac{\partial \tilde{\mathcal{G}}}{\partial A}$  and  $\frac{\partial \tilde{\mathcal{G}}}{\partial B}$  given in (I.7),(I.8); where  $\eta_c$ ,  $\eta_s$  and  $\eta_p$  are independent gaussian noises, with zero means and correlations  $\mathbb{E}[\eta_c(t_1)\eta_c(t_2)] = \mathbb{E}[\eta_s(t_1)\eta_s(t_2)] = C_0\delta(t_1 - t_2)$  and  $\mathbb{E}[\eta_p(\mathbf{r}_1, t_1)\eta_p(\mathbf{r}_2, t_2)] = C_p(\mathbf{r}_1 - \mathbf{r}_2)\delta(t_1 - t_2)$  with  $C_0$  and  $C_p$  defined by (I.4); where the operators  $N L_U$  and  $D_U$  are given in (I.15), (I.16) and the linear operator reads

$$L_U[\omega_p] = L_U^0[\omega_p] + \kappa \int d\mathbf{r}' C_p(\mathbf{r} - \mathbf{r}') (\omega_p + \psi_p), \quad (7.51)$$

where

$$L_U^0[\omega_p] = U \partial_x (\omega_p + \psi_p), \quad (7.52)$$

with the large-scale zonal jet velocity profile  $U(y) = A \sin y - B \cos y$ .

Note that the most probable vorticity  $\omega^*$  corresponds to a zonal flow at leading order in  $\gamma$ , but it can have non-zonal corrections of order  $\gamma$ . This means that in general, the average perturbation  $\omega_p$  in the statistically stationary state of (7.48),(7.49),(7.50) is non-zero, and is of order  $\gamma$ . This non-zero average value is related to the non-linear terms in (7.50).

In equations (7.48),(7.49),(7.50), we readily see that the typical time scale of evolution of the large-scale flow coefficients  $A(t)$  and  $B(t)$  is of order  $1/\gamma \gg 1$ , while the typical time scale of evolution of the perturbation flow  $\omega_p(\mathbf{r}, t)$  is of order 1.

In contrast with the non-equilibrium case studied in chapter 3, here the time scale separation regime  $\gamma \ll 1$  is not the regime of small dissipation  $\kappa \ll 1$ . Instead, time scale separation between large scales and small scales is due to the very particular structure of the dissipation term, related to the choice of potential (7.40). Such artificial time scale separation is somehow similar to the asymmetric damping used for instance in [33], where the evolution of the jet is artificially slowed down using a smaller linear friction rate in the equation for the zonal vorticity than in the equation for the non-zonal perturbations. Asymmetric damping in a barotropic model can be regarded as a simplified model for a baroclinic flow, where the upper zonal jet is less damped than the baroclinic eddies [33].

In particular, because here the small parameter  $\gamma$  is not the parameter controlling the rate of energy dissipation, we will not encounter theoretical difficulties similar to those discussed in chapters 3, 4 and 5 in the limit of time scale separation  $\gamma \rightarrow 0$ .

In the following, we will apply the stochastic averaging tools described in chapter 2, like we did for the stochastic barotropic equation in chapter 3.

In the case of equations (7.48),(7.49),(7.50), the analogy with the generic slow-

fast system (2.8) reads<sup>4</sup>

$$\begin{aligned}
\alpha &\equiv \gamma, \quad z \equiv (A, B), \quad w \equiv \omega_p \\
f(z, w) &\equiv \left( \langle \mathbf{v}_p \cdot \nabla \omega_p, \cos \rangle + \kappa C_0 \frac{\partial \tilde{\mathcal{G}}}{\partial A}, \langle \mathbf{v}_p \cdot \nabla \omega_p, \sin \rangle + \kappa C_0 \frac{\partial \tilde{\mathcal{G}}}{\partial B} \right) \\
\eta_0 &\equiv (\sqrt{\kappa} \eta_c, \sqrt{\kappa} \eta_s), \quad \eta \equiv \sqrt{\kappa} \eta_p \\
L_z \cdot w &\equiv L_U[\omega_p] \\
b_1(z, w) &\equiv -N L_U[\omega_p] - \sqrt{\gamma} \kappa D_U[\omega_p].
\end{aligned} \tag{7.53}$$

The resulting effective equation for the evolution of  $(A, B)$  will be given in section 7.3.3.

### Stationary distribution of the fast variable

Using the analogy (7.53), the virtual fast process (2.9) reads in this case

$$\partial_t \omega_p + L_U[\omega_p] = \sqrt{2\kappa} \eta_p, \tag{7.54}$$

where  $U(y)$  is the fixed zonal jet velocity profile. Explicitly,

$$\partial_t \omega_p + L_U^0[\omega_p] = -\kappa \int d\mathbf{r}' C_p(\mathbf{r} - \mathbf{r}') \frac{\delta \mathcal{G}_2}{\delta \omega_p(\mathbf{r}')} + \sqrt{2\kappa} \eta_p, \tag{7.55}$$

with the inertial linear operator  $L_U^0[\omega_p] = U \partial_x (\omega_p + \psi_p)$ , with the potential

$$\mathcal{G}_2[\omega_p] = \frac{1}{2} \int d\mathbf{r} (\omega_p^2 + \omega_p \psi_p), \tag{7.56}$$

and where  $\eta_p$  has correlations  $\mathbb{E}[\eta_p(\mathbf{r}_1, t_1) \eta_p(\mathbf{r}_2, t_2)] = C_p(\mathbf{r}_1 - \mathbf{r}_2) \delta(t_1 - t_2)$ . The potential (7.56) is conserved by the inertial part of the linearized dynamics:

$$\int d\mathbf{r} L_U^0[\omega_p] \frac{\delta \mathcal{G}_2}{\delta \omega_p(\mathbf{r})} = \int d\mathbf{r} U(y) \partial_x (\omega_p + \psi_p) \cdot (\omega_p + \psi_p) = 0, \tag{7.57}$$

where the last equality can be found performing an integration by parts with respect to  $x$ .

As a consequence, the linearized dynamics (7.54) is a Langevin dynamics with potential  $\mathcal{G}_2$ . We thus know its stationary distribution, it is the gaussian distribution

$$G[\omega_p] \equiv \frac{1}{Z} \exp(-\mathcal{G}_2[\omega_p]). \tag{7.58}$$

Note that  $G$  does not depend on the large-scale flow  $U$ . We will thus denote by  $\mathbb{E}_\infty[O]$  the average of an observable  $O[\omega_p]$  over the distribution  $G$ .

---

<sup>4</sup>The term of order  $\sqrt{\gamma}$  in the expression of  $b_1(z, w)$  could be easily included in the formal derivation of stochastic averaging, chapter 2 and appendix A.

### 7.3.3 Effective dynamics of the zonal jet

Using the results of section 2.2 (equation (2.19) in page 32) and the analogy (7.53), we get

$$\partial_t A = \kappa C_0 \gamma \mathbb{E}_\infty \left[ \frac{\partial \tilde{\mathcal{G}}}{\partial A} \right] + \sqrt{2\kappa\gamma} \eta_c + \gamma F_c + \gamma^{3/2} F_{1,c} + \gamma \xi_c, \quad (7.59)$$

$$\partial_t B = \kappa C_0 \gamma \mathbb{E}_\infty \left[ \frac{\partial \tilde{\mathcal{G}}}{\partial B} \right] + \sqrt{2\kappa\gamma} \eta_s + \gamma F_s + \gamma^{3/2} F_{1,s} + \gamma \xi_s, \quad (7.60)$$

where  $\eta_c$  and  $\eta_s$  are the same noises as in (7.48),(7.49), and where  $\xi_c$  and  $\xi_s$  are gaussian random noises with zero means and correlations (for fixed  $(A, B)$ )  $\mathbb{E} [\xi_c(t_1)\xi_c(t_2)] = \Xi_c(A, B)\delta(t_1-t_2)$ ,  $\mathbb{E} [\xi_c(t_1)\xi_s(t_2)] = \Xi_{cs}(A, B)\delta(t_1-t_2)$  and  $\mathbb{E} [\xi_s(t_1)\xi_s(t_2)] = \Xi_s(A, B)\delta(t_1-t_2)$ . These correlation functions are given by the Central Limit Theorem (2.20), here<sup>5</sup>

$$\Xi_c(A, B) = 2 \int_0^\infty ds \mathbb{E}_U [\langle \mathbf{v}_p \cdot \nabla \omega_p, \cos \rangle (s) \langle \mathbf{v}_p \cdot \nabla \omega_p, \cos \rangle (0)], \quad (7.61)$$

$$\Xi_s(A, B) = 2 \int_0^\infty ds \mathbb{E}_U [\langle \mathbf{v}_p \cdot \nabla \omega_p, \sin \rangle (s) \langle \mathbf{v}_p \cdot \nabla \omega_p, \sin \rangle (0)], \quad (7.62)$$

$$\begin{aligned} \Xi_{cs}(A, B) = \int_0^\infty ds \mathbb{E}_U [\langle \mathbf{v}_p \cdot \nabla \omega_p, \cos \rangle (s) \langle \mathbf{v}_p \cdot \nabla \omega_p, \sin \rangle (0) \\ + \langle \mathbf{v}_p \cdot \nabla \omega_p, \sin \rangle (s) \langle \mathbf{v}_p \cdot \nabla \omega_p, \cos \rangle (0)]. \end{aligned} \quad (7.63)$$

The drift terms in (7.59),(7.60) are given by the Law of Large Numbers,

$$F_c = \mathbb{E}_\infty [\langle \mathbf{v}_p \cdot \nabla \omega_p, \cos \rangle] \quad , \quad F_s = \mathbb{E}_\infty [\langle \mathbf{v}_p \cdot \nabla \omega_p, \sin \rangle], \quad (7.64)$$

and  $F_{1,c}$ ,  $F_{1,s}$  are given in appendix A.

In the above expressions, we recall that  $\mathbb{E}_\infty[\cdot]$  and  $\mathbb{E}_U[\cdot]$  denote respectively the average and the covariance over the stationary distribution of the fast variable (7.58). In particular, we know from the results of section 7.2 that  $F_c = F_s = 0$ . This means that in this class of Langevin models, the drift in the effective evolution of the large scale jet is given at leading order by the dissipation terms only. At next order, the drift terms  $F_{1,c}$ ,  $F_{1,s}$  describe the corrections due to the non-linear terms in (7.50).

### 7.3.4 Fluctuation-dissipation relations

The Langevin structure of the system (7.48),(7.49),(7.50) implies constraints on the effective dynamics (7.59),(7.60), called fluctuation-dissipation relations. These relations were derived in a very abstract and general setting in section 7.1.3. Here we give the explicit expression of those relations for the dynamics (7.59),(7.60), and discuss some consequences.

<sup>5</sup>The dissipative drift terms  $\frac{\partial \tilde{\mathcal{G}}}{\partial A}$  and  $\frac{\partial \tilde{\mathcal{G}}}{\partial B}$  (given in (I.7),(I.8)) do not depend on  $\omega_p$  at leading order. Then, their covariance is of order  $\sqrt{\gamma}$ , and is negligible here.

The first fluctuation-dissipation relation (7.17) relates the inertial terms in the effective equations (7.59),(7.60) at equilibrium, namely,

$$\begin{aligned} \frac{\partial}{\partial A} \left\{ -F_{1,c}R_{\text{eq}} + \sqrt{\gamma} \frac{\partial}{\partial A} (\Xi_c R_{\text{eq}}) \right\} + \frac{\partial}{\partial B} \left\{ -F_{1,s}R_{\text{eq}} + \sqrt{\gamma} \frac{\partial}{\partial B} (\Xi_s R_{\text{eq}}) \right\} \\ + 2\sqrt{\gamma} \frac{\partial^2}{\partial A \partial B} (\Xi_{cs} R_{\text{eq}}) = O(\gamma), \end{aligned} \quad (7.65)$$

with  $R_{\text{eq}} = G^{-1} \mathcal{P} P_{\text{eq}}$  the equilibrium distribution of the jet amplitudes. Here we have used  $F_c = F_s = 0$ .

We stress again on the fact that (7.65) is an equality up to terms of order  $\gamma$ . Thus, if we expand  $R_{\text{eq}}$  as

$$R_{\text{eq}} = R_{\text{eq}}^0 + \sqrt{\gamma} R_{\text{eq}}^1 + O(\gamma) \quad (7.66)$$

and the drift terms  $F_{1,c}, F_{1,s}$  as

$$F_{1,c/s} = F_{1,c/s}^0 + \sqrt{\gamma} F_{1,c/s}^1 + O(\gamma), \quad (7.67)$$

then at order  $\gamma^0$  equation (7.65) becomes

$$\frac{\partial}{\partial A} \{ F_{1,c}^0 R_{\text{eq}}^0 \} + \frac{\partial}{\partial B} \{ F_{1,s}^0 R_{\text{eq}}^0 \} = 0, \quad (7.68)$$

and at order  $\sqrt{\gamma}$  we get

$$\begin{aligned} \frac{\partial}{\partial A} \left\{ -F_{1,c}^0 R_{\text{eq}}^1 - F_{1,c}^1 R_{\text{eq}}^0 + \frac{\partial}{\partial A} (\Xi_c R_{\text{eq}}^0) \right\} + \frac{\partial}{\partial B} \left\{ -F_{1,s}^0 R_{\text{eq}}^1 - F_{1,s}^1 R_{\text{eq}}^0 + \frac{\partial}{\partial B} (\Xi_s R_{\text{eq}}^0) \right\} \\ + 2 \frac{\partial^2}{\partial A \partial B} (\Xi_{cs} R_{\text{eq}}^0) = 0. \end{aligned} \quad (7.69)$$

Those relations are very difficult to obtain from the explicit expressions of  $F_{1,c/s}, \Xi_{c/s/cs}$  and  $R_{\text{eq}}$  given in appendix A. Despite the simplicity of the proof given in section 7.1.3, such fluctuation-dissipation are not trivial in general. In particular, they can lead to cases where the stochastic term  $\Xi$  could be expressed simply as a function of the drift term  $F_0$ . It turns out that in all the cases studied during this thesis, the physically relevant drift term (average Reynolds' stress divergence) is zero (see section 7.2). This is why no simple numerical application of this study is possible at that point. Generalizations are discussed in section 7.4.

The second fluctuation-dissipation relation (7.18) relates the terms in (7.59),(7.60) coming from forcing and dissipation, namely,

$$\frac{\partial}{\partial A} \left\{ -\mathbb{E}_\infty \left[ \frac{\partial \tilde{\mathcal{G}}}{\partial A} \right] R_{\text{eq}} + \frac{\partial R_{\text{eq}}}{\partial A} \right\} + \frac{\partial}{\partial B} \left\{ -\mathbb{E}_\infty \left[ \frac{\partial \tilde{\mathcal{G}}}{\partial B} \right] R_{\text{eq}} + \frac{\partial R_{\text{eq}}}{\partial B} \right\} = O(\gamma^{3/2}). \quad (7.70)$$

The relation (7.70) can actually be guessed from the approximate expression of  $R_{\text{eq}}$ . Using (I.6) in appendix I, we have

$$\begin{aligned} P_{\text{eq}}[\omega] &= \frac{1}{Z} \exp \left( -\tilde{\mathcal{G}}[A, B, \omega_p] \right) \\ &= \frac{1}{Z} \exp \left( -g(A, B) - \mathcal{G}_2[\omega_p] + O(\sqrt{\gamma}) \right) \end{aligned} \quad (7.71)$$

with

$$g(A, B) = \frac{\epsilon}{\gamma} 2\pi^2 l_x (A^2 + B^2) + \frac{\epsilon}{\gamma} \int d\mathbf{r} f(-A \cos y - B \sin y), \quad (7.72)$$

and  $\mathcal{G}_2$  given by (7.56) (remember that  $|\epsilon| \sim \gamma$ ).

In equation (7.71), we recognize both the general expression  $P_{\text{eq}} = G R_{\text{eq}} + O(\sqrt{\gamma})$ , and the fact that at leading order, the fast variable  $\omega_p$  is distributed according to the equilibrium distribution (7.58) with potential  $\mathcal{G}_2$ .

From (7.71), the equilibrium distribution of the jet amplitudes is

$$R_{\text{eq}}(A, B) = \frac{1}{Z'} \exp(-g(A, B)) + O(\sqrt{\gamma}). \quad (7.73)$$

By construction (see eq. (7.71)), we have  $\frac{\partial g}{\partial A} = \frac{\partial \tilde{\mathcal{G}}}{\partial A} + O(\sqrt{\gamma})$  and  $\frac{\partial g}{\partial B} = \frac{\partial \tilde{\mathcal{G}}}{\partial B} + O(\sqrt{\gamma})$ . Note also that at leading order,  $\frac{\partial \tilde{\mathcal{G}}}{\partial A}$  and  $\frac{\partial \tilde{\mathcal{G}}}{\partial B}$  do not depend on  $\omega_p$  (see appendix I), so they are equal to their average values  $\mathbb{E}_\infty \left[ \frac{\partial \tilde{\mathcal{G}}}{\partial A} \right]$  and  $\mathbb{E}_\infty \left[ \frac{\partial \tilde{\mathcal{G}}}{\partial B} \right]$ , plus corrections of order  $\sqrt{\gamma}$ .

As a consequence, the equality (7.70) at order  $\gamma^0$  (i.e. with  $O(\sqrt{\gamma})$  on the r.h.s) can be obtained directly from the expansion of  $P_{\text{eq}}$  (7.71).

## 7.4 Perspectives

We have studied in this chapter the effective dynamics for a particular class of 2D stochastic Euler equations, where some quantities of interest can be computed explicitly. In particular, we have proposed a method to compute the average Reynolds' stress divergence, averaged over the stationary distribution of the linearized dynamics close to a fixed base flow. It turns out that in all the cases studied here, this quantity is exactly zero, so the effective jet dynamics is driven at leading order by dissipation and non-linear corrections, in contrast with what is observed in the non-equilibrium case (see chapter 3).

An interesting perspective of this work is the generalization to Langevin models where the detailed balance assumption involves the inertial advection terms of the fluid mechanics equation:

$$\begin{aligned} \frac{\partial \omega}{\partial t} &= -\mathbf{v} \cdot \nabla \omega - \kappa \omega + \nu \Delta \omega + \sqrt{2\gamma} \eta \\ &= \mathcal{F}[\omega] - \int d\mathbf{r}' C(\mathbf{r} - \mathbf{r}') \frac{\delta \mathcal{G}}{\delta \omega(\mathbf{r}')} + \sqrt{2\gamma} \eta \end{aligned} \quad (7.74)$$

where  $\mathcal{F}$  and  $\mathcal{G}$  satisfy a Liouville property  $\int d\mathbf{r} \frac{\delta \mathcal{F}}{\delta \omega(\mathbf{r})} = 0$  and an orthogonality condition  $\int d\mathbf{r} \mathcal{F}[\omega](\mathbf{r}) \frac{\delta \mathcal{G}}{\delta \omega(\mathbf{r})} = 0$ . Then, like for the Langevin model (7.1), the stationary state is given by the equilibrium distribution  $P_{\text{eq}}[\omega] \propto \exp(-\mathcal{G}[\omega]/\gamma)$ .

In a regime of parameters where a time scale separation exists between a large-scale flow and small-scales turbulent perturbations, a stochastic averaging procedure could be applied to (7.74), and it is easy to show that fluctuation-dissipation relations would hold. The interest of such a study would be to construct realistic—with a realistic dissipation—explicitly solvable models, where the average Reynolds'

stress divergence would be non-zero and would probably depend on the zonal jet characteristics.

Another motivation of this work is to make explicit predictions for the rare transitions between attractors, using large deviation theory. For instance, in [10, 61] is presented the computation of the probability of transition between two attractors of the stochastic barotropic equation upon a topography, corresponding to two different zonal jet configurations. In the results presented in [61], the transition occurs through zonally invariant states only. The results of this chapter enable to take into account the non-zonal degrees of freedom (eddies) in such transitions (inertial terms in the effective equations (7.59),(7.60), and inertial fluctuation-dissipation relation (7.65)). Again, a case with a non-zero leading order drift term (average Reynolds' stress divergence) would be more interesting from a physical point of view.

# Conclusion

We have studied in this thesis the dynamics of zonal jets in stochastic barotropic models, in the regime of weak forces and dissipation. This framework is expected to give a qualitative description of the dynamics of the polar jet stream in the atmosphere, or of the zonal jet structure observed in the outer layer of giant gaseous planets.

We have seen that in the regime of weak forces and dissipation (characterized by a small parameter  $\alpha \ll 1$ ), most of the kinetic energy concentrates into the zonal jet, which evolves much slower than the surrounding turbulent perturbations. This allows a quasi-static description of zonal jet dynamics and statistics, where small-scale turbulence is averaged out. Our approach is similar to the kinetic theory for systems of particles, which provides an effective description of the macroscopic behaviour of the system. We also go beyond the classical kinetic approach in order to describe fluctuations of zonal jets, at higher orders in  $\alpha$ . These fluctuations are of great importance in the dynamics of the polar jet stream, and can lead in some cases to a brutal change in the configuration of the jets.

Using kinetic theory, we have obtained an equation that describes the effective slow evolution of zonal jets. At leading order in  $\alpha \ll 1$ , this equation is equivalent to a closure at second order in the hierarchy of cumulants of the vorticity, already studied in the past on a phenomenological ground (S3T in [2], CE2 in [104, 106]). With our perturbative expansion, we thus justify theoretically those previous approaches, and explain why the regime  $\alpha \ll 1$  and  $K \gg 1$  where  $K$  is the number of forced modes, is the most natural regime to apply such closure. An important physical consequence is that in this regime, the main energy transfer mechanism from the forcing scale to the scale of the jet is a non-local one, through Reynolds' stresses. This is in contrast with the common picture of jet formation through an upscale turbulent energy cascade.

Our approach also allows to go beyond classical closures in order to describe zonal jet fluctuations. This is a very original point of view in the study of zonal jet dynamics. In particular, we have proved that in the general case, the small fluctuations of Reynolds' stresses are actually not negligible in the zonal jet energy balance.

From a theoretical point of view, we have addressed the validity of the kinetic theory in the regime  $\alpha \ll 1$ . In the simplest case with no differential rotation, no viscosity, and when the stochastic forcing spectrum is localized, we have proved that the perturbative expansion actually leads to divergences, also interpreted as a lack of ergodicity for the dynamics of fast turbulent perturbations. We have also discussed how those divergences could be regularized by considering a forcing acting on a very

large number of modes  $K \gg 1$  (with a constant energy input). This is actually the case considered in previous numerical studies [2, 104, 106], this explains why those divergences were never observed before.

It would be very interesting to study more precisely different regimes, such as  $K \gg 1$  or with non-zero viscosity, and investigate from a theoretical point of view the effect of differential rotation (beta-effect). This would be very interesting for geophysical applications, and it would bridge the gap with previous numerical studies [2, 104, 106].

Another important part of this thesis deals with the study of rare events in zonal jet dynamics, such as transitions between different configurations of jets. Such rare events are extremely difficult to study using direct numerical simulations, and yet no theoretical approach was ever attempted to describe these events in this system. We have also explained why kinetic theory is not able to describe rare events either.

Instead, we have chosen to use Large Deviation Theory. In the regime of time scale separation  $\alpha \ll 1$ , the large deviation principle gives the probability of arbitrarily large fluctuations of the zonal jet acceleration. We have developed original methods in order to implement the large deviation principle, and to compute explicitly or numerically such probabilities. We have applied those methods to the stochastic barotropic model, and we have observed significant differences between the actual probability of rare events and the probability predicted by kinetic theory, as expected.

This work is the first step towards a Large Deviation Theory of zonal jet statistical dynamics. Computing the probability of fluctuations leading to a transition between attractors of the dynamics and the most probable path of such transition is the most interesting perspective of this work, both from a theoretical point of view and for geophysical applications.

In a last chapter, we have presented an academic model of barotropic dynamics, analogous to the Langevin model for Brownian motion. The interest of this model is that the stationary distribution of the flow is known explicitly. We have studied the effective slow dynamics of zonal jets within this model, and derived fluctuation-dissipation relations which give the stationary distribution of the jet amplitude.

The tools developed in this thesis could be generalized to more complex climate models, and in order to study the dynamics of other large scale coherent structures such as giant vortices, ocean rings and currents. In particular, the possible brutal climate changes (related to changes in the thermohaline circulation for instance [91]) are very difficult to study through direct climate modelling [50], this calls for extended theoretical investigation.

# Appendix A

## Stochastic averaging — Formal derivation

### A.1 Perturbative expansion of the Fokker–Planck equation

We consider the slow-fast system  $(z, w)$  evolving according to (2.8) (page 29), described by the Fokker-Planck equation (2.10). We recall the definition of the slow part of the PDF  $P_s(z, w, t) = \mathcal{P}P(z, w, t) = G_z(w)R(z, t)$  and of the fast part  $P_f = (1 - \mathcal{P})P$ , where  $\mathcal{P}\cdot = G_z \int dw \cdot$  is the projector onto the space of PDF's with the fast variable  $w$  relaxed to its stationary distribution  $G_z$ . As explained in section 2.2, in the case of interest  $G_z$  is a gaussian distribution, given by (2.15).

The stochastic averaging is a perturbative expansion of  $P_f$  as a function of  $P_s$ , in powers of  $\alpha \ll 1$ . To obtain this expansion, we project the Fokker-Planck equation (2.10) using  $\mathcal{P}$  and  $1 - \mathcal{P}$ :

$$\frac{\partial P_s}{\partial t} = \alpha \mathcal{P} \mathcal{L}_s (P_s + P_f) \quad (\text{A.1})$$

$$\frac{\partial P_f}{\partial t} = \mathcal{L}_0 P_f + \sqrt{\alpha} \mathcal{L}_1 (P_s + P_f) + \alpha (1 - \mathcal{P}) \mathcal{L}_s (P_s + P_f), \quad (\text{A.2})$$

where we have used  $\mathcal{P} \mathcal{L}_0 = \mathcal{P} \mathcal{L}_1 = 0$  (this is because  $\mathcal{L}_0$  and  $\mathcal{L}_1$  are divergences with respect to  $w$ ) and  $\mathcal{L}_0 \mathcal{P} = 0$  (this is because by definition,  $\mathcal{L}_0 G_z = 0$ ). To solve formally (A.1), (A.2), we consider the Laplace transform, defined for any function of time  $\phi(t)$  by

$$\hat{\phi}(s) = LT[\phi](s) = \int_0^\infty \phi(t) e^{-ts} dt.$$

By integration by parts, we have  $LT[\partial_t \phi](s) = -\phi(0) + s \hat{\phi}(s)$ , so (A.2) becomes

$$(s - \mathcal{L}_0 - \sqrt{\alpha} \mathcal{L}_1 - \alpha(1 - \mathcal{P}) \mathcal{L}_s) \hat{P}_f(s) = (\sqrt{\alpha} \mathcal{L}_1 - \alpha(1 - \mathcal{P}) \mathcal{L}_s) \hat{P}_s(s) + P_f(0).$$

As  $P_f$  evolves very fast, the initial condition  $P_f(0)$  is not important and can be taken to be zero without loss of generality. Then,

$$\hat{P}_f(s) = \sqrt{\alpha} (s - \mathcal{L}_0 - \sqrt{\alpha} \mathcal{L}_1 - \alpha(1 - \mathcal{P}) \mathcal{L}_s)^{-1} (\mathcal{L}_1 - \sqrt{\alpha} (1 - \mathcal{P}) \mathcal{L}_s) \hat{P}_s(s). \quad (\text{A.3})$$

This is still exact. We can now perform a perturbative expansion of (A.3) in powers of  $\alpha$ ,

$$\hat{P}_f(s) = \sqrt{\alpha} [(s - \mathcal{L}_0)^{-1} + (s - \mathcal{L}_0)^{-1} (\sqrt{\alpha} \mathcal{L}_1) (s - \mathcal{L}_0)^{-1}] (\mathcal{L}_1 - \sqrt{\alpha} (1 - \mathcal{P}) \mathcal{L}_s) \hat{P}_s(s) + O(\alpha^{3/2}).$$

Now using the fact that  $(s - \mathcal{L})^{-1}$  is the Laplace transform of  $e^{t\mathcal{L}}$ , and the fact that the inverse Laplace transform of a product is a convolution product, we get

$$P_f(t) = \sqrt{\alpha} \int_0^\infty e^{t'\mathcal{L}_0} (\mathcal{L}_1 - \sqrt{\alpha} (1 - \mathcal{P}) \mathcal{L}_s) P_s(t - t') dt' + \alpha \int_0^\infty e^{t'\mathcal{L}_0} \mathcal{L}_1 \int_0^\infty e^{t''\mathcal{L}_0} \mathcal{L}_1 P_s(t - t' - t'') dt' dt'' + O(\alpha^{3/2}).$$

We observe now that the evolution equation for  $P_s$  contains memory terms. However, from (A.1) we have  $\partial P_s \partial t = O(\alpha)$ , so we can replace  $P_s(t - t')$  by  $P_s(t) + O(\alpha)$ . This approximation is the equivalent of Bogolyubov's hypothesis in kinetic theory [4]. The evolution equation for  $P_s$  is then

$$\frac{\partial P_s(t)}{\partial t} = \alpha \left[ \mathcal{P} \mathcal{L}_s + \sqrt{\alpha} \mathcal{P} \mathcal{L}_s \int_0^\infty dt' e^{t'\mathcal{L}_0} (\mathcal{L}_1 - \sqrt{\alpha} (1 - \mathcal{P}) \mathcal{L}_s) + \alpha \mathcal{P} \mathcal{L}_s \int_0^\infty dt' e^{t'\mathcal{L}_0} \mathcal{L}_1 \int_0^\infty dt'' e^{t''\mathcal{L}_0} \mathcal{L}_1 \right] P_s(t) + O(\alpha^{5/2}).$$

## A.2 Explicit computation of the operators

The next step is to evaluate explicitly each term appearing in this equation.

- The first term gives the Large Deviation Principle,

$$\mathcal{P} \mathcal{L}_s P_s(w, z) = -G_z(w) \nabla_z [F(z) R(z)].$$

- The second term reads

$$\begin{aligned} \mathcal{P} \mathcal{L}_s \int_0^\infty dt' e^{t'\mathcal{L}_0} \mathcal{L}_1 G_z(w) R(z) &= -G_z(w) \nabla_z [\tilde{F}_1(z) R(z)] \\ &- G_z(w) \nabla_z \nabla_z \left[ \int_0^\infty dt' \int dw e^{t'\mathcal{L}_0} \nabla_w (b_1(z, w) G_z(w)) R(z) \right] \end{aligned}$$

with

$$\tilde{F}_1(z) = - \int_0^\infty dt' \mathbb{E}_z [f(z, \tilde{w}_z(t')) \nabla_w [b_1(z, \tilde{w}_z(0)) G_z(\tilde{w}_z(0))] G_z^{-1}(\tilde{w}_z(0))] \quad (\text{A.4})$$

In the second term, the integral over  $w$  can be rewritten as an average over  $G_z$  of a function of  $(z, \tilde{w}_z(t'))$ . This is an average in the stationary state of the process  $\tilde{w}_z$ , so it does not depend on time  $t'$ . Then, it is just the integral over  $w$  of a divergence with respect to  $w$ , so it vanishes. The first term is non-zero in general.

- For the third term, we have

$$\begin{aligned}
 (1 - \mathcal{P})\mathcal{L}_s P_s(z, w) &= -\nabla_z [f(z, w)G_z(w)R(z)] + G_z(w)\nabla_z [F(z)R(z)] \\
 \mathcal{P}\mathcal{L}_s e^{t'\mathcal{L}_0} (1 - \mathcal{P})\mathcal{L}_s P_s(z, w) &= -G_z(w)\nabla_z \int dw f(z, w)e^{t'\mathcal{L}_0} \{-\nabla_z [f(z, w)G_z(w)R(z)] + G_z(w)\nabla_z [F(z)R(z)]\} \\
 &= G_z(w)\nabla_z \nabla_z \int dw f(z, w)e^{t'\mathcal{L}_0} f(z, w)G_z R - G_z \nabla_z \int dw \nabla_z [f(z, w)e^{t'\mathcal{L}_0}] f(z, w)G_z R \\
 &\quad - G_z \nabla_z \nabla_z \int dw f(z, w)e^{t'\mathcal{L}_0} G_z F R + G_z \nabla_z \int dw \nabla_z [f(z, w)e^{t'\mathcal{L}_0} G_z] F R \\
 &= G_z \nabla_z \nabla_z \{\mathbb{E}_z [f(t') (f(0) - F)] R\} - G_z \nabla_z \left\{ \mathbb{E}_z \left[ \nabla_z [f(z, w)e^{t'\mathcal{L}_0}] (f(z, w) - F) \right] R \right\} \\
 &\quad - G_z \nabla_z \left\{ \mathbb{E}_z \left[ f(t') \left( \frac{1}{G_z} (\nabla_z G_z) F \right) (0) \right] R \right\}
 \end{aligned}$$

where we use the notation  $\phi(t') = \phi(z, \tilde{w}_z(t'))$ , with  $\tilde{w}_z$  the solution of the virtual fast process (2.9). Now, defining

$$\Xi(z) \equiv 2 \int_0^\infty \mathbb{E}_z [f(t') (f(0) - F)] dt' = 2 \int_0^\infty \mathbb{E}_z [(f(t') - F) (f(0) - F)] dt'$$

and

$$\tilde{F}_2(z) = \int_0^\infty \left\{ \mathbb{E}_z \left[ \nabla_z [f(z, w)e^{t'\mathcal{L}_0}] (f(z, w) - F) \right] + \mathbb{E}_z \left[ f(t') \left( \frac{1}{G_z} (\nabla_z G_z) F \right) (0) \right] \right\} dt',$$

we get

$$\mathcal{P}\mathcal{L}_s \int_0^\infty e^{t'\mathcal{L}_0} (1 - \mathcal{P})\mathcal{L}_s P_s(z, w) = G_z(w)\nabla_z \left\{ -\tilde{F}_2(z)R(z) + \frac{1}{2}\nabla_z (\Xi(z)R(z)) \right\}.$$

- For the last term, we write

$$e^{t'\mathcal{L}_0} \mathcal{L}_1 e^{t''\mathcal{L}_0} \mathcal{L}_1 G_z(w) = M(z, w)(t', t'')G_z(w).$$

The function  $M$  could be written explicitly using the expression of  $G_z(w)$ , but this is not necessary here. Then,

$$\mathcal{P}\mathcal{L}_s e^{t'\mathcal{L}_0} \mathcal{L}_1 e^{t''\mathcal{L}_0} \mathcal{L}_1 P_s = G_z \nabla_z [\mathbb{E}_z [f(z, w)M(z, w)(t', t'')] R] + \nabla_z [\mathbb{E}_z [M(z, w)(t', t'')] R].$$

We first consider the average value of  $M$ . As  $\mathbb{E}_z$  is an average over the stationary distribution  $G_z$ , we have

$$\mathbb{E}_z [M(z, w)(t', t'')] = \mathbb{E}_z [M_1(z, w)(t' - t'')]$$

with  $M_1$  defined by

$$\mathcal{L}_1 e^{(t'-t'')\mathcal{L}_0} \mathcal{L}_1 G_z(w) = M_1(z, w)(t' - t'')G_z(w).$$

Using the expression of  $\mathcal{L}_1$  as a divergence with respect to  $w$ , we then have  $\mathbb{E}_z [M(z, w)(t', t'')] = 0$ , so that

$$\mathcal{P}\mathcal{L}_s \int_0^\infty e^{t'\mathcal{L}_0} \mathcal{L}_1 \int_0^\infty e^{t''\mathcal{L}_0} \mathcal{L}_1 dt' dt'' P_s(z, w, t) = -G_z(w)\nabla_z [\tilde{F}_3(z)R(z, t)]$$

with  $\tilde{F}_3(z) = -\int_0^\infty \int_0^\infty \mathbb{E}_z [f(z, w)M(z, w)(t', t'')] dt' dt''$ .

The slow Fokker-Planck equation thus reads

$$\frac{\partial R}{\partial t} = -\alpha \nabla_z [(F + \sqrt{\alpha} F_1) R] + \frac{1}{2} \alpha^2 \nabla_z \nabla_z [\Xi R] \quad (\text{A.5})$$

with  $F_1 = \tilde{F}_1 + \sqrt{\alpha}(\tilde{F}_2 + \tilde{F}_3)$ .

# Appendix B

## Large Deviation Principle — Formal derivation

### B.1 The Gärtner–Ellis theorem applied to the slow process

The formal computations presented in this appendix are directly inspired by the work of Eric Vanden-Eijnden, that will be published soon [16]. The corresponding theorem was first published by Freidlin and Wentzell [39], see also [114] and references therein.

Consider the slow-fast system (2.1) (in page 26). For simplicity, we perform the change of time variable  $t \rightarrow \alpha t$ , so the relevant time scale for the slow process is of order one:

$$\begin{cases} \frac{\partial z}{\partial t} = f(z, w) \\ \frac{\partial w_i}{\partial t} = \frac{1}{\alpha} b_i(z, w) + \frac{1}{\sqrt{\alpha}} \eta_i \end{cases} \quad (\text{B.1})$$

We will consider the paths  $\{z(t), w(t)\}_{t \in [0, T]}$  where  $T$  is fixed and with a given initial state  $(z_0, w_0) \equiv (z(0), w(0))$ .

In order to apply the Gärtner-Ellis theorem, consider the scaled cumulant generating functional

$$\lambda[k] \equiv \lim_{\alpha \rightarrow 0} \alpha \ln \mathbb{E} \left[ \exp \left( \frac{1}{\alpha} \int_0^T k(t) z(t) dt \right) \right], \quad (\text{B.2})$$

where the average is taken over the distribution of  $\{z(t), w(t)\}_{t \in [0, T]}$  with initial condition  $(z(0), w(0)) = (z_0, w_0)$ . This is a direct generalization of the SCGF  $\lambda(k)$  defined in section 2.3.1 (page 32) for infinite dimensional random variables (random processes). Assuming that  $\lambda[k]$  is well-defined (finite and functionally differentiable with respect to  $k$ ), the Gärtner-Ellis theorem implies that the process  $\{z(t)\}_{t \in [0, T]}$  satisfies a Large Deviation Principle for  $\alpha \rightarrow 0$  with rate function

$$I[z] = \sup_{\{k(t)\}_{t \in [0, T]}} \left\{ \int_0^T k(t) z(t) dt - \lambda[k] \right\}. \quad (\text{B.3})$$

We will prove that

$$\lambda[k] = \theta(0)z_0 + \int_0^T H(z(t), \theta(t)) dt \quad (\text{B.4})$$

for  $\theta(t)$  such that  $\dot{\theta}(t) = -k(t)$  and  $\theta(T) = 0$ , and where  $H$  is the SCGF defined in equation (2.26) (page 34). Then, the condition that  $\lambda[k]$  is functionally differentiable with respect to  $k$  resumes to the condition that  $H(z, \cdot)$  is differentiable.

Performing an integration by parts in (B.3) and using (B.4), we get

$$\begin{aligned} I[z] &= \sup_{\{\theta(t)\}_{t \in [0, T]}} \left\{ \int_0^T (\theta(t)\dot{z}(t) - H(z(t), \theta(t))) dt \right\} \\ &= \int_0^T \sup_{\theta(t)} \{\theta(t)\dot{z}(t) - H(z(t), \theta(t))\} dt, \end{aligned}$$

which is exactly the action functional  $S[z]$  defined in section 2.3.2.

We now have to prove (B.4) to finish the proof of the Large Deviation Principle for  $z$ . Performing an integration by parts in (B.2) and using (B.1), we get

$$\begin{aligned} \lambda[k] &= \lim_{\alpha \rightarrow 0} \alpha \ln \mathbb{E} \left[ e^{\frac{1}{\alpha} \theta(0) z_0} \exp \left( \frac{1}{\alpha} \int_0^T \theta(t) f(z(t), w(t)) dt \right) \right] \\ &= \theta(0) z_0 + \lim_{\alpha \rightarrow 0} \alpha \ln u(T, z_0, w_0) \end{aligned}$$

with

$$u(T, z, w) \equiv \mathbb{E} \left[ \exp \left( \frac{1}{\alpha} \int_0^T \theta(t) f(z(t), w(t)) dt \right) \middle| z(0) = z, w(0) = w \right]. \quad (\text{B.5})$$

In the following,  $\theta$  (or  $k$ ) will be fixed so we don't denote its dependency in  $u$ . In contrast, the initial conditions  $(z(0), w(0)) = (z, w)$  are important in the definition of  $u$ . Indeed, the evolution equation of  $u$  is given by [16]

$$\frac{\partial u}{\partial T} = \left( f(z, w) \nabla_z + \frac{1}{\alpha} b(z, w) \nabla_w + \frac{1}{2\alpha} C : \nabla_w \nabla_w + \frac{1}{\alpha} \theta f(z, w) \right) u \quad (\text{B.6})$$

with  $\theta = \theta(0)$ . We look for a solution of this equation under the form  $u(T, z, w) = v(T, z, w) \exp(\frac{1}{\alpha} \phi(T, \alpha z, w))$ , where  $v$  and  $\phi$  are assumed to be of order one with respect to  $\alpha$ . Injecting this ansatz in (B.6) and collecting terms of leading order, we get  $\nabla_w \phi = 0$ . Then at order  $1/\alpha$ ,

$$\left( b(z, w) \nabla_w + \frac{1}{2} C : \nabla_w \nabla_w + \theta f(z, w) - K \right) v = 0 \quad (\text{B.7})$$

with  $K = \partial_T \phi(T, 0)$ <sup>1</sup>. The first two terms in the parenthesis are related to the evolution of the virtual fast process  $\tilde{w}_z$  defined in (2.4) (page 28), while  $z$ ,  $T$  and  $\theta$

<sup>1</sup>A more precise definition of  $K$  goes through the Hamilton-Jacobi equation [16]

are simple parameters. Then,  $v$  is the stationary solution of an equation similar to (B.6), so (B.7) can be solved as

$$\begin{aligned} v(T, z, w) &= \lim_{\Delta t \rightarrow \infty} \mathbb{E} \left[ \exp \left( \theta \int_0^{\Delta t} f(z, \tilde{w}_z(s)) ds - \Delta t K \right) \right] \\ &= \lim_{\Delta t \rightarrow \infty} e^{-\Delta t K} \mathbb{E}_z \left[ \exp \left( \theta \int_0^{\Delta t} f(z, \tilde{w}_z(s)) ds \right) \right] \end{aligned}$$

where  $\mathbb{E}_z$  is the average over the stationary distribution of the virtual fast process  $\tilde{w}_z$  with  $z$  held fixed. A sufficient condition for  $v$  to be finite is that

$$K = \lim_{\Delta t \rightarrow \infty} \frac{1}{\Delta t} \ln \mathbb{E}_z \left[ \exp \left( \theta \int_0^{\Delta t} f(z, \tilde{w}_z(s)) ds \right) \right] < \infty.$$

We then recognize  $K = H(z, \theta)$ . Using this relation and the definitions of  $K$  and  $\phi$ , we get

$$\lim_{\alpha \rightarrow 0} \alpha \ln u(T, z(T), w(T)) = \phi(T) = \int_0^T H(z(t), \theta(t)) dt$$

and (B.4) is proved.

## B.2 Expansion of the SCGF in powers of $\theta$

In this section we prove (2.30). This relation is a direct consequence of the property of cumulant generating functions,

$$\ln \mathbb{E} [e^x] \simeq \mathbb{E} [x] + \frac{1}{2} \mathbb{E} [x^2 - \mathbb{E} [x]^2] + O(x^3),$$

which can be found expanding  $\exp(x)$  and  $\ln(1+x)$  around  $x=0$ . Applied to the definition of the SCGF for the slow process  $z$  (2.26), this gives

$$\begin{aligned} H(z, \theta) &\simeq \lim_{\Delta t \rightarrow \infty} \frac{1}{\Delta t} \left\{ \theta \mathbb{E}_z \left[ \int_0^{\Delta t} f(z, \tilde{w}_z(s)) ds \right] \right. \\ &\quad \left. - \frac{1}{2} \theta^2 \mathbb{E}_z \left[ \left( \int_0^{\Delta t} f(z, \tilde{w}_z(s)) ds \right)^2 - \mathbb{E}_z \left[ \int_0^{\Delta t} f(z, \tilde{w}_z(s)) ds \right]^2 \right] + O(\theta^3) \right\}. \end{aligned}$$

At first order in  $\theta$ , we have

$$\begin{aligned} \lim_{\Delta t \rightarrow \infty} \frac{1}{\Delta t} \mathbb{E}_z \left[ \int_0^{\Delta t} f(z, \tilde{w}_z(s)) ds \right] &= \lim_{\Delta t \rightarrow \infty} \frac{1}{\Delta t} \int_0^{\Delta t} \mathbb{E}_z [f(z, \tilde{w}_z(s))] ds \\ &= \lim_{\Delta t \rightarrow \infty} \frac{1}{\Delta t} \int_0^{\Delta t} F(z) ds \\ &= F(z). \end{aligned}$$

At second order in  $\theta$ , we have

$$\begin{aligned}
 H_2 &\equiv \mathbb{E}_z \left[ \left( \int_0^{\Delta t} f(z, \tilde{w}_z(s)) \, ds \right)^2 - \mathbb{E}_z \left[ \int_0^{\Delta t} f(z, \tilde{w}_z(s)) \, ds \right]^2 \right] \\
 &= \mathbb{E}_z \left[ \int_0^{\Delta t} f(z, \tilde{w}_z(s)) \, ds \int_0^{\Delta t} f(z, \tilde{w}_z(s')) \, ds' - \left( \int_0^{\Delta t} \mathbb{E}_z [f(z, \tilde{w}_z(s))] \, ds \right)^2 \right] \\
 &= \int_0^{\Delta t} ds \int_0^{\Delta t} ds' \mathbb{E}_z [f(z, \tilde{w}_z(s)) f(z, \tilde{w}_z(s')) - F(z)^2] \\
 &= 2 \int_0^{\Delta t} ds \int_0^s ds' \mathbb{E}_z [f(z, \tilde{w}_z(s)) f(z, \tilde{w}_z(s')) - F(z)^2],
 \end{aligned}$$

where we have used that the integrand is invariant under  $(s, s') \rightarrow (s', s)$ . With the change of variable  $(s, s') \rightarrow (t + \tau, t)$ ,

$$H_2 = 2 \int_0^{\Delta t} dt \int_0^t d\tau \mathbb{E}_z [f(z, \tilde{w}_z(t + \tau)) f(z, \tilde{w}_z(t)) - F(z)^2].$$

Now using the fact that  $\mathbb{E}_z$  is an average over the stationary state of  $\tilde{w}_z$ , we have

$$\mathbb{E}_z [f(z, \tilde{w}_z(t + \tau)) f(z, \tilde{w}_z(t)) - F(z)^2] = \mathbb{E}_z [[f(z, \tilde{w}_z(\tau)) f(z, \tilde{w}_z(0))]] .$$

Assuming that the following limit exists

$$\Xi(z) = 2 \lim_{t \rightarrow \infty} \int_0^t d\tau \mathbb{E}_z [[f(z, \tilde{w}_z(\tau)) f(z, \tilde{w}_z(0))]] ,$$

we get  $H_2 \underset{\Delta t \rightarrow \infty}{\sim} \Delta t \Xi(z)$  so finally

$$\lim_{\Delta t \rightarrow \infty} \frac{1}{\Delta t} \mathbb{E}_z \left[ \left( \int_0^{\Delta t} f(z, \tilde{w}_z(s)) \, ds \right)^2 - \mathbb{E}_z \left[ \int_0^{\Delta t} f(z, \tilde{w}_z(s)) \, ds \right]^2 \right] = \Xi(z).$$

# Appendix C

## Kinetic equation from the generalized LMN hierarchy

### C.1 The LMN hierarchy for the 2D stochastic Euler equation

Consider the 2D stochastic Euler equation

$$\frac{\partial \omega}{\partial t} + \mathbf{v} \cdot \nabla \omega = -\alpha \omega + \sqrt{2\alpha} \eta, \quad (\text{C.1})$$

with  $\eta$  a Gaussian noise with zero mean and correlation

$$\mathbb{E}[\eta(\mathbf{r}_1, t_1) \eta(\mathbf{r}_2, t_2)] = C(\mathbf{r}_1 - \mathbf{r}_2) \delta(t_1 - t_2). \quad (\text{C.2})$$

The generalization to the barotropic equation ( $\beta \neq 0$ ) and to the Navier-Stokes equation ( $\nu \neq 0$ ) would be straightforward, we do not present these generalizations here.

We are interested in the evolution of the  $n$ -points equal-time vorticity distribution, that we will denote for simplicity

$$p_n(1, \dots, n) \equiv p_n(\mathbf{r}_1, \sigma_1, \dots, \mathbf{r}_n, \sigma_n, t) = \mathbb{E}[\delta(\omega(\mathbf{r}_1, t) - \sigma_1) \dots \delta(\omega(\mathbf{r}_n, t) - \sigma_n)]. \quad (\text{C.3})$$

In the inertial limit  $\alpha = 0$ , the derivation of the evolution equation of  $p_n$  is easy [40], it reads

$$\frac{\partial p_n}{\partial t} + NL_n[p_{n+1}] = 0, \quad (\text{C.4})$$

where the local average of the advection term is given by

$$NL_n[p_{n+1}](1, \dots, n) = \sum_{k=1}^n \nabla_{\mathbf{r}_k} \cdot \left[ \int d\mathbf{r} \mathbf{G}(\mathbf{r}_k - \mathbf{r}) \int_{\mathbb{R}} d\sigma \sigma p_{n+1}(1, \dots, n, \mathbf{r}, \sigma) \right], \quad (\text{C.5})$$

with  $\mathbf{G}$  the Green function of the velocity, i.e. such that  $\mathbf{v} = \mathbf{G} * \omega$ . Note that in this case, the average  $\mathbb{E}[\cdot]$  is made over a set of different initial conditions. When  $\alpha \neq 0$ , the evolution equation for  $p_n$  is obtained applying Itô's formula to the function

$$\phi_n(\omega_1, \sigma_1, \dots, \omega_n, \sigma_n) = \delta(\omega_1 - \sigma_1) \dots \delta(\omega_n - \sigma_n), \quad (\text{C.6})$$

where  $\omega_k = \omega(\mathbf{r}_k, t)$ , and averaging. Using  $\frac{\partial \phi_n}{\partial \omega_k} = -\frac{\partial \phi_n}{\partial \sigma_k}$  and  $\omega(\mathbf{r}_k, t)\phi_n = \sigma_k \phi_n$ , we get

$$\frac{\partial p_n}{\partial t} + NL_n [p_{n+1}] = \alpha \sum_{k=1}^n \frac{\partial}{\partial \sigma_k} \left[ \sigma_k p_n + \sum_{l=1}^n C(\mathbf{r}_k - \mathbf{r}_l) \frac{\partial p_n}{\partial \sigma_l} \right]. \quad (\text{C.7})$$

In section C.2, we discuss a special class of solutions of equation (C.4), and the link with the equilibrium statistical mechanics theory of the 2D Euler equation. Then in section C.3, we perform a closure of the hierarchy defined by (C.7) based on the assumption that  $\alpha \ll 1$ .

## C.2 Young measure solution in the inertial limit

We prove here that Young measures form a special class of solutions of (C.4). Young measures are defined by

$$\forall n, \quad p_n(1, \dots, n) = p(1) \dots p(n) \quad (\text{C.8})$$

with  $p \equiv p_1$ . Distributed according to this measure, vorticity values at different points are statistically independent random variables. This means that Young measures represent the mean-field behaviour of the system.

An important consequence is that velocity and vorticity, distributed according to (C.8), are independent random fields. Indeed, using that the velocity Green function  $\mathbf{G}$  is continuous, the velocity field  $\mathbf{v} = \mathbf{G} * \omega$  can be seen as a (weighted) sum of independent random variables. By the Law of Large Numbers, we thus conclude that the distribution of  $\mathbf{v}(\mathbf{r}_1)$  is a delta function centered on the average velocity

$$\bar{\mathbf{v}}(\mathbf{r}_1) \equiv (\mathbf{G} * \bar{\omega})(\mathbf{r}_1) = \int d\mathbf{r} \mathbf{G}(\mathbf{r}_1 - \mathbf{r}) \int_{\mathbb{R}} d\sigma \sigma p(\mathbf{r}, \sigma, t), \quad (\text{C.9})$$

see [15] for a more detailed derivation. This result can be extended to investigate the joint probability distribution of velocity and vorticity, and the result is that velocity and vorticity are independent random fields [15]. As a consequence, the evolution of  $p$  reads

$$\partial_t p + \bar{\mathbf{v}} \cdot \nabla p = 0, \quad (\text{C.10})$$

and equation (C.4) is fulfilled for  $n = 1$ . It is now easy to prove that the Young measure (C.8) is a solution of the whole hierarchy of equations (C.4), using (C.10),

$$\begin{aligned} \partial_t p_n(1, \dots, n) &= \sum_{k=1}^n \partial_t p(k) \prod_{l \neq k} p(l) \\ &= - \sum_{k=1}^n \nabla_{\mathbf{r}_k} \cdot \left[ \int d\mathbf{r} \mathbf{G}(\mathbf{r}_k - \mathbf{r}) \int_{\mathbb{R}} d\sigma \sigma p(k) p(\mathbf{r}, \sigma, t) \right] \prod_{l \neq k} p(l) \\ &= - \sum_{k=1}^n \nabla_{\mathbf{r}_k} \cdot \left[ \int d\mathbf{r} \mathbf{G}(\mathbf{r}_k - \mathbf{r}) \int_{\mathbb{R}} d\sigma \sigma p_{n+1}(1, \dots, n, \mathbf{r}, \sigma, t) \right]. \end{aligned} \quad (\text{C.11})$$

Young measures are of particular importance in the equilibrium statistical mechanics theory of the 2D Euler equation, indeed the microcanonical measure is a Young measure defined by

$$p(\mathbf{r}, \sigma) = \frac{1}{Z(\mathbf{r})} e^{\tilde{\beta} \sigma \bar{\psi}(\mathbf{r}) - \lambda(\sigma)} \quad (\text{C.12})$$

where  $\tilde{\beta}$  and  $\lambda$  are the Lagrange parameters associated with the conservation of energy and vorticity levels distribution,  $\bar{\psi}$  is the average stream function, and  $Z$  is a normalisation constant. More generally, it can be shown that the mean-field approximation is exact for the 2D Euler equation [15], so Young measures are a natural type of measure to describe the statistical mechanics of this system.

### C.3 Comparison with stochastic averaging

In this section we will use brackets to denote the (non-normalized) symmetric part of an expression, for example  $\{f(1, 2)\} = f(1, 2) + f(2, 1)$ .

#### C.3.1 Perturbative expansion in powers of $\alpha$

We have seen in the previous section that when forcing and dissipation vanish, a natural solution of (C.7) is a Young measure (C.8). When forcing and dissipation are small but non-zero ( $0 < \alpha \ll 1$  in (C.1)), we thus consider perturbations of the Young measure solution as

$$p_2(1, 2) = p(1)p(2) + \alpha q_2(1, 2), \quad (\text{C.13})$$

$$p_3(1, 2, 3) = p(1)p(2)p(3) + \alpha \{q_2(1, 2)p(3)\} + \alpha^2 q_3(1, 2, 3), \quad (\text{C.14})$$

and so on. These expressions define the functions  $q_n$ , our assumption in the following is thus that  $q_n = \mathcal{O}(1)$  as  $\alpha \rightarrow 0$ . This type of ansatz has been proposed since the beginning of the study of the LMN hierarchy, using an analogy with the BBGKY hierarchy of the classical kinetic theory of plasmas [63].

The functions  $q_n$  are called the connected parts of the probability distribution functions  $p_n$ . They describe the correction to the equilibrium statistical mechanics theory due to the small forcing and dissipation present in (C.1).

To get the time evolution of  $q_2$ , we will compare  $\partial_t p_2$  computed from (C.13) using (C.7) (for  $n = 1$ ) on one hand and from (C.7) (for  $n = 2$ ) using (C.14) on the other hand. We analyse this computation for each order in  $\alpha$ :

- At order zero in  $\alpha$ , this amounts at checking that the leading order expressions of  $p_2$  and  $p_3$  solve the first two equations of the inertial hierarchy. This is obviously true, as we have seen in section C.2 that Young measures are particular solutions of the inertial LMN hierarchy, which motivated the ansatz (C.13),(C.14).
- The terms of order  $\alpha$  in the time derivative of (C.13) come from two parts, first

$$\{p(2) \cdot \partial_t p(1)\} = \mathcal{O}(1) + \alpha \left\{ -p(2)NL_1[q_2](1) + p(2) \frac{\partial}{\partial \sigma_1} \left[ \sigma_1 p(1) + C(\mathbf{0}) \frac{\partial p(1)}{\partial \sigma_1} \right] \right\},$$

and  $\alpha \partial_t q_2(1, 2)$ . The terms of order  $\alpha$  in (C.7) (for  $n = 2$ ) read

$$\begin{aligned} NL_2[\{q_2(1, 2)p(3)\}](1, 2) &= \sum_{k=1}^2 \nabla_{\mathbf{r}_k} \cdot \left[ \int d\mathbf{r} \mathbf{G}(\mathbf{r}_k - \mathbf{r}) \int d\sigma \sigma \{q_2(1, 2)p(\mathbf{r}, \sigma)\} \right] \\ &= \left\{ \bar{\mathbf{v}}(1) \cdot \nabla_1 q_2(1, 2) + p(2) NL_1[q_2](1) \right. \\ &\quad \left. + \int d\mathbf{r} \mathbf{G}(\mathbf{r}_1 - \mathbf{r}) \int d\sigma \sigma q_2(2, \mathbf{r}, \sigma) \cdot \nabla_1 p(1) \right\} \end{aligned}$$

for the advection part and

$$\begin{aligned} &\sum_{k=1}^2 \frac{\partial}{\partial \sigma_k} \left[ \sigma_k p(1)p(2) + \sum_{l=1}^2 C(\mathbf{r}_k - \mathbf{r}_l) \frac{\partial}{\partial \sigma_l} p(1)p(2) \right] \\ &= \left\{ p(2) \frac{\partial}{\partial \sigma_1} \left[ \sigma_1 p(1) + C(0) \frac{\partial p(1)}{\partial \sigma_1} \right] \right\} + 2C(1, 2) \frac{\partial p(1)}{\partial \sigma_1} \frac{\partial p(2)}{\partial \sigma_2} \end{aligned}$$

for the dissipation and forcing part.

- The terms of order  $\alpha^2$  in (C.7) (for  $n = 2$ ) are  $NL_2[q_3]$  and the dissipation and forcing term

$$\sum_{k=1}^2 \frac{\partial}{\partial \sigma_k} \left[ \sigma_k q_2 + \sum_{l=1}^2 C(\mathbf{r}_k - \mathbf{r}_l) \frac{\partial q_2}{\partial \sigma_l} \right].$$

Finally, the evolution equation of  $q_2$  reads

$$\begin{aligned} \partial_t q_2 &= - \left\{ \bar{\mathbf{v}}(1) \cdot \nabla_1 q_2(1, 2) + \int d\mathbf{r} \mathbf{G}(\mathbf{r}_1 - \mathbf{r}) \int d\sigma \sigma q_2(2, \mathbf{r}) \cdot \nabla_1 p(1) \right\} \\ &\quad + 2C(1, 2) \frac{\partial p(1)}{\partial \sigma_1} \frac{\partial p(2)}{\partial \sigma_2} - \alpha NL_2[q_3] + \alpha \sum_{k=1}^2 \frac{\partial}{\partial \sigma_k} \left[ \sigma_k q_2 + \sum_{l=1}^2 C(\mathbf{r}_k - \mathbf{r}_l) \frac{\partial q_2}{\partial \sigma_l} \right]. \end{aligned} \quad (\text{C.15})$$

This equation still involves  $q_3$ . Our closure in the hierarchy consists in neglecting terms of order  $\alpha$  in (C.15). The truncated hierarchy is thus made of equation (C.7) for  $n = 1$ ,

$$\partial_t p + \bar{\mathbf{v}} \cdot \nabla p + \alpha NL_1[q_2] = \alpha \frac{\partial}{\partial \sigma} \left[ \sigma p + C(\mathbf{0}) \frac{\partial p}{\partial \sigma} \right]. \quad (\text{C.16})$$

and of

$$\begin{aligned} \partial_t q_2 &= - \left\{ \bar{\mathbf{v}}(1) \cdot \nabla_1 q_2(1, 2) + \int d\mathbf{r} \mathbf{G}(\mathbf{r}_1 - \mathbf{r}) \int d\sigma \sigma q_2(2, \mathbf{r}) \cdot \nabla_1 p(1) \right\} \\ &\quad + 2C(1, 2) \frac{\partial p(1)}{\partial \sigma_1} \frac{\partial p(2)}{\partial \sigma_2} \end{aligned} \quad (\text{C.17})$$

The system (C.17), (C.16) is a closed set of equations. It describes the leading order correction to the equilibrium statistical mechanics theory of the inertial 2D Euler equation (Young measure). In this sense, it should be equivalent to the leading order result we obtained using stochastic averaging. To observe this equivalence, we derive the evolution equations for the average and the two-points correlation function.

$$\bar{\omega}(\mathbf{r}_1, t) = \mathbb{E}[\omega(\mathbf{r}_1, t)] = \int d\sigma_1 \sigma_1 p(\mathbf{r}_1, \sigma_1, t), \quad (\text{C.18})$$

$$\tilde{g}(\mathbf{r}_1, \mathbf{r}_2, t) \equiv \mathbb{E} [\omega(\mathbf{r}_1, t)\omega(\mathbf{r}_2, t)] = \int d\sigma_1 d\sigma_2 \sigma_1 \sigma_2 p_2(1, 2) = \bar{\omega}(\mathbf{r}_1, t)\bar{\omega}(\mathbf{r}_2, t) + \alpha g(\mathbf{r}_1, \mathbf{r}_2, t), \quad (\text{C.19})$$

with  $g(\mathbf{r}_1, \mathbf{r}_2, t) \equiv \int d\sigma_1 d\sigma_2 \sigma_1 \sigma_2 q_2(1, 2)$ . For  $\bar{\omega}$ , we get

$$\partial_t \bar{\omega} + \bar{\mathbf{v}} \cdot \nabla \bar{\omega} + \alpha \int d\mathbf{r} \mathbf{G}(\mathbf{r}_1 - \mathbf{r}) \cdot \nabla_{\mathbf{r}_1} g(\mathbf{r}_1, \mathbf{r}, t) = -\alpha \bar{\omega}. \quad (\text{C.20})$$

For  $g$ , we get

$$\partial_t g + \left( L_{\bar{\omega}}^{0(1)} + L_{\bar{\omega}}^{0(2)} \right) g = 2C \quad (\text{C.21})$$

with

$$L_{\bar{\omega}}^0 [f](\mathbf{r}_1) \equiv \bar{\mathbf{v}}(\mathbf{r}_1) \cdot \nabla_{\mathbf{r}_1} f(\mathbf{r}_1) + \int d\mathbf{r} \mathbf{G}(\mathbf{r}_1 - \mathbf{r}) f(\mathbf{r}) \cdot \nabla_{\mathbf{r}_1} \bar{\omega}(\mathbf{r}_1), \quad (\text{C.22})$$

and where  $L_{\bar{\omega}}^{0(k)}$  is the operator  $L_{\bar{\omega}}^0$  acting on the variable  $\mathbf{r}_k$ . We recognize in (C.21) the Lyapunov equation associated with the Ornstein-Uhlenbeck process

$$\partial_t \omega + L_{\bar{\omega}}^0[\omega] = \sqrt{2}\eta, \quad (\text{C.23})$$

with the same noise  $\eta$  as in the original equation (C.1). Moreover, the last term in the left-hand side of (C.20) is exactly the Reynolds forcing associated with the two-points correlation function  $g$ , acting on the mean flow  $\bar{\omega}$ . The leading order correction to the mean-field behaviour is thus described by a quasi-linear approximation of the dynamics, like in the stochastic averaging approach. If we assume that the mean flow is a steady state of the Euler equation, the non-linear term  $\bar{\mathbf{v}} \cdot \nabla \bar{\omega}$  in (C.20) vanishes. Then the dynamics of  $\bar{\omega}$  occurs on a time scale of order  $1/\alpha$ , while the time scale of evolution of  $g$  is of order 1, consistently with the time scale separation used for the stochastic averaging procedure.

### C.3.2 The case of a zonal jet

To understand more precisely the analogy between the two approaches, let's now consider the case where the mean flow is a parallel flow in the  $x$  direction,  $\bar{\mathbf{v}}(\mathbf{r}) = \bar{U}(y)\mathbf{e}_x$ . Then the advection term  $\bar{\mathbf{v}} \cdot \nabla \bar{\omega}$  in (C.20) vanishes, and the linear operator  $L_{\bar{\omega}}^0$  in the Lyapunov equation (C.21) reads

$$L_{\bar{U}}^0 [f](\mathbf{r}_1) = \bar{U}(y_1) \cdot \partial_{x_1} f(\mathbf{r}_1) - \bar{U}''(y_1) \cdot \partial_{x_1} \Delta^{-1} f(\mathbf{r}_1), \quad (\text{C.24})$$

where we have used the incompressibility of the flow under the form  $G_y = \partial_x H$  with  $H$  the Green function of the Laplacian.

We now have to prove (i) that only the non-zonal degrees of freedom contribute to the Reynolds forcing in (C.20) and (ii) that the zonal jet solution is consistent in time evolution, i.e. if  $\bar{\omega}(\mathbf{r}, t = 0) = \bar{\omega}(y, 0)$  then  $\bar{\omega}(\mathbf{r}, t) = \bar{\omega}(y, t)$  for all  $t \geq 0$ . We decompose the forcing and the two-points correlation function into zonal and non-zonal parts,  $C = C_z + C_m$  and  $g = g_z + g_m$  with the zonal projection operator

$$h_z(y_1, y_2) \equiv \langle h(\mathbf{r}_1, \mathbf{r}_2) \rangle \equiv \int \frac{dx_1}{2\pi l_x} \frac{dx_2}{2\pi l_x} h(\mathbf{r}_1, \mathbf{r}_2). \quad (\text{C.25})$$

Using that  $L_{\bar{U}}^0[f](\mathbf{r}_1)$  in (C.24) is the derivative with respect to  $x_1$  of a periodic function, we have  $\langle L_{\bar{U}}^0[f] \rangle = 0$ , so the projected Lyapunov equations read

$$\partial_t g_z = 2C_z, \quad (\text{C.26})$$

$$\partial_t g_m + \left( L_{\bar{U}}^{0(1)} + L_{\bar{U}}^{0(2)} \right) g_m = 2C_m. \quad (\text{C.27})$$

The contribution of  $g_z$  in the mean flow equation is zero:

$$\int d\mathbf{r} \mathbf{G}(\mathbf{r}_1 - \mathbf{r}) \cdot \nabla_{\mathbf{r}_1} g_z(y_1, y) = - \int d\mathbf{r} \partial_x [H(\mathbf{r}_1 - \mathbf{r})] \partial_{y_1} g_z(y_1, y) = 0, \quad (\text{C.28})$$

so the zonal part of the forcing  $C_z$  doesn't contribute to the evolution of the mean flow  $\bar{\omega}$ . Note that if the forcing is invariant under translations in the zonal direction, then the two-points correlation function  $g_m$  is also invariant under zonal translations. Then, the Reynolds forcing in (C.20) reads

$$\int d\mathbf{r} \mathbf{G}(\mathbf{r}_1 - \mathbf{r}) \cdot [\nabla_{\mathbf{r}_1} g_m](x_1 - x, y_1, y) = \int d\mathbf{r} \mathbf{G}(\mathbf{r}) \cdot [\nabla_{\mathbf{r}_1} g_m](x, y_1, y_1 - y), \quad (\text{C.29})$$

which does not depend on the zonal coordinate  $x_1$ . This means that an initially parallel mean flow remains parallel as time goes on. We have thus proved (i) and (ii).

The resulting equations

$$\partial_t \bar{\omega}(y_1, t) + \alpha \int d\mathbf{r} \mathbf{G}(\mathbf{r}) \cdot [\nabla_{\mathbf{r}_1} g_m](x, y_1, y_1 - y) = -\alpha \bar{\omega}(y_1, t), \quad (\text{C.30})$$

together with (C.27) thus form a closed system of equations that describe the evolution of the jet at leading order in  $\alpha$ . As explained in the end of the previous section, when  $\alpha \ll 1$  the time scale of evolution of  $\bar{\omega}$  is much larger than the time scale of evolution of  $g_m$ . Then, one can consider that  $g_m$  in (C.30) can be replaced by its stationary value, given by (C.27) with  $\bar{\omega}$  held fixed.

### C.3.3 Discussion

When  $C_z = 0$ , the system (C.27), (C.30) describes the evolution of the average zonal jet  $\bar{U}(y, t)$  where the perturbation flow evolves according to the linearized equation close to the fixed background flow  $\bar{U}$ . On the other hand, when  $C_z \neq 0$ , the kinetic equation obtained through stochastic averaging describes the quasi-linear evolution of a *non-fluctuating* zonal jet  $U$ . Then  $U = \bar{U}$ , we can say that the stochastic averaging and the perturbative expansion of the LMN hierarchy are equivalent at first order in  $\alpha$ .

When  $C_z \neq 0$ , the stochastic noise directly affects the evolution of the zonal degrees of freedom. Then, the zonal jet  $U$  described by the kinetic equation fluctuates, and these fluctuations lead to fluctuations of the two-points correlation function of the non-zonal fields. This effect is not reproduced by the truncated LMN hierarchy approach. This is due to the fact that the  $n$ -points vorticity distribution functions contain the information of moments up to order  $n$ , while the functional PDF used in stochastic averaging contains all the information about the fluctuations of the fields. Moreover, equation (C.26) does not admit a stationary solution for  $C_z \neq 0$ ,

which means that the connected part of the two-points vorticity distribution  $q_2$  is not well-defined.

This case illustrates one of the weaknesses of this approach: we have made the assumption that the connected parts  $q_n$  remain of order 1 as  $\alpha \rightarrow 0$ , but there is no proof of the self-consistency of this assumption. To prevent the blowing out of  $g_z$ , one could find a way to keep some dissipation in the equation for  $q_2$ , like in the stochastic averaging procedure. This would require another ansatz for the perturbative expansion of the hierarchy, and another way to truncate it. The arbitrariness of the truncation is the other main weakness of this approach. Indeed, there exist many ways to truncate the hierarchy [71], probably leading to different effective equations.

# Appendix D

## Convergence of the vorticity auto-correlation function to a distribution

In this appendix we study the convergence properties in the limit  $\alpha \rightarrow 0$  of the vorticity stationary auto-correlation function

$$g^\alpha kl(\mathbf{r}_1, \mathbf{r}_2) = \frac{1}{2} e^{ik(x_1 - x_2)} \mathbb{E}_U^\alpha [\omega_{kl}(y_1) \omega_{kl}^*(y_2)] + \text{c.c.}$$

where  $\omega_{kl}$  is the Ornstein-Uhlenbeck process

$$\frac{\partial \omega_{kl}}{\partial t} + L_{U,k}^0 [\omega_{kl}] = -\alpha \omega_{kl} + \sqrt{2} e^{ily} \eta_{kl},$$

with the inertial linear operator  $L_{U,k}^0 [\omega] = ikU\omega - ikU'' \Delta_k^{-1} \omega$ . For simplicity in the notations we will drop the indices  $k, l$ , and denote  $g = g^\alpha$ .

We will use an expression of  $g$  that is slightly different from (4.16) given in section 4.2.2. The stochastic equation for  $\omega$  can be solved as

$$\omega(y, t) = \sqrt{2} \int_0^t \tilde{\omega}(y, t_1) e^{-\alpha t_1} dW(t_1),$$

where  $\tilde{\omega}$  is the solution of the deterministic equation  $\partial_t \tilde{\omega} + L_{U,k}^0 [\tilde{\omega}] = 0$  with initial condition  $\tilde{\omega}(y, 0) = e^{ily}$ . Then,

$$g(\mathbf{r}_1, \mathbf{r}_2) = e^{ik(x_1 - x_2)} \tilde{g}(y_1, y_2) + \text{c.c.}$$

with

$$\tilde{g}(y_1, y_2) = \int_0^\infty \tilde{\omega}(y_1, t_1) \tilde{\omega}^*(y_2, t_1) e^{-2\alpha t_1} dt_1. \quad (\text{D.1})$$

In section D.1 we present the Sokhotskyi–Plemelj formula, that will be useful in the following. In section D.2 we present a more complete version of the Orr mechanism for  $\tilde{\omega}$ . Then in section D.3 we prove that (D.1) converges to a distribution in the limit  $\alpha \rightarrow 0$ .

## D.1 Sokhotskyi–Plemelj formula

The Sokhotskyi–Plemelj formula (Plemelj formula in the following) adapted to our notations is

$$\int_0^\infty e^{-ity} dt = \lim_{\lambda \rightarrow 0^+} \frac{-i}{y - i\lambda} = \pi\delta(y) - iPV\left(\frac{1}{y}\right), \quad (\text{D.2})$$

where  $PV$  is the Cauchy Principal Value distribution.

### D.1.1 Regularization due to a small linear friction

We consider the following function for some  $\lambda > 0$

$$F_\lambda(y) = \frac{-i}{y - i\lambda} = \frac{\lambda}{y^2 + \lambda^2} - i\frac{y}{y^2 + \lambda^2}$$

where the real part of  $F_\lambda$  is even while the imaginary part is odd. From (D.2), the real part of  $F_\lambda$  is a regularization of  $\pi\delta(y)$ ,

$$\lim_{\lambda \rightarrow 0^+} \text{Re}[F_\lambda(y)] = \lim_{\lambda \rightarrow 0^+} \frac{\lambda}{y^2 + \lambda^2} = \pi\delta(y),$$

and the imaginary part of  $F_\lambda$  is a regularization of  $-PV(1/y)$ ,

$$\lim_{\lambda \rightarrow 0^+} \text{Im}[F_\lambda(y)] = -\lim_{\alpha \rightarrow 0} \frac{y}{y^2 + \lambda^2} = -PV\left(\frac{1}{y}\right).$$

We note that for a fixed  $y > 0$ ,  $\lim_{\lambda \rightarrow 0^+} \text{Re}[F_\lambda(y)] = 0$ , and  $\lim_{\lambda \rightarrow 0^+} \text{Im}[F_\lambda(y)] = 1/y$ .

### D.1.2 Expressions of the Cauchy Principal Value distribution

By definition,

$$\int^* \frac{f(y)}{y} dy \equiv \int PV\left(\frac{1}{y}\right) f(y) dy \equiv \lim_{\epsilon \rightarrow 0^+} \left[ \int_{-\infty}^{-\epsilon} + \int_{\epsilon}^{+\infty} \right] \frac{f(y)}{y} dy.$$

Using  $\int^* dy/y = 0$ , we get

$$\int^* \frac{f(y)}{y} dy = \int \frac{f(y) - f(0)}{y} dy, \quad (\text{D.3})$$

where the integral on the right-hand side is now a usual Riemann integral if  $f$  is continuous at  $y = 0$ . All these formulas are easily generalizable to the case of a singularity around  $y_0 \neq 0$  by a change of variable.

## D.2 Resolvent of the linearized Euler operator

The Laplace transform of the vorticity is defined by<sup>1</sup>

$$\hat{\omega}(y, c + i\epsilon) = \int_0^\infty dt \tilde{\omega}(y, t) e^{ik(c+i\epsilon)t}. \quad (\text{D.4})$$

---

<sup>1</sup>This definition of the Laplace transform differs from the one used in appendix A by a change of variable.

The inverse Laplace transform is then given by

$$\tilde{\omega}(y, t) = \frac{|k|}{2\pi} \lim_{\epsilon \rightarrow 0^+} \int_{-\infty}^{\infty} dc \hat{\omega}(y, c + i\epsilon) e^{-ikct}. \quad (\text{D.5})$$

It is also useful to define the Laplace transform of the stream function  $\phi \equiv \hat{\psi}$ ; this quantity is usually referred in literature as the resolvent of the operator  $L_{U,k}$ . It is related to  $\hat{\omega}$  through  $\hat{\omega}(y, c + i\epsilon) = \left(\frac{d^2}{dy^2} - k^2\right) \phi(y, c + i\epsilon)$  and is the solution of the linear ordinary differential equation

$$\left(\frac{d^2}{dy^2} - k^2\right) \phi - \frac{U''(y)}{U(y) - c - i\epsilon} \phi = \frac{e^{ily}}{ik(U(y) - c - i\epsilon)}. \quad (\text{D.6})$$

The homogeneous part of this equation (with zero right-hand side) is known as the Rayleigh equation [35]. For all  $\epsilon > 0$ , this equation is a regular ODE. When  $\epsilon \rightarrow 0^+$ , this equation becomes singular at the critical layer  $c = U(y)$ . It can be shown that  $\phi(y, c + i\epsilon) \rightarrow \phi_+(y, c)$  as  $\epsilon \rightarrow 0^+$ , where  $\phi_+$  is continuous over  $c \in \mathbb{R}$ , with either a logarithmic singularity in its first derivative with respect to  $c$  if  $U'(y) \neq 0$ , or a logarithmic singularity in its second derivative if  $U'(y) = 0$  [11]. We will first consider the case  $U'(y) \neq 0$ . Then we can write, for all  $c$ ,

$$\phi_+(y, c) = \phi_2(y, c) \cdot (U(y) - c) \ln |U(y) - c| + \phi_1(y, c), \quad (\text{D.7})$$

where  $\phi_1, \phi_2$  are analytic functions of  $c$  [11].

Using (D.5), (D.6) and Plemelj formula (D.2) to evaluate the limit  $\epsilon \rightarrow 0^+$ , we get

$$\tilde{\omega}(y, t_1) = \tilde{\omega}^\infty(y) e^{-ikU(y)t_1} + \int^* \frac{dc}{2\pi i} \frac{ikU''(y)\phi_+(y, c) + e^{ily}}{U(y) - c} e^{-ikct}, \quad (\text{D.8})$$

where

$$\tilde{\omega}^\infty(y) = ikU''(y)\phi_+(y, U(y)) + e^{ily}, \quad (\text{D.9})$$

and where we recall that  $\int^*$  denotes the Cauchy Principal Value of the integral.

The first term is the classical Orr mechanism (4.20), the second term decays for large  $t_1$  as  $1/t_1^\gamma$ , where  $\gamma > 0$  depends on the order of differentiability of  $c \rightarrow \phi_+(y, c)$ . Then, as  $c \rightarrow \phi_+(y, c)$  is smoother at points  $y$  such that  $U'(y) = 0$  than at points such that  $U'(y) \neq 0$ , we can focus on the latter case.

## D.3 Proof of the convergence

### D.3.1 Points such that $U(y_1) = U(y_2)$

The Orr mechanism (D.8) can be written  $\tilde{\omega}(y, t_1) = \tilde{\omega}^\infty(y) e^{-ikU(y)t_1} + \tilde{\omega}^r(y, t_1)$  where  $\tilde{\omega}^r(y, t_1) = O(t_1^{-\gamma})$  as  $t_1 \rightarrow \infty$ , with  $\gamma > 0$ . Using this expression of the deterministic vorticity and (D.1), we get

$$\tilde{g}(y_1, y_2) = \frac{\tilde{\omega}^\infty(y_1)\tilde{\omega}^{\infty*}(y_2)}{ik(U(y_1) - U(y_2)) + 2\alpha} + \tilde{g}^r(y_1, y_2),$$

where  $\tilde{g}^r$  contains the corrections involving  $\tilde{\omega}^r$ . From Plemelj formula (D.2), the first term converges to a distribution in the limit  $\alpha \rightarrow 0^+$ , as described in section 5.1.1. In particular, it diverges point-wise as  $1/\alpha$  at points such that  $U(y_1) = U(y_2)$ . We now prove that the remainder  $\tilde{g}^r$  is negligible compared to this  $1/\alpha$  divergence at such points.

The most divergent part of  $\tilde{g}^r$  is of the form  $G_\alpha = \int_0^\infty f(t) dt$  where  $f$  is bounded and  $f(t) = O(e^{-2\alpha t} t^{-\gamma})$  as  $t \rightarrow \infty$ . The behaviour for small  $\alpha$  of  $G_\alpha$  depends on the value of  $\gamma$ .

- if  $\gamma < 1$ , there exists some  $K > 0$  such that

$$|G_\alpha| \leq K \int_0^\infty \frac{e^{-2\alpha t}}{t^\gamma} dt,$$

which is finite for all  $\alpha > 0$  because the integrand is integrable close to  $t = 0$ . With the change of variable  $u = \alpha t$ , we get  $|G_\alpha| \leq K' \alpha^{\gamma-1}$  with  $K' = K \int_0^\infty e^{-2u} u^{-\gamma} du$ .

- if  $\gamma = 1$ , taking the derivative with respect to  $\alpha$  and with the change of variable  $u = \alpha t$  we get

$$\frac{\partial G_\alpha}{\partial \alpha} = \frac{1}{\alpha} \int_0^\infty e^{-2u} g\left(\frac{u}{\alpha}\right) du$$

with a bounded function  $g$  such that  $g(t) = O(1)$  as  $t \rightarrow \infty$ . By the theorem of dominated convergence,

$$\int_0^\infty e^{-2u} g\left(\frac{u}{\alpha}\right) du \xrightarrow{\alpha \rightarrow 0} K'' \equiv \int_0^\infty e^{-2u} \lim_{\infty} g du,$$

so by integration  $G_\alpha \sim -K'' \ln \alpha$ .

- if  $\gamma > 1$  we directly have  $G_\alpha \rightarrow G_0 < \infty$  as  $\alpha \rightarrow 0$  by the theorem of dominated convergence.

In all three cases,  $G_\alpha$  is negligible with respect to  $1/\alpha$  as  $\alpha \rightarrow 0$ . We conclude that  $\tilde{g}^r(y_1, y_2)$  is negligible with respect to the  $1/\alpha$  divergence of  $\tilde{g}(y_1, y_2)$  at points such that  $U(y_1) = U(y_2)$ .

At points such that  $U(y_1) \neq U(y_2)$ , the first term in the expression of  $\tilde{g}(y_1, y_2)$  converges to a finite value, so we need to prove that  $\tilde{g}^r(y_1, y_2)$  also converges. This is done in next paragraph.

### D.3.2 Points such that $U(y_1) \neq U(y_2)$

Using (D.1), (D.5) and (D.6) we get

$$\tilde{g}(y_1, y_2) = \lim_{\epsilon_1, \epsilon_2 \rightarrow 0^+} \int \frac{dc_1}{2\pi} \frac{dc_2}{2\pi} \hat{\omega}(y_1, c_1 + i\epsilon_1) (\hat{\omega}(y_2, c_2 + i\epsilon_2))^* \frac{1}{ik(c_1 - c_2) + 2\alpha} \quad (\text{D.10})$$

with  $\hat{\omega}(y, c + i\epsilon) = \frac{ikU''(y)\phi(y, c+i\epsilon)+e^{iy}}{U(y)-c-i\epsilon}$ . We easily realize that the infinite bounds of this double integral are not sources of divergence. The only possible sources of divergence come from the critical layers  $c = U(y)$  when  $\alpha \rightarrow 0^+$ . When  $U(y_1) =$

$U(y_2)$ , we know that  $\tilde{g}$  is equivalent to  $1/\alpha$  as  $\alpha \rightarrow 0$ . We now consider the case  $U(y_1) \neq U(y_2)$ .

Consider a fixed  $\alpha > 0$ ,  $\tilde{g}$  is of the form

$$I_\alpha = \lim_{\epsilon_1 \rightarrow 0^+} \int dx_1 \frac{f_1(x_1)}{x_1 - a_1 - i\epsilon_1} \lim_{\epsilon_2 \rightarrow 0^+} \int dx_2 \frac{f_2(x_2)}{x_2 - a_2 - i\epsilon_2} \frac{1}{x_1 - x_2 - i\alpha},$$

where the functions  $x \rightarrow f_k(x)$  are continuous with a logarithmic singularity in their first derivative at  $x = a_k$ . We also assume that  $a_1 \neq a_2$ . Using Plemelj formula (D.2) to estimate successively the limits  $\epsilon_2 \rightarrow 0^+$  and  $\epsilon_1 \rightarrow 0^+$ , we get

$$\begin{aligned} I_\alpha &= \frac{\pi^2 f_1(a_1) f_2(a_2)}{a_1 - a_2 - i\alpha} - i\pi f_2(a_2) \int^* dx_1 \frac{f_1(x_1)}{x_1 - a_1} \frac{1}{x_1 - a_2 - i\alpha} \\ &\quad - i\pi f_1(a_1) \int^* dx_2 \frac{f_2(x_2)}{x_2 - a_2} \frac{1}{a_1 - x_2 - i\alpha} \\ &\quad - \int^* dx_1 \frac{f_1(x_1)}{x_1 - a_1} \int^* dx_2 \frac{f_2(x_2)}{x_2 - a_2} \frac{1}{x_1 - x_2 - i\alpha}, \end{aligned} \quad (\text{D.11})$$

where all the principal value integrals are finite because  $f_1$  and  $f_2$  are continuous, and because  $\alpha > 0$ . We now study the convergence of each term as  $\alpha \rightarrow 0^+$ .

- The first term  $\frac{\pi^2 f_1(a_1) f_2(a_2)}{a_1 - a_2 - i\alpha}$  converges to  $\frac{\pi^2 f_1(a_1) f_2(a_2)}{a_1 - a_2}$ , which is finite for  $a_1 \neq a_2$ . This term corresponds to the most divergent part when  $a_1 = a_2$  (or  $U(y_1) = U(y_2)$  in  $\tilde{g}$ ). It also means that the convergence of the remaining terms in (D.11) depends directly on the value of  $\gamma$  in the Orr mechanism, or equivalently on the regularity of the resolvent  $c \rightarrow \phi_+(y, c)$ .
- For the second term, Plemelj formula (D.2) can be applied to estimate the limit  $\alpha \rightarrow 0^+$  because the singularities at  $x_1 = a_1$  and  $x_1 = a_2$  are not confounded:

$$\int^* dx_1 \frac{f_1(x_1)}{x_1 - a_1} \frac{1}{x_1 - a_2 - i\alpha} \xrightarrow{\alpha \rightarrow 0^+} \pi \frac{f_1(a_2)}{a_2 - a_1} - i \int^* dx_1 \frac{f_1(x_1)}{(x_1 - a_1)(x_1 - a_2)}$$

The same result applies to the third term.

- For the last term, let's consider the function

$$J(x_1) = \lim_{\alpha \rightarrow 0^+} \int^* dx_2 \frac{f_2(x_2)}{x_2 - a_2} \frac{1}{x_1 - x_2 - i\alpha}.$$

At any point such that  $x_1 \neq a_2$ , this can be estimated using Plemelj formula (D.2),

$$J(x_1) = \frac{\pi f_2(x_1)}{x_1 - a_2} - i \int^* dx_2 \frac{f_2(x_2)}{(x_2 - a_2)(x_1 - x_2)},$$

where both terms are finite because  $x_1 \neq a_2$ . To estimate the limit at the point  $x_1 = a_2$ , we first use (D.3),

$$J(a_2) = \lim_{\alpha \rightarrow 0^+} \int dx_2 \frac{1}{x_2 - a_2} \left( \frac{f_2(x_2)}{a_2 - x_2 - i\alpha} - \frac{f_2(a_2)}{-i\alpha} \right)$$

and the expression of the resolvent (D.7), here  $f_2(x_2) = g(x_2)(x_2 - a_2) \ln |x_2 - a_2| + h(x_2)$ , where  $g$  and  $h$  are analytic functions,

$$J(a_2) = - \lim_{\alpha \rightarrow 0^+} \left[ \int dx_2 \frac{g(x_2) \ln |x_2 - a_2|}{x_2 - a_2 + i\alpha} + \int^* dx_2 \frac{h(x_2)}{x_2 - a_2} \frac{1}{x_2 - a_2 + i\alpha} \right], \quad (\text{D.12})$$

where we have used again (D.3) in order to express the second integral as a Principal Value. The first term in the brackets finite for all  $\alpha > 0$  because  $x \rightarrow \ln x$  is integrable around  $x = 0$ . This term converges in the limit  $\alpha \rightarrow 0$ :

$$\begin{aligned} \int dx_2 \frac{g(x_2) \ln |x_2 - a_2|}{x_2 - a_2 + i\alpha} &\underset{\alpha \rightarrow 0^+}{\sim} \int dx_2 \frac{g(x_2) \ln |x_2 - a_2 + i\alpha|}{x_2 - a_2 + i\alpha} \\ &= \int dx_2 g(x_2) \frac{1}{2} \frac{d}{dx_2} \ln^2 |x_2 - a_2 + i\alpha| \\ &= -\frac{1}{2} \int dx_2 g'(x_2) \ln^2 |x_2 - a_2 + i\alpha| \\ &\xrightarrow{\alpha \rightarrow 0^+} -\frac{1}{2} \int dx_2 g'(x_2) \ln^2 |x_2 - a_2|, \end{aligned}$$

where the first and last equivalents follow from continuity of  $z \rightarrow \ln |z|$ . This expression is finite because  $g$  is analytic and  $x \rightarrow \ln^2(x)$  is integrable around  $x = 0$ . In the second term in (D.12), we use that  $h$  can be expanded in its Taylor series,  $h(x_2) = h_0 + h_1(x_2 - a_2) + o(x_2 - a_2)$ , so

$$\int^* dx_2 \frac{h(x_2)}{x_2 - a_2} \frac{1}{x_2 - a_2 + i\alpha} = \int^* dx_2 \frac{h_0}{x_2 - a_2} \frac{1}{x_2 - a_2 + i\alpha} + \int dx_2 \frac{h_1 + o(1)}{x_2 - a_2 + i\alpha},$$

where the last integral is now a usual Riemann integral because the divergence has been cancelled. The term involving  $h_0$  can be computed explicitly for any  $\alpha > 0$ ,

$$\int^* dx_2 \frac{1}{x_2 - a_2} \frac{1}{x_2 - a_2 + i\alpha} = \frac{1}{i\alpha} \lim_{\epsilon \rightarrow 0^+} [\ln |x_2 - a_2 + i\alpha| - \ln |x_2 - a_2|]_{a_2 + \epsilon}^{a_2 - \epsilon} = 0.$$

Then,

$$\int^* dx_2 \frac{h(x_2)}{x_2 - a_2} \frac{1}{x_2 - a_2 + i\alpha} = \int dx_2 \frac{h(x_2) - h(a_2)}{x_2 - a_2 + i\alpha} \xrightarrow{\alpha \rightarrow 0^+} \int dx_2 \frac{h(x_2) - h(a_2)}{x_2 - a_2},$$

which is finite. We conclude that  $J(x_1)$  is a finite quantity for all  $x_1$ , and is continuous at  $x_1 = a_1 \neq a_2$ . Then,

$$\lim_{\alpha \rightarrow 0^+} \int^* dx_1 \frac{f_1(x_1)}{x_1 - a_1} \int^* dx_2 \frac{f_2(x_2)}{x_2 - a_2} \frac{1}{x_1 - x_2 - i\alpha} = \int^* dx_1 \frac{f_1(x_1)}{x_1 - a_1} J(x_1),$$

which is finite.

We conclude that  $I_\alpha$  has a finite limit for  $\alpha \rightarrow 0^+$ , so  $\tilde{g}(y_1, y_2)$  is finite for all points such that  $U(y_1) \neq U(y_2)$ .

# Appendix E

## Algorithms to compute the average Reynolds' forcing

### E.1 Integral Lyapunov equation

By definition, the stationary vorticity autocorrelation function  $\tilde{g}_{kl}^\infty(y_1, y_2) \equiv \mathbb{E}_U^\alpha [\omega_{kl}(y_1)\omega_{kl}^*(y_2)]$  is the solution of the stationary Lyapunov equation (here with friction and no viscosity)

$$\left( L_{U,k}^{(1)} + L_{U,-k}^{(2)} \right) \tilde{g}_{kl}^\alpha = e^{il(y_1 - y_2)} \quad (\text{E.1})$$

where

$$L_{U,k} = ikU - ik(U'' - \beta)\Delta_k^{-1} + \alpha,$$

and where  $L_{U,k}^{(j)}$  is the operator applied to the variable  $y_j$ . We define  $h_{kl}^\alpha(y_1, y_2) \equiv \mathbb{E}_U^\alpha [\omega_{kl}(y_1)\psi_{kl}^*(y_2)]$ , such that  $\tilde{g}_{kl}^\alpha = \Delta_k^{(2)} h_{kl}^\alpha$ , where  $\Delta_k^{(2)}$  is the Laplacian operator with respect to the second variable. Using (4.25), the average Reynolds' forcing can be directly computed from  $h_{kl}^\alpha$ , with

$$f_{kl}^\alpha(y) = 2k\pi l_x \text{Im} [h_{kl}^\alpha(y, y)].$$

In terms of  $h_{kl}^\alpha$ , the stationary Lyapunov equation (E.1) becomes

$$\Delta_k^{(2)} h_{kl}^\alpha(y_1, y_2) = \frac{ik(U''(y_1) - \beta)(h_{kl}^\alpha)^*(y_2, y_1) - ik(U''(y_2) - \beta)h_{kl}^\alpha(y_1, y_2) + e^{il(y_1 - y_2)}}{ik(U(y_1) - U(y_2)) + 2\alpha}. \quad (\text{E.2})$$

We note that this equation is not a differential equation for  $h_{kl}^\alpha(y_1, y_2)$  for each  $y_1$  fixed, as it involves  $(h_{kl}^\alpha)^*(y_2, y_1)$ .

In section 5.1, we have shown that  $\tilde{g}_{kl}^\alpha = \Delta_k^{(2)} h_{kl}^\alpha$  diverge point-wise for  $U(y_1) = U(y_2)$  in the limit  $\alpha \rightarrow 0$ . This is related to the vanishing of the denominator for  $\alpha = 0$  and  $U(y_1) = U(y_2)$  in equation (E.2). On the other hand, it can be proved, with a very similar reasoning to the one used in section 5.1.1 for the velocity auto-correlation function  $E_{kl}$ , that  $h_{kl}^\alpha$  is well-defined as a function, even in the limit  $\alpha \rightarrow 0$ . Thus, we chose to turn (E.2) to an integral equation. Inverting the Laplacian operator using the Green function  $H_k$ , we obtain

$$\begin{aligned} h_{kl}^\alpha(y_1, y_2) = & -\frac{i}{k} \int \frac{H_k(y_2, y'_2) e^{il(y_1 - y'_2)}}{U(y_1) - U(y'_2) - \frac{2i\alpha}{k}} dy'_2 \\ & + \int \frac{H_k(y_2, y'_2)}{U(y_1) - U(y'_2) - \frac{2i\alpha}{k}} [(U''(y_1) - \beta)(h_{kl}^\alpha)^*(y'_2, y_1) - (U''(y'_2) - \beta)h_{kl}^\alpha(y_1, y'_2)] dy'_2. \end{aligned} \quad (\text{E.3})$$

The generalization to the 2D barotropic equation upon a topography  $h(y)$  is straightforward, replacing  $\beta$  by  $h'(y)$  in (E.3). The main advantage of this equation is that it involves only well-behaved functions, even in the limit of no dissipation  $\alpha \rightarrow 0$ . Indeed, in this limit, the integrals converge to their Cauchy principal values. Moreover, the fact that it doesn't involve any space derivative will make it easy to solve numerically, as discussed in next section.

### Numerical implementation

In order to numerically compute solutions of Eq. (E.3), we chose an iterative scheme. We compute the sequence  $\{h_N\}_{N \geq 0}$  with

$$h_{N+1} = S + T[h_N],$$

where  $S$  is the first term in the right hand side of Eq. (E.3) and  $T$  is the integral operator of the second term. If this sequence converges, then  $h_{kl}^\alpha = \lim_{N \rightarrow \infty} h_N$ .

We note that we have not been able to establish conditions for which  $T$  is contracting. As a consequence, the convergence of the algorithm is not guaranteed, and we establish the convergence empirically on a case by case basis. More precisely, the convergence of the iterative algorithm is checked by plotting  $\log \|h_N - h_{N-1}\|$  as a function of the number of iterations  $N$ , where  $\|\cdot\|$  is the  $L^2$  norm.

The computation of integrals of the form  $\int \frac{f_k(y, y')}{U(y) - U(y') - 2i\alpha/k} dy'$  requires a particular attention. Indeed, the singularity of the denominator at the points such that  $U(y') = U(y)$  can be the source of important numerical errors, and we find that the result strongly depends on the resolution if it is not precise enough. The resolution required to get robust results is easily understood: in order to avoid numerical errors, the denominator must satisfy  $|U(y) - U(y \pm \Delta y)| \ll \frac{2\alpha}{k}$  for a discretization step  $\Delta y$ . More precisely, for sufficiently small  $\Delta y$ , we have  $U(y) - U(y \pm \Delta y) \simeq \pm U'(y)\Delta y$ , so that the condition becomes  $\Delta y \ll \frac{2\alpha}{k|U'|}$ . The numerical results confirm this scaling, for base flows with no stationary points. This is an important remark, because the iterative algorithm may converge and yet give a wrong result if the condition  $\Delta y \ll \frac{2\alpha}{k|U'|}$  is not respected. For base flows with stationary points, the iterative algorithm often gives problems of convergence in the small  $\alpha$  limit.

### Results in the case of a parabolic base flow

We consider the case of the 2D Euler equations ( $\beta = h = 0$ ) in the channel  $(x, y) \in [0, 2\pi] \times [-1, 1]$  with rigid boundary conditions  $\psi_m(x, \pm 1) = 0$ ,  $\mathbf{v}_m(x + 2\pi, y) = \mathbf{v}_m(x, y)$ , and with a parabolic base flow  $U(y) = A(y+2)^2 - U_0$ , where the constants  $A$  and  $U_0$  are chosen so that the total energy is 1 and the total momentum is 0. This flow has no inflection point, whence its linear stability by direct application of Rayleigh's inflection point theorem [35]. Moreover, this flow has no stationary points ( $y_0$  such that  $U'(y_0) = 0$ ). We chose here, for sake of simplicity, to force only one mode  $k = l = 1$ . This corresponds to the forcing correlation function  $C(\mathbf{r}) = c_{11} \cos(x + y)$ , with  $c_{11} = 4.72$ .

We have numerically computed the solution of (E.3) with the iterative scheme previously explained. As mentioned above, the necessary resolution to use depends on the value of  $\alpha$ ; in the present case, it ranges from  $\Delta y = 1/60$  for the largest value  $\alpha = 0.1$  to  $\Delta y = 1/300$  for the smallest one,  $\alpha = 0.005$ . Figure E.1 shows the

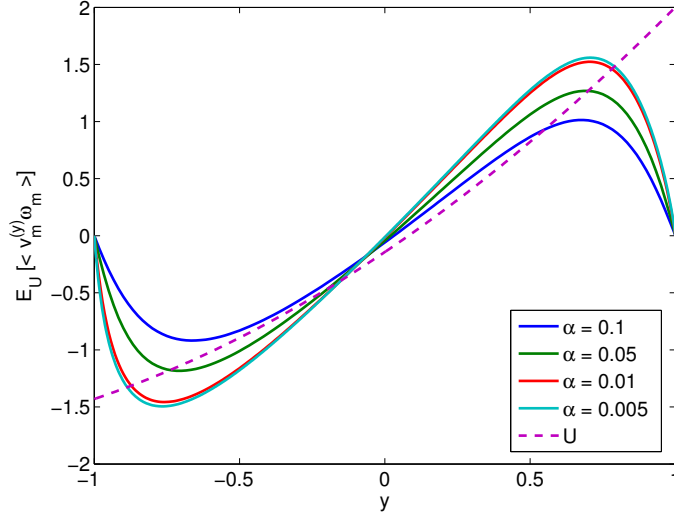


Figure E.1: The Reynolds stress divergence  $F^\alpha(y) = \mathbb{E}_U^\alpha \langle v_m \omega_m \rangle = 2k\pi c_{kl} \text{Im} [h_{kl}^\alpha(y, y)]$  in the case of a parabolic base profile in a channel geometry, with  $k = l = 1$  and different values of the friction coefficient  $\alpha$ . We check the convergence of  $F^\alpha$  to a smooth function in the inertial limit, as theoretically predicted in section 4.3.

Reynolds stress divergence  $F^\alpha(y) = 2k\pi c_{kl} \text{Im} [h_{kl}^\alpha(y, y)]$  and it clearly illustrates the convergence of  $F^\alpha$  for  $\alpha \rightarrow 0$ , as theoretically described in section 4.3. We also note that the Reynolds' forcing and the base flow profile  $U$  have the same sign, except in a small region near  $y = 0$ . This implies that the Reynolds stress is actually forcing the zonal flow.

## E.2 Integration of the resolvent over frequencies

The analog of (4.16) for the vorticity-stream function correlation is

$$h_{k,l}^\alpha(y_1, y_2) = \int_{-\infty}^{\infty} dt \tilde{\omega}_{k,l}(y_1, t) \tilde{\psi}_{k,l}^*(y_2, t), \quad (\text{E.4})$$

where  $\tilde{\omega}_{k,l}(y, t)$  is the vorticity field obeying the deterministic initial value problem

$$\forall t > 0, \quad \partial_t \tilde{\omega}_{k,l}(y, t) + L_{U,k} [\tilde{\omega}_{k,l}](y, t) = 0,$$

$$\tilde{\omega}_{k,l}(y, 0) = e^{ily},$$

$$\forall t < 0, \quad \tilde{\omega}_{k,l}(y, t) = 0,$$

and  $\tilde{\psi}_{k,l}(y, t)$  is the associated stream function.

We move now to the frequency domain. The Laplace transform of the vorticity is defined by

$$\hat{\omega}_{k,l}(y, c) = \int_0^{\infty} dt \tilde{\omega}_{k,l}(y, t) e^{ickt} = \int_{-\infty}^{\infty} dt \tilde{\omega}_{k,l}(y, t) e^{ikct}. \quad (\text{E.5})$$

For all  $\alpha > 0$ , the deterministic vorticity field  $\tilde{\omega}_{k,l}$  decays to 0 for  $t \rightarrow \infty$ . Then, the Laplace transform defined by (E.5) for real values of  $c$  coincides with the Fourier transform with respect to  $t$ . As a consequence, it can be simply inverted as

$$\tilde{\omega}_{k,l}(y, t) = \frac{|k|}{2\pi} \int_{-\infty}^{\infty} dc \hat{\omega}_{k,l}(y, c) e^{-ikct}. \quad (\text{E.6})$$

We stress that this property is valid only for decaying fields  $\tilde{\omega}_{k,l}$ , and thus only when  $\alpha \neq 0$ .

The Laplace transform of the associated stream function is the resolvent  $\phi_{kl}$ , defined in appendix D.2. Using (E.6) and (D.6) in (E.4), and performing the integration over  $t$ , we get

$$h_{k,l}^{\alpha}(y, y) = \frac{|k|}{2\pi} \int_{-\infty}^{\infty} dc \frac{(U''(y) - \beta)\phi_{k,l}(y, c) + e^{ily}/ik}{U(y) - c - i\frac{\alpha}{k}} \phi_{k,l}^*(y, c). \quad (\text{E.7})$$

The numerical computation of the resolvent  $\phi_{k,l}$  is a very easy task, an algorithm is detailed in [11]<sup>1</sup>. Then, the computation of the integral (E.7) is a matter of a few minutes, with a very good accuracy (of the order of  $10^{-3}$ ). The computation can take up to 15 minutes for the smallest values of  $\alpha$ . An example of application of this method is given in figure E.2.

**Results in the case of a cosine base flow** Consider the zonal base flow  $U(y) = \cos y$  in the domain  $(x, y) = [0, 2\pi l_x) \times [-\pi, \pi)$  with periodic boundary conditions, which is usually referred to as the Kolmogorov flow [11]. This flow is stable and the linearized operator associated to this flow has no normal modes for aspect ratio  $l_x < 1$  [11]. We choose the parameters  $l_x = 0.5$ ,  $k = 2$ ,  $l = 0$ , corresponding to the forcing correlation function  $C(\mathbf{r}) = c_{20} \cos(2x)$ , with  $c_{20} = 1.29$ . The Reynolds stress divergence  $F^{\alpha}$  is plotted in figure E.2. It converges to a smooth function in the inertial limit. For all points such that  $U'(y) \neq 0$ , this was expected from the theoretical results of section 4.3. We note that we have also a convergence of  $F^{\alpha}(y)$  to a finite limit at the stationary points  $y = 0, \pi$ , as discussed at the end of section 4.3.1. We observe that the Reynolds stress is forcing the flow except in some regions around the zeros of  $U$ , like in the case of the parabolic zonal flow.

### E.3 Using the pseudomomentum balance

Using (4.30) and (D.9), we get

$$\lim_{\alpha \rightarrow 0} f_{kl}^{\alpha}(y) = k\pi l_x (kU''(y) |\phi_{+}(y, U(y))|^2 - 2\text{Im}(\phi_{+}(y, U(y))e^{ily})).$$

We see explicitly that this quantity does not diverge at the inflexion points of the base flow  $U''(y) = 0$ . Using the numerical method described in [11] to compute the resolvent  $\phi_{+}$ , we directly get the average Reynolds' forcing with the above expression. This method is much simpler than the previous one because we need to compute  $\phi_{+}(y, c)$  only for some values of  $c$ , depending on the desired spatial resolution for  $F_0(y)$ . Computing the average Reynolds' forcing with this method is a matter

---

<sup>1</sup>This method is based on the classical theory of linear ODEs of second order in order to solve (D.6).

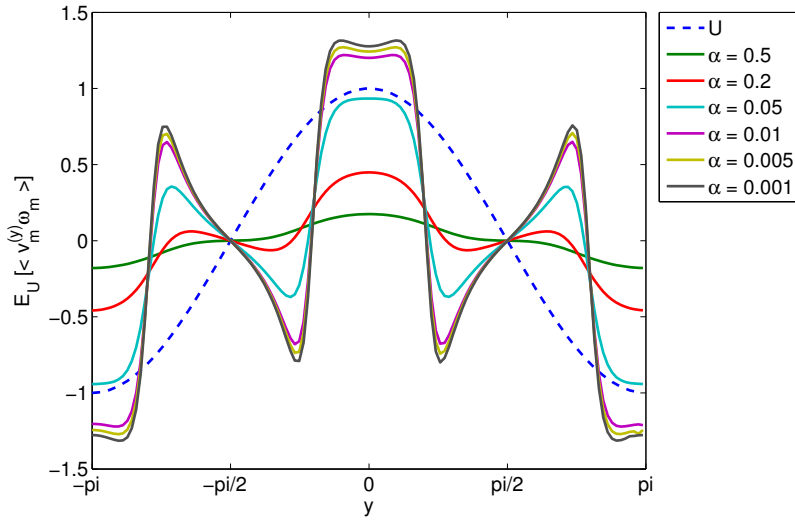


Figure E.2: The Reynolds stress divergence  $F^\alpha(y) = \mathbb{E}_U^\alpha \langle v_m \omega_m \rangle = 2k\pi l_x c_{kl} \text{Im} [h_{kl}^\alpha(y, y)]$  in the case of a cosine base profile  $U(y) = \cos y$  in a periodic geometry, with  $k = 2$ ,  $l = 0$  and different values of the friction coefficient  $\alpha$ . Again, we observe the convergence of  $F^\alpha$  towards a smooth function when  $\alpha \rightarrow 0$ , even at the stationary points  $y = 0$  and  $y = \pi$  where we do not have full theoretical predictions.

of a fraction of seconds, and almost does not depend on  $\alpha$ . An example of such computation is shown in figure 4.2, page 59.

Note that the two methods based on the computation of the resolvent  $\phi_+$  are expected to be accurate only in the inertial regime  $\alpha \rightarrow 0$ , because in this limit we can identify the limit  $\epsilon \rightarrow 0$  in (D.5) and the limit  $\alpha \rightarrow 0$ . In contrast, the integral equation (E.3) is rigorously equivalent to the original Lyapunov equation, so it gives an accurate estimation of  $F_0$  even for relatively large values of  $\alpha$ . However in practice, we observe that the two methods based on the resolvent are much more stable when small values of  $\alpha$  are considered (typically smaller than  $10^{-2}$ ), and this is the regime we are ultimately interested in.

# Appendix F

## Fluctuations of the Reynolds' forcing for any background flow

In this appendix we study the behaviour for small  $\alpha$  of the integrated autocorrelation function  $\Xi^\alpha[U]$  defined in (4.36) (page 61). More precisely, we prove (5.15) (page 73). We recall the following definitions:

$$\Xi^\alpha[U](y_1, y_2) = \sum_{(k,l) \in \mathbb{Z}^2} c_{kl}^2 \{ \Xi_{kl}^\alpha(y_1, y_2) + \Xi_{kl}^\alpha(y_2, y_1) \} \quad (\text{F.1})$$

with  $\Xi_{kl}^\alpha(y_1, y_2) = C_{kl}^\alpha(y_1, y_2, T_0 = 0) + D_{kl}^\alpha(y_1, y_2, T_0 = 0)$  where

$$C_{kl}^\alpha(y_1, y_2, T_0) = \frac{1}{4} \int_{T_0}^{\infty} \mathbb{E}_U^\alpha [v_{kl}(y_1, s)v_{-k,-l}(y_2, 0)] \mathbb{E}_U^\alpha [\omega_{-k,-l}(y_1, s)\omega_{kl}(y_2, 0)] ds \quad (\text{F.2})$$

and

$$D_{kl}^\alpha(y_1, y_2, T_0) = \frac{1}{4} \int_{T_0}^{\infty} \mathbb{E}_U^\alpha [v_{kl}(y_1, s)\omega_{-k,-l}(y_2, 0)] \mathbb{E}_U^\alpha [\omega_{-k,-l}(y_1, s)v_{kl}(y_2, 0)] ds. \quad (\text{F.3})$$

For future simplicity, we have introduced the variable  $T_0$ . Indeed, we are only interested in the large  $s$  behavior of the integrands above because there are no convergence problems around  $s = 0$ . In the following,  $T_0$  will be fixed and assumed to be very large.

In section F.1 we study the large- $s$  behaviour of the two-points correlation functions  $T_{\omega\omega}^\alpha$ ,  $T_{vv}^\alpha$ ,  $T_{v\omega}^\alpha$  and  $T_{\omega v}^\alpha$  given by (4.40–4.43), using the Orr mechanism (4.24). Then, we will be able to study the small- $\alpha$  behaviour of  $C_{kl}^\alpha$  and  $D_{kl}^\alpha$  given by (F.2, F.3). This is done in section F.2.

### F.1 Two–points correlation functions

#### Large time behavior of $T_{\omega\omega}^\alpha$

We report (4.40) for convenience,

$$T_{\omega\omega}^\alpha(k, l, y_1, y_2, s) \equiv \frac{1}{2} \mathbb{E}_U^\alpha [\omega_{-k,-l}(y_1, s)\omega_{k,l}(y_2, 0)] = \int_0^\infty dt_1 \tilde{\omega}_{-k,-l}(y_1, s+t_1)\tilde{\omega}_{k,l}(y_2, t_1). \quad (\text{F.4})$$

The computations presented in appendix D for the convergence of  $g_{kl}^\alpha$  can be generalized to the computation of  $T_{\omega\omega}^\alpha$ , leading to a similar conclusion:

$$T_{\omega\omega}^\alpha(k, l, y_1, y_2, s) = \frac{\tilde{\omega}_{-k,-l}^\infty(y_1)\tilde{\omega}_{kl}^\infty(y_2)}{ik(U(y_1) - U(y_2)) + 2\alpha} e^{ikU(y_1)s - \alpha s} + T_{\omega\omega}^{r,\alpha}(k, l, y_2, y_2, s), \quad (\text{F.5})$$

where  $T_{\omega\omega}^{r,\alpha}(k, l, y_2, y_2, s)$  is finite for all  $(k, l, y_2, y_2, s)$  such that  $U(y_1) \neq U(y_2)$ , and is negligible with respect to  $1/\alpha$  if  $U(y_1) = U(y_2)$ . Also,  $T_{\omega\omega}^{r,\alpha}(k, l, y_2, y_2, s)$  is a bounded function of  $s$ .

### Large time behavior of $T_{vv}^\alpha$

We report (4.41) for convenience,

$$T_{vv}^\alpha(k, l, y_1, y_2, s) \equiv \frac{1}{2} \mathbb{E}_U^\alpha [v_{k,l}(y_1, s)v_{-k,-l}(y_2, 0)] = \int_0^\infty dt_1 \tilde{v}_{k,l}(y_1, s+t_1)\tilde{v}_{-k,-l}(y_2, t_1). \quad (\text{F.6})$$

We show here that  $T_{vv}^\alpha$  decays as or faster than  $1/s^2$ .

We have

$$|T_{vv}^\alpha(k, l, y_1, y_2, s)| \leq \int_0^\infty dt_1 |\tilde{v}_{k,l}(y_1, t_1 + s)| |\tilde{v}_{-k,-l}(y_2, t_1)|. \quad (\text{F.7})$$

Because  $T_0 \gg 1$ , we can chose in the above formula  $s \gg 1$ . We thus have

$$|T_{vv}^\alpha(k, l, y_1, y_2, s)| \leq \left| \frac{\tilde{\omega}_{k,l}^\infty(y)}{ik(U'(y))^2} \right| \int_0^\infty dt_1 |\tilde{v}_{-k,-l}(y_2, t_1)| \left\{ \frac{1}{(t_1 + s)^2} + o\left(\frac{1}{(t_1 + s)^2}\right) \right\}. \quad (\text{F.8})$$

Using the results in section F.3, we have

$$|T_{vv}^\alpha(k, l, y_1, y_2, s)| \underset{s \rightarrow \infty}{\lesssim} \frac{R_{vv}(k, l, y_1, y_2)}{s^2} + o\left(\frac{1}{s^2}\right), \quad (\text{F.9})$$

where  $R_{vv}$  is a positive, bounded function of  $(y_1, y_2)$ . It is important to note that  $R_{vv}$  does not depend on  $\alpha$ .

### Large time behavior of $T_{v\omega}^\alpha$

We report (4.42) for convenience,

$$T_{v\omega}^\alpha(k, l, y_1, y_2, s) \equiv \frac{1}{2} \mathbb{E}_U^\alpha [v_{k,l}(y_1, s)\omega_{-k,-l}(y_2, 0)] = \int_0^\infty dt_1 \tilde{v}_{k,l}(y_1, s+t_1)\tilde{\omega}_{-k,-l}(y_2, t_1). \quad (\text{F.10})$$

The large- $s$  behavior of  $T_{v\omega}^\alpha(k, l, y_1, y_2, s)$  is different if  $U(y_1) = U(y_2)$  or if  $U(y_1) \neq U(y_2)$ . Indeed, in the first case, the asymptotic oscillations of the integral cancel out and the large- $s$  decay is slower: it decays as  $1/s$  in the  $\alpha \rightarrow 0$  limit. In the second one, the oscillations do not cancel out and the decay is as  $1/s^{\min\{1+\gamma, 2\}}$ , where  $\gamma > 0$  is the exponent of the decay of  $\tilde{\omega}_{kl}^r$ .

We have

$$T_{v\omega}^\alpha(k, l, y_1, y_2, s) \underset{s \rightarrow \infty}{\sim} \frac{\tilde{\omega}_{k,l}^\infty(y_1)}{ik(U'(y_1))^2} e^{-ikU(y_1)s - \alpha s} \left\{ \tilde{\omega}_{-k,-l}^\infty(y_2) \int_0^\infty dt_1 \frac{e^{-i[kU(y_1) - kU(y_2)]t_1 - 2\alpha t_1}}{(t_1 + s)^2} + \int_0^\infty dt_1 \frac{e^{-ikU(y_1)t_1 - 2\alpha t_1}}{(t_1 + s)^2} \tilde{\omega}_{-k,-l}^r(y_2, t_1) \right\}. \quad (\text{F.11})$$

We now see that the decay in  $s$  of the expression in parenthesis is different if  $U(y_1) = U(y_2)$  or  $U(y_1) \neq U(y_2)$ .

If  $U(y_1) = U(y_2)$ , the first integral dominates. We have

$$\int_0^\infty dt_1 \frac{e^{-i[kU(y_1)-kU(y_2)]t_1-2\alpha t_1}}{(t_1+s)^2} = \int_0^\infty dt_1 \frac{e^{-2\alpha t_1}}{(t_1+s)^2} \leq \frac{1}{s}. \quad (\text{F.12})$$

Observe that the equality holds in the  $\alpha \rightarrow 0$  limit. We conclude that, if  $U(y_1) = U(y_2)$ ,

$$|T_{v\omega}^\alpha(k, l, y_1, y_2, s)| \underset{s \rightarrow \infty}{\lesssim} \frac{R_{v\omega}^{\text{slow}}(k, l, y_1, y_2)}{s} e^{-\alpha s}, \quad (\text{F.13})$$

where

$$R_{v\omega}^{\text{slow}}(k, l, y_1, y_2) = \frac{\tilde{\omega}_{k,l}^\infty(y_1)\tilde{\omega}_{-k,-l}^\infty(y_2)}{ik(U'(y_1))^2} \quad (\text{F.14})$$

is a regular function which does not depend on  $\alpha$ .

If  $U(y_1) \neq U(y_2)$ , the asymptotic oscillations on the first term in the parenthesis of Eq. (F.11) do not cancel out. Using the results of section F.3, we conclude that

$$\left| \int_0^\infty dt_1 \frac{e^{-i[kU(y_1)-kU(y_2)]t_1-2\alpha t_1}}{(t_1+s)^2} \right| \leq \left| \int_0^\infty dt_1 \frac{e^{-i[kU(y_1)-kU(y_2)]t_1}}{(t_1+s)^2} \right| \sim \frac{1}{s^2}. \quad (\text{F.15})$$

For what concerns the second term in the parenthesis of Eq. (F.11), we have

$$\left| \int_0^\infty dt_1 \frac{e^{-ikU(y_1)t_1-2\alpha t_1}}{(t_1+s)^2} \tilde{\omega}_{-k,-l}^r(y_2, t_1) \right| \leq \int_0^\infty dt_1 \frac{|\tilde{\omega}_{-k,-l}^r(y_2, t_1)|}{(t_1+s)^2} \underset{s \rightarrow \infty}{\sim} \frac{A(k, l, y_2)}{s^{1+\gamma}}, \quad (\text{F.16})$$

where  $A$  is a positive function which does not depend on  $\alpha$ . The formula given above is valid for  $0 < \gamma < 1$  or  $\gamma > 1$  but not for  $\gamma = 1$ , in which there is a logarithmic correction, see sections F.3. The logarithmic correction is not important for the following, so we do not consider it here.

We thus conclude that, for  $U(y_1) \neq U(y_2)$

$$|T_{v\omega}^\alpha(k, l, y_1, y_2, s)| \underset{s \rightarrow \infty}{\lesssim} \frac{R_{v\omega}^{\text{fast}}(k, l, y_1, y_2)}{s^{\min\{1+\gamma, 2\}}} e^{-\alpha s} \quad (\text{F.17})$$

where

$$R_{v\omega}^{\text{fast}}(k, l, y_1, y_2) = \frac{\tilde{\omega}_{k,l}^\infty(y_1)}{ik(U'(y_1))^2} A(k, l, y_2). \quad (\text{F.18})$$

### Large time behaviour of $T_{\omega v}^\alpha$

We report (4.43) for convenience,

$$T_{\omega v}^\alpha(k, l, y_1, y_2, s) \equiv \frac{1}{2} \mathbb{E}_U^\alpha [\omega_{-k,-l}(y_1, s) v_{k,l}(y_2, 0)] = \int_0^\infty dt_1 \tilde{\omega}_{-k,-l}(y_1, s+t_1) \tilde{v}_{k,l}(y_2, t_1). \quad (\text{F.19})$$

We show here that  $T_{\omega v}^\alpha$  defined in Eq. (4.43) is bounded by a function of  $(k, l, y_1, y_2)$ , independent of  $\alpha$ .

We have

$$|T_{\omega v}^\alpha(k, l, y_1, y_2, s)| \leq e^{-\alpha s} \|\tilde{\omega}\|_\infty(y_1) \int_0^\infty dt_1 |\tilde{v}_{k,l}(y_2, t_1)|, \quad (\text{F.20})$$

where  $\|\tilde{\omega}\|_\infty = \max_{t_1} \tilde{\omega}_{-k,-l}(y_1, t_1)$  is finite thanks to the Orr mechanism. Using that  $|\tilde{v}_{k,l}(y_2, t_1)|$  is a bounded function of both  $y_2$  and  $t_1$ , and that it decays as  $1/t_1^2$  for  $t_1 \rightarrow \infty$ , we conclude that

$$|T_{\omega v}^\alpha(k, l, y_1, y_2, s)| \leq R_{\omega v}(k, l, y_1, y_2) e^{-\alpha s}. \quad (\text{F.21})$$

where  $R_{\omega v}(k, l, y_1, y_2)$  is a positive, bounded function of  $(y_1, y_2)$  which does not depend on  $\alpha$ .

## F.2 Four-points correlation functions

### Behavior of $C_{kl}^\alpha$ in the limit $\alpha \rightarrow 0$

Using (F.9) and (5.21) in the definition (F.2),

$$\begin{aligned} C_{kl}^\alpha(y_1, y_2, T_0) &\lesssim \frac{\tilde{\omega}_{-k,-l}^\infty(y_1) \tilde{\omega}_{k,l}^\infty(y_2) R_{vv}(k, l, y_1, y_2)}{ik [U(y_1) - U(y_2)] + 2\alpha} \int_{T_0}^\infty ds \left( \frac{1}{s^2} + o\left(\frac{1}{s^2}\right) \right) e^{-\alpha s} \\ &\quad + R_{vv}(k, l, y_1, y_2) \int_{T_0}^\infty ds T_{\omega\omega}^{r,\alpha}(k, l, y_1, y_2, s) e^{-\alpha s} \left( \frac{1}{s^2} + o\left(\frac{1}{s^2}\right) \right). \end{aligned}$$

From the properties of  $T_{\omega\omega}^{r,\alpha}$ , we conclude that

- if  $U(y_1) = U(y_2)$ ,

$$C_{kl}^\alpha(y_1, y_2, T_0) \underset{\alpha \rightarrow 0}{=} \frac{A_1(k, l, y_1, y_2)}{2\alpha} + o\left(\frac{1}{\alpha}\right) \underset{\alpha \rightarrow 0}{=} \frac{A_1(k, l, y_1, y_2) + o(1)}{2\alpha}$$

where

$$A_1(k, l, y_1, y_2) = \tilde{\omega}_{-k,-l}^\infty(y_1) \tilde{\omega}_{k,l}^\infty(y_2) \int_{T_0}^\infty ds T_{vv}^\alpha(k, l, y_1, y_2, s) \Big|_{\alpha=0},$$

which is finite.

- if  $U(y_1) \neq U(y_2)$ ,

$$C_{kl}^\alpha(y_1, y_2, T_0) \underset{\alpha \rightarrow 0}{=} \frac{A_1(k, l, y_1, y_2)}{ik [U(y_1) - U(y_2)]} + A_2(k, l, y_1, y_2)$$

where

$$A_2(k, l, y_1, y_2) = \int_{T_0}^\infty ds T_{vv}^\alpha(k, l, y_1, y_2, s) T_{\omega\omega}^{r,\alpha}(k, l, y_1, y_2, s) \Big|_{\alpha=0},$$

which is finite.

### Behavior of $D_{kl}^\alpha$ in the limit $\alpha \rightarrow 0$

Using (F.13), (F.17) and (F.21) in the definition (F.3), we have:

- if  $U(y_1) = U(y_2)$ ,

$$|D_{kl}^\alpha(y_1, y_2, T_0)| \lesssim R_{vw}^{slow}(k, l, y_1, y_2) R_{\omega v}(k, l, y_1, y_2) \int_{T_0}^{\infty} ds \frac{e^{-2\alpha s}}{s}.$$

We can now observe that

$$\int_{T_0}^{\infty} ds \frac{e^{-2\alpha s}}{s} \underset{\alpha \rightarrow 0}{\sim} \log \alpha T_0$$

so  $D_{kl}^\alpha(y_1, y_2, T_0) = \ln \alpha B_1(k, l, y_1, y_2)$  where  $B_1$  is finite and doesn't depend on  $\alpha$ .

- if  $U(y_1) \neq U(y_2)$ ,

$$|D_{kl}^\alpha(y_1, y_2, T_0)| \lesssim R_{vw}^{fast}(k, l, y_1, y_2) R_{\omega v}(k, l, y_1, y_2) \int_{T_0}^{\infty} ds \frac{e^{-2\alpha s}}{s^{\min(1+\gamma, 2)}}. \quad (\text{F.22})$$

We can now observe that

$$\int_{T_0}^{\infty} ds \frac{e^{-2\alpha s}}{s^{\min(1+\gamma, 2)}} < \infty \quad \forall \alpha \geq 0 \quad (\text{F.23})$$

so  $D_{kl}^\alpha(y_1, y_2, T_0) = B_2(k, l, y_1, y_2)$  where  $B_2$  is finite and doesn't depend on  $\alpha$ .

### Conclusion for $\Xi_{kl}^\alpha$

Collecting the previous results and using  $\Xi_{kl}^\alpha = C_{kl}^\alpha + D_{kl}^\alpha$ , we have

- if  $U(y_1) = U(y_2)$ ,

$$\Xi_{kl}^\alpha(y_1, y_2) \underset{\alpha \rightarrow 0}{=} \frac{A_1(k, l, y_1, y_2) + o(1) + 2\alpha \ln \alpha B_1(k, l, y_1, y_2)}{2\alpha} \underset{\alpha \rightarrow 0}{=} \frac{A_1(k, l, y_1, y_2)}{2\alpha}.$$

- if  $U(y_1) \neq U(y_2)$ ,

$$\Xi_{kl}^\alpha(y_1, y_2) \underset{\alpha \rightarrow 0}{=} \frac{A_1(k, l, y_1, y_2) + ik [U(y_1) - U(y_2)] [A_2(k, l, y_1, y_2) + B_2(k, l, y_1, y_2)]}{ik [U(y_1) - U(y_2)]}.$$

We conclude that for all  $(y_1, y_2)$ ,

$$\Xi_{kl}^\alpha(y_1, y_2) \underset{\alpha \rightarrow 0}{\sim} \frac{A_{kl}(y_1, y_2)}{ik [U(y_1) - U(y_2)] + 2\alpha},$$

with  $A_{kl}(y_1, y_2) = A_1(k, l, y_1, y_2) + ik [U(y_1) - U(y_2)] [A_2(k, l, y_1, y_2) + B_2(k, l, y_1, y_2)]$ .

## F.3 Temporal decay of some integrals

### Some oscillating integrals

Consider integrals of the form

$$F(t) = \int_0^{\infty} du e^{-igu} f(t+u) \quad f(u) \underset{u \rightarrow \infty}{\sim} \frac{1}{u^N} \quad g \neq 0, \quad (\text{F.24})$$

where  $f$  is a smooth real function and  $N > 0$ . We prove here that

$$F(t) \underset{t \rightarrow \infty}{\sim} \frac{1}{t^N}. \quad (\text{F.25})$$

Let us perform the change of variable  $w = 1 + u/t$ :

$$F(t) = t e^{-igt} \int_1^\infty dw e^{-igtw} f(tw) = t e^{-igt} \int_1^\infty dw e^{-igtw} h_t(w), \quad (\text{F.26})$$

where we have introduced the function  $h_t(w) = f(tw)$ ; clearly,  $h_t(w) \underset{t, w \rightarrow \infty}{\sim} \frac{1}{t^N w^N}$ .

We also have  $h_t^{(n)}(1) \underset{t \rightarrow \infty}{\sim} \frac{1}{t^N}$  for all  $n$ , where  $h_t^{(n)}$  indicates the  $n$ -th derivative.

Now perform part integration iteratively on the last expression, for example after two parts integrations:

$$F(t) \underset{t \gg 1}{\sim} e^{-igt} \left\{ \frac{-i}{g} h_t(1) + \frac{1}{g^2 t} h_t^{(1)}(1) - \frac{1}{g^2 t} \int_1^\infty dw e^{-igtw} h_t^{(2)}(w) \right\}. \quad (\text{F.27})$$

Each successive term converges faster to zero than the previous one in the limit  $t \ll 1$ , thanks to the relation  $h_t^{(n)}(1) \underset{t \rightarrow \infty}{\sim} \frac{1}{t^N}$  for all  $n$ . We thus have the desired result.

### Non oscillating integrals

Consider integrals of the form

$$G(t) = \int_0^\infty du \frac{g(u)}{(u+t)^2} \quad \int_0^\infty du g(u) < \infty; \quad (\text{F.28})$$

where  $g(u) \geq 0$  everywhere in  $[0, \infty)$ . We prove here that

$$G(t) \underset{t \rightarrow \infty}{\sim} \frac{A}{t^2} \quad 0 < \int_0^\infty du \frac{g(u)}{(1+u)^2} < A < \int_0^\infty du g(u). \quad (\text{F.29})$$

We have

$$G(t) = \frac{1}{t^2} \int_0^\infty du \frac{g(u)}{(1 + \frac{u}{t})^2}; \quad (\text{F.30})$$

let us observe that

$$\frac{1}{(1+u)^2} \underset{t > 1}{\leq} \frac{1}{(1 + \frac{u}{t})^2} < 1 \quad (\text{F.31})$$

where in the first passage we assumed  $t > 1$  as we are interested in the  $t \rightarrow \infty$  limit of  $G$ . Then,

$$\frac{1}{t^2} \int_0^\infty du \frac{g(u)}{(1+u)^2} \underset{t > 1}{\leq} G(t) < \frac{1}{t^2} \int_0^\infty du g(u). \quad (\text{F.32})$$

We have then proved the desired result in Eq. (F.29).

These results can be easily extended to the case of integrals of the form

$$G(t) = \int_0^\infty du \frac{g(u)}{(u+t)^N} \quad \int_0^\infty du g(u) < \infty \quad N > 0 \quad (\text{F.33})$$

and one would obtain the result

$$G(t) \underset{t \rightarrow \infty}{\sim} \frac{A}{t^N} \quad 0 < \int_0^\infty du \frac{g(u)}{(1+u)^N} < A < \int_0^\infty du g(u). \quad (\text{F.34})$$

**Non oscillating integrals where the previous estimation does not work**

Consider integrals of the form

$$G(t) = \int_0^\infty du \frac{g(u)}{(u+t)^2} \quad g(u) \underset{u \rightarrow \infty}{\sim} \frac{1}{u^\gamma} \quad 0 < \gamma \leq 1, \quad (\text{F.35})$$

where  $g(u) \geq 0$  everywhere in  $[0, \infty)$ . In this case, the hypothesis of the previous section do not work because  $\int_0^\infty du g(u) = \infty$ .

We prove in this subsection that

$$G(t) \underset{t \rightarrow \infty}{\lesssim} \frac{A_1}{t^{1+\gamma}} \quad 0 < \gamma < 1 \quad (\text{F.36})$$

and

$$G(t) \underset{t \rightarrow \infty}{\lesssim} \frac{A_2}{t^2} \log t \quad \gamma=1 \quad (\text{F.37})$$

where  $A_1$  and  $A_2$  are suitable positive constants. As usual the symbol  $\underset{t \rightarrow \infty}{\lesssim}$  means that there is a function  $G_1(t)$  which dominates  $G(t)$  and behaves as described for  $t \rightarrow \infty$ .

The proof of Eq. (F.36) and (F.37) is easily done by observing that  $g$  can be majorated for every  $u$  by

$$g(u) \leq \frac{a_1}{u^\gamma} \quad \text{if} \quad 0 < \gamma < 1 \quad (\text{F.38})$$

and

$$g(u) \leq \frac{a_2}{u + a_3} \quad \text{if} \quad \gamma = 1. \quad (\text{F.39})$$

where  $a_1$ ,  $a_2$  and  $a_3$  are positive constants. The case  $0 < \gamma < 1$  is easily completed by observing that

$$G(t) < G_1(t) \equiv \int_0^\infty du \frac{1}{(u+t)^2} \frac{a_1}{u^\gamma} = a_1 \pi \left(\frac{1}{t}\right)^{1+\gamma} \gamma \text{Csc}[\pi\gamma] \underset{t \rightarrow \infty}{\sim} \frac{A_1}{t^{1+\gamma}}. \quad (\text{F.40})$$

where Csc is the cosecant<sup>1</sup>

The case  $\gamma = 1$  is also easily accomplished by observing that

$$G(t) < G_2(t) \equiv \int_0^\infty du \frac{1}{(u+t)^2} \frac{a_2}{u + a_3} = \frac{a_2(a_3 - t - t \ln a_3 + t \ln t)}{(a_3 - t)^2 t} \underset{t \rightarrow \infty}{\sim} \frac{A_2}{t^2} \ln t. \quad (\text{F.41})$$

---

<sup>1</sup>Csc( $x$ ) <  $\infty$  if  $x \neq n\pi$  with  $n$  integer.

# Appendix G

## Large deviations of quadratic forms of gaussian processes

### G.1 Derivation of the Ricatti equation

Like for the derivation of the Large Deviation Principle for  $z$  (see appendix B.1 in page 136), consider the function

$$u(t, z, w, \theta) \equiv \mathbb{E}_z \exp \left( \theta \int_0^t f(z, \tilde{w}_z(s)) \, ds \right), \quad (\text{G.1})$$

such that  $H(z, \theta) = \lim_{t \rightarrow \infty} \frac{1}{t} \ln u(t, z, w, \theta)$ , where  $w = \tilde{w}_z(0)$  is the fixed initial condition (which is naturally lost in the limit  $t \rightarrow \infty$  when computing  $H$ ). We recall that we consider here the class of systems such that  $f(z, w) = r_z + w^T s_z + w^T M_z w$ , and that  $\tilde{w}_z$  is the virtual fast process (6.10) with  $z$  held fixed.

The evolution equation for  $u$  is given by [16]

$$\frac{\partial u}{\partial t} = \left( -L_z \cdot w \nabla_w + \frac{1}{2} C : \nabla_w \nabla_w + \theta f(z, w) \right) u. \quad (\text{G.2})$$

We look for a solution under the form of a gaussian in  $w$ ,

$$u(t, z, w, \theta) = K(t, z, \theta) \exp \left( w^T m(t, z, \theta) + w^T N(t, z, \theta) w \right), \quad (\text{G.3})$$

for some unknowns  $m(t, z, \theta)$  and  $N(t, z, \theta)$ . Then (dropping the dependencies in  $z$  for simplicity of notations), (G.2) leads to

$$\frac{1}{K} \frac{\partial K}{\partial t} = \frac{1}{2} C : (2N(t, \theta) + m(t, \theta) m(t, \theta)^T) + \theta r \quad (\text{G.4})$$

$$\frac{\partial m}{\partial t} = -L^T m(t, \theta) + 2N(t, \theta) C m(t, \theta) + \theta s \quad (\text{G.5})$$

$$\frac{\partial N}{\partial t} = -L^T N(t, \theta) - N(t, \theta) L + 2N(t, \theta) C N(t, \theta) + \theta M \quad (\text{G.6})$$

where we have collected terms of order 0, 1 and 2 in  $w$ . Assume that (G.6) has a stationary solution  $N_\infty(\theta)$ , then (G.5) has the stationary solution

$$m_\infty(\theta) = \theta (L^T - 2N_\infty(\theta) C)^{-1} s, \quad (\text{G.7})$$

and  $K(t, \theta)$  satisfies

$$\ln K(t, \theta) \underset{t \rightarrow \infty}{\sim} t \left( \theta r + \text{tr}(CN_\infty(\theta)) + \frac{1}{2} m_\infty(\theta)^T C m_\infty(\theta) \right), \quad (\text{G.8})$$

where we have used  $C : N = \text{tr}(CN)$  and  $C : mm^T = m^T C m$ . Injecting (G.8) in (G.3), we get for the Hamiltonian

$$H(\theta) = \theta r + \text{tr}(CN_\infty(\theta)) + \frac{1}{2} m_\infty(\theta)^T C m_\infty(\theta). \quad (\text{G.9})$$

Using (G.7), it means that the Hamiltonian can be computed directly from the stationary solution of the matricial Ricatti equation (G.6). Note that this equation may have more than one solution: we should take the one such that  $N_\infty(0) = 0$ , so that  $H(0) = 0$ .

## G.2 Explicit solution of the Ricatti equation

Consider first the stationary Lyapunov equation (we drop the dependency in  $z$  for simplicity of notations)

$$gL + L^T g = 2C.$$

It can be solved as

$$g = 2 \int_0^\infty dt e^{-tL^T} C e^{-tL}.$$

In the case where  $CL = L^T C$ , we then have the simple solution  $G = L^{-T} C$  with  $L^{-T} = (L^{-1})^T$ .

We now try to extend this result to the Ricatti equation (G.6). Expand  $N_\infty$  as  $N_\infty(\theta) = N_\infty^{(1)}\theta + N_\infty^{(2)}\theta^2 + \dots$ , so that  $H(\theta = 0) = 0$ . The equation for  $N_\infty^{(1)}$  is

$$N_\infty^{(1)} L + L^T N_\infty^{(1)} = M$$

from which  $N_\infty^{(1)} = \int_0^\infty dt e^{-tL^T} M e^{-tL}$ . With the assumption  $ML = L^T M$ , we then have  $N_\infty^{(1)} = \frac{1}{2} L^{-T} M$ .

At higher orders, the equation for  $N_\infty^{(k)}$  reads

$$N_\infty^{(k)} L + L^T N_\infty^{(k)} = 2 \sum_{i=1}^{k-1} N_\infty^{(i)} C N_\infty^{(k-i)}$$

from which  $N_\infty^{(k)} = 2 \int_0^\infty dt e^{-tL^T} \sum_{i=1}^{k-1} N_\infty^{(i)} C N_\infty^{(k-i)} e^{-tL}$ . With the assumption that  $L^T$  commutes with  $MC$ , we can prove by mathematical induction that for all  $k \geq 1$ ,

$$N_\infty^{(k)} = \phi_k (L^{-T})^{2k-1} (MC)^{k-1} M,$$

where  $\phi_k$  is a numerical sequence given by the recursion relation

$$\phi_k = \sum_{i=1}^{k-1} \phi_i \phi_{k-i}, \quad \phi_1 = 1/2. \quad (\text{G.10})$$

Defining  $\phi(\theta) = \sum_{k \geq 1} \phi_k \theta^k$  and using the recursion relation on  $\phi_k$  we have  $\phi^2(\theta) = \phi(\theta) - \phi_1 \theta$ , from which

$$\phi(\theta) = \frac{1 - \sqrt{1 - 2\theta}}{2}.$$

Thus,

$$N_\infty(\theta)C = \frac{1}{2} \left[ L - \sqrt{L^2 - 2\theta CM} \right]^T$$

whenever the square root  $\sqrt{L^2 - 2\theta CM}$  exists. We can then compute the hamiltonian using (G.9),

$$\text{tr}(CN_\infty) = \frac{1}{2} \text{tr} \left[ L - \sqrt{L^2 - 2\theta CM} \right]$$

and

$$\begin{aligned} m_\infty(\theta)^T C m_\infty(\theta) &= \theta^2 s^T (L^{2T} - 2\theta MC)^{-T/2} C (L^{2T} - 2\theta MC)^{-1/2} s \\ &= \theta^2 s^T (L^2 - 2\theta CM) C s, \end{aligned}$$

so

$$H(\theta) = \theta r + \frac{1}{2} \text{tr} \left[ L - \sqrt{L^2 - 2\theta CM} \right] + \frac{1}{2} \theta^2 s^T (L^2 - 2\theta CM)^{-1} C s.$$

# Appendix H

## Most probable state of the equilibrium distribution

In this appendix we characterize the most probable state of the equilibrium energy-casimir distribution  $P_{\text{eq}} = \frac{1}{Z} \exp\left(-\frac{1}{\gamma}\mathcal{G}\right)$ , with

$$\mathcal{G}[\omega] = \int d\mathbf{r} \left( \frac{1-\epsilon}{2} \omega \Delta^{-1} \omega + \frac{1}{2} \omega^2 + \epsilon f(\omega) \right) \equiv \mathcal{G}_0[\omega] + \epsilon \mathcal{H}[\omega] + \text{cte} \quad (\text{H.1})$$

where  $\mathcal{G}_0[\omega] = \frac{1}{2} \int d\mathbf{r} (\omega \Delta^{-1} \omega + \omega^2)$  and  $\mathcal{H}$  contains all higher-order terms. Any large-scale jet  $\omega_0(\mathbf{r}) = -A \cos y - B \sin y$ <sup>1</sup> is a minimizer (and a zero) of  $\mathcal{G}_0$ .

For  $\epsilon = 0$ , we recover the energy-entropy potential studied in section 7.2. We know that the most probable state of this distribution is a large-scale jet  $\omega_0$ .

For  $\epsilon \neq 0$ , we can write the minimizer of the full potential as  $\omega^* = \omega_0^* + \epsilon \delta\omega^*$ , with  $\omega_0^*(y) = -A^* \cos y - B^* \sin y$ . Let's now see how the values  $(A^*, B^*)$  are selected. A Taylor expansion gives

$$\mathcal{G}[\omega_0 + \epsilon \delta\omega] = \mathcal{G}[\omega_0] + \epsilon \int d\mathbf{r} \frac{\delta\mathcal{G}}{\delta\omega(\mathbf{r})}[\omega_0] \delta\omega(\mathbf{r}) + O(\epsilon^2). \quad (\text{H.2})$$

The first term in the right-hand side reads

$$\mathcal{G}[\omega_0] = \mathcal{G}_0[\omega_0] + \epsilon \mathcal{H}[\omega_0] = \epsilon \mathcal{H}[\omega_0]. \quad (\text{H.3})$$

Using  $\mathcal{G} = \mathcal{G}_0 + \epsilon \mathcal{H}$ , the second term in the right-hand side of (H.2) involves

$$\frac{\delta\mathcal{G}}{\delta\omega(\mathbf{r})}[\omega_0] = \frac{\delta\mathcal{G}_0}{\delta\omega(\mathbf{r})}[\omega_0] + O(\epsilon) = 0 + O(\epsilon) \quad (\text{H.4})$$

where we have used that  $\omega_0$  is the minimizer of  $\mathcal{G}_0$ .

Then, (H.2) reads

$$\mathcal{G}[\omega_0 + \epsilon \delta q] = \epsilon \mathcal{H}[\omega_0] + O(\epsilon^2). \quad (\text{H.5})$$

The values of  $(A^*, B^*)$  in  $\omega_0^*$  are thus given at leading order in  $\epsilon$  by minimizing the functional  $\omega_0 \rightarrow \mathcal{H}[\omega_0]$ . Equivalently, we can write  $\mathcal{H}[\omega_0] = \theta(A, B)$  where  $\omega_0(y) = -A \cos y - B \sin y$ . Then,  $A^*$  and  $B^*$  are given by

$$\frac{\partial\theta}{\partial A}(A^*, B^*) = \frac{\partial\theta}{\partial B}(A^*, B^*) = 0. \quad (\text{H.6})$$

---

<sup>1</sup>We use this notation in agreement with the one used in section 7.3, and in the reference papers [10, 19, 61].

---

We now make sure that the expansion  $\omega^* = \omega_0^* + \epsilon \delta\omega^*$  is self-consistent. By definition,  $\frac{\delta\mathcal{G}}{\delta\omega(\mathbf{r})}[\omega^*] = 0$ . Using the fact that  $\mathcal{G}_0$  is a quadratic functional, we get

$$\frac{\delta\mathcal{G}_0}{\delta\omega(\mathbf{r})}[\omega_0^*] + \epsilon \frac{\delta\mathcal{G}_0}{\delta\omega(\mathbf{r})}[\delta\omega^*] + \epsilon \frac{\delta\mathcal{H}}{\delta\omega(\mathbf{r})}[\omega^*] = 0. \quad (\text{H.7})$$

By definition of  $\omega_0$ , the first term is exactly zero. Using a Taylor expansion in the last term and using the explicit expression of  $\mathcal{G}_0$ , we get

$$\delta\psi^* + \delta\omega^* = -\frac{\delta\mathcal{H}}{\delta\omega(\mathbf{r})}[\omega_0^*] + O(\epsilon). \quad (\text{H.8})$$

This equation gives  $\delta\omega^*$  at leading order in  $\epsilon$ . It has a stationary solution if and only if the forcing term on the right hand side has no resonant harmonics ( $\cos y, \sin y$ ). The amplitude of these harmonics are given by

$$\mathcal{A} = -\int d\mathbf{r} \frac{\delta\mathcal{H}}{\delta\omega(\mathbf{r})}[\omega_0^*] \cos y \quad , \quad \mathcal{B} = -\int d\mathbf{r} \frac{\delta\mathcal{H}}{\delta\omega(\mathbf{r})}[\omega_0^*] \sin y. \quad (\text{H.9})$$

We then have  $\delta\omega^* = O(1)$  if and only if  $\mathcal{A} = \mathcal{B} = 0$ . Differentiating the change of variable  $\mathcal{H}[\omega_0] = \theta(A, B)$ , we have

$$\delta\mathcal{H} = \int d\mathbf{r} \frac{\delta\mathcal{H}}{\delta\omega(\mathbf{r})}[\omega_0] \delta\omega_0 = \frac{\partial\theta}{\partial A} \delta A + \frac{\partial\theta}{\partial B} \delta B \quad (\text{H.10})$$

for an infinitesimal variation  $\delta\omega_0(\mathbf{r}) = \delta A \cos y + \delta B \sin y$ . Using (H.6), equation (H.10) evaluated at  $(A^*, B^*)$  gives  $\delta\mathcal{H} = 0$ . Then,  $\mathcal{A} = \mathcal{B} = 0$ . The expansion  $\omega^* = \omega_0^* + \epsilon \delta q^*$  is thus self-consistent.

# Appendix I

## Decomposition of the Langevin equation

In this appendix we describe the decomposition of the Langevin equation (7.1), that we report here for convenience,

$$\partial_t \omega + \mathbf{v} \cdot \nabla \omega = -\alpha \int d\mathbf{r}' C(\mathbf{r} - \mathbf{r}') \frac{\delta \mathcal{G}}{\delta \omega(\mathbf{r}')} + \sqrt{2\alpha\gamma} \eta, \quad (\text{I.1})$$

into its large-scale and small-scales components. We recall the definition of the large-scale component of the potential vorticity field  $A = -\langle \omega, \cos \rangle = -\frac{1}{2\pi^2 l_x} \int d\mathbf{r} \omega(\mathbf{r}) \cos y$ ,  $B = -\langle \omega, \sin \rangle = -\frac{1}{2\pi^2 l_x} \int d\mathbf{r} \omega(\mathbf{r}) \sin y$  and of the small-scale component  $\sqrt{\gamma} \omega_p(\mathbf{r}) = \omega(\mathbf{r}) + (A \cos y + B \sin y)$ .

### I.1 Advection term

The large-scale velocity field  $\mathbf{V}_0(\mathbf{r}) = U(y)\mathbf{e}_x$  with  $U(y) = A \sin y - B \cos y$  is a purely shear flow, as a consequence  $\mathbf{V}_0 \cdot \nabla \omega_0 = 0$ , where  $\omega_0 = -A \cos y - B \sin y$  is the large-scale potential vorticity. The linearized operator close to  $\mathbf{V}_0$  reads  $L_U^0[\omega] = U \partial_x \omega - U'' \partial_x \psi = U \partial_x (\omega + \psi)$ . It satisfies  $\langle L_U^0[\omega], \cos \rangle = \langle L_U^0[\omega], \sin \rangle = 0$ , so that the decomposition of the advection term reads

$$\begin{aligned} \mathbf{v} \cdot \nabla \omega &= \sqrt{\gamma} L_U^0[\omega] + \gamma \mathbf{v}_p \cdot \nabla \omega_p \\ &= \gamma [\langle \mathbf{v}_p \cdot \nabla \omega_p, \cos \rangle \cos y + \langle \mathbf{v}_p \cdot \nabla \omega_p, \sin \rangle \sin y] + \sqrt{\gamma} [L_A^0[\omega_p] + \sqrt{\gamma} NL^0[\omega_p]]. \end{aligned} \quad (\text{I.2})$$

with  $NL^0[\omega_p] = \mathbf{v}_p \cdot \nabla \omega_p - [\langle \mathbf{v}_p \cdot \nabla \omega_p, \cos \rangle \cos y + \langle \mathbf{v}_p \cdot \nabla \omega_p, \sin \rangle \sin y]$ .

### I.2 Dissipation term

We perform the change of variable  $\mathcal{G}[-A \cos y - B \sin y + \sqrt{\gamma} \omega_p] = \gamma \tilde{\mathcal{G}}[A, B, \omega_p]$ . Differentiating this change of variable gives

$$\delta \mathcal{G} = \int d\mathbf{r} \frac{\delta \mathcal{G}}{\delta \omega(\mathbf{r})} \delta q(\mathbf{r}) = -\gamma \delta A \frac{\partial \tilde{\mathcal{G}}}{\partial A} - \gamma \delta B \frac{\partial \tilde{\mathcal{G}}}{\partial B} + \gamma \int d\mathbf{r} \frac{\delta \tilde{\mathcal{G}}}{\delta \omega_p(\mathbf{r})} \delta \omega_p(\mathbf{r}), \quad (\text{I.3})$$

with  $\delta A = -\langle \delta \omega, \cos \rangle$ ,  $\delta B = -\langle \delta \omega, \sin \rangle$  and  $\sqrt{\gamma} \delta \omega_p = \delta \omega + (\delta A \cos y + B \sin y)$ . This formula plus the prescription  $\left\langle \frac{\delta \tilde{\mathcal{G}}}{\delta \omega_p(\mathbf{r})}, \cos \right\rangle = \left\langle \frac{\delta \tilde{\mathcal{G}}}{\delta \omega_p(\mathbf{r})}, \sin \right\rangle = 0$  defines unambiguously  $\frac{\delta \tilde{\mathcal{G}}}{\delta \omega_p(\mathbf{r})}$ .

We write the noise correlation function as

$$C(\mathbf{r} - \mathbf{r}') = C_0 \cos(y - y') + C_p(\mathbf{r} - \mathbf{r}') \quad (\text{I.4})$$

with  $C_p(\mathbf{r}) = \sum_{\mathbf{k} \neq (0,1)} c_{\mathbf{k}} \cos \mathbf{k} \cdot \mathbf{r}$ . Applying (I.3) to  $\delta\omega(\mathbf{r}') = C(\mathbf{r} - \mathbf{r}')$  for a fixed  $\mathbf{r}$  gives

$$\int d\mathbf{r}' \frac{\delta\mathcal{G}}{\delta\omega(\mathbf{r}')} C(\mathbf{r} - \mathbf{r}') = \gamma C_0 \cos y \frac{\partial\tilde{\mathcal{G}}}{\partial A} + \gamma C_0 \sin y \frac{\partial\tilde{\mathcal{G}}}{\partial B} + \sqrt{\gamma} \int d\mathbf{r}' \frac{\delta\tilde{\mathcal{G}}}{\delta\omega_p(\mathbf{r}')} C_p(\mathbf{r} - \mathbf{r}'), \quad (\text{I.5})$$

where we have used  $\int dy' \cos(y - y') \cos y' = \pi \cos y$  and  $\int dy' \cos(y - y') \sin y' = \pi \sin y$ .

Let's now compute explicitly the gradients of  $\tilde{\mathcal{G}}$ . Using the expression of  $\mathcal{G}$  (7.40) and the fact that  $\langle \omega_p, \cos \rangle = \langle \omega_p, \sin \rangle = 0$ , we have

$$\tilde{\mathcal{G}}[A, B, \omega_p] = \frac{\epsilon}{\gamma} 2\pi^2 l_x (A^2 + B^2) + \frac{1}{2} \int d\mathbf{r} ((1 - \epsilon)\omega_p \psi_p + \omega_p^2) + \frac{\epsilon}{\gamma} \int d\mathbf{r} f(\omega). \quad (\text{I.6})$$

First consider the function  $A \rightarrow \tilde{\mathcal{G}}[A, B, \omega_p]$  and derive it for fixed  $(B, \omega_p)$ . It gives

$$\frac{\partial\tilde{\mathcal{G}}}{\partial A} = \frac{\epsilon}{\gamma} 2\pi^2 l_x [2A - \langle f'(\omega), \cos \rangle], \quad (\text{I.7})$$

where  $f'$  denotes the derivative of  $f$  with respect to its argument. Similarly,

$$\frac{\partial\tilde{\mathcal{G}}}{\partial B} = \frac{\epsilon}{\gamma} 2\pi^2 l_x [2B - \langle f'(\omega), \sin \rangle], \quad (\text{I.8})$$

Now consider the functional  $\omega_p \rightarrow \tilde{\mathcal{G}}[A, B, \omega_p]$  and derive it for fixed  $(A, B)$ . Recalling that we impose  $\langle \frac{\delta\tilde{\mathcal{G}}}{\delta\omega_p(\mathbf{r})}, \cos \rangle = \langle \frac{\delta\tilde{\mathcal{G}}}{\delta\omega_p(\mathbf{r})}, \sin \rangle = 0$ , we get

$$\frac{\delta\tilde{\mathcal{G}}}{\delta\omega_p} = (1 - \epsilon)\psi_p + \omega_p + \frac{\epsilon}{\sqrt{\gamma}} [f'(\omega) - (\langle f'(\omega), \cos \rangle \cos y + \langle f'(\omega), \sin \rangle \sin y)]. \quad (\text{I.9})$$

Note that, due to the factor  $1/\gamma$  in the definition of  $\tilde{\mathcal{G}}$  and to the fact that  $\gamma \sim |\epsilon| \ll 1$ , the gradients of  $\tilde{\mathcal{G}}$  are all of order one.

We will need to decompose  $\frac{\delta\tilde{\mathcal{G}}}{\delta\omega_p}$  in powers of  $\gamma$ . Using  $\omega = \omega_0 + \sqrt{\gamma}\omega_p$ , we can write  $f'(\omega) = f'(\omega_0) + \sqrt{\gamma}\omega_p f''(\omega_0) + O(\gamma)$ . This will be useful in the following.

## I.3 Decomposed equations

The equations for  $A$  and  $B$  are obtained applying the projections  $\langle \cdot, \cos \rangle$  and  $\langle \cdot, \sin \rangle$  onto (I.1). Using (I.2) and (I.5), we have

$$\partial_t A = \gamma \langle \mathbf{v}_p \cdot \nabla \omega_p, \cos \rangle + \alpha \gamma C_0 \frac{\partial\tilde{\mathcal{G}}}{\partial A} + \sqrt{2\alpha\gamma} \eta_c, \quad (\text{I.10})$$

$$\partial_t B = \gamma \langle \mathbf{v}_p \cdot \nabla \omega_p, \sin \rangle + \alpha \gamma C_0 \frac{\partial\tilde{\mathcal{G}}}{\partial B} + \sqrt{2\alpha\gamma} \eta_s, \quad (\text{I.11})$$

with  $\frac{\partial \tilde{\mathcal{G}}}{\partial A}$  and  $\frac{\partial \tilde{\mathcal{G}}}{\partial B}$  given in (I.7),(I.8) and where  $\eta_c = \langle \eta, \cos \rangle$  and  $\eta_s = \langle \eta, \sin \rangle$ . The remaining terms in (I.2) and (I.5) give the equation for the perturbation  $\omega_p$ ,

$$\partial_t \omega_p + L_U^0[\omega_p] + \sqrt{\gamma} NL^0[\omega_p] = -\alpha \int d\mathbf{r}' C_p(\mathbf{r} - \mathbf{r}') \frac{\delta \tilde{\mathcal{G}}}{\delta \omega_p(\mathbf{r}')} + \sqrt{2\alpha} \eta_p, \quad (\text{I.12})$$

where  $\eta_p(\mathbf{r}, t) = \eta(\mathbf{r}, t) - \eta_c(t) \cos y - \eta_s(t) \sin y$ . Using the structure (I.4) of the noise correlation function, it can be shown that  $\eta_c$ ,  $\eta_s$  and  $\eta_p$  are independent gaussian noises, with zero mean and correlations  $\mathbb{E}[\eta_c(t_1)\eta_c(t_2)] = \mathbb{E}[\eta_s(t_1)\eta_s(t_2)] = C_0\delta(t_1 - t_2)$  and  $\mathbb{E}[\eta_p(\mathbf{r}_1, t_1)\eta_p(\mathbf{r}_2, t_2)] = C_p(\mathbf{r}_1 - \mathbf{r}_2)\delta(t_1 - t_2)$ .

Using the explicit computations (I.7),(I.8),(I.9), we can decompose the equation on  $\omega_p$  in powers of  $\gamma$ ,

$$\partial_t \omega_p + L_U[\omega_p] + \sqrt{\gamma} NL_U[\omega_p] + \gamma D_U[\omega_p] = \sqrt{2\alpha} \eta_p \quad (\text{I.13})$$

with

$$L_U[\omega_p] = L_U^0[\omega_p] + \alpha \int d\mathbf{r}' C_p(\mathbf{r} - \mathbf{r}') (\omega_p + \psi_p), \quad (\text{I.14})$$

$$NL_U[\omega_p] = NL^0[\omega_p] + \frac{\alpha\epsilon}{\gamma} \int d\mathbf{r}' C_p(\mathbf{r} - \mathbf{r}') [f'(\omega_0) - (\langle f'(\omega_0), \cos \rangle \cos y + \langle f'(\omega_0), \sin \rangle \sin y)], \quad (\text{I.15})$$

and

$$D_U[\omega_p] = \frac{\alpha\epsilon}{\gamma} \int d\mathbf{r}' C_p(\mathbf{r} - \mathbf{r}') \{ \psi_p - \omega_p [f''(\omega_0) - (\langle f''(\omega_0), \cos \rangle \cos y + \langle f''(\omega_0), \sin \rangle \sin y)] \} + O(\sqrt{\gamma}) \quad (\text{I.16})$$

# Bibliography

- [1] Farid Ait-Chaalal and Tapio Schneider. Why eddy momentum fluxes are concentrated in the upper troposphere. *Journal of the Atmospheric Sciences*, 72(4):1585–1604, 2015.
- [2] Nikolaos A Bakas, Navid C Constantinou, and Petros J Ioannou. S3T stability of the homogeneous state of barotropic beta-plane turbulence. *Journal of the Atmospheric Sciences*, 72(5):1689–1712, 2015.
- [3] Nikolaos A Bakas and Petros J Ioannou. A theory for the emergence of coherent structures in beta-plane turbulence. *Journal of Fluid Mechanics*, 740:312–341, 2014.
- [4] Radu Balescu. *Statistical dynamics – Matter out of equilibrium*. Imperial College Press, 1997.
- [5] NJ Balmforth and PJ Morrison. Normal modes and continuous spectra. *Annals of the New York Academy of Sciences*, 773(1):80–94, 1995.
- [6] Jacob Bedrossian and Nader Masmoudi. Inviscid damping and the asymptotic stability of planar shear flows in the 2d euler equations. *Publications mathématiques de l’IHÉS*, pages 1–106, 2013.
- [7] P Berloff, I Kamenkovich, and Joseph Pedlosky. A model of multiple zonal jets in the oceans: Dynamical and kinematical analysis. *Journal of Physical Oceanography*, 39(11):2711–2734, 2009.
- [8] Pavel Berloff, Igor Kamenkovich, and Joseph Pedlosky. A mechanism of formation of multiple zonal jets in the oceans. *Journal of Fluid Mechanics*, 628:395–425, 2009.
- [9] Guido Boffetta and Robert E Ecke. Two-dimensional turbulence. *Annual Review of Fluid Mechanics*, 44:427–451, 2012.
- [10] F. Bouchet, J. Laurie, and O. Zaboronski. Langevin Dynamics, Large Deviations and Instantons for the Quasi-Geostrophic Model and Two-Dimensional Euler Equations. *Journal of Statistical Physics*, 156(6):1066–1092, September 2014.
- [11] F. Bouchet and H. Morita. Large time behavior and asymptotic stability of the 2D Euler and linearized Euler equations. *Physica D Nonlinear Phenomena*, 239:948–966, June 2010.

- 
- [12] F Bouchet, C Nardini, and T Tangarife. Stochastic averaging, large deviations and random transitions for the dynamics of 2d and geostrophic turbulent vortices. *Fluid Dynamics Research*, 46(6):061416, 2014.
- [13] F. Bouchet and E. Simonnet. Random Changes of Flow Topology in Two-Dimensional and Geophysical Turbulence. *Physical Review Letters*, 102(9):094504, March 2009.
- [14] F. Bouchet and A. Venaille. Statistical mechanics of two-dimensional and geophysical flows. *Physics Reports*, 515:227–295, 2012.
- [15] Freddy Bouchet and Marianne Corvellec. Invariant measures of the 2D Euler and Vlasov equations. *Journal of Statistical Mechanics: Theory and Experiment*, 2010(08):P08021, 2010.
- [16] Freddy Bouchet, Tobias Grafke, Tomás Tangarife, and Eric Vanden-Eijnden. Large deviations in fast-slow systems. *preprint, to be submitted to the Journal of Statistical Physics*, arXiv:1510.02227, 2015.
- [17] Freddy Bouchet, J Brad Marston, and Tomás Tangarife. Large deviations of reynolds’ stresses in zonal jet dynamics. *in preparation*, 1:1, 2015.
- [18] Freddy Bouchet, Cesare Nardini, and Tomás Tangarife. Kinetic theory of jet dynamics in the stochastic barotropic and 2D Navier-Stokes equations. *Journal of Statistical Physics*, 153(4):572–625, 2013.
- [19] Freddy Bouchet, Cesare Nardini, and Tomás Tangarife. *5th Warsaw School of Statistical Physics*, chapter 1: Non-equilibrium Statistical Mechanics of the Stochastic Navier-Stokes Equations and Geostrophic Turbulence. Warsaw University Press, 2014.
- [20] Freddy Bouchet, Cesare Nardini, and Tomás Tangarife. *Zonal Jets*, chapter 5: Kinetic theory of jet dynamics. Cambridge University Press, 2016.
- [21] Charles-Edouard Bréhier. Strong and weak orders in averaging for spdes. *Stochastic Processes and their Applications*, 122(7):2553–2593, 2012.
- [22] SN Brown and K Stewartson. On the algebraic decay of disturbances in a stratified linear shear flow. *J. Fluid Mech*, 100(part 4):811–816, 1980.
- [23] G. Brunet and P. H. Haynes. The Nonlinear Evolution of Disturbances to a Parabolic Jet. *Journal of Atmospheric Sciences*, 52:464–477, 1995.
- [24] G. Brunet and T. Warn. Rossby Wave Critical Layers on a Jet. *Journal of Atmospheric Sciences*, 47:1173–1178, 1990.
- [25] George F Carnevale and Paul C Martin. Field theoretical techniques in statistical fluid dynamics: with application to nonlinear wave dynamics. *Geophysical & Astrophysical Fluid Dynamics*, 20(1-2):131–163, 1982.
- [26] Frédéric Cérou and Arnaud Guyader. Adaptive multilevel splitting for rare event analysis. *Stochastic Analysis and Applications*, 25(2):417–443, 2007.

- [27] Jule G. Charney and John G. DeVore. Multiple flow equilibria in the atmosphere and blocking. *Journal of the Atmospheric Sciences*, 36(7):1205–1216, July 1979.
- [28] Y Chavaillaz, F Codron, and M Kageyama. Southern westerlies in LGM and future (RCP4. 5) climates. *Climate of the Past Discussions*, 8:3693–3717, 2012.
- [29] P. H. Chavanis. Quasilinear Theory of the 2D Euler Equation. *Physical Review Letters*, 84:5512–5515, June 2000.
- [30] P. H. Chavanis. Kinetic theory of point vortices: Diffusion coefficient and systematic drift. *Phys. Rev. E*, 64(2):026309, 2001.
- [31] Colm P Connaughton, Balasubramanya T Nadiga, Sergey V Nazarenko, and Brenda E Quinn. Modulational instability of rossby and drift waves and generation of zonal jets. *Journal of Fluid Mechanics*, 654:207–231, 2010.
- [32] Navid Constantinou. *Formation of large-scale structures by turbulence in rotating planets*. PhD thesis, University of Athens, 2015.
- [33] Navid C Constantinou, Brian F Farrell, and Petros J Ioannou. Emergence and equilibration of jets in beta-plane turbulence: applications of stochastic structural stability theory. *J. Atmos. Sci.*, 71(5):1818–1842, 2014.
- [34] Sergey Danilov and David Gurarie. Scaling spectra and zonal jets in beta-plane turbulence. *Physics of Fluids*, 16(7):2592–2603, 2004.
- [35] P. G. Drazin and W. H. Reid. *Hydrodynamic stability*. Cambridge university press, 2004, second edition.
- [36] DG Dritschel and ME McIntyre. Multiple jets as pv staircases: the phillips effect and the resilience of eddy-transport barriers. *Journal of the Atmospheric Sciences*, 65(3):855–874, 2008.
- [37] Jinqiao Duan and Wei Wang. *Effective dynamics of stochastic partial differential equations*. Elsevier, 2014.
- [38] Brian F Farrell and Petros J Ioannou. Structural stability of turbulent jets. *Journal of the atmospheric sciences*, 60(17):2101–2118, 2003.
- [39] Mark I Freidlin and Alexander D Wentzell. *Random perturbations of dynamical systems, Second Edition*, volume 260. Springer, 1998.
- [40] R. Friedrich, A. Daitche, O. Kamps, J. Lulff, M. Vosskuhle, and M. Wilczek. The Lundgren-Monin-Novikov hierarchy: kinetic equations for turbulence. *C. R. Physique*, 13:929–953, 2012.
- [41] Basile Gallet and William R Young. A two-dimensional vortex condensate at high reynolds number. *Journal of Fluid Mechanics*, 715:359–388, 2013.
- [42] Boris Galperin, Semion Sukoriansky, and Nadejda Dikovskaya. Geophysical flows with anisotropic turbulence and dispersive waves: flows with a  $\beta$ -effect. *Ocean Dynamics*, 60(2):427–441, 2010.

- 
- [43] Boris Galperin, Roland MB Young, Semion Sukoriansky, Nadejda Dikovskaya, Peter L Read, Andrew J Lancaster, and David Armstrong. Cassini observations reveal a regime of zonostrophic macroturbulence on jupiter. *Icarus*, 229:295–320, 2014.
- [44] C. W. Gardiner. *Handbook of stochastic methods for physics, chemistry and the natural sciences*. Springer Series in Synergetics, Berlin: Springer, —c1994, 2nd ed. 1985. Corr. 3rd printing 1994, 1994.
- [45] Daniel T. Gillespie. Exact numerical simulation of the Ornstein-Uhlenbeck process and its integral. *Phys. Rev. E*, 54:2084–2091, Aug 1996.
- [46] Natsuki Hashitsume, Morikazu Toda, Ryogo Kubo, and Nobuhiko Saitō. *Statistical physics II: nonequilibrium statistical mechanics*, volume 30. Springer Science & Business Media, 1991.
- [47] Isaac M Held and Peter J Phillips. Linear and nonlinear barotropic decay on the sphere. *Journal of the atmospheric sciences*, 44(1):200–207, 1987.
- [48] Huei-Ping Huang and Walter A Robinson. Two-dimensional turbulence and persistent zonal jets in a global barotropic model. *Journal of the atmospheric sciences*, 55(4):611–632, 1998.
- [49] James W Hurrell. Decadal trends in the north atlantic oscillation: regional temperatures and precipitation. *Science*, 269(5224):676–679, 1995.
- [50] Intergovernmental Panel on Climate Change [Core Writing Team, R.K. Pachauri and L.A. Meyer (eds.)]. *Climate Change 2014: Synthesis Report. Contribution of Working Groups I, II and III to the Fifth Assessment Report of the Intergovernmental Panel on Climate Change*. IPCC, Geneva, Switzerland, 2014.
- [51] Harold Jeffreys. On the dynamics of geostrophic winds. *Quarterly Journal of the Royal Meteorological Society*, 52(217):85–104, 1926.
- [52] E. Kalnay and Coauthors. The NCEP/NCAR reanalysis 40-year project. *Bull. Amer. Meteor. Soc.*, 77:437–471, 1996.
- [53] Akira Kasahara. Effect of zonal flows on the free oscillations of a barotropic atmosphere. *Journal of the Atmospheric Sciences*, 37(5):917–929, 1980.
- [54] Masahide Kimoto and Michael Ghil. Multiple flow regimes in the northern hemisphere winter. part i: Methodology and hemispheric regimes. *Journal of the Atmospheric Sciences*, 50(16):2625–2644, 1993.
- [55] R H Kraichnan and D Montgomery. Two-dimensional turbulence. *Reports on Progress in Physics*, 43(5):547, 1980.
- [56] Werner Krauth. *Statistical mechanics: algorithms and computations*, volume 13. Oxford University Press, 2006.
- [57] S. Kravtsov, A. W. Robertson, and M. Ghil. Bimodal Behavior in the Zonal Mean Flow of a Baroclinic  $\beta$ -Channel Model. *Journal of Atmospheric Sciences*, 62:1746–1769, 2005.

- [58] Hsiao-Lan Kuo. Dynamical aspects of the general circulation and the stability of zonal flow. *Tellus*, 3(4):268–284, 1951.
- [59] Paul Langevin. Sur la théorie du mouvement brownien. *CR Acad. Sci. Paris*, 146(530-533), 1908.
- [60] Jason Laurie, Guido Boffetta, Gregory Falkovich, Igor Kolokolov, and Vladimir Lebedev. Universal profile of the vortex condensate in two-dimensional turbulence. *Physical review letters*, 113(25):254503, 2014.
- [61] Jason Laurie and Freddy Bouchet. Computation of rare transitions in the barotropic quasi-geostrophic equations. *New Journal of Physics*, 17(1):015009, 2015.
- [62] Douglas K Lilly. Numerical simulation of two-dimensional turbulence. *Physics of Fluids (1958-1988)*, 12(12):II–240, 1969.
- [63] T. S. Lundgren. Distribution functions in the statistical theory of turbulence. *Phys. Fluids*, 10:969–975, 1967.
- [64] Andrew Majda and Xiaoming Wang. *Nonlinear dynamics and statistical theories for basic geophysical flows*. Cambridge University Press, 2006.
- [65] Vladislav Mantič-Lugo, Cristóbal Arratia, and François Gallaire. Self-consistent mean flow description of the nonlinear saturation of the vortex shedding in the cylinder wake. *Physical review letters*, 113(8):084501, 2014.
- [66] JB Marston. Statistics of the general circulation from cumulant expansions. *Chaos*, 20(4), 2010.
- [67] JB Marston, E Conover, and Tapio Schneider. Statistics of an unstable barotropic jet from a cumulant expansion. *Journal of the Atmospheric Sciences*, 65(6):1955–1966, 2008.
- [68] JB Marston, Wanming Qi, and SM Tobias. Direct statistical simulation of a jet. *arXiv preprint arXiv:1412.0381*, 2014.
- [69] Jonathan Miller. Statistical mechanics of euler equations in two dimensions. *Physical review letters*, 65(17):2137, 1990.
- [70] A. S. Monin. Equations of turbulent motion. *Prikl. Mat. Mekh.*, 31:1057, 1967.
- [71] A S Monin and A M Yaglom. *Statistical fluid mechanics, Volume II*. Dover, 1975.
- [72] Clément Mouhot and Cédric Villani. On landau damping. *Acta mathematica*, 207(1):29–201, 2011.
- [73] C. Nardini, S. Gupta, S. Ruffo, T. Dauxois, and F. Bouchet. Kinetic theory for non-equilibrium stationary states in long-range interacting systems. *Journal of Statistical Mechanics: Theory and Experiment*, 1:L01002, January 2012.

- 
- [74] Cesare Nardini, Shamik Gupta, Stefano Ruffo, Thierry Dauxois, and Freddy Bouchet. Kinetic theory of nonequilibrium stochastic long-range systems: phase transition and bistability. *Journal of Statistical Mechanics: Theory and Experiment*, 2012(12):P12010, 2012.
- [75] Sergey Nazarenko. *Wave turbulence*, volume 825. Springer Science & Business Media, 2011.
- [76] Sergey Nazarenko and Brenda Quinn. Triple cascade behavior in quasi-geostrophic and drift turbulence and generation of zonal jets. *Physical review letters*, 103(11):118501, 2009.
- [77] Mark EJ Newman and Gerard T Barkema. *Monte Carlo methods in statistical physics*, volume 13. Clarendon Press Oxford, 1999.
- [78] D. Nicholson. *Introduction to plasma theory*. Wiley, New-York, 1983.
- [79] E. A. Novikov. Kinetic equations for a vortex field. *Sov. Phys. Dokl.*, 12:1006–1008, 1968.
- [80] Paul A O’Gorman and Tapio Schneider. Recovery of atmospheric flow statistics in a general circulation model without nonlinear eddy-eddy interactions. *Geophysical Research Letters*, 34(22), 2007.
- [81] Lars Onsager. Statistical hydrodynamics. *Il Nuovo Cimento (1943-1954)*, 6:279–287, 1949.
- [82] W. M. F. Orr. The stability or instability of the steady motions of a perfect liquid and of a viscous liquid. *Proc. Roy. Irish Acad*, pages 9–69, 1907.
- [83] George C Papanicolaou. Some probabilistic problems and methods in singular perturbations. *Journal of Mathematics*, 6(4), 1976.
- [84] George C Papanicolaou. Introduction to the asymptotic analysis of stochastic equations. *Modern modeling of continuum phenomena (Ninth Summer Sem. Appl. Math., Rensselaer Polytech. Inst., Troy, NY, 1975)*, 16:109–147, 1977.
- [85] Jeffrey B. Parker and John A. Krommes. Generation of zonal flows through symmetry breaking of statistical homogeneity. *New Journal of Physics*, 16:035006, 2014.
- [86] Grigoris Pavliotis and Andrew Stuart. *Multiscale methods: averaging and homogenization*, volume 53. Springer, 2008.
- [87] J. Pedlosky. *Geophysical fluid dynamics*. Springer, 1982.
- [88] José P Peixóto and Abraham H Oort. Physics of climate. *Reviews of Modern Physics*, 56(3):365, 1984.
- [89] Stephen B Pope. *Turbulent flows*. Cambridge university press, 2000.
- [90] Carolyn C Porco *et. al.* Cassini imaging of jupiter’s atmosphere, satellites, and rings. *Science*, 299:1541, 2003.

- [91] Stefan Rahmstorf. Ocean circulation and climate during the past 120,000 years. *Nature*, 419(6903):207–214, 2002.
- [92] Osborne Reynolds. On the dynamical theory of incompressible viscous fluids and the determination of the criterion. *Proceedings of the Royal Society of London*, 56(336-339):40–45, 1894.
- [93] Hannes Risken. *The Fokker-Planck equation, Method of solution and applications*. Springer, 1984.
- [94] Raoul Robert and Joel Sommeria. Statistical equilibrium states for two-dimensional flows. *Journal of Fluid Mechanics*, 229:291–310, 1991.
- [95] John Hubert Rogers. *The giant planet Jupiter*. Number 6 in Practical Astronomy Handbooks. Cambridge University Press, 1995.
- [96] Christian M Rohwer, Florian Angeletti, and Hugo Touchette. Convergence of large deviation estimators. *arXiv preprint arXiv:1409.8531v2*, 2015.
- [97] Joran Rolland and Eric Simonnet. Statistical behaviour of adaptive multi-level splitting algorithms in simple models. *Journal of Computational Physics*, 283:541–558, 2015.
- [98] C.-G. Rossby. Relation between variations in the intensity of the zonal circulation of the atmosphere and the displacements of the semi-permanent centers of action. *J. Mar. Res.*, 2:38–55, 1939.
- [99] Rick Salmon. *Lectures on geophysical fluid dynamics*, volume 378. Oxford University Press Oxford, 1998.
- [100] Colette Salyk, Andrew P Ingersoll, Jean Lorre, Ashwin Vasavada, and Anthony D Del Genio. Interaction between eddies and mean flow in jupiter’s atmosphere: Analysis of cassini imaging data. *Icarus*, 185(2):430–442, 2006.
- [101] D. A. Schecter, D. H. E. Dubin, K. S. Fine, and C. F. Driscoll. Vortex crystals from 2D Euler flow: Experiment and simulation. *Phys. Fluids*, 11:905–914, 1999.
- [102] Tapio Schneider and Junjun Liu. Formation of jets and equatorial superrotation on jupiter. *Journal of the Atmospheric Sciences*, 66(3):579–601, 2009.
- [103] Theodore G Shepherd. A spectral view of nonlinear fluxes and stationary-transient interaction in the atmosphere. *Journal of the atmospheric sciences*, 44(8):1166–1179, 1987.
- [104] K. Srinivasan and W. R. Young. Zonostrophic Instability. *Journal of the atmospheric sciences*, 69(5):1633–1656, 2011.
- [105] Semion Sukoriansky, Nadejda Dikovskaya, and Boris Galperin. On the arrest of inverse energy cascade and the rhines scale. *Journal of the Atmospheric Sciences*, 64(9):3312–3327, 2007.
- [106] SM Tobias and JB Marston. Direct statistical simulation of out-of-equilibrium jets. *Physical Review Letters*, 110(10):104502, 2013.

- 
- [107] JR Toggweiler, Joellen L Russell, and SR Carson. Midlatitude westerlies, atmospheric CO<sub>2</sub>, and climate change during the ice ages. *Paleoceanography*, 21(2):PA2005, 2006.
- [108] Hugo Touchette. The large deviation approach to statistical mechanics. *Physics Reports*, 478(1):1–69, 2009.
- [109] F. R. Ulinich and B. Ya. Lyubimov. The statistical theory of turbulence of an incompressible fluid at large Reynolds numbers. *Sov. Phys. JETP*, 28:494–500, 1969.
- [110] Geoffrey K. Vallis. *Atmospheric and Oceanic Fluid Dynamics: Fundamentals and Large-scale Circulation*. Cambridge University Press, November 2006.
- [111] Geoffrey K Vallis, Edwin P Gerber, Paul J Kushner, and Benjamin A Cash. A mechanism and simple dynamical model of the north atlantic oscillation and annular modes. *Journal of the atmospheric sciences*, 61(3):264–280, 2004.
- [112] Geoffrey K Vallis and Matthew E Maltrud. Generation of mean flows and jets on a beta plane and over topography. *Journal of physical oceanography*, 23(7):1346–1362, 1993.
- [113] N G Van Kampen. On the theory of stationary waves in plasmas. *Physica*, 21(6):949–963, 1955.
- [114] A Yu Veretennikov. On large deviations for sdes with small diffusion and averaging. *Stochastic processes and their applications*, 89(1):69–79, 2000.
- [115] Heinz Wanner, Stefan Brönnimann, Carlo Casty, Dimitrios Gyalistras, Jürg Luterbacher, Christoph Schmutz, David B Stephenson, and Eleni Xoplaki. North atlantic oscillation—concepts and studies. *Surveys in geophysics*, 22(4):321–381, 2001.
- [116] E. R. Weeks, Y. Tian, J. S. Urbach, K. Ide, H. L. Swinney, and M. Ghil. Transitions Between Blocked and Zonal Flows in a Rotating Annulus. *Science*, 278:1598, 1997.
- [117] Peter D Welch. The use of fast fourier transform for the estimation of power spectra: a method based on time averaging over short, modified periodograms. *IEEE Transactions on audio and electroacoustics*, 15(2):70–73, 1967.
- [118] Ashraf Youssef and Philip S Marcus. The dynamics of jovian white ovals from formation to merger. *Icarus*, 162(1):74–93, 2003.
- [119] Christian Zillinger. Linear inviscid damping for monotone shear flows. *arXiv preprint arXiv:1410.7341*, 2014.
- [120] Christian Zillinger. Linear inviscid damping for monotone shear flows in a finite periodic channel, boundary effects, blow-up and critical sobolev regularity. *arXiv preprint arXiv:1506.04010*, 2015.

# Publications

Part of the work presented in this thesis has been published in peer-reviewed journals:

[18] F. Bouchet, C. Nardini and T. Tangarife. Kinetic theory of jet dynamics in the stochastic barotropic and 2D Navier-Stokes equations. *Journal of Statistical Physics*, 153(4):572–625, 2013.

[12] F. Bouchet, C. Nardini and T. Tangarife. Stochastic averaging, large deviations, and random transitions for the dynamics of 2D and geostrophic turbulent vortices. *Fluid Dyn. Res.* 46(6):061416, 2014.

Two more papers will be published soon:

[17] F. Bouchet, J.B. Marston and T. Tangarife. Large deviations of Reynolds' stresses in zonal jet dynamics.

[16] F. Bouchet, T. Grafke, T. Tangarife and E. Vanden-Eijnden. Large deviations in fast-slow systems. *preprint, to be submitted to the Journal of Statistical Physics*, arXiv:1510.02227.

Finally, a part of this thesis is presented in the following books, one of which is already published:

[19] F. Bouchet, C. Nardini and T. Tangarife. *5th Warsaw School of Statistical Physics*, chapter 1: Non-equilibrium Statistical Mechanics of the Stochastic Navier-Stokes Equations and Geostrophic Turbulence. Warsaw University Press (2014).

[20] F. Bouchet, C. Nardini and T. Tangarife. *Zonal Jets*, chapter 5: Kinetic theory of jet dynamics. Cambridge University Press (2016).

# Main results

## In chapter 3

- Derivation of an effective equation for the evolution of zonal jets in the time scale separation regime (kinetic equation), using stochastic averaging (equation (3.7) in page 39).
- Alternative derivation of the leading order part of the kinetic equation using a generalization of the Lundgren-Monin-Novikov hierarchy (section 3.2.2 in page 43).

## In chapter 4

- Simple expression of the average Reynolds' stress divergence (drift term in the kinetic equation) for the linearized stochastic barotropic equation in the inviscid limit (equation (4.30) in page 57).
- Development of an efficient method to compute numerically the average Reynolds' stress divergence in the inviscid limit (section 4.3.2 in page 58).

## In chapter 5

- Estimation of the typical fluctuations of the Reynolds' stress divergence for the linearized stochastic barotropic equation in the inviscid limit (equation (5.15) in page 73 and section 5.3.2 in page 77).
- Proof that ergodicity for the Reynolds' stress divergence is not fulfilled point-wise in the case of a localized forcing spectrum and in the absence of rotation and viscosity (section 5.3.3 in page 78).

## In chapter 6

- Estimation of the large deviation rate function for the time-averaged Reynolds' stress divergence, from direct numerical simulations of the linearized stochastic barotropic equation (sections 6.1 in page 83 and 6.5.3 in page 106).
- Direct computation of probabilities of rare events for the time-averaged Reynolds' stress divergence, through a matrix Riccati equation (equation (6.12) in page 88 and section 6.5.3 in page 106).
- Explicit computation of the large deviation function for a class of quasi-linear slow-fast systems (equation (6.17) in page 89).

## In chapter 7

- Derivation of the effective slow dynamics of zonal jets in a class of Langevin models for the barotropic equation (equations (7.59),(7.60) in page 126).
- Derivation of fluctuation-dissipation relations for the effective Langevin dynamics in a very general setting (equation (7.65) in page 127).
- Derivation of an explicit solution of the Lyapunov equation (section 7.2.2 in page 119).

# Résumé

Cette thèse porte sur la dynamique des grandes échelles des écoulements géophysiques turbulents, en particulier sur les écoulements parallèles orientés dans la direction est-ouest (jets zonaux). Ces structures ont la particularité d'évoluer sur des périodes beaucoup plus longues que la turbulence qui les entoure. D'autre part, on observe dans certains cas, sur ces échelles de temps longues, des transitions brutales entre différentes configurations des jets zonaux (multistabilité).

L'approche proposée dans cette thèse consiste à moyenniser l'effet des degrés de liberté turbulents rapides de manière à obtenir une description effective des grandes échelles spatiales de l'écoulement, en utilisant les outils de moyennisation stochastique et la théorie des grandes déviations. Ces outils permettent d'étudier à la fois les attracteurs, les fluctuations typiques et les fluctuations extrêmes de la dynamique des jets. Cela permet d'aller au-delà des approches antérieures, qui ne décrivent que le comportement moyen des jets.

Le premier résultat est une équation effective pour la dynamique lente des jets, la validité de cette équation est étudiée d'un point de vue théorique, et les conséquences physiques sont discutées. De manière à décrire la statistique des événements rares tels que les transitions brutales entre différentes configurations des jets, des outils issus de la théorie des grandes déviations sont employés. Des méthodes originales sont développées pour mettre en œuvre cette théorie, ces méthodes peuvent par exemple être appliquées à des situations de multistabilité.

# Abstract

This thesis deals with the dynamics of geophysical turbulent flows at large scales, more particularly their organization into east-west parallel flows (zonal jets). These structures have the particularity to evolve much slower than the surrounding turbulence. Besides, over long time scales, abrupt transitions between different configurations of zonal jets are observed in some cases (multistability).

Our approach consists in averaging the effect of fast turbulent degrees of freedom in order to obtain an effective description of the large scales of the flow, using stochastic averaging and the theory of large deviations. These tools provide the attractors, the typical fluctuations and the large fluctuations of jet dynamics. This allows to go beyond previous studies, which only describe the average jet dynamics.

Our first result is an effective equation for the slow dynamics of jets, the validity of this equation is studied from a theoretical point of view, and the physical consequences are discussed. In order to describe the statistics of rare events such as abrupt transitions between different jet configurations, tools from large deviation theory are employed. Original methods are developed in order to implement this theory, those methods can be applied for instance in situations of multistability.